

*TK des 1002 S*

Stellingen

behorende bij het proefschrift

" Macroscopic Theory of Two-Phase Bubbly Flow "

van

A.J.N. Vreenegoor

- [1] De drukverdelingen aan de expansiekant van een supersonische delta-vleugel, bepaald met behulp van reeksooplossingen van de conische potentiaalvergelijking, blijken erg gevoelig te zijn voor de positie van de 'inboard shock' (Vreenegeoor & Bakker 1986).

Vreenegeoor, A. J. N. & Bakker, P. G. 1986 Berekening drukverdelingen op supersonische delta-vleugels m.b.v. stuwpunts-oplossingen. *Rapport LR-484*, TU Delft.

- [2] De bewering van Kapteijn (1989), dat Kok (1989) heeft aangetoond dat de theorie van Geurst (1985) voor vloeistof/bellenmengsels geen bel-interactie bevat bij marginale stabiliteit, is onjuist.

Kapteijn, C. 1989 *Measurements on concentration waves in bubbly liquids*. Ph.D. Thesis, Twente University, Enschede, The Netherlands.

Kok, J. B. W. 1989 *Dynamics of gas bubbles moving through liquid*. Ph.D. Thesis, Twente University, Enschede, The Netherlands.

Geurst, J. A. 1985 Virtual mass in two-phase bubbly flow. *Physica A* 129, 233-261.

- [3] Om milieutechnische redenen dient men vervuilende continu-processen te vervangen door beter te beheersen batch-processen.

Een schoon voorbeeld hiervan vormt de fabricage van opencellig schuimplastic, waarbij het batch-proces de mogelijkheid biedt een groot gedeelte van het schadelijke blaasmiddel Freon terug te winnen (Vreenegeoor 1987).

Vreenegeoor, N. C. 1988 Environmental considerations in the production of flexible slabstock. *Cellular Polymers* 8, 16-32.

- [4] Het pulseren van een enkele gasbel in een oneindige vloeistof, beschreven door de Rayleigh–Plesset vergelijking, kan door middel van een variationele formulering op systematische wijze opgenomen worden in een macroscopische theorie voor vloeistof/bellenmengsels (Vreenegoor 1990).

Vreenegoor, A. J. N. 1990 Bubble pulsations in gas/liquid two-phase flow.  
*Technical Note*, TU Delft.

- [5] ‘Loss-of-coolant accidents’, die kunnen leiden tot de ‘melt down’ van een kernreactor, worden gesimuleerd met behulp van bewegingsvergelijkingen, die zowel op fysische als op mathematische gronden verworpen zouden moeten worden.

- [6] Dat het trekken van conclusies uit meetresultaten zeer zorgvuldig dient te geschieden bleek al in 1610 toen Galileo de ring van Saturnus interpreteerde als twee manen en bleek in 1989 opnieuw bij de zogenaamde ontdekking van kernfusie bij kamertemperatuur (Fleischmann & Pons en Jones et al. 1989).

Fleischmann, M. & Pons, S. 1989 Electrochemically induced nuclear fusion of deuterium. *J. Electroanal. Chem.* **261**, 301–308.

Jones, S. E. et al. 1989 Observation of cold nuclear fusion in condensed matter. *Nature* **338**, 737–740.

- [7] Door herhaaldelijk en nadrukkelijk de revolutie in Oost-Europa (1989) als onomkeerbaar te kwalificeren, gaven een aantal vooraanstaande Westerse regeringsleiders blijk van hun vrees dat deze revolutie alsnog tot stilstand gebracht zou kunnen worden.

- [8] Ten aanzien van de ontwikkeling van de Engelse economie had de Kanaaltunnel geen slechtere ligging kunnen hebben.
- [9] Vele golfverschijnselen kunnen een heilzame werking hebben op de mens. Gezien de onbetrouwbare eigenschappen van het medium en de daaruit voortvloeiende schadelijke bijverschijnselen moet het evenwel ten zeerste afgeraden worden zich bloot te stellen aan een wave in een voetbalstadion.
- [10] De houding van de voetbalverslaggevers van Studio Sport werd duidelijk gedemonstreerd door Evert ten Napel, die zich tijdens de wedstrijd PSV – Steaua Boekarest (5 – 1; 1-11-1989) verontschuldigde voor zijn enthousiasme.
- [11] In sommige etappes verdienen de deelnemers aan de Ronde van Frankrijk het predikaat tourist.

500dag  
30.9.2017  
T. P. van der Meer

**TR diss  
1802**

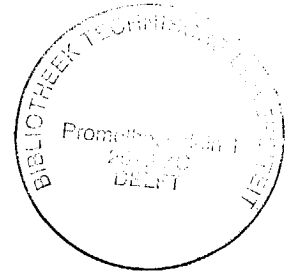
**MACROSCOPISCHE THEORIE VAN  
TWEE-FASENSTROMING MET BELLEN**

Omslag: *Galatea of the Spheres* .

© Salvador Dalí, 1952 c/o Beeldrecht Amsterdam.

# MACROSCOPIC THEORY OF TWO-PHASE BUBBLY FLOW

## PROEFSCHRIFT



ter verkrijging van de graad van doctor  
aan de Technische Universiteit Delft,  
op gezag van de Rector Magnificus,  
Prof. drs. P.A. Schenck,  
in het openbaar te verdedigen  
ten overstaan van een commissie  
aangewezen door het College van Dekanen  
op dinsdag 13 maart 1990 te 14.00 uur

door

**ALOYSIUS JOHANNES NICOLAAS VREENEGOOR ,**

geboren te Hillegom,  
wiskundig ingenieur.

**Dit proefschrift is goedgekeurd door de promotor:**

Prof. dr. J.A. Geurst

**Promotiecommissie:**

Prof. dr. ir. H.E.A. van den Akker

Prof. dr. ir. P.G. Bakker

Prof. dr. ir. A.J. Hermans

Dr. ir. R.V.A. Oliemans

Prof. dr. ir. Steketee

Prof dr. ir. P. Wesseling



**Aan mijn ouders**

# Contents

<b>I</b>	<b>Introduction</b>	<b>1</b>
1.1	Two-phase flow	1
1.2	Basic model	4
1.3	Momentum balances	7
1.4	Averaging methods	7
1.5	Three-fluid models	11
1.6	Variational methods	14
1.7	Comparison of various models	19
<b>II</b>	<b>Variational approach to bubble deformation in two-phase flow</b>	<b>25</b>
2.1	Introduction	25
2.2	Variational formulation and two-phase flow equations	26
2.3	Conservation equations: The Clebsch–Bateman principle	32
2.4	Linear stability analysis	36
2.5	Adjustment of the flow equations to the dynamics of a separate deformable bubble	42
2.6	Acoustic modes and breakdown of bubbly flow	47
2.7	Conclusions	49
	Appendix	51

<b>III</b>	<b>Nonlinear void–fraction waves in bubbly two–phase flow</b>	<b>53</b>
3.1	Introduction	53
3.2	Inviscid two–phase bubbly flow	54
3.3	Nonlinear void–fraction waves	59
3.4	Variational principle	64
3.5	Nonlinear void–fraction waves and bubble deformation	66
3.6	Nonlinear void–fraction waves and gas motion inside bubbles	71
3.7	Conclusions	77
<b>IV</b>	<b>Numerical and analytical investigation of waves and wave–interactions in bubbly two–phase flow</b>	<b>79</b>
4.1	Introduction	79
4.2	Flow equations	81
4.3	Some remarks on stability	83
4.3.1	Eigenvalues and eigenvectors	83
4.3.2	Effect of the functional form of $m(\alpha)$ on the eigenvalues of model 1	88
4.4	Numerical method and results	91
4.4.1	Numerical method	91
4.4.2	Testing the method	94
4.4.3	Numerical investigation of wave–interaction	98
4.4.4	Stability of nonlinear concentration waves and linear stability of model 1	102
4.5	Linear theory and acoustics	106
4.5.1	Waves originating from a disturbance in the gas pressure (linear theory)	106
4.5.2	Interaction of an acoustic wave and a discontinuous concentration wave (linear theory)	109
4.5.3	Acoustics of bubbly two–phase flow	116
4.5.4	Comparison with ordinary acoustics	122
4.6	Conclusions	127

<b>V</b>	<b>Two-phase bubbly flow through vertical tube: void-fraction distribution and velocity profiles</b>	<b>129</b>
5.1	Introduction	129
5.2	Equations governing non-dissipative bubbly flow	133
5.3	Additional terms required near solid boundary	138
5.4	Dissipative effects and external forces	140
5.5	Bubbly flow through vertical tube: asymptotic solution	144
5.6	Numerical results	153
5.7	Higher order asymptotic solution	161
5.8	Conclusions	166
	<b>References</b>	<b>167</b>
	<b>Acknowledgment</b>	<b>173</b>
	<b>Summary</b>	<b>175</b>
	<b>Samenvatting</b>	<b>177</b>
	<b>Curriculum vitae</b>	<b>179</b>

## CHAPTER I

### INTRODUCTION

#### 1.1 Two-phase flow

Two-phase flow is encountered in many different forms, including for instance the entrainment of particles by a gas flow, fluidized beds, sedimentation, liquid-liquid flow and gas-liquid flow. In this thesis only the last type of flow is considered.

On its turn, gas-liquid flow may exhibit a variety of different flow patterns. Figure 1.1.1 shows the fundamentally different types of gas-liquid two-phase flow which may occur in a vertical pipe. In horizontal flow the same flow patterns may be encountered, supplemented

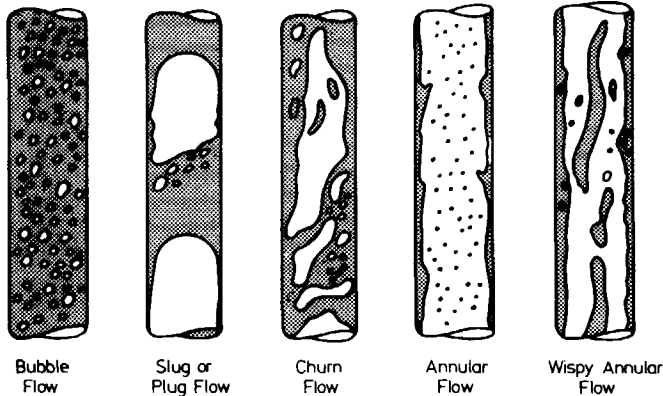


*Figure 1.1.1 Two-phase flow patterns in vertical gas-liquid flow.*

by stratified flow in which the buoyancy force plays a dominant part. For many industrial applications it is of crucial importance to know when and where a definite flow pattern may be expected and to understand the mechanisms which control the transition of one type of flow to the other. The results of experimental investigations of those transitions are usually presented in the form of flow-pattern maps. See figure 1.1.2, where the type of flow is given as a function of the momentum flux of the liquid (L) and the momentum flux of the gas (G).

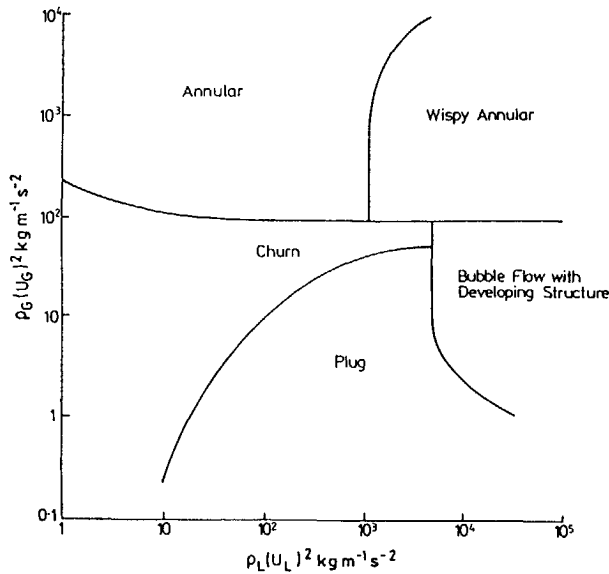


*Figure 1.1.2 Flow-pattern map according to Hewitt & Roberts (1969) for vertical two-phase upward flow*

Due to the complex nature of the different flow patterns and of the transitions between them a general theory of two-phase flow covering all states is still far from being realised. The present state of the art is that each state (annular, plug, bubble, etc.) is modelled separately. Many fundamental problems, however, remain in view of the fact that the major part of the models depends heavily on correlations obtained from experiments. This thesis focuses on the field of bubbly flow. It comprises the dynamics of small gas bubbles dispersed in a liquid.

Bubbly two-phase flows are encountered frequently in nature and in industry. Violent water movements due to waves rolling over and breaking at the beach may cause air being trapped in the water in the form of bubbles. Fast running mountain brooks may contain vapour bubbles as a result of cavitation. The pulsations of these bubbles producing sound in the audible range (approximately 1 kHz) provide an explanation for the appearance of so-called "singing" brooks. Geysers contain bubbly mixtures due to boiling processes.

Bubbly flows may also occur in cooling systems of nuclear power stations during a loss of coolant accident. A reliable simulation of such an accident is essential for the safe construction of those power stations. Bubble column reactors are widely used in the process industry and biotechnology due to their simplicity and the absence of moving parts. Among others, they are used for the purpose of absorption and stripping and in waste-water purification. We finally mention that cavitation around the propellers of ships produces large amounts of bubbles which may radiate sound waves due to pulsations. This effect will make the hull resonate, thus leading to unwanted vibrations and noises.

Many attempts have been made to describe bubbly flows mathematically, yet no generally accepted model exists for this type of flow. Roughly spoken, bubbly two-phase flow may be approached in two ways, viz., microscopically or macroscopically. In the microscopic formulation the path of each bubble through the liquid is governed by an equation of motion, which possibly takes into account the interactions with other bubbles. However, when one considers a volume of one cubic meter filled for 10 percent with bubbles having a diameter of 1 mm, one needs to calculate the paths of approximately  $2 \times 10^8$  bubbles. Clearly, that is not a practical approach. Macroscopically the behaviour of the gas bubbles is modelled more efficiently by introducing the gas fraction  $\alpha$ . Several techniques may now be applied to derive the equations of motion for groups of bubbles in a control volume (compare with the kinetic gas theory). Although this may seem quite straightforward the complex nature of bubbly two-phase flows has led to the existence of many different models with a variety of fundamental shortcomings. Supported by the review articles of Drew (1983) and van den Akker (1986) we discuss in this chapter the basic techniques of modelling, various sets of equations and some of the key difficulties. Pressure terms and interaction effects associated with the virtual mass of the gas bubbles receive some special attention since they have caused the severest problems. It is shown in section 1.6 how the application of variational techniques by Geurst ((1985a)(1985b)(1986)) solved those problems. The variational approach accordingly constitutes the basis of this thesis. For simplicity only one-dimensional instationary flows are considered in the present chapter.

## 1.2 Basic model

The basic model contains some simplifying assumptions which also apply to the other models discussed in this chapter. First, the liquid is assumed to be incompressible with a constant mass density  $\rho_\ell$ . Secondly, the flow is assumed to proceed under isothermal flow conditions with constant temperature  $T$ . The gas is considered to be perfect, with the gas pressure  $p_g$  determined by

$$p_g = \frac{RT}{M} \rho_g, \quad (1.2.1)$$

where  $\rho_g$  is the mass density of the pure gas,  $R$  denotes the gas constant and  $M$  the molecular weight of the gas. Viscous effects are neglected. When we introduce the relative densities  $\rho_1$  and  $\rho_2$  of the liquid and the gas by means of

$$\rho_1 = \rho_\ell (1 - \alpha), \quad (1.2.2)$$

$$\rho_2 = \rho_g \alpha \quad (1.2.3)$$

and denote the mass averaged velocities of the liquid and the gas by  $u_1$  and  $u_2$ , the equations expressing the conservation of mass become

$$\frac{\partial \rho_1}{\partial t} + \frac{\partial}{\partial x} (\rho_1 u_1) = 0 \quad (1.2.4)$$

and

$$\frac{\partial \rho_2}{\partial t} + \frac{\partial}{\partial x} (\rho_2 u_2) = 0. \quad (1.2.5)$$

A subscript "1" refers to the liquid, a subscript "2" to the gas. The mass conservation equations (1.2.4) and (1.2.5) are generally accepted and form no point of discussion, unless boiling effects are taken into account. However, boiling effects are not considered in this thesis. The gas fraction  $\alpha$ , already mentioned in the previous section, describes the percentage of gas present in a volume element. Quite often it is referred to as void fraction.

The basic model is based on the assumption that the Euler equations known from one-phase fluid dynamics hold for the liquid as well as for the gas. The equations of motion for the



liquid and the gas are accordingly written

$$\left[ \frac{\partial}{\partial t} + u_1 \frac{\partial}{\partial x} \right] u_1 = -\frac{1}{\rho_l} \frac{\partial p_l}{\partial x}, \quad (1.2.6)$$

$$\left[ \frac{\partial}{\partial t} + u_2 \frac{\partial}{\partial x} \right] u_2 = -\frac{1}{\rho_g} \frac{\partial p_g}{\partial x}. \quad (1.2.7)$$

It is further assumed that there is a local balance between the liquid pressure  $p_l$  and the gas pressure  $p_g$  inside the control volume :  $p_l = p_g$ . Gravity and drag forces may be added to the right hand sides of (1.2.6) and (1.2.7). Equations (1.2.4) to (1.2.7) constitute the basic model, complemented by (1.2.1) and the equal pressure assumption. For practical applications it is the most frequently used model (see Drew 1983) and is applied to the complete variety of gas-liquid flows displayed in figure 1.1.1 despite the absence of terms describing the actual structure of the flow. In the case of bubbly flows the flow structure is sometimes accounted for by adding virtual-mass forces on the right hand sides of the equations of motion (1.2.6) and (1.2.7). In general those interaction terms are incorporated in an incorrect and ad hoc fashion. Some modifications of the basic model may be found in the review article by Stewart & Wendroff (1984). For the purpose of comparison with other models we also give the equations of motion in the form

$$\frac{\partial}{\partial t} (\rho_1 u_1) + \frac{\partial}{\partial x} (\rho_1 u_1^2) = -(1 - \alpha) \frac{\partial p_g}{\partial x}, \quad (1.2.8)$$

$$\frac{\partial}{\partial t} (\rho_2 u_2) + \frac{\partial}{\partial x} (\rho_2 u_2^2) = -\alpha \frac{\partial p_g}{\partial x}, \quad (1.2.9)$$

where the mass conservation equations (1.2.4), (1.2.5) and the equal pressure assumption have been used.

Obviously, a constant uniform flow is an exact solution of the basic model. A linear stability analysis reveals, however, that this solution is linearly unstable. Since (1.2.4)–(1.2.7) form a homogeneous set of partial differential equations the basic model possesses complex characteristics as well and is ill-posed in the sense of Hadamard (see Stewart & Wendroff 1984). The fast modes corresponding to acoustic waves are characterised by real roots. The slow modes, however, are associated with complex conjugate roots. The imaginary part becomes zero when the gas bubbles travel with the liquid velocity ( $u_2 = u_1$ ). For that reason

some scientists believe that the basic model only describes stratified flows, where a Kelvin–Helmholz instability appears when  $u_2 \neq u_1$ . On the other hand, Ransom & Hicks (1984) emphasize that hydrodynamical instabilities should evolve from models with real characteristics. Therefore, they present a hyperbolic two–pressure model for stratified flows. In the case of bubbly flows the majority of the scientists also believes that reliable predictions should come from hyperbolic models. Moreover, in practice (slow) concentration waves (see Chapter III), or void–fraction waves, are observed which necessarily have to be connected to real roots of the dispersion equation (or characteristic polynomial). Therefore, on mathematical as well as on physical grounds the basic model should be rejected as a model for bubbly two–phase flow. That this has not been done appears from the fact that popular computer codes like PHOENIX (–84) and TRAC still make use of the basic model (see Assimacopoulos 1986 and Stewart & Wendroff 1984, respectively). Instabilities are suppressed by initially taking  $u_2 = u_1$ , by adding large drag forces and by increasing the numerical viscosity. Computations on the acoustic time scale may be performed without severe problems since the complex roots are associated with the slowly propagating concentration waves.

A different way of dealing with the complex characteristics is making them real by modifying the pressure terms at the right hand side of (1.2.8) and (1.2.9). This may be achieved by replacing those terms by  $-\partial/\partial x((1-\alpha)p_g)$  and  $-\partial/\partial x(\alpha p_g)$ , respectively. Naturally, this is also an ad hoc solution of the problem since there are no physical grounds for making that modification. In fact, it is generally accepted that the pressure terms related to the gas pressure  $p_g$  should appear in the form presented by equations (1.2.8) and (1.2.9) (see van den Akker 1986). Nevertheless, quite recently a thesis has been written on the numerical simulation of two–phase flows based on the above mentioned erroneous form of the pressure terms (Ranaivoson 1988).

We may conclude that the basic model should not be used for the prediction of transient bubbly two–phase flows in cases, where the difference velocity between the two phases does not vanish. Interaction terms accounting for the virtual mass of the gas bubbles should be included. However, those terms are too complicated for being postulated, as will appear in the subsequent sections of this chapter. Therefore, a systematic approach is required to overcome those difficulties and to avoid the appearance of complex characteristics. At the same time it may be investigated in which way the pressure terms should be included in the equations of motion.

### 1.3 Momentum balances

From one-phase fluid dynamics it is known that the Navier-Stokes equations for an isothermal fluid may be derived by considering the momentum transport in a volume element  $\Delta x \Delta y \Delta z$  for a short period  $\Delta t$  and taking the limit  $\Delta x, \Delta y, \Delta z, \Delta t \rightarrow 0$ . The Euler equations follow by neglecting the viscous terms. The same procedure is discussed by van den Akker (1986) but now applied to each phase separately in a dispersed two-phase flow. The exchange of momentum between the bubbles and the liquid gives rise to an interaction term which appears in the form of an integral over the surfaces of the bubbles. That term is interpreted as an added-mass force. When Reynolds stress terms and shear stress terms are neglected, the basic model is recovered with an extra term on the right hand side of equations (1.2.8) and (1.2.9), viz., the added-mass force. The pressure terms follow in a systematic way. The added-mass force should solve the occurrence of complex characteristics but to achieve this it is necessary to express the surface integral in terms of the flow variables  $\rho_1, \rho_2, \alpha$  and the difference velocity  $w = u_2 - u_1$ . This is an additional exercise which has to be performed; the momentum balances do not yield such an expression. Therefore, it still requires a lot of effort to complete the model resulting from momentum balances. Assumptions have to be made concerning the form of the added-mass force and since it appears to be a force of a complex nature errors easily slip in. Nevertheless, the equations of motion now have a solid foundation.

### 1.4 Averaging methods

Averaging methods start with assuming that the different phases may be described as a continuum. Each phase satisfies an equation expressing the conservation of mass, viz.,

$$\frac{\partial \rho}{\partial t} + \nabla \cdot \rho \mathbf{v} = 0 \quad (1.4.1)$$

and an equation expressing the conservation of linear momentum:

$$\frac{\partial \rho \mathbf{v}}{\partial t} + \nabla \cdot \rho \mathbf{v} \mathbf{v} = \nabla \cdot \mathbf{T} + \rho \mathbf{f}, \quad (1.4.2)$$

where  $\mathbf{T}$  is the stress tensor and  $\mathbf{f}$  the body force density. Each phase has its own density  $\rho$  and its own velocity field  $\mathbf{v}$ . At the interface separating the two phases conservation of mass and linear momentum appear in the form of jump conditions. In order to obtain equations of

motion that do not contain every detail of the flow averaging processes are applied. Several averaging methods are available: time averages, space averages, weighted space averages, combinations of averages and ensemble averages. A more or less complete account of the literature concerning averaging methods is given by Drew (1983). Following Drew (1983), we choose the weighted space average to elucidate some of the key aspects of averaging methods.

A phase function  $X_k(\mathbf{x}, t)$ , ( $k = 1, 2$ ), is defined by

$$X_k(\mathbf{x}, t) = \begin{cases} 1 & \text{if } \mathbf{x} \text{ is in phase } k \text{ at time } t \\ 0 & \text{otherwise.} \end{cases} \quad (1.4.3)$$

We recall that a subscript "1" refers to the liquid, a subscript "2" to the gas. The equations of motion (1.4.1) and (1.4.2) which hold for the liquid and the gas are now multiplied by  $X_1(\mathbf{x}, t)$  and  $X_2(\mathbf{x}, t)$ , respectively, and the result is averaged over a control volume. After defining averaged variables, omitting the symbols denoting space averages and assuming a one-dimensional flow, we arrive at the mass conservation equations (1.2.4) and (1.2.5) supplemented by the equations of motion

$$\frac{\partial}{\partial t} (\rho_1 u_1) + \frac{\partial}{\partial x} (\rho_1 u_1^2) = - (1 - \alpha) \frac{\partial p_g}{\partial x} + M_1^d, \quad (1.4.4)$$

$$\frac{\partial}{\partial t} (\rho_2 u_2) + \frac{\partial}{\partial x} (\rho_2 u_2^2) = - \alpha \frac{\partial p_g}{\partial x} + M_2^d. \quad (1.4.5)$$

Shear stress has been neglected, the equal pressure assumption at the interface has been made and it is assumed that there is no transfer of mass across the interface.  $M_k^d$ , ( $k=1, 2$ ), denote the interfacial force densities. From the jump conditions it follows that

$$M_1^d + M_2^d = 0. \quad (1.4.6)$$

Again we recognize the basic model and notice that the pressure terms appear in the same form as they follow from momentum balances. An expression for  $M_1^d$  (or  $M_2^d$ ) is required to complete the model.

The structure of the flow (bubble, slug, etc.) is not yet included in the model in an explicit way. An expression for  $M_1^d$  has to be assumed to describe the interaction between the liquid and the gas phase. In the case of bubbly flow Drew (1983) postulates a certain expression for  $M_1^d$  which still contains a set of undetermined parameters. By demanding that the interfacial force density should be objective, or material frame indifferent, a complete expression for  $M_1^d$  is obtained. For one-dimensional flow it is given by

$$M_1^d = \frac{\partial}{\partial t} \{C_{vm} \rho_\ell \alpha (u_2 - u_1)\} + \frac{\partial}{\partial x} \{C_{vm} \rho_\ell \alpha u_2(u_2 - u_1)\}. \quad (1.4.7)$$

Drag forces are not taken into account. The constant  $C_{vm}$  is referred to as virtual-volume density by Drew (1983). Here, we will call it the virtual-mass coefficient<sup>†</sup>). The virtual-mass coefficient of a spherical bubble is equal to 1/2 and we may therefore take  $C_{vm} = 1/2$ . The virtual-mass density of a dispersion of bubbles is expressed by  $C_{vm} \rho_\ell \alpha$ , a term which appears in expression (1.4.7) for  $M_1^d$ . Clearly, bubble interactions are not taken into account, since terms  $O(\alpha^2)$  are not present. A very essential aspect of expression (1.4.7) is that virtual-mass effects do not only appear as a flux in the  $\partial/\partial x$  term but also take part in the time derivative. This may be understood when one realizes that an accelerating bubble induces an acceleration of some part of the liquid as well.

The influence of the interfacial force density  $M_1^d$  on the complex characteristics of the basic model has been investigated by Lahey et al. (1980). For  $C_{vm} = 1/2$  the characteristics are still complex, unless somewhat non-physical assumptions are made. Nevertheless, virtual mass has a stabilizing effect in the sense that the growth rate of the unstable modes decreases. Drew (1983) concludes that virtual mass does not seem to be the total answer to the ill-posed nature of the model. However, it must be realized that  $M_1^d$  has been postulated

---

†) *The virtual mass of a body consists of the sum of its actual mass and the added mass. The added mass is associated with the kinetic energy of the liquid due to the relative motion of the body. The definition of added mass is given by Milne-Thomson (1965, p. 247). Due to the fact that the mass density of the gas is much smaller than the mass density of the liquid, the term virtual mass is often used in the literature of bubbly two-phase flows while added mass is understood.*

and that bubble interaction effects are not taken into account. In section 1.6 it is demonstrated that those two aspects indeed play an important role.

Space averages, time averages and composite averages are discussed by Delhaye (1981) and by Bouré & Delhaye (1982), among others. A complete account of those techniques lies beyond the scope of the present work. We therefore focus on some of the important consequences resulting from the application of those methods. Averaging methods lead to averages of products. To write the averaged equations in the form of a two-fluid model like the basic model, averages of products have to be split in products of averages. When  $\langle \cdot \rangle$  denotes an averaging operator it is assumed that  $\langle fg \rangle = \langle f \rangle \langle g \rangle$  holds. In doing so, one possibly introduces a supplementary dependent variable and as a consequence the number of variables and equations are not in balance. An extra equation is required to close the model : a so-called closure law. The closure problem is discussed by Bouré (1987). A similar difficulty is encountered in the theory of turbulence. A closure relation is not always needed, as is demonstrated by Delhaye (1981) who simplifies the composite-averaged equations to the basic model with on the right hand side of the equations of motion (1.2.8) and (1.2.9) some additional interface integrals. At the interface constitutive laws are required which describe the momentum transfer between the liquid and the gas. Ishii (1987) discusses the interfacial transfer terms and emphasizes that they are among the most essential factors in the modelling of two-phase flows. We conclude that the averaging methods discussed above require questionable assumptions and still leave us with some complex difficulties.

Ensemble averages are applied by Biesheuvel & van Wijngaarden (1984). By assuming that the bubbly mixture constitutes a statistically homogeneous medium the ensemble averages become equivalent to volume averages. As a consequence the techniques developed in a number of papers by Batchelor may be used (see Biesheuvel & van Wijngaarden 1984). The ensemble-averaged stress tensor and the ensemble-averaged momentum-flux tensor are defined for the mixture and are determined by assuming a potential flow around a test bubble. The potential solution depends on the liquid velocity at infinity  $U_0$ , which is taken equal to the total volume flux:

$$U_0 = (1-\alpha) u_1 + \alpha u_2. \quad (1.4.8)$$

The equation of motion for the ensemble of the two phases follows by equating the rate of change of momentum to the divergence of the stress tensor. The equation of motion for the gas is derived by averaging the hydrodynamic force exerted on the bubbles by the surrounding fluid and using the fact that the net force on the approximately massless

bubbles must vanish. The form of the last equation presented by Biesheuvel & van Wijngaarden (1984) is incorrect since it contains no spatial derivatives. As a result, the equation of motion for the gas phase is not invariant with respect to a Galilean transformation as pointed out by Geurst (1986). Later, Biesheuvel & van Wijngaarden modified the equation by replacing the time derivatives by convective derivatives with respect to the gas velocity. The modified equation may be inferred from Kok (1989, relation (1.4)). The equation of motion for the mixture and the equation of motion for the gas phase (after correction of a typing error) read

$$\frac{\partial u_1}{\partial t} + u_1 \frac{\partial u_1}{\partial x} = -\frac{1}{\rho_1} \frac{\partial p_g}{\partial x}, \quad (1.4.9)$$

$$\left[ \frac{\partial}{\partial t} + u_2 \frac{\partial}{\partial x} \right] \left\{ \frac{1}{2} \tau (u_2 - U_0) \right\} = \tau \left[ \frac{\partial}{\partial t} + u_2 \frac{\partial}{\partial x} \right] U_0. \quad (1.4.10)$$

The equal pressure assumption has been made, drag and gravity are neglected and terms related to pulsations of the bubbles are omitted. The inertia of the gas bubbles has been neglected as well. The bubble volume  $\tau$  is related to the gas density  $\rho_g$  by means of  $\rho_g \tau = \text{constant}$ , which expresses that only bubbles of equal mass are considered. The mass conservation equations (1.2.4) and (1.2.5) complete the model, which only holds for dilute dispersions of bubbles in liquid. The characteristics of the model are claimed to be real. Two roots are associated with pressure waves and two roots, both equal to the gas velocity  $u_2$ , are identified with a concentration wave. The presentation by Kok (1989) therefore suggests that ensemble averaging might lead to a hyperbolic model.

### 1.5 Three-fluid models

Three-fluid models have been developed by Wallis (1978), by Cook & Harlow (1984) and by Kowe et al. (1988). Wallis constructed a one-dimensional model while Cook & Harlow (1984) derived in an equivalent way, but independently, the three-dimensional form. We discuss the Cook-Harlow model as it is presented by Wallis (1987). For completeness we mention that Wallis (1987) also makes a comparison with models developed by Pauchon & Banerjee (1986), by Drew & Wood (1985), by Lhuillier (1985), by Nigmatulin (1979) and by Geurst ((1985a)(1985b)(1986)).

A unit cell is considered which contains liquid and gas. The cell is divided into three parts: the fraction occupied by the gas ( $\alpha$ ), the fraction of liquid entrained with the gas ( $1-\alpha-1/\beta$ ) and the unentrained fraction of the liquid ( $1/\beta$ ). The unentrained liquid velocity  $u'_1$  is related to the liquid velocity  $u_1$  and the gas velocity  $u_2$  by means of

$$u'_1 = u_1 - D w, \quad (1.5.1)$$

where  $w$  is the difference velocity  $w = u_2 - u_1$ .  $D$  denotes a quantity called the *exertia* given by

$$D = (1 - \alpha) \beta - 1. \quad (1.5.2)$$

For a random suspension of spheres (1.5.2) reduces to  $D = (1/2)\alpha$ . Note that the entrained liquid travels with the velocity of the gas bubbles  $u_2$ . That is the reason why only two velocity fields are required to describe the flow. It is shown in a straightforward way that the unentrained fluid satisfies an equation of motion of the form known from single phase flows:

$$\rho_l \left[ \frac{\partial u'_1}{\partial t} + u'_1 \frac{\partial u'_1}{\partial x} \right] = - \frac{\partial p}{\partial x}, \quad (1.5.3)$$

where  $p$  denotes the *hydrodynamic* pressure. The equation of motion for the combined phases is derived by making a momentum balance on the entire contents of a unit cell. The construction of the momentum-flux tensor for the mixture requires quite some effort (see Wallis 1987). We therefore simply give the equation of motion for the mixture as

$$\rho_1 \left[ \frac{\partial u_1}{\partial t} + u_1 \frac{\partial u_1}{\partial x} + Z \right] + \rho_2 \left[ \frac{\partial u_2}{\partial t} + u_2 \frac{\partial u_2}{\partial x} \right] = - \frac{\partial p}{\partial x}, \quad (1.5.4)$$

with

$$Z = \frac{1}{\rho_1} \frac{\partial}{\partial x} \{ \rho_1 D w^2 \}. \quad (1.5.5)$$

The equations of motion for the liquid and the gas are obtained from (1.5.3) and (1.5.4) by applying (1.5.1) and using the mass conservation equations (1.2.4), (1.2.5) and an additional equation expressing the conservation of the entrained part of the liquid. They read, respectively,



$$\begin{aligned} \frac{\partial u_1}{\partial t} + u_1 \frac{\partial u_1}{\partial x} + Z + D \left\{ \frac{\partial u_1}{\partial t} + u_1 \frac{\partial u_1}{\partial x} + Z - \frac{\partial u_2}{\partial t} - u_2 \frac{\partial u_2}{\partial x} \right\} = \\ = -\frac{1}{\rho_\ell} \frac{\partial p}{\partial x} \end{aligned} \quad (1.5.6)$$

and

$$\begin{aligned} \frac{\partial u_2}{\partial t} + u_2 \frac{\partial u_2}{\partial x} - D \frac{\rho_1}{\rho_2} \left\{ \frac{\partial u_1}{\partial t} + u_1 \frac{\partial u_1}{\partial x} + Z - \frac{\partial u_2}{\partial t} - u_2 \frac{\partial u_2}{\partial x} \right\} = \\ = -\frac{1}{\rho_g} \frac{\partial p}{\partial x} \end{aligned} \quad (1.5.7)$$

The appropriate choice for the hydrodynamic pressure seems to be the volumetric average pressure

$$p = (1-\alpha) p_\ell + \alpha p_g, \quad (1.5.8)$$

with the hydrodynamic pressure jump between the liquid and the gas taken equal to

$$p_\ell - p_g = \frac{1}{2} \rho_1 w^2 \frac{dD}{d\alpha}. \quad (1.5.9)$$

The term on the right hand side of (1.5.9) accounts for the Bernoullian effects which contribute to the pressure  $p$  in the case of a non-vanishing difference velocity  $w$ .

The mutual nature of the added-mass force is clearly demonstrated by (1.5.6) and (1.5.7): multiplying (1.5.6) by  $\rho_1$ , (1.5.7) by  $\rho_2$  and adding the results cancels the terms multiplied by the inertia  $D$ . In addition it is seen that the interaction terms contain convective derivatives. By taking  $D \equiv 0$  the basic model is recovered. Whether the introduction of added-mass terms suppresses the appearance of complex characteristics or not is not discussed by Wallis (1987).

We conclude that three-fluid techniques form a systematic approach to the modelling of two-phase flows. Added-mass forces are included containing time as well as space derivatives and a hydrodynamic pressure is introduced which is not necessarily equal to the gas pressure. However, the construction of the momentum-flux tensor for the mixture and the definition of the hydrodynamic pressure still require some detailed considerations on the microscopic level. Whether the set of equations of the Cook-Harlow model is hyperbolic or

not has not yet been investigated, to our knowledge.

## 1.6 Variational methods

The previous sections demonstrate that several mathematical techniques and physical models have been used for the derivation of macroscopic two-phase flow equations. As a result of the complicated nature of that type of flow many models now exist which are essentially different. The previous sections only present a limited selection. The present state is that there is no agreement about the definition of the hydrodynamic pressure and the way virtual-mass terms should be incorporated. Clearly, this situation leads to contradictory conclusions: while Ramshaw & Trapp (1978) and Lahey et al. (1980) state that neglecting virtual mass will lead to complex characteristics, Pauchon & Banerjee (1988) conclude that neglecting their virtual-mass force tends to keep the characteristics real. In view of those major discrepancies the modelling of bubbly two-phase flow requires a clear and systematic approach. Variational methods fulfil those requirements, as is demonstrated in the present section. A great advantage of the application of variational methods is that for an inviscid description of bubbly flow it suffices to define the kinetic energy density and the free energy density on the *macroscopic* level. Interaction effects may be included and will appear in a consistent way in the equations of motion by performing the independent variations. Subsequently, Noether's first invariance theorem may be applied to derive the equations expressing the conservation of linear momentum and the conservation of energy.

Bedford & Drumheller (1978) choose for a Lagrangian setting and write Hamilton's extended variational principle as

$$\int_{t_1}^{t_2} (\delta T - \delta U + \delta W) dt = 0, \quad (1.6.1)$$

where  $T$  and  $U$  are the kinetic and potential energies and  $\delta W$  denotes the virtual work due to the forces not represented by a potential. Their theory is kept quite general and applies for mixtures of an arbitrary amount of constituents which remain physically separate. In the case of bubbly liquid-gas mixtures they demonstrate how pulsations of the bubbles may be included in a consistent way by means of the kinetic energy  $T$ . Interaction effects are attributed to the virtual work  $\delta W$ , which should be associated with unrecoverable energy (see Drew 1983). Virtual-mass effects are not incorporated in that way.

It was first shown by Geurst ((1985a)(1985b)(1986)) that interaction effects associated with the virtual mass of the gas bubbles could be accounted for in a systematic way by means of the kinetic energy density of the mixture. That crucial step leads to a consistent theory, free of any ad hoc assumptions, and to the solution of several of the existing problems. Since Geurst's approach forms the basis of the present thesis, it is treated here in more detail.

Geurst (1985a) starts from a generalised form of Hamilton's variational principle in an Eulerian setting by writing

$$\delta \int_{t_1}^{t_2} dt \int_{x_1}^{x_2} dx L = 0 . \quad (1.6.2)$$

During the variations the constraints expressing the conservation of mass of the two phases given by (1.2.4) and (1.2.5) should remain fulfilled. The Lagrangian energy density  $L$  is defined by

$$L = K - F , \quad (1.6.3)$$

where  $K$  denotes the kinetic energy density and  $F$  the free energy density. The kinetic energy density is taken equal to

$$K = \frac{1}{2} \rho_1 u_1^2 + \frac{1}{2} \rho_2 u_2^2 + \frac{1}{2} \rho_\ell m(\alpha) (u_2 - u_1)^2 . \quad (1.6.4)$$

It consists of three parts: the first two terms account for the kinetic energies of the liquid and the gas, the last term includes the kinetic energy associated with the virtual mass of the gas bubbles. For spherical bubbles at low void fraction  $\alpha$  the virtual-mass coefficient  $m(\alpha)$  takes the form  $m(\alpha) = (1/2)\alpha + O(\alpha^2)$ . Under isothermal flow conditions the thermodynamics, contained in  $F$ , is completely characterised by the relations

$$dF = \mu_1 d\rho_1 + \mu_2 d\rho_2 \quad (1.6.5)$$

and

$$d\mu_1 = \frac{dp_g}{\rho_\ell} , \quad (1.6.6)$$

$$d\mu_2 = \frac{dp_g}{\rho_g}, \quad (1.6.7)$$

where  $\mu_1$  and  $\mu_2$  denote the thermodynamic potentials.

Introducing Lagrange multipliers  $\varphi_1$  and  $\varphi_2$  to account for the constraints (1.2.4) and (1.2.5) we arrive at the equivalent variational principle

$$\delta \int_{t_1}^{t_2} dt \int_{x_1}^{x_2} dx \hat{L} = 0, \quad (1.6.8)$$

with the modified Lagrangian density given by

$$\hat{L} = L + \varphi_1 \left[ \frac{\partial \rho_1}{\partial t} + \frac{\partial}{\partial x} (\rho_1 u_1) \right] + \varphi_2 \left[ \frac{\partial \rho_2}{\partial t} + \frac{\partial}{\partial x} (\rho_2 u_2) \right]. \quad (1.6.9)$$

Partial integration of (1.6.8) yields

$$\delta \int_{t_1}^{t_2} dt \int_{x_1}^{x_2} dx L^* = 0, \quad (1.6.10)$$

where  $L^*$  reads

$$L^* = L - \rho_1 \left[ \frac{\partial \varphi_1}{\partial t} + u_1 \frac{\partial \varphi_1}{\partial x} \right] - \rho_2 \left[ \frac{\partial \varphi_2}{\partial t} + u_2 \frac{\partial \varphi_2}{\partial x} \right]. \quad (1.6.11)$$

The Euler–Lagrange equations follow quite simply from (1.6.10) by performing the independent variations of the four variables  $\rho_1, \rho_2, u_1, u_2$ :

$$\delta \rho_1: \frac{1}{2} u_1^2 - \frac{1}{2} m'(\alpha)(u_2 - u_1)^2 - \mu_1 - \frac{\partial \varphi_1}{\partial t} - u_1 \frac{\partial \varphi_1}{\partial x} = 0, \quad (1.6.12)$$

$$\delta \rho_2: \frac{1}{2} u_2^2 - \mu_2 - \frac{\partial \varphi_2}{\partial t} - u_2 \frac{\partial \varphi_2}{\partial x} = 0, \quad (1.6.13)$$

$$\delta u_1: \rho_1 u_1 - \rho_1 m(\alpha)(u_2 - u_1) - \rho_1 \frac{\partial \varphi_1}{\partial x} = 0, \quad (1.6.14)$$

$$\delta u_2: \rho_2 u_2 + \rho_l m(\alpha)(u_2 - u_1) - \rho_2 \frac{\partial \varphi_2}{\partial x} = 0, \quad (1.6.15)$$

where  $m'(\alpha)$  denotes  $(d/d\alpha)m(\alpha)$ . The equations of motion are derived by eliminating the Lagrange multipliers. The equation of motion for the liquid reads

$$\left[ \frac{\partial}{\partial t} + u_1 \frac{\partial}{\partial x} \right] \left\{ u_1 - \frac{\rho_l m(\alpha)}{\rho_1} (u_2 - u_1) \right\} - \frac{\rho_l m(\alpha)}{\rho_1} (u_2 - u_1) \frac{\partial u_1}{\partial x} + \frac{\partial}{\partial x} \left\{ \mu_1 + \frac{1}{2} m'(\alpha)(u_2 - u_1)^2 \right\} = 0. \quad (1.6.16)$$

For the gas it is given by

$$\left[ \frac{\partial}{\partial t} + u_2 \frac{\partial}{\partial x} \right] \left\{ u_2 + \frac{\rho_l m(\alpha)}{\rho_2} (u_2 - u_1) \right\} + \frac{\rho_l m(\alpha)}{\rho_2} (u_2 - u_1) \frac{\partial u_2}{\partial x} + \frac{\partial \mu_2}{\partial x} = 0. \quad (1.6.17)$$

The application of Noether's first invariance theorem (see Geurst 1985a and Logan 1977) yields the equation expressing the conservation of energy

$$\frac{\partial H}{\partial t} + \frac{\partial Q}{\partial x} = 0 \quad (1.6.18)$$

and the equation expressing the conservation of linear momentum

$$\frac{\partial P}{\partial t} + \frac{\partial \Pi}{\partial x} = 0. \quad (1.6.19)$$

The energy density  $H$  and the energy flux  $Q$  are given by

$$H = K + F, \quad (1.6.20)$$

$$\begin{aligned}
 Q = & \rho_1 u_1 \left\{ \frac{1}{2} u_1^2 - \frac{\rho_\ell m(\alpha)}{\rho_1} u_1 (u_2 - u_1) + \mu_1 + \frac{1}{2} m'(\alpha) (u_2 - u_1)^2 \right\} + \\
 & + \rho_2 u_2 \left\{ \frac{1}{2} u_2^2 + \frac{\rho_\ell m(\alpha)}{\rho_2} u_2 (u_2 - u_1) + \mu_2 \right\}, \quad (1.6.21)
 \end{aligned}$$

while the momentum density  $P$  and the momentum flux  $\Pi$  are determined by

$$P = \rho_1 u_1 + \rho_2 u_2, \quad (1.6.22)$$

$$\begin{aligned}
 \Pi = & \rho_1 u_1^2 + \rho_2 u_2^2 + \rho_\ell m(\alpha) (u_2 - u_1)^2 + \\
 & + p_g + \frac{1}{2} \rho_\ell \{ m(\alpha) + (1-\alpha) m'(\alpha) \} (u_2 - u_1)^2. \quad (1.6.23)
 \end{aligned}$$

In a three-dimensional formulation the last two terms of the momentum flux  $\Pi$  are multiplied by the unit isotropic tensor. That suggests the introduction of the hydrodynamic pressure  $p$  according to

$$p = p_g + \frac{1}{2} \rho_\ell \{ m(\alpha) + (1-\alpha) m'(\alpha) \} (u_2 - u_1)^2. \quad (1.6.24)$$

At the same time it is shown that

$$L^* = p. \quad (1.6.25)$$

The variational principle (1.6.10) based on  $L^*$  therefore constitutes a generalisation of Bateman's variational principle known from classical one-phase fluid dynamics (see Bateman 1959, chapter II).

When the equations for the conservation of mass (1.2.4) and (1.2.5) and the equations of motion (1.6.16) and (1.6.17) are subjected to a linear stability analysis, it follows that marginal stability is obtained only when the virtual-mass coefficient  $m(\alpha)$  satisfies two differential equations:

$$1 + 3 \frac{m(\alpha)}{1-\alpha} + 2 m'(\alpha) + \frac{1}{2} (1-\alpha) m''(\alpha) = 0 \quad (1.6.26)$$

and

$$1 - \frac{1-3\alpha}{\alpha^2(1-\alpha)} m(\alpha) + \frac{m'(\alpha)}{\alpha} = 0 . \quad (1.6.27)$$

Equations (1.6.26) and (1.6.27) possess the *common* solution

$$m(\alpha) = \frac{1}{2} \alpha (1 - \alpha) ( \hat{m} - (\hat{m}+2) \alpha ) , \quad (1.6.28)$$

which reduces to  $m(\alpha) = (1/2) \alpha + O(\alpha^2)$  for dilute dispersions of spherical gas bubbles ( $\hat{m}=1$ ). The coinciding roots at marginal stability are equal to the gas velocity  $u_2$  and are associated with concentration waves. The acoustic modes are real as well (see Geurst 1985a). Since for a homogeneous set of equations the characteristic roots are equal to the roots of the dispersion equation, the equations presented by Geurst (1985a) constitute a model with real characteristics, provided  $m(\alpha)$  is given by (1.6.28). At the critical void fraction  $\alpha_c = \hat{m}/(\hat{m}+2)$  the virtual-mass coefficient  $m(\alpha)$  vanishes. Higher void fractions would yield a negative contribution to the kinetic energy density  $K$  which on physical grounds can not be accepted. It is therefore concluded that bubbly flow ceases to exist at the critical void fraction and that a transition to a different flow pattern like slug flow must take place. Recent measurements by Matuszkiewicz et al. (1987) report bubble-slug flow pattern transitions at void fractions varying from .3 to .45.

We conclude that variational techniques as applied by Geurst ((1985a)(1985b)(1986)) include interaction effects and pressure terms in a systematic way. Free from any dubious assumptions the theory allows a clear physical interpretation. A comparison with the other methods is made in the following section, thus highlighting the advantages of the application of variational principles.

### 1.7 Comparison of various models

A comparison of Geurst's method and equations with the other methods and equations reviewed in this chapter leads to some interesting conclusions.

The basic model (section 1.2) is recovered from Geurst's equations of motion (1.6.16) and (1.6.17) by taking  $m(\alpha) \equiv 0$  and using relations (1.6.6) and (1.6.7) for the thermodynamic potentials. After rewriting the equations the pressure terms appear as in (1.2.8) and (1.2.9).

We may also conclude that neglecting the virtual mass of the gas bubbles leads to complex characteristics.

Momentum balances (section 1.3) yield similar pressure terms related to  $p_g$  but require a postulated added-mass force. That important force does not have to be postulated when variational techniques are used, which is a great advantage since the force is of a complicated nature.

Averaging techniques (section 1.4) require a postulated virtual-mass force as well (Drew 1983, Delhaye 1981). Geurst (1986) rewrote the equations and derived a three-dimensional form of the interaction force. In a one-dimensional theory it reduces to

$$\begin{aligned} \tilde{M}_1^d = \frac{\partial}{\partial t} \{ \rho_\ell m(\alpha) (u_2 - u_1) \} + \frac{\partial}{\partial x} \{ \rho_\ell m(\alpha) u_2 (u_2 - u_1) \} + \\ + \rho_\ell m(\alpha) (u_2 - u_1) \frac{\partial u_2}{\partial x} . \end{aligned} \quad (1.7.1)$$

For small values of the void fraction  $\alpha$  the first two terms of equation (1.7.1) become equal to the interaction force  $M_1^d$  (equation (1.4.7)) postulated by Drew (1983) ( $\hat{m}=1$ ,  $C_{vm}=1/2$ ).

A three-dimensional comparison demonstrates that Drew's interaction force contains a term which is not comprised by Geurst's equations. Nevertheless, both forces appear to be objective. Geurst's version of (1.4.4) (see Geurst 1986, equation (5.7)) also shows that some momentum fluxes associated with virtual-mass effects are missing in (1.4.4). Those discrepancies eventually lead to the occurrence of complex characteristics in the model treated by Drew. Pressure terms related to  $p_g$  are included in a similar way. The hydrodynamic pressure is not discussed by Drew. For further details we refer to the comparison made by Geurst (1986).

In relation to the equations presented by Delhaye (1981) we mention that closure laws are closely connected with averaging methods. They are not encountered when variational techniques are used. Constitutive laws (Ishii 1987) are not required either.

The equations presented by Biesheuvel & van Wijngaarden (1984) (section 1.4) clearly have some aspects in common with Geurst's equations. When the equal pressure assumption is not made, Biesheuvel & van Wijngaarden (1984) show that equation (1.4.9) is written



$$\frac{\partial \rho_l u_1}{\partial t} + \frac{\partial}{\partial x} \left\{ \rho_l u_1^2 + \frac{1}{2} \rho_\ell \alpha (u_2 - U_0)^2 + \langle p \rangle \right\} = 0, \quad (1.7.2)$$

where the bulk pressure  $\langle p \rangle$  is given by

$$\langle p \rangle = p_g + \frac{1}{4} \rho_\ell (u_2 - U_0)^2. \quad (1.7.3)$$

These results may be obtained from Geurst's equations (1.6.19) and (1.6.22)–(1.6.24) by neglecting  $\rho_2$ , by considering small void fractions  $\alpha$  and by replacing  $u_1$  by  $U_0$ , which become equal in the limit  $\alpha \rightarrow 0$  according to (1.4.8). Geurst (1986) showed that for small void fractions and spherical bubbles of a constant radius the equation of motion for the gas (1.6.17) simplifies to

$$\left[ \frac{\partial}{\partial t} + u_2 \frac{\partial}{\partial x} \right] u_2 = 3 \left[ \frac{\partial}{\partial t} + u_1 \frac{\partial}{\partial x} \right] u_1, \quad (1.7.4)$$

which expresses that the acceleration of the bubbles equals three times the acceleration of the liquid: a result which was already known to hold for one spherical bubble. We may therefore conclude that Geurst's equations contain the microscopic behaviour of one bubble in the correct way, despite the fact that the equations are derived from macroscopic principles. Equation (1.4.10) of Biesheuvel & van Wijngaarden reduces to an equation which is similar to (1.7.4) when small void fractions  $\alpha$  are considered. In their case *both* convective derivatives occur with respect to the gas velocity  $u_2$ . This does not seem to be correct and might be a result of the fact that the interaction of the bubbles with the surrounding liquid is analysed in a frame of reference moving with the volume flux  $U_0$ . In the theory of sedimentation it has become customary to work in such a frame, as is demonstrated by the new theory for fluidized beds and sedimentation proposed by Batchelor (1988). Since the work of Biesheuvel & van Wijngaarden is closely related to Batchelor's work, they have chosen for the same frame of reference. Virtual-mass effects form a problem for Batchelor (1988) as well: in a somewhat loosely way a simple form for the mean fluid force on the particles is proposed which is not complete.

Wallis (1987) compared the three-fluid model of Cook & Harlow (section 1.5) with Geurst's equations. For small void fractions the kinetic energy density  $K$  and the momentum flux for the mixture  $\Pi$  become equivalent. The hydrodynamic pressure (1.6.24) proposed by Geurst is not compatible with the relations (1.5.8) and (1.5.9) given by Wallis. However, alternative definitions given by Geurst (1986) lead to relations which are compatible with (1.5.8) and

(1.5.9). The exertia  $D$  should be identified with  $m(\alpha)/(1-\alpha)$ . The added-mass force follows from (1.5.6) and (1.5.7). It is given by

$$\bar{M}_1^2 = \rho_1 D \left\{ \frac{\partial u_2}{\partial t} + u_2 \frac{\partial u_2}{\partial x} - \frac{\partial u_1}{\partial t} - u_1 \frac{\partial u_1}{\partial x} - Z \right\} \quad (1.7.5)$$

and a comparison with Geurst's (1.7.1) shows some major differences. Nevertheless, a number of other similarities may be discovered, for which we refer to Wallis ((1987)(1988a)). We further mention that Geurst (1988) transformed an extended version of his equations (see Chapter II) into a three-fluid model and also made a comparison with the model of Cook & Harlow (1984).

We conclude that the comparison made above decides in favour of variational methods. Other techniques generally lead to complicated difficulties which are not encountered when variational methods are applied, as has been demonstrated by Geurst ((1985a)(1985b)(1986)). Moreover, several recent two-fluid models have been subjected to three test cases by Wallis (1988b) and only Geurst's equations pass these tests. The calculus of variations is therefore chosen as a sound basis for the present thesis. Several extensions of Geurst's equations are derived and used for a further investigation of bubbly two-phase flows.

All previous models assume that the bubbles have a spherical shape. In reality, however, the bubbles become oblate ellipsoids when they have a velocity relative to the liquid. In Chapter II it is demonstrated how the variational principle (1.6.2) may be extended to include that effect.

Many models presented in the literature suffer from complex characteristics, related to the inadequate inclusion of concentration waves. That type of waves is treated in Chapter III. In particular, nonlinear concentration waves are discussed which appear as nonlinear exact solutions of Geurst's equations and of the extended version presented in Chapter II. The waves are found to be closely related to the virtual-mass coefficient.

Due to the occurrence of complex characteristics many models are not suitable for stable and reliable numerical computations. The numerical investigation of the interaction of acoustic waves and nonlinear concentration waves is used in Chapter IV as a test for the numerical suitability of Geurst's model and the extended model. At the same time the stability of nonlinear concentration waves for acoustic disturbances is investigated. Linear theory is used to verify the numerical results. A variational formulation of the linearised equations shows

that the acoustics of a bubbly liquid/gas mixture may be considered as a generalisation of the acoustics of one-component fluids.

In Chapter V stationary vertical pipe flow is considered. That type of flow has been studied experimentally and has received quite some attention in the literature. The reason for this is that the void-fraction profiles for upward flows show a distinct peak near the pipe wall, as was already reported by Malnes in 1966 (see Serizawa et al. 1975). Since then, many attempts have been made for a theoretical explanation of this interesting effect. However, an explanation starting from a general model has not yet been given. In Chapter V dissipative terms and corrections in the case of high gradients are systematically included in the two-phase flow equations. That general theory is subsequently used in order to investigate void-fraction and velocity profiles in stationary vertical two-phase flows. The governing ordinary differential equations are solved numerically and by means of perturbation theory. The results are compared with measurements.



## CHAPTER II

# VARIATIONAL APPROACH TO BUBBLE DEFORMATION IN TWO-PHASE FLOW †)

### 2.1 Introduction

All models treated in the previous chapter have in common that they assume bubbles of a constant shape. In general the bubbles are taken spherical, which is only exact in the case where the difference velocity vanishes. As the relative velocity increases the bubbles deviate from their spherical form to become oblate ellipsoids in a good approximation. In addition, the presence of the bubbles is taken into account only by means of the void fraction. However, a definite void fraction  $\alpha$  may be realised by a small amount of large bubbles as well as by a large amount of small bubbles. The models mentioned above do not distinguish between those cases. They do not include the energy related to surface tension either.

Section 1.6 demonstrates the importance and advantages of variational methods. Virtual-mass effects associated with the motion of the bubbles relative to the liquid may be included systematically in that way. In the present chapter the variational principle of Geurst (1985a) ‡) will be extended by including the deformations of the bubbles induced by their relative motion to the surrounding liquid. Since the deformations are related to the surface energy of the bubbles, that energy has to be included. In addition a constraint expressing the conservation of the number of bubbles is required.

Bubble deformation effects may be related to the value of the Weber number which expresses the ratio of the pressure variation induced by the relative flow and the pressure contribution due to surface tension. In fact the shape of the bubble is determined by the mutual balance of those pressures. The Weber number is introduced in the Lagrangian density as an additional quantity in order to model the flow induced bubble deformations. In Geurst's equations (see section 1.6) the fixed streamline contours of the gas bubbles

---

†) *Parts of this chapter were communicated at ICIAM 87, June - July 1987, Paris, France (see Geurst & Vreenegoor 1987).*

‡) *Hereafter referred to as G (1985a).*

determine the constant value of  $\hat{m}$  (see expression (1.6.28) for  $m(\alpha)$ ). In the present formulation bubble deformation effects are taken into account by allowing the virtual-mass coefficient to depend on the Weber number. As a consequence the critical value  $\alpha_c$  of the void fraction at which the virtual-mass coefficient vanishes will also depend on the Weber number. It is investigated how bubble deformations affect that critical value and how they influence the phase velocities of the acoustic modes.

The flow equations are subjected to a linear stability analysis. Marginal stability is investigated by analysing the common solution of two partial differential equations (compare with the ordinary differential equations (1.6.26) and (1.6.27) for  $m(\alpha)$ ), which in addition contain derivatives with respect to the Weber number. By considering the limit of vanishingly small values of the void fraction  $\alpha$  the solution is made compatible with the results known to hold for a separate oblate ellipsoid. At the same time the solution allows the inclusion of the surface tension energy in a simple way.

The analysis is confined to the one-dimensional non-dissipative behaviour of a bubbly liquid/gas mixture. A three-dimensional formulation is presented in Chapter V, where also dissipative effects are included.

## 2.2 Variational formulation and two-phase flow equations

The derivation of the two-phase flow equations including bubble deformation effects starts from an extended form of Hamilton's principle of least action. The derivation proceeds parallel to Geurst's approach which is treated in section 1.6. The liquid is considered to be incompressible, the gas ideal and the flow is assumed to occur at isothermal conditions. The coalescence and break-up of bubbles are not taken into account. The analysis is confined to one-dimensional motion for the sake of convenience.

The variational principle reads

$$\delta \int_{t_1}^{t_2} dt \int_{x_1}^{x_2} dx L = 0, \quad (2.2.1)$$

where  $L = L(\rho_1, \rho_2, n, u_1, u_2)$ . The number density of the gas bubbles  $n$  is included as an additional variable. It is related to the void fraction  $\alpha$  and the equivalent bubble radius  $a$  by means of

$$\alpha = n \tau , \tag{2.2.2}$$

where the local average  $\tau$  of the bubble volume is defined by

$$\tau = \frac{4\pi}{3} a^3 . \tag{2.2.3}$$

The Lagrangian density  $L$  is given by

$$L = K - F ; \tag{2.2.4}$$

$K = K(\rho_1, \rho_2, n, u_1, u_2)$  denotes the kinetic energy density of the liquid/gas mixture and  $F = F(\rho_1, \rho_2)$  the free energy density. The thermodynamics of the bubbly mixture is contained in  $F$  and is partially treated in section 1.6. An additional relation, convenient for the present section, is written

$$\rho_1 \mu_1 + \rho_2 \mu_2 = F + p_g . \tag{2.2.5}$$

The kinetic energy density  $K$  is modified to include the effect of bubble deformation:

$$K = \frac{1}{2} \rho_1 u_1^2 + \frac{1}{2} \rho_2 u_2^2 + \frac{1}{2} \rho_\ell m(\alpha, We) (u_2 - u_1)^2 . \tag{2.2.6}$$

The virtual-mass effects associated with the relative motion are now represented by the coefficient  $m(\alpha, We)$ . That coefficient is allowed to depend not only on the void fraction  $\alpha$  but also on the Weber number  $We$  defined by

$$We = \frac{\rho_\ell (u_2 - u_1)^2}{(\gamma/2a)} \tag{2.2.7}$$

in order to model the flow induced deformation of the bubbles in addition to their mutual interaction. The bubble number density  $n$  enters the kinetic energy density  $K$  as a result of the fact that the Weber number depends on the equivalent bubble radius  $a$ . The surface tension coefficient is denoted by  $\gamma$ . The Weber number is a ratio of two pressures, viz., the hydrodynamic pressure variation induced by the relative flow and the pressure contribution due to surface tension. When the bubbles travel with the liquid the hydrodynamic pressure of the liquid on the bubbles is nearly constant and the bubbles are spherical with a Weber number equal to zero. The possible form of the function  $m(\alpha, We)$  is investigated in sections

2.4 and 2.5. It appears that the energy associated with surface tension may be accounted for by including terms in the mass-coefficient  $m(\alpha, We)$  which are inversely proportional to the Weber number. As a result, the coefficient  $m(\alpha, We)$  should not be identified with the virtual-mass coefficient  $m(\alpha)$ . In the present case the actual virtual-mass coefficient  $m^*(\alpha, We)$  must be defined as (see expression (2.3.16) for the new kinetic energy density  $K^*$ )

$$m^* = m + We m_{We}, \quad (2.2.8)$$

where  $m_{We}$  denotes  $(\partial/\partial We)m(\alpha, We)$ . As a result of expression (2.2.8)  $m^*(\alpha, We)$  does not contain terms which are inversely proportional to the Weber number so that only pure bubble deformation effects are included in the virtual-mass coefficient. Note that the free energy density  $F$  does not contain any terms related to surface tension. The last term on the right hand side of (2.2.6), however, may contain all surface tension effects.

The variations in (2.2.1) are restricted by the constraints (1.2.4) and (1.2.5), expressing the conservation of mass for the liquid and the gas, and by

$$\frac{\partial n}{\partial t} + \frac{\partial}{\partial x} (n u_2) = 0. \quad (2.2.9)$$

Equation (2.2.9) describes the conservation of the number of bubbles in the case where the coalescence and fragmentation of bubbles are neglected. Equation (1.2.5) and (2.2.9) may be combined to

$$\frac{\partial}{\partial t} (\rho_g \tau) + u_2 \frac{\partial}{\partial x} (\rho_g \tau) = 0, \quad (2.2.10)$$

where (2.2.2) and (1.2.3) have been used. It expresses that the mass  $\rho_g \tau$  inside a bubble remains constant in a frame of reference moving with the bubble velocity  $u_2$ .

When the constraints (1.2.4), (1.2.5) and (2.2.9) are introduced in the variational principle by means of Lagrange multipliers, the Lagrangian density  $L$  is modified into

$$\hat{L} = L + \sum_{i=1}^2 \varphi_i \left[ \frac{\partial \rho_i}{\partial t} + \frac{\partial}{\partial x} (\rho_i u_i) \right] + \lambda \left[ \frac{\partial n}{\partial t} + \frac{\partial}{\partial x} (n u_2) \right]. \quad (2.2.11)$$



Integrating by parts we obtain the equivalent Lagrangian density  $L^*$  given by

$$L^* = L - \sum_{i=1}^2 \rho_i \left[ \frac{\partial}{\partial t} + u_i \frac{\partial}{\partial x} \right] \varphi_i - n \left[ \frac{\partial}{\partial t} + u_2 \frac{\partial}{\partial x} \right] \lambda . \quad (2.2.12)$$

The variation applies to the independent variables  $\rho_1$ ,  $\rho_2$ ,  $n$ ,  $u_1$ ,  $u_2$  and the Lagrange multipliers  $\varphi_1$ ,  $\varphi_2$  and  $\lambda$ . The variation of the independent variables yields the Euler-Lagrange equations

$$\delta\rho_1 : \frac{1}{2} u_1^2 - \mu_1^* - \left[ \frac{\partial}{\partial t} + u_1 \frac{\partial}{\partial x} \right] \varphi_1 = 0 , \quad (2.2.13)$$

$$\delta\rho_2 : \frac{1}{2} u_2^2 - \mu_2 - \left[ \frac{\partial}{\partial t} + u_2 \frac{\partial}{\partial x} \right] \varphi_2 = 0 , \quad (2.2.14)$$

$$\delta n : -\frac{1}{6} \rho_\ell \frac{We}{n} m_{We} (u_2 - u_1)^2 - \left[ \frac{\partial}{\partial t} + u_2 \frac{\partial}{\partial x} \right] \lambda = 0 , \quad (2.2.15)$$

$$\delta u_1 : \rho_1 u_1 - \rho_\ell m^* (u_2 - u_1) - \rho_1 \frac{\partial \varphi_1}{\partial x} = 0 , \quad (2.2.16)$$

$$\delta u_2 : \rho_2 u_2 + \rho_\ell m^* (u_2 - u_1) - \rho_2 \frac{\partial \varphi_2}{\partial x} - n \frac{\partial \lambda}{\partial x} = 0 . \quad (2.2.17)$$

The modified thermodynamic potential  $\mu_1^*$  is defined according to

$$\mu_1^* = \mu_1 + \frac{1}{2} \left( m_\alpha + \frac{We}{3\alpha} m_{We} \right) (u_2 - u_1)^2 , \quad (2.2.18)$$

where  $m_\alpha$  denotes  $(\partial/\partial\alpha)m(\alpha, We)$ . When we compare equations (2.2.16) and (2.2.17) with Geurst's (1.6.14) and (1.6.15) it may already be anticipated that  $m^*(\alpha, We)$  should be named the virtual-mass coefficient and not  $m(\alpha, We)$ .

The total mass velocity  $u$  follows by adding (2.2.16) and (2.2.17) and is determined by

$$\rho u = \sum_{i=1}^2 \rho_i u_i = \sum_{i=1}^2 \rho_i \frac{\partial \varphi_i}{\partial x} + n \frac{\partial \lambda}{\partial x} . \quad (2.2.19)$$

The total mass density  $\rho$  reads

$$\rho = \rho_1 + \rho_2 . \quad (2.2.20)$$

Multiplying (2.2.16) by  $u_1$ , (2.2.17) by  $u_2$  and adding the results we obtain

$$\sum_{i=1}^2 \rho_i u_i \frac{\partial \varphi_i}{\partial x} + n u_2 \frac{\partial \lambda}{\partial x} = \sum_{i=1}^2 \rho_i u_i^2 + \rho_\ell m^* (u_2 - u_1)^2 . \quad (2.2.21)$$

When equations (2.2.13)–(2.2.15) are respectively multiplied by  $\rho_1$ ,  $\rho_2$  and  $n$  and the resulting equations are added, it is derived that

$$\begin{aligned} & \sum_{i=1}^2 \rho_i \frac{\partial \varphi_i}{\partial t} + n \frac{\partial \lambda}{\partial t} + K + F + p_g + \\ & + \frac{1}{2} \rho_\ell \{ m + (1-\alpha) m_\alpha + \left( \frac{1}{3\alpha} + 2 \right) We m_{We} \} (u_2 - u_1)^2 = 0 , \end{aligned} \quad (2.2.22)$$

where (2.2.21) and (2.2.5) have been used. Equation (2.2.22) constitutes a generalisation of the Bernoullian theorem, known from the classical hydrodynamics of one-phase fluids.

The equations of motion for the liquid and the gas phase are obtained by eliminating the Lagrange multipliers. Differentiating (2.2.13) and (2.2.14) with respect to  $x$  and using (2.2.15)–(2.2.17) and the conservation equations (1.2.4), (1.2.5), (2.2.9) and (2.2.10), we derive the equation of motion for the liquid phase as

$$\begin{aligned} \left[ \frac{\partial}{\partial t} + u_1 \frac{\partial}{\partial x} \right] \left\{ u_1 - \frac{\rho_\ell m^*}{\rho_1} (u_2 - u_1) \right\} - \frac{\rho_\ell m^*}{\rho_1} (u_2 - u_1) \frac{\partial u_1}{\partial x} + \\ + \frac{\partial \mu_1^*}{\partial x} = 0 \end{aligned} \quad (2.2.23)$$

and determine the equation of the gas phase to be

$$\left[ \frac{\partial}{\partial t} + u_2 \frac{\partial}{\partial x} \right] \left\{ u_2 + \frac{\rho_\ell m^*}{\rho_2} (u_2 - u_1) \right\} + \frac{\rho_\ell m^*}{\rho_2} (u_2 - u_1) \frac{\partial u_2}{\partial x} + \frac{\partial \mu_2^*}{\partial x} - \frac{1}{6} \rho_\ell \frac{We}{n} m_{We} (u_2 - u_1)^2 \frac{\partial}{\partial x} \left[ \frac{n}{\rho_2} \right] = 0. \quad (2.2.24)$$

The modified thermodynamic potential  $\mu_2^*$  is defined by

$$\mu_2^* = \mu_2 + \frac{1}{6} \rho_\ell \frac{We}{\rho_2} m_{We} (u_2 - u_1)^2. \quad (2.2.25)$$

Equations (2.2.23) and (2.2.24) may also be written

$$\frac{\partial}{\partial t} \left\{ u_1 - \frac{\rho_\ell m^*}{\rho_1} (u_2 - u_1) \right\} + \frac{\partial}{\partial x} \left\{ \frac{1}{2} u_1^2 - \frac{\rho_\ell m^*}{\rho_1} u_1 (u_2 - u_1) + \mu_1^* \right\} = 0 \quad (2.2.26)$$

and

$$\frac{\partial}{\partial t} \left\{ u_2 + \frac{\rho_\ell m^*}{\rho_2} (u_2 - u_1) \right\} + \frac{\partial}{\partial x} \left\{ \frac{1}{2} u_2^2 + \frac{\rho_\ell m^*}{\rho_2} u_2 (u_2 - u_1) + \mu_2^* \right\} + \frac{1}{6} \rho_\ell \frac{We}{n} m_{We} (u_2 - u_1)^2 \frac{\partial}{\partial x} \left[ \frac{n}{\rho_2} \right] = 0. \quad (2.2.27)$$

The non-dissipative two-phase flow of deformable bubbles dispersed in a continuous liquid is determined by equations (1.2.4), (1.2.5), (2.2.9), (2.2.23) and (2.2.24), which describe the evolution in time of the independent variables  $\rho_1$ ,  $\rho_2$ ,  $n$ ,  $u_1$  and  $u_2$ . For the sake of convenience we refer to those equations as model 2. Geurst's equations (1.2.4), (1.2.5), (1.6.16) and (1.6.17) are referred to as model 1.

When we compare equations (2.2.23) and (2.2.24) with Geurst's equations (1.6.16) and (1.6.17), it becomes clear that  $m^*(\alpha, We)$  has replaced  $m(\alpha)$  and should be identified as the virtual-mass coefficient. From equation (2.2.26) it is concluded that the equation of motion for the liquid may be written formally in conservation form. Equation (2.2.27) demonstrates,

however, that the equation of motion for the gas can not be written in conservation form, unlike Geurst's equation (1.6.17). This has some consequences for the application of certain numerical schemes, as is shown in Chapter IV.

The evolution in time of the difference velocity  $w = u_2 - u_1$  is derived by subtracting (2.2.27) and (2.2.26). The result may be written as

$$\begin{aligned} & \frac{\partial}{\partial t} \left[ \left\{ \left[ \frac{1}{2} + \frac{\rho_\ell m^*}{\rho_1} \right] + \left[ \frac{1}{2} + \frac{\rho_\ell m^*}{\rho_2} \right] \right\} (u_2 - u_1) \right] + \\ & + \frac{\partial}{\partial x} \left[ \left\{ \left[ \frac{1}{2} + \frac{\rho_\ell m^*}{\rho_1} \right] u_1 + \left[ \frac{1}{2} + \frac{\rho_\ell m^*}{\rho_2} \right] u_2 \right\} (u_2 - u_1) + \mu_2^* - \mu_1^* \right] + \\ & - \frac{1}{6} \rho_\ell \frac{We}{n} m_{We} (u_2 - u_1)^2 \frac{\partial}{\partial x} \left[ \frac{n}{\rho_2} \right] = 0 . \end{aligned} \quad (2.2.28)$$

### 2.3 Conservation equations: the Clebsch-Bateman principle

The conservation equations for energy and linear momentum may be derived by means of Noether's first invariance theorem (see G 1985a and Logan 1977). It will be obvious that those equations may also be obtained from the Euler-Lagrange equations (2.2.13)-(2.2.17) though it takes a lot more effort this way. For completeness we give the main results of the invariance theorem.

When a Lagrangian density  $L$  depends on the field quantities  $\psi_\sigma$  with the subscript  $\sigma$  belonging to a finite discrete set, the conservation of energy is expressed by

$$\frac{\partial H}{\partial t} + \frac{\partial Q}{\partial x} = 0 , \quad (2.3.1)$$

with the energy density  $H$  and the energy flux  $Q$  given by

$$H = \sum_{\sigma} \frac{\partial L}{\partial(\partial\psi_{\sigma}/\partial t)} \frac{\partial\psi_{\sigma}}{\partial t} - L \quad (2.3.2)$$

and

$$Q = \sum_{\sigma} \frac{\partial L}{\partial(\partial\psi_{\sigma}/\partial x)} \frac{\partial\psi_{\sigma}}{\partial t} . \quad (2.3.3)$$

The equation for the conservation of linear momentum is written

$$\frac{\partial P}{\partial t} + \frac{\partial \Pi}{\partial x} = 0 , \quad (2.3.4)$$

where the momentum density P and the momentum flux  $\Pi$  are determined by

$$P = - \sum_{\sigma} \frac{\partial L}{\partial(\partial\psi_{\sigma}/\partial t)} \frac{\partial\psi_{\sigma}}{\partial x} \quad (2.3.5)$$

and

$$\Pi = - \sum_{\sigma} \frac{\partial L}{\partial(\partial\psi_{\sigma}/\partial x)} \frac{\partial\psi_{\sigma}}{\partial x} + L . \quad (2.3.6)$$

In our theory of bubbly two-phase flow  $\{\psi_{\sigma}\}$  represents the set  $\{\rho_1, \rho_2, n, u_1, u_2\}$ . Noether's theorem is most readily applied to the Lagrangian density  $L^*$  given by (2.2.12). The energy density H follows as

$$\begin{aligned} H &= - \sum_{i=1}^2 \rho_i \frac{\partial\varphi_i}{\partial t} - n \frac{\partial\lambda}{\partial t} - L^* \\ &= K + F + \rho_{\ell} We m_{We} (u_2 - u_1)^2 \end{aligned} \quad (2.3.7)$$

with the use of (2.2.16) and (2.2.17). The energy flux Q is determined by

$$\begin{aligned}
 Q &= -\sum_{i=1}^2 \rho_i u_i \frac{\partial \varphi_i}{\partial t} - n u_2 \frac{\partial \lambda}{\partial t} \\
 &= \rho_1 u_1 \left\{ \frac{1}{2} u_1^2 - \frac{\rho_\ell m^*}{\rho_1} u_1 (u_2 - u_1) + \mu_1^* \right\} + \\
 &+ \rho_2 u_2 \left\{ \frac{1}{2} u_2^2 + \frac{\rho_\ell m^*}{\rho_2} u_2 (u_2 - u_1) + \mu_2^* \right\}, \tag{2.3.8}
 \end{aligned}$$

where now the Euler–Lagrange equations (2.2.13)–(2.2.17) have been used. The total momentum density  $P$  follows from (2.3.5) as

$$P = \sum_{i=1}^2 \rho_i \frac{\partial \varphi_i}{\partial x} + n \frac{\partial \lambda}{\partial x} = \sum_{i=1}^2 \rho_i u_i = \rho u, \tag{2.3.9}$$

while the momentum flux  $\Pi$  reads

$$\begin{aligned}
 \Pi &= \sum_{i=1}^2 \rho_i u_i \frac{\partial \varphi_i}{\partial x} + n u_2 \frac{\partial \lambda}{\partial x} + L^* \\
 &= \sum_{i=1}^2 \rho_i u_i^2 + \rho_\ell m^* (u_2 - u_1)^2 + p. \tag{2.3.10}
 \end{aligned}$$

The hydrodynamic pressure  $p$  of the bubbly liquid/gas mixture is defined by

$$p = p_g + \frac{1}{2} \rho_\ell \left\{ m + (1-\alpha) m_\alpha + \frac{We}{3\alpha} m_{We} \right\} (u_2 - u_1)^2. \tag{2.3.11}$$

Equations (2.3.7)–(2.3.11) are a generalisation of Geurst’s equations (1.6.20)–(1.6.24) (see section 1.6). The form of the momentum flux  $\Pi$  again determines the pressure  $p$ . Rewriting expression (2.2.12) for  $L^*$  by means of the Euler–Lagrange equations yields

$$p = L^*. \tag{2.3.12}$$

Similar to the results of section 1.6, the present variational principle also constitutes a Clebsch–Bateman principle.

A somewhat unexpected difference with Geurst's results is governed by equation (2.3.7) for the total energy density  $H$ . Obviously,  $H$  does not equal the sum of the kinetic and free energy densities  $K$  and  $F$ . That discrepancy may be solved, however, by introducing a new kinetic energy density  $K^*$  and a new free energy density  $F^*$  according to

$$H = K^* + F^* , \quad L = K^* - F^* . \quad (2.3.13)$$

From (2.3.13), (2.3.7) and (2.2.4) it is derived that

$$K^* = K + \frac{1}{2} \rho_\ell \text{We} m_{\text{We}} (u_2 - u_1)^2 \quad (2.3.14)$$

and

$$F^* = F + \frac{1}{2} \rho_\ell \text{We} m_{\text{We}} (u_2 - u_1)^2 . \quad (2.3.15)$$

Combining (2.3.14) and (2.2.6) we have

$$K^* = \frac{1}{2} \rho_1 u_1^2 + \frac{1}{2} \rho_2 u_2^2 + \frac{1}{2} \rho_\ell m^* (u_2 - u_1)^2 . \quad (2.3.16)$$

Clearly,  $m^*(\alpha, \text{We})$  should be identified as the virtual-mass coefficient. The redefinition of  $K$  and  $F$  transports the energy associated with surface tension from the kinetic to the free energy density. That energy may be included in  $m(\alpha, \text{We})$  by means of terms which are inversely proportional to the Weber number (see section 2.5). As a result, the new kinetic energy density  $K^*$  is allowed to depend only on those surface tension effects which change the kinetic energy due to the deformations of the bubbles. Note that the last term on the right hand side of (2.3.7) is invariant with respect to a Galilean transformation and may be attributed to the kinetic as well as the free energy density.

It follows from (2.3.11), (2.3.14) and (2.3.15) that the Bernoullian theorem (2.2.22) may be written in the form

$$\sum_{i=1}^2 \rho_i \frac{\partial \varphi_i}{\partial t} + n \frac{\partial \lambda}{\partial t} + K^* + F^* + p = 0 . \quad (2.3.17)$$

Compared to (2.2.22), equation (2.3.17) may be recognised more easily as a generalisation of the Bernoullian theorem valid for classical fluids.

### 2.4 Linear stability analysis

In order to investigate the linear stability of the evolution equations (1.2.4), (1.2.5), (2.2.9), (2.2.23) and (2.2.24) we write the field quantities  $\rho_1, \rho_2, n, u_1, u_2$  in the form

$$u(x,t) = u_0 + \hat{u} \exp\{i(\omega t - kx)\} . \quad (2.4.1)$$

The steady-state value  $u_0$  is constant and  $\hat{u}$  represents the amplitude of a small perturbation of the steady state. Products of perturbations in the evolution equations are neglected. When the velocity perturbations  $\hat{u}_1$  and  $\hat{u}_2$  are eliminated by means of the mass balance equations (1.2.4) and (1.2.5) we arrive at the following system of linearised equations:

$$\begin{aligned} a_{11} \bar{\rho}_1 + a_{12} \bar{\rho}_2 &= 0 , \\ a_{21} \bar{\rho}_1 + a_{22} \bar{\rho}_2 &= 0 , \end{aligned} \quad (2.4.2)$$

$$y \bar{\rho}_2 - y \bar{n} = 0 ,$$

where

$$\begin{aligned} a_{11} = \{ & 1 + \frac{1}{1-\alpha} m + \frac{5}{1-\alpha} We m_{We} + \frac{2}{1-\alpha} We^2 m_{WeWe} \} y^2 + \\ & + 2w_0 \{ 1 + \frac{2}{1-\alpha} m + m_\alpha + \frac{2+16\alpha}{3\alpha(1-\alpha)} We m_{We} + We m_{\alpha We} + \\ & + \frac{1+5\alpha}{3\alpha(1-\alpha)} We^2 m_{WeWe} \} y + \\ & + w_0^2 \{ 1 + \frac{3}{1-\alpha} m + 2 m_\alpha + \frac{-1+14\alpha+50\alpha^2}{9\alpha^2(1-\alpha)} We m_{We} + \frac{1-\alpha}{2} m_{\alpha\alpha} + \\ & + \frac{1+5\alpha}{3\alpha} We m_{\alpha We} + \frac{1+10\alpha+25\alpha^2}{18\alpha^2(1-\alpha)} We^2 m_{WeWe} \} + \\ & - \frac{RT}{M} \beta \frac{1-\alpha}{\alpha} , \end{aligned} \quad (2.4.3)$$



$$\begin{aligned}
 a_{12} = & - \left\{ \frac{1}{1-\alpha} m + \frac{5}{1-\alpha} We m_{We} + \frac{2}{1-\alpha} We^2 m_{WeWe} \right\} y^2 + \\
 & - w_0 \left\{ \frac{1}{1-\alpha} m + m_\alpha + \frac{2+11\alpha}{3\alpha(1-\alpha)} We m_{We} + We m_{\alpha We} + \right. \\
 & \qquad \qquad \qquad \left. + \frac{1+4\alpha}{3\alpha(1-\alpha)} We^2 m_{WeWe} \right\} y + \\
 & + w_0^2 \left\{ \frac{1+11\alpha}{18\alpha(1-\alpha)} We m_{We} + \frac{1}{6} We m_{\alpha We} + \frac{1+5\alpha}{18\alpha(1-\alpha)} We^2 m_{WeWe} \right\} + \\
 & \qquad \qquad \qquad - \frac{RT}{M} \beta, \tag{2.4.4}
 \end{aligned}$$

$$a_{21} = \frac{1-\alpha}{\beta\alpha} a_{12}, \tag{2.4.5}$$

$$\begin{aligned}
 a_{22} = & \frac{1}{\beta\alpha} \left\{ \beta\alpha + m + 5 We m_{We} + 2 We^2 m_{WeWe} \right\} y^2 + \\
 & - \frac{1}{\beta\alpha} w_0 \left\{ 2m + \frac{10}{3} We m_{We} + \frac{2}{3} We^2 m_{WeWe} \right\} y + \\
 & + \frac{1}{\beta\alpha} w_0^2 \left\{ \frac{2}{9} We m_{We} + \frac{1}{18} We^2 m_{WeWe} \right\} - \frac{RT}{M} \tag{2.4.6}
 \end{aligned}$$

and

$$\bar{\rho}_1 = \frac{\hat{\rho}_1}{\rho_{1,0}}, \quad \bar{\rho}_2 = \frac{\hat{\rho}_2}{\rho_{2,0}}, \quad \bar{n} = \frac{\hat{n}}{n_0}. \tag{2.4.7}$$

The Doppler-shifted phase velocity  $y$  and the unperturbed difference velocity  $w_0$  are given by

$$y = \frac{\omega}{k} - u_{2,0}, \tag{2.4.8}$$

$$w_0 = u_{2,0} - u_{1,0}. \tag{2.4.9}$$

The zero subscripts denoting the unperturbed steady-state values of  $\alpha$  and  $We$  have been deleted in the expressions (2.4.3)–(2.4.6) for the sake of convenience. The quantity  $\beta$  is defined by

$$\beta = \frac{\rho_{g,0}}{\rho_l}. \tag{2.4.10}$$

The velocity perturbations are determined by

$$\hat{u}_1 = (y + w_0) \bar{\rho}_1 \tag{2.4.11}$$

and

$$\hat{u}_2 = y \bar{\rho}_2 . \tag{2.4.12}$$

The system (2.4.2) of linear equations admits a non-trivial solution if and only if the determinant of the coefficient matrix vanishes. That condition yields the dispersion equation, which is written

$$y ( a_{11} a_{22} - a_{12} a_{21} ) = 0 . \tag{2.4.13}$$

Obviously, it is a fifth degree algebraic equation in  $y$ . It determines the phase velocities of the linear modes. The uniform solution of the system of partial differential equations is linearly unstable when the dispersion equation contains complex conjugate roots. We therefore consider the discriminant  $D_0$  of the equation (2.4.13). It is shown in section 1.6 that when bubble deformation effects are not included  $D_0$  vanishes for a specific form of the virtual-mass coefficient  $m(\alpha)$  (see expression (1.6.28)). When the virtual mass of the bubbles is neglected,  $D_0$  becomes negative, the dispersion equation possesses complex roots and the steady-state solution is unstable. We now investigate what form of  $m(\alpha, We)$  might correspond to marginal stability ( $D_0 = 0$ ).

By substituting the coefficients  $a_{ij}$ , ( $i, j=1, 2$ ), into equation (2.4.13) the dispersion equation takes the form

$$y \sum_{k=0}^4 c_k y^k = 0 . \tag{2.4.14}$$

The discriminant  $D_0$  of the fourth order equation which is multiplied by  $y$  in (2.4.14) is determined by the coefficients  $c_k$ , ( $k=1, \dots, 4$ ). We analyse the discriminant for small values of  $w_0$  by writing it as a power series expansion in the difference velocity. From the theory of fourth degree algebraic equations (see e.g. Turnbull 1944) it follows that the leading term in the expansion of the discriminant is determined by the coefficients  $c_1$  and  $c_0$ , which are given by

$$c_1 = -2 \frac{RT}{M} PDV_1 w_0 + O(w_0^3) \quad (2.4.15)$$

and

$$c_0 = -\frac{RT}{M} PDV_0 w_0^2 + O(w_0^4) . \quad (2.4.16)$$

The partial differential equations  $PDV_1$  and  $PDV_0$  read

$$\begin{aligned} PDV_1 = 1 + \frac{3\alpha-1}{\alpha^2(1-\alpha)} m + \frac{1}{\alpha} m_\alpha + \frac{7\alpha-1}{\alpha^2(1-\alpha)} We m_{We} + \frac{1}{\alpha} We m_{We\alpha} + \\ + \frac{2}{\alpha(1-\alpha)} We^2 m_{WeWe} \end{aligned} \quad (2.4.17)$$

and

$$\begin{aligned} PDV_0 = 1 + \frac{3}{1-\alpha} m + 2 m_\alpha + \frac{7}{1-\alpha} We m_{We} + \frac{1-\alpha}{2} m_{\alpha\alpha} + 2 We m_{We\alpha} + \\ + \frac{2}{1-\alpha} We^2 m_{WeWe} . \end{aligned} \quad (2.4.18)$$

The structure of the discriminant may be written

$$D_0 = g(\alpha, We; \beta) \{ h(\alpha, We; \beta) PDV_0 - (PDV_1)^2 \} w_0^2 + O(w_0^3) , \quad (2.4.19)$$

where the functions  $g(\cdot)$  and  $h(\cdot)$  depend additionally on the parameter  $\beta$ . As a consequence, the discriminant vanishes for small relative velocities  $w_0$  independently of the value of  $\beta$  if and only if the partial differential equations  $PDV_1$  and  $PDV_0$  for  $m(\alpha, We)$  satisfy

$$PDV_1 = 0 \quad \text{and} \quad PDV_0 = 0 . \quad (2.4.20)$$

Note that  $m(\alpha, We)$  does not depend on  $\beta$ . By introducing the function  $f(\alpha, We)$  which is related to  $m(\alpha, We)$  according to

$$m(\alpha, We) = \alpha (1-\alpha) f(\alpha, We) , \quad (2.4.21)$$

(2.4.20) may be shown to be equivalent to the two partial differential equations

$$(1-\alpha)We f_{\alpha We} + 2 We^2 f_{WeWe} + 5 We f_{We} + (1-\alpha) f_{\alpha} + f + 1 = 0, \quad (2.4.22)$$

$$\frac{1}{2} \alpha (1-\alpha) f_{\alpha\alpha} + (2\alpha-1) We f_{\alpha We} - 2 We^2 f_{WeWe} - 3 We f_{We} = 0. \quad (2.4.23)$$

A *common* solution of (2.4.22) and (2.4.23) would yield marginal stability for small relative velocities  $w_0$ . We investigate the common solution by introducing the characteristic coordinates  $(\eta, \varphi)$  of equation (2.4.22) by means of

$$\eta = We (1-\alpha)^2, \quad (2.4.24)$$

$$\varphi = 1 - \alpha.$$

The equations (2.4.22) and (2.4.23) are now transformed into

$$\varphi\eta \hat{f}_{\eta\varphi} + \varphi \hat{f}_{\varphi} - \eta \hat{f}_{\eta} - \hat{f} - 1 = 0, \quad (2.4.25)$$

$$\eta\varphi \hat{f}_{\eta\varphi} - \eta \hat{f}_{\eta} + \frac{1}{2} \varphi^2 (1-\varphi) \hat{f}_{\varphi\varphi} = 0, \quad (2.4.26)$$

where  $\hat{f}(\eta, \varphi)$  denotes the function  $f$  expressed in characteristic coordinates. The equation (2.4.25) may be solved exactly according to

$$\hat{f}(\eta, \varphi) = \varphi C(\eta) + \frac{1}{\eta} D(\varphi) - 1, \quad (2.4.27)$$

where  $C(\eta)$  and  $D(\varphi)$  are unknown functions of the characteristic coordinates  $\eta$  and  $\varphi$ . Substitution of (2.4.27) in (2.4.26) yields an ordinary differential equation for  $D(\varphi)$ , viz.,

$$\frac{1}{2} \varphi (1-\varphi) \frac{d^2 D}{d\varphi^2} - \frac{dD}{d\varphi} + \frac{1}{\varphi} D = 0. \quad (2.4.28)$$

The general solution of (2.4.28) reads

$$D(\varphi) = A \varphi + B \frac{\varphi}{1-\varphi}, \quad (2.4.29)$$

where A and B are unknown constants. The *common* solution of the two partial differential equations (2.4.25) and (2.4.26) is accordingly determined by

$$\hat{f}(\eta, \varphi) = \varphi C(\eta) + \frac{1}{\eta} ( A \varphi + B \frac{\varphi}{1-\varphi} ) - 1 . \quad (2.4.30)$$

Combining (2.4.21), (2.4.24) and (2.4.30) we conclude that steady two-phase flow is marginally stable for small relative velocities  $w_0$  if and only if the function  $m(\alpha, We)$  satisfies

$$m(\alpha, We) = \alpha(1-\alpha) \{ (1-\alpha) C(We(1-\alpha)^2) + \frac{1}{We(1-\alpha)} ( A + \frac{B}{\alpha} ) - 1 \} . \quad (2.4.31)$$

The virtual-mass coefficient  $m^*(\alpha, We)$  follows by means of (2.2.8) as

$$m^*(\alpha, We) = \alpha (1-\alpha) \{ (1-\alpha) E(We(1-\alpha)^2) - 1 \} , \quad (2.4.32)$$

where

$$E(\eta) = \frac{d}{d\eta} ( \eta C(\eta) ) . \quad (2.4.33)$$

By making the substitution

$$E(\eta) = 1 + \frac{1}{2} \tilde{m}(\eta) \quad (2.4.34)$$

we may write the virtual-mass coefficient as

$$m^*(\alpha, We) = \frac{1}{2} \alpha (1-\alpha) \{ \tilde{m} - (\tilde{m}+2) \alpha \} , \quad (2.4.35)$$

where  $\tilde{m}$  is a function of  $\eta = We(1-\alpha)^2$ . When we compare the virtual-mass coefficient  $m^*(\alpha, We)$  given by (2.4.35) with Geurst's virtual-mass coefficient  $m(\alpha)$  given by (1.6.28), it becomes clear that the inclusion of bubble deformation effects replaced the constant  $\tilde{m}$  by a function  $\tilde{m}(\eta)$  which depends on the Weber number through the quantity  $\eta$ .

Substitution of expression (2.4.31) for  $m(\alpha, We)$  in the coefficients  $a_{ij}$ , ( $i, j=1, 2$ ), and writing out the determinant given by (2.4.14) reveals that the higher order terms in  $w_0$  which occur in the coefficients  $c_1$  and  $c_0$  vanish as well. We may therefore conclude that expression (2.4.31) for  $m(\alpha, We)$  implies marginal stability of uniform bubbly two-phase flow without any further restrictions on the physical variables. The coinciding roots  $y = 0$  correspond to

wave velocities equal to the gas velocity  $u_2$ . They may be partly associated with concentration waves, or void-fraction waves. In practice concentration waves are observed to travel with a velocity lying between the liquid and the gas velocity but with a distinct preference for the gas velocity (see G 1985a and the references contained therein). Void-fraction waves will be treated extensively in Chapter III.

It follows from the dispersion equation (2.4.14) that expression (2.4.31) for  $m(\alpha, We)$  makes the bubble velocity  $u_2$  a triple root. The additional third root already anticipated by equation (2.2.10) may be defined as a bubble-size wave. That wave was first mentioned by Geurst in a private communication to the author. It is also discussed by Chaabane (1989). The quantities which vary in a bubble-size wave are the bubble radius  $a$ , or the bubble volume  $\tau$ , the number density  $n$  and the gas pressure  $p_g$ . They vary in such a way that the variation of the gas pressure  $p_g$  equals the pressure jump  $2\gamma/a$  due to surface tension. Since the void fraction is kept constant, the wave may consist of transitions from a large concentration of small bubbles with a relatively high gas pressure to a small concentration of large bubbles with a relatively low gas pressure.

The unknown constants  $A$  and  $B$  and the unknown function  $C(\cdot)$  which appear in expression (2.4.31) for  $m(\alpha, We)$  are determined in the following section by considering the limiting case  $\alpha \rightarrow 0$  (a separate deformable bubble). In section 2.6 formulas are presented which determine the velocity of propagation of the acoustic modes including bubble deformation effects.

### **2.5 Adjustment of the flow equations to the dynamics of a separate deformable bubble**

The evolution in time of the five quantities  $\rho_1$ ,  $\rho_2$ ,  $n$ ,  $u_1$  and  $u_2$  described by model 2 still depends on the form of the mass coefficients  $m(\alpha, We)$  and  $m^*(\alpha, We)$  which are related by means of (2.2.8). The requirement of marginal stability of model 2 determines  $m(\alpha, We)$  and  $m^*(\alpha, We)$  as functions of  $\alpha$  and  $We$  which still contain two unknown constants  $A$  and  $B$  and an unknown function  $C(\eta)$ , where  $\eta = We(1-\alpha)^2$ . It is shown in the present section that  $C(\eta)$  may be determined by considering the limiting behaviour of the virtual-mass coefficient  $m^*(\alpha, We)$  at small values of the void fraction  $\alpha$  and using the results known to hold for a separate deformable bubble. The constants  $A$  and  $B$  may be determined by including the energy associated with surface tension.

First, however, the requirement of marginal stability needs some elucidation. It is still unclear why model 1 (Geurst's equations treated in section 1.6) and model 2 (present

chapter) should be *marginally* stable. A physical interpretation must justify that choice. The first physical support to the choice of marginal stability is given by the void–fraction waves. As is already mentioned in the previous section those waves are observed to travel with a velocity close to the velocity of the gas bubbles. Since only one type of concentration wave is observed, the roots necessarily have to coincide which results in marginal stability. An exception to that situation form the experiments by Bouré (1988) who reports at high void fractions two types of concentration waves with distinct velocities of propagation. At low void fractions one mode is absent. Those results, however, may still be very well in accordance with our models since model 1 and model 2 do not include any dissipative (viscosity) or dispersive (high gradients, bubble pulsations) effects. Obviously, the inclusion of those effects present in most practical situations will make the coinciding roots split. The influence of those effects on the coinciding root  $u_2$  still remains to be investigated.

A second physical support to the choice of marginal stability follows from a consideration of the distribution of the bubbles. The distribution of the bubbles influences the bubble interactions and therefore determines the coefficients of the higher order terms in  $\alpha$  that appear in the virtual–mass coefficient. A random distribution is unstable, as is mentioned in section 1.7 and demonstrated by figure 4.3.2.1 (Chapter IV). A well–stirred bubbly mixture will therefore leave that distribution and will strive for a stable situation. Coming from an unstable region the first stable distribution the mixture encounters is the marginally stable situation. As soon as the mixture finds itself in that situation there is no reason for further changing the obtained equilibrium. Obviously, the fixed expression for the virtual–mass coefficient (1.6.28) implies that the distribution of the bubbles adopts the state of equilibrium instantaneously when the flow is subjected to some changes. In practice, however, the distribution of the bubbles is a dynamically determined quantity whose state of equilibrium will be disturbed by changes in the flow. In Chapter IV the coefficients of the higher order terms in  $\alpha$  are perturbed to investigate the influence of the form of  $m(\alpha)$  close to marginal stability on the roots of the dispersion equation. Geurst (1988) demonstrates how the virtual–mass coefficient may be included as an independent variable in model 2. That formulation may be used for a systematic inclusion of terms which account for perturbations from the marginally stable state.

We now come to the full determination of the coefficients  $m(\alpha, We)$  and  $m^*(\alpha, We)$ . For small values of the void fraction expression (2.4.35) for the virtual–mass coefficient  $m^*(\alpha, We)$  may be written as

$$m^*(\alpha, We) = \frac{1}{2} \alpha \tilde{m}(We) + O(\alpha^2). \quad (2.5.1)$$

The term  $(1/2)\check{m}(We)$  represents the virtual-mass coefficient taken per unit volume of gas in a dilute dispersion of bubbles in liquid. Clearly, interaction effects are neglected. Some information concerning the function  $\check{m}(We)$  might therefore be obtained by considering the inertial properties of the separate gas bubbles moving through the liquid. When the bubbles are spherical, for example, the Weber number is zero and  $\check{m}(0)$  must be equal to one.

We consider a separate deformable gas bubble moving through an infinite liquid with a relative velocity  $U$ . Its Weber number  $\check{We}$  is defined according to

$$\check{We} = \frac{\rho_l U^2}{\gamma/2 a} \tag{2.5.2}$$

Moore (1965) mentions that for a Weber number  $\check{We} = O(1)$  it is a fair approximation to assume that the bubble is an oblate ellipsoid. The virtual-mass coefficient  $(1/2)\check{m}$  of an oblate ellipsoid is given by (see Lamb 1945)

$$\frac{1}{2} \check{m} = \frac{\tan z - z}{z - \sin z \cos z}, \tag{2.5.3}$$

where  $z = \cos^{-1}(q/r)$  and  $q/r$  denotes the ratio of the length of the parallel axis to the length of the cross-stream axis of the ellipsoid. Moore (1965) presents the following approximation of the associated Weber number:

$$\check{We} = 4 \sqrt[3]{\cos z} (1 + \cos^2 z - 2 \cos^3 z) \left( \frac{z - \sin z \cos z}{\sin^3 z} \right)^2. \tag{2.5.4}$$

With the use of the Computer-Algebra system Macsyma (1985) relations (2.5.3) and (2.5.4) were combined to derive the first five terms of a Taylor series expansion of  $\check{m}$  around  $\check{We} = 0$ , i.e.,

$$\check{m} = 1 + \sum_{k=1}^4 b_k \check{We}^k + O(\check{We}^5). \tag{2.5.5}$$

The exact values of the coefficients  $b_k$ , ( $k=1, \dots, 4$ ), are given in the appendix. A numerical approximation reads

$$\begin{aligned} b_1 &= .17, & b_2 &= .34 \times 10^{-1}, \\ b_3 &= .73 \times 10^{-2}, & b_4 &= .16 \times 10^{-2}. \end{aligned} \tag{2.5.6}$$



For completeness we mention that Benjamin (1987) gives an approximation of the Weber number  $We$  which is slightly more accurate than (2.5.4), viz.,

$$We = \frac{\sqrt[3]{\cos z}}{\sin^3 z} \left( \frac{z - \sin z \cos z}{3 + \tan^2 z} - \frac{3 \tan z}{3} \right)^2 \left\{ 6 + 4 \tan^2 z + \right. \\ \left. - \frac{4 - \cos^2 z}{\sin z} \ln \left( \frac{1 + \sin z}{1 - \sin z} \right) \right\}. \quad (2.5.7)$$

A numerical comparison of (2.5.4) and (2.5.7) demonstrated only small differences. For reasons of simplicity we used expression (2.5.4).

In a dilute dispersion of gas bubbles in liquid the kinetic energies associated with the motions of the separate gas bubbles may be added, because interaction effects between the bubbles are negligible. When it is assumed that the velocities of the gas bubbles relative to the liquid are nearly equal, the virtual masses of the separate bubbles may be added also. We therefore infer from (2.2.7), (2.5.2) and (2.5.5) that

$$\bar{m}(We) = 1 + \sum_{k=1}^4 b_k We^k + O(We^5). \quad (2.5.8)$$

It has been assumed that the diameters of the gas bubbles are nearly equal. It follows from (2.4.33), (2.4.34) and (2.5.8) that

$$C(\eta) = \frac{C_0}{\eta} + \frac{1}{2} \left( 3 + \sum_{k=1}^4 \frac{b_k}{k+1} \eta^k \right) + O(\eta^5), \quad (2.5.9)$$

where  $C_0$  is an unknown constant. According to (2.4.30) the constant  $C_0$  may be taken equal to zero without affecting the generality of the expression for  $\hat{f}(\eta, \varphi)$ .

The terms in the expression (2.4.31) for  $m(\alpha, We)$  that contain the constants  $A$  and  $B$  are inversely proportional to the Weber number  $We$ . As a result, they contribute to the free energy density  $F^*$ , but not to the kinetic energy density  $K^*$ . Those terms may be used to take into account the surface tension energy  $F_\gamma$  which was not included in the free energy density  $F$ .

In the limit  $We \rightarrow 0$ , the gas bubbles have a spherical shape. The surface tension energy  $F_\gamma$  is accordingly given by

$$F_\gamma = n \gamma 4\pi a^2 = \frac{3\gamma\alpha}{a}. \quad (2.5.10)$$

According to (2.3.15), (2.4.31) and (2.5.9) ( $C_0 = 0$ ) the difference of the free energy densities  $F^*$  and  $F$  is determined by

$$\begin{aligned} F^* - F &= \frac{1}{2} \rho_l We m_{We} (u_2 - u_1)^2 \\ &= \frac{3\gamma\alpha}{a} \left\{ -\frac{A}{12} - \frac{B}{12\alpha} + \frac{1}{48} b_1 (1-\alpha)^4 We^2 + O(We^3) \right\}. \end{aligned} \quad (2.5.11)$$

Taking the limit  $We \rightarrow 0$  and comparing with (2.5.10) we derive that

$$A = -12, \quad B = 0. \quad (2.5.12)$$

The final expressions for  $m(\alpha, We)$  and the virtual-mass coefficient  $m^*(\alpha, We)$  follow from (2.4.31) and (2.4.35), where the function  $C(\eta)$  is given by (2.5.9) ( $C_0 = 0$ ), the constants  $A$  and  $B$  are given by (2.5.12) and the function  $\tilde{m}(\eta)$  is determined by (2.5.8). The expressions read

$$\begin{aligned} m(\alpha, We) &= \frac{1}{2} \alpha (1-\alpha) \left\{ 1 - 3\alpha + \sum_{k=1}^4 \frac{b_k}{k+1} (1-\alpha)^{2k+1} We^k \right\} + \\ &\quad - \frac{1}{2} \frac{2\alpha}{We} + O(We^5) \end{aligned} \quad (2.5.13)$$

and

$$m^*(\alpha, We) = \frac{1}{2} \alpha (1-\alpha) \left\{ 1 - 3\alpha + \sum_{k=1}^4 b_k (1-\alpha)^{2k+1} We^k \right\} + O(We^5) \quad (2.5.14)$$

and account for the microscopic behaviour of deformable bubbles. When the Weber number approaches the value three the rectilinear motion of deformed bubbles becomes unstable (see van Bekkum 1985 and Benjamin 1987). As a result Moore's (1965) approximation (2.5.4) is no more valid there. The expressions (2.5.13) and (2.5.14) for  $m(\alpha, We)$  and  $m^*(\alpha, We)$  should therefore only be used for Weber numbers smaller than, approximately, three.

Substitution of (2.5.13) in expression (2.3.11) for the hydrodynamic pressure  $p$  shows that the term  $-12\alpha/We$  yields the well-known pressure difference  $-2\gamma/a$  associated with surface tension.

## 2.6 Acoustic modes and breakdown of bubbly flow

In section 2.4 it is mentioned that expression (2.4.31) for  $m(\alpha, We)$  makes the coefficients  $c_1$  and  $c_0$  of the dispersion equation (2.4.14) vanish. In the case of marginal stability the dispersion equation may therefore be written as

$$(a_0 + a_1 y + a_2 y^2) y^3 = 0. \quad (2.6.1)$$

In a first order approximation with respect to the Weber number the coefficients  $a_i$ , ( $i=0,1,2$ ), are given by

$$\begin{aligned} a_0 = & -\frac{1}{\alpha} \left\{ \frac{1}{2} w^2 (1-\alpha)^2 \left[ 1 + \frac{9}{40} (1-\alpha)^2 We \right]^2 + \right. \\ & + \left[ \frac{RT}{M} \beta - \frac{4}{3We} \left( 1 + \frac{9}{1280} (1-\alpha)^4 We^2 \right) w^2 \right] \times \\ & \left. \times \left[ 2\beta + 1 + \frac{81}{160} (1-\alpha)^2 We \right] \right\} + O(We^2), \end{aligned} \quad (2.6.2)$$

$$\begin{aligned} a_1 = & 2\beta \left( 3 + \frac{9}{40} (1-\alpha)^2 We \right) (1-\alpha) w + \frac{9}{16} (1-\alpha)^3 We w + \\ & + O(We^2), \end{aligned} \quad (2.6.3)$$

$$\begin{aligned} a_2 = & 1 - 3\alpha + \frac{81}{160} (1-\alpha)^3 We + \beta \left( 2 + 3\alpha + \frac{81}{160} \alpha (1-\alpha)^2 We \right) + \\ & + O(We^2). \end{aligned} \quad (2.6.4)$$

The exact value  $b_1 = 27/160$  (see the appendix) has been used and for the sake of convenience the subscript zero has been omitted. The acoustic phase velocities follow from the solution of the quadratic equation which makes part of (2.6.1). The Doppler-shifted phase velocity  $y$  is expressed by (2.4.8). When the terms depending on the Weber number are omitted in (2.6.2)–(2.6.4), expression (6.16) derived by G (1985a, p. 253) is recovered. Due to the fact that  $a_1 \neq 0$  the acoustic phase velocities are not symmetrically centered around the gas velocity  $u_2$ , unless the difference velocity  $w$  vanishes. When bubble deformations are not taken into account that effect is small since  $\beta = \rho_g/\rho_\ell \cong 10^{-3}$ . It will be clear that the value of the void fraction for which  $a_2$  becomes zero and the acoustic velocities

become infinite increases as a result of the inclusion of bubble deformation effects. In addition it may be inferred from the relations (2.6.1) to (2.6.4) that the acoustic waves travel slower when the deformation of the bubbles is accounted for. The behaviour of acoustic waves travelling through a mixture of deformable bubbles is further demonstrated in the numerical experiments presented in Chapter IV.

In section 1.6 a breakdown of bubbly flow is associated with the vanishing of the virtual-mass coefficient. Model 1 predicts such a breakdown to occur at a critical void fraction  $\alpha_c = 1/3$  in the case of spherical bubbles. We now investigate the influence of bubble deformation on the critical void fraction by analysing for which values of  $\alpha$  the virtual-mass coefficient  $m^*(\alpha, We)$  vanishes.

Expression (2.5.14) for  $m^*(\alpha, We)$  relates the critical void fraction  $\alpha_c$  and the Weber number by means of

$$1 - 3 \alpha_c + \sum_{k=1}^4 b_k (1-\alpha_c)^{2k+1} We^k = 0 . \quad (2.6.5)$$

For small Weber numbers it is deduced from (2.6.5) that

$$\alpha_c = \frac{1}{3} + \frac{1}{60} We + \frac{19}{80640} We^2 + O(We^3) , \quad (2.6.6)$$

where the exact values for  $b_1$  and  $b_2$  (see the appendix) are substituted. The breakdown of bubbly flow is therefore shifted to larger values of the void fraction in cases where the gas bubbles are deformed by the flow as a result of a finite value of the surface tension coefficient  $\gamma$ . A numerical treatment of expression (2.6.5) presents  $\alpha_c$  as a function of the Weber number  $We$  in figure 2.6.1. The figure shows that breakdown may occur at void fractions varying from  $1/3$  to  $.4$ , depending on the value of the Weber number. This result is supported experimentally by Matuszkiewicz et al. (1987), who observe bubble-slug flow pattern transitions at void fractions varying from  $.3$  to  $.45$ .

In a first order approximation in the Weber number the coefficient  $a_2$  (equation (2.6.4)) which occurs in the denominator of the acoustic phase velocities becomes equal to

$$a_2 = \frac{1}{10} We + \beta \left( 3 + \frac{1}{8} We \right) + O(We^2) \quad (2.6.7)$$

at the critical void fraction  $\alpha_c$  given by (2.6.6). As a consequence the value of  $a_2$  is small when breakdown occurs and the acoustic velocities will be large. For Weber numbers of order one it is seen, however, that bubble deformation effects become dominant in expression (2.6.7) and tend to decrease the acoustic phase velocities in the region of breakdown.

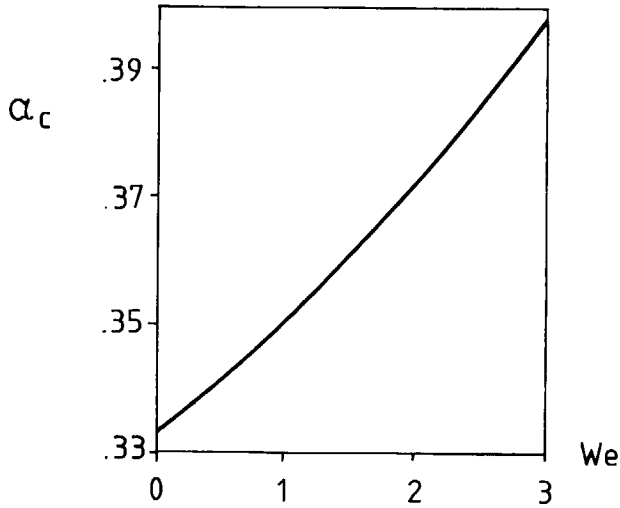


*Figure 2.6.1 The critical void-fraction  $\alpha_c$  as a function of the Weber number  $We$ .*

## 2.7 Conclusions

The variational principle presented by G (1985a) (see section 1.6) is extended to include bubble deformation effects and surface tension energy by introducing the Weber number as an additional quantity. The inclusion of the equation which expresses the conservation of the number of bubbles introduces a new type of wave, viz., a bubble-size wave. The equations of motion are systematically derived from the extended variational principle. The expression for the total energy density  $H$  obtained from Noether's first invariance theorem suggests a redefinition of the kinetic and free energy densities. As a result, the surface tension energy is moved from the kinetic energy density to the free energy density. The variational principle may be given the form of a Clebsch-Bateman principle.

A linear stability analysis shows that marginal stability is achieved if and only if the mass coefficient  $m(\alpha, We)$  takes a specific form, which also determines the virtual-mass coefficient  $m^*(\alpha, We)$ . A few physical arguments are given motivating the requirement of marginal stability. At marginal stability three roots of the characteristic (dispersion) equation become equal to the velocity  $u_2$  of the gas bubbles. One of these roots is related to a bubble-size wave, the other two roots may be associated with a concentration wave. Expressions for the acoustic phase velocities are presented which depend on the Weber number. All roots of the characteristic equation are real.

The virtual-mass coefficient  $m^*(\alpha, We)$  is adjusted to the dynamics of a separate deformable bubble. The surface tension energy is included by means of the mass coefficient  $m(\alpha, We)$ . The value of the void fraction at which breakdown occurs becomes dependent on the Weber number. The transition from bubble to slug flow may now occur at void fractions varying from  $1/3$  to  $.4$ , which is physically more acceptable than the fixed value for  $\alpha_c$  in the case of model 1. The values of  $\alpha_c$  are in agreement with experiments.

The flow equations presented in the present chapter include the microscopic properties of bubbly two-phase flow with greater detail than the models treated in the introductory chapter. Several physical effects are included which are not accounted for in the major part of the models presented in the literature. The use of variational techniques enabled a reliable and systematic refinement of Geurst's model treated in section 1.6.

**Appendix**

The exact values of the coefficients  $b_k$ , ( $k=1,\dots,4$ ), which appear in expression (2.5.5) for  $\check{m}$  read

$$\begin{aligned} b_1 &= \frac{27}{160}, & b_2 &= \frac{48519}{1433600}, \\ b_3 &= \frac{6727941}{91750400}, & b_4 &= \frac{59439630519}{36171677696000}. \end{aligned} \tag{2.A.1}$$

The values follow from expressions (2.5.3) and (2.5.4) and are determined with the use of the Computer–Algebra system Macsyma (1985).





## CHAPTER III

# NONLINEAR VOID-FRACTION WAVES IN BUBBLY TWO-PHASE FLOW †)

### 3.1 Introduction

The stability of two-phase flow of bubbly liquid/gas mixtures constitutes a wellknown theoretical problem (see the review article by Drew (1983)). Although the introduction of virtual-mass terms may have some stabilising effect (see Lahey et al. (1980)), two-phase flow computations are usually faced with unwanted instabilities. The occurrence of the instabilities is associated with the fact that the equations possess two characteristics, that are complex conjugate.

In a recent paper (Geurst (1985a)<sup>‡</sup>) the stability problem was reconsidered. It was shown after an extensive and detailed analysis that marginal stability of two-phase bubbly flow can be achieved by means of a proper choice of the virtual-mass coefficient  $m(\alpha)$  as a function of the void fraction  $\alpha$ . At marginal stability the two complex conjugate roots become real. In the case of spherical bubbles the functional dependence is given by

$$m(\alpha) = \frac{1}{2} \alpha (1 - \alpha) (1 - 3\alpha) . \quad (3.1.1)$$

The unwanted instability concerns a linear mode which is allowed by the equations in addition to the acoustic mode. When the additional mode is marginally stabilised by means of (3.1.1), it contains a void-fraction wave propagating with the drift velocity of the gas bubbles. The gas density and the drift velocity of the gas bubbles are not perturbed by the linear void-fraction wave. Since the bubble concentration varies while the bubble size remains constant, void-fraction waves are sometimes called concentration waves.

---

†) Published in *ZAMP* (with the exception of sections 3.5 and 3.6). See Geurst & Vreenegoor (1988).

‡) Hereafter referred to as *G* (1985a).

The analysis in G (1985a) is confined to linear modes and linear stability. In the present chapter *non-linear* void-fraction waves are introduced. They are characterised by the property that the gas density and the drift velocity of the gas bubbles remain constant. It is demonstrated that nonlinear void-fraction waves constitute exact solutions of the two-phase flow equations, when the virtual-mass coefficient is given by (3.1.1). It is shown at the same time that the validity of (3.1.1) is not only a sufficient but also a necessary condition for the possibility of nonlinear void-fraction waves. A remarkable and non-trivial result is that the greater part of the physical quantities associated with a nonlinear void-fraction wave is a *linear* function of the void fraction. The analysis suggests a particular form of Hamilton's variational principle.

Dissipative effects are not considered in the present chapter. They may be introduced in a systematic way according to the thermodynamics of irreversible processes (see the appendix of G (1985a) and Chapter V).

Void-fraction waves are observed experimentally. Some recent experimental results are reported in Matuszkiewicz et al. (1987).

### 3.2 Inviscid two-phase bubbly flow

The equations governing the two-phase flow of a bubbly liquid/gas mixture were derived in G (1985a) by using variational methods. Starting point of the derivations was an extended form of Hamilton's variational principle of least action. The two-phase flow equations are presented here briefly (see also Geurst (1986)<sup>†</sup>) and section 1.6 of Chapter I).

The bubbly liquid/gas mixture is composed of a continuous phase, the liquid phase with constant density  $\rho_l$ , and a discrete phase, the gas phase (density  $\rho_g$ , pressure  $p_g$ ) which obeys the ideal gas law. The void fraction or volume density of the gas phase is denoted by  $\alpha$ . The flow is assumed to proceed isothermally. That assumption is usually made in cases, where mass exchange between the two phase may be neglected (see e.g. Drew (1983)). For the sake of convenience the analysis is restricted to one-dimensional flow. The effects of gravity and viscosity are disregarded. When the reduced densities  $\rho_1$  and  $\rho_2$  are introduced according to

---

†) Hereafter referred to as G (1986).

$$\rho_1 = \rho_\ell (1 - \alpha), \quad \rho_2 = \rho_g \alpha, \quad (3.2.1)$$

the conservation of mass for the liquid and the gas are expressed by

$$\frac{\partial \rho_1}{\partial t} + \frac{\partial}{\partial x} (\rho_1 u_1) = 0 \quad (3.2.2)$$

and

$$\frac{\partial \rho_2}{\partial t} + \frac{\partial}{\partial x} (\rho_2 u_2) = 0. \quad (3.2.3)$$

Here,  $u_1$  and  $u_2$  denote the mass averaged velocities of, respectively, the liquid and the gas phase.

The Euler–Lagrange equations obtained by means of the variational approach are given by the two Bernoulli equations

$$\left[ \frac{\partial}{\partial t} + u_1 \frac{\partial}{\partial x} \right] \varphi_1 + \mu_1 + \frac{1}{2} m'(\alpha) (u_2 - u_1)^2 - \frac{1}{2} u_1^2 = 0 \quad (3.2.4)$$

and

$$\left[ \frac{\partial}{\partial t} + u_2 \frac{\partial}{\partial x} \right] \varphi_2 + \mu_2 - \frac{1}{2} u_2^2 = 0, \quad (3.2.5)$$

and the two equations expressing the velocities  $u_1$  and  $u_2$  in terms of the potentials  $\varphi_1$  and  $\varphi_2$ , viz.,

$$u_1 - \frac{\rho_\ell m(\alpha)}{\rho_1} (u_2 - u_1) = \frac{\partial \varphi_1}{\partial x} \quad (3.2.6)$$

and

$$u_2 + \frac{\rho_\ell m(\alpha)}{\rho_2} (u_2 - u_1) = \frac{\partial \varphi_2}{\partial x}. \quad (3.2.7)$$

Note that  $m'(\alpha)$  denotes  $(d/d\alpha)m(\alpha)$ .

The thermodynamic potentials  $\mu_1$  and  $\mu_2$  are defined by

$$dF = \mu_1 d\rho_1 + \mu_2 d\rho_2, \quad (3.2.8)$$

where  $F$  denotes the free energy density. The virtual-mass coefficient  $m(\alpha)$  is introduced by means of the expression for the total kinetic energy  $K$ , viz.,

$$K = \frac{1}{2} \rho_1 u_1^2 + \frac{1}{2} \rho_2 u_2^2 + \frac{1}{2} \rho_\ell m(\alpha) (u_2 - u_1)^2. \quad (3.2.9)$$

The first two terms at the right-hand side of (3.2.9) represent the kinetic energy densities connected with the motion of the local centres of mass of the liquid and the gas. The last term, which contains the virtual-mass coefficient, takes account of the kinetic energy associated with the local backflow around the gas bubbles in the case, where the drift velocity of the bubbles relative to the liquid does not vanish. Some useful thermodynamic relations are

$$d\mu_1 = \frac{dp_g}{\rho_\ell}, \quad d\mu_2 = \frac{dp_g}{\rho_g} \quad (3.2.10)$$

and

$$\rho_1 \mu_1 + \rho_2 \mu_2 = F + p_g. \quad (3.2.11)$$

The surface energy of the gas bubbles may be added to the free energy density  $F$ .

Eliminating the potentials  $\varphi_1$  and  $\varphi_2$  in the equations (3.2.4) to (3.2.7) we obtain the following equations of motion for the liquid and the gas phase:

$$\left[ \frac{\partial}{\partial t} + u_1 \frac{\partial}{\partial x} \right] \left\{ u_1 - \frac{\rho_\ell m(\alpha)}{\rho_1} (u_2 - u_1) \right\} - \frac{\rho_\ell m(\alpha)}{\rho_1} (u_2 - u_1) \frac{\partial u_1}{\partial x} + \frac{\partial}{\partial x} \left\{ \frac{1}{2} m'(\alpha) (u_2 - u_1)^2 \right\} = - \frac{1}{\rho_\ell} \frac{\partial p_g}{\partial x}. \quad (3.2.12)$$

and

$$\left[ \frac{\partial}{\partial t} + u_2 \frac{\partial}{\partial x} \right] \left\{ u_2 + \frac{\rho_\ell m(\alpha)}{\rho_2} (u_2 - u_1) \right\} + \frac{\rho_\ell m(\alpha)}{\rho_2} (u_2 - u_1) \frac{\partial u_2}{\partial x} = -\frac{1}{\rho_g} \frac{\partial p_g}{\partial x} . \quad (3.2.13)$$

The generalised momenta per unit mass  $\pi_1$  and  $\pi_2$  are given by (see G (1986))

$$\pi_1 = u_1 - \frac{\rho_\ell m(\alpha)}{\rho_1} (u_2 - u_1) \quad (3.2.14)$$

and

$$\pi_2 = u_2 + \frac{\rho_\ell m(\alpha)}{\rho_2} (u_2 - u_1) . \quad (3.2.15)$$

The mass-conservation equations (3.2.2) and (3.2.3) and the equations of motion (3.2.12) and (3.2.13) constitute a complete set of four evolution equations for the determination of  $\rho_1$ ,  $\rho_2$ ,  $u_1$  and  $u_2$  as functions of position and time.

The equation for the conservation of momentum is given by

$$\frac{\partial P}{\partial t} + \frac{\partial \Pi}{\partial x} = 0 , \quad (3.2.16)$$

where the momentum density  $P$  and the momentum flux  $\Pi$  are determined, respectively, by

$$P = \rho_1 u_1 + \rho_2 u_2 \quad (3.2.17)$$

and

$$\Pi = \rho_1 u_1^2 + \rho_2 u_2^2 + \rho_\ell m(\alpha) (u_2 - u_1)^2 + p . \quad (3.2.18)$$

The pressure  $p$  is given by

$$p = p_g + \frac{1}{2} \rho_\ell \{ m(\alpha) + (1-\alpha) m'(\alpha) \} (u_2 - u_1)^2 . \quad (3.2.19)$$

The equation expressing the conservation of energy reads

$$\frac{\partial H}{\partial t} + \frac{\partial Q}{\partial x} = 0, \quad (3.2.20)$$

where the energy density H and the energy flux Q are determined, respectively, by

$$H = K + F \quad (3.2.21)$$

and

$$Q = \rho_1 u_1 \left\{ \frac{1}{2} u_1^2 - \frac{\rho_\ell m(\alpha)}{\rho_1} u_1 (u_2 - u_1) + \mu_1 + \frac{1}{2} m'(\alpha)(u_2 - u_1)^2 \right\} + \\ + \rho_2 u_2 \left\{ \frac{1}{2} u_2^2 + \frac{\rho_\ell m(\alpha)}{\rho_2} u_2 (u_2 - u_1) + \mu_2 \right\}. \quad (3.2.22)$$

The following relations may be helpful for deriving (3.2.16) and (3.2.20) from (3.2.2), (3.2.3), (3.2.12) and (3.2.13):

$$dP = \pi_1 d\rho_1 + \pi_2 d\rho_2 + \rho_1 d\pi_1 + \rho_2 d\pi_2 \quad (3.2.23)$$

and

$$dH = \left\{ u_1 \pi_1 - \frac{1}{2} u_1^2 + \mu_1 + \frac{1}{2} m'(\alpha)(u_2 - u_1)^2 \right\} d\rho_1 + \\ + \left\{ u_2 \pi_2 - \frac{1}{2} u_2^2 + \mu_2 \right\} d\rho_2 + \rho_1 u_1 d\pi_1 + \rho_2 u_2 d\pi_2. \quad (3.2.24)$$

### 3.3 Nonlinear void–fraction waves

A nonlinear void–fraction wave propagating in an otherwise undisturbed two–phase medium may be characterised by the following two properties:

- (i) the gas density  $\rho_g$  is constant;
- (ii) the drift velocity  $u_2$  of the gas bubbles is constant.

The analysis in G (1985a) shows that linear void–fraction waves satisfy those requirements. The definition of a non–linear concentration wave according to (i) and (ii) seems therefore justified. Since the flow is assumed to proceed isothermally, the gas pressure is constant.

The following remark may illustrate the concept of a void–fraction wave. When a bubbly liquid\gas mixture is at rest and the volumes of the bubbles are constant, the liquid and the gas bubbles may be rearranged in an arbitrary way without changing the value of the free energy of the bubbly liquid\gas mixture. The rearrangement of the bubbles accordingly does not induce any dynamical effect. When considered macroscopically an inhomogeneous arrangement of bubbles constitutes a void–fraction wave. The void–fraction wave in this case does not propagate, since the medium is at rest.

It follows from (3.2.3) that for a nonlinear void–fraction wave in general

$$\alpha = f(x - u_2 t) . \tag{3.3.1}$$

The functional dependence (3.3.1) expresses that the void–fraction wave propagates with the gas velocity  $u_2$ . It is derived from the mass–conservation equation (3.2.2) for the liquid phase that

$$u_1 = u_2 - \frac{c}{1 - \alpha} , \tag{3.3.2}$$

where  $c$  is a constant velocity. It is immediately inferred from the Euler–Lagrange equations (3.2.4) to (3.2.7) that the potentials  $\varphi_i$ , ( $i = 1, 2$ ), should take the form

$$\varphi_i = \beta_i t - \nu_i x + \hat{\varphi}_i(x - u_2 t) , \quad (i = 1, 2), \tag{3.3.3}$$

where  $\beta_i$  and  $\nu_i$  represent unknown constants.

By using (3.3.2), (3.3.3) and the equations (3.2.6) and (3.2.7), the Bernoulli equations (3.2.4) and (3.2.5) may be reduced to

$$\mu_1 + \frac{1}{2} \left[ 1 + 2 \frac{m(\alpha)}{1 - \alpha} + m'(\alpha) \right] \frac{c^2}{(1 - \alpha)^2} - \frac{1}{2} u_2^2 + c_1 = 0 \quad (3.3.4)$$

and

$$\mu_2 - \frac{1}{2} u_2^2 + c_2 = 0, \quad (3.3.5)$$

where

$$c_i = \beta_i - u_2 \nu_i, \quad (i = 1, 2). \quad (3.3.6)$$

Note that according to (3.2.10) the thermodynamic potentials  $\mu_1$  and  $\mu_2$  depend only on  $\rho_g$ . The equation (3.3.5) determines the value of  $c_2$ . The equation (3.3.4) can be satisfied if and only if the second term at the left-hand side takes a constant value, i.e.,

$$\frac{1}{2} \left[ 1 + 2 \frac{m(\alpha)}{1 - \alpha} + m'(\alpha) \right] \frac{1}{(1 - \alpha)^2} = \frac{1}{4} (\hat{m} + 2), \quad (3.3.7)$$

where  $\hat{m}$  is a constant. The expression for the constant at the right-hand side of (3.3.7) has been chosen in such a way that the final result (3.3.11) conforms to the notation in G (1985a). When (3.3.7) is satisfied, equation (3.3.4) simplifies to

$$\mu_1 - \frac{1}{2} u_2^2 + \frac{1}{4} (\hat{m} + 2) c^2 + c_1 = 0. \quad (3.3.8)$$

Equation (3.3.8) determines the value of  $c_1$ . Note that the quantity  $c$  is a parameter characterising a nonlinear void-fraction wave according to (3.3.2).

Equation (3.3.7) constitutes a differential equation for the virtual-mass coefficient  $m(\alpha)$ . It may be written in the form

$$\frac{d}{d\alpha} \{ (1 - \alpha)^{-2} m(\alpha) \} + (1 - \alpha)^{-2} = \frac{1}{2} (\hat{m} + 2). \quad (3.3.9)$$



The virtual–mass coefficient should fulfil the requirement

$$m(0) = 0 . \tag{3.3.10}$$

The solution of (3.3.9) satisfying the condition (3.3.10) reads

$$m(\alpha) = \frac{1}{2} \alpha (1 - \alpha) ( \hat{m} - (\hat{m}+2) \alpha ) . \tag{3.3.11}$$

A similar expression for the virtual–mass coefficient was obtained in G (1985a) after an elaborate stability analysis of a uniform two–phase flow. In the case of spherical gas bubbles ( $\hat{m} = 1$ ) the expression (3.3.11) reduces to (3.1.1). The derivation shows that nonlinear void–fraction waves are possible in a two–phase bubbly medium if and only if the virtual–mass coefficient satisfies (3.3.11).

It will be clear from (3.3.2) that the liquid velocity  $u_1$  of a nonlinear void–fraction wave is in general a nonlinear function of the void–fraction. The greater part of the kinematic and dynamic quantities, however, is a linear function of  $\alpha$ . The mass fluxes, e.g., are given by

$$\rho_1 u_1 = \rho_\ell (u_2 - c) - \alpha \rho_\ell u_2 \tag{3.3.12}$$

and

$$\rho_2 u_2 = \alpha \rho_g u_2 , \tag{3.3.13}$$

while the generalised momenta per unit mass are expressed by

$$\pi_1 = u_2 - c - \alpha \frac{1}{2} (\hat{m} + 2) c \tag{3.3.14}$$

and

$$\pi_2 = u_2 + \frac{\rho_\ell}{2\rho_g} \hat{m} c - \alpha \frac{\rho_\ell}{2\rho_g} (\hat{m} + 2) c . \tag{3.3.15}$$

Furthermore

$$\begin{aligned} u_1 \pi_1 + \frac{1}{2} m'(\alpha) (u_2 - u_1)^2 - \frac{1}{2} u_1^2 &= \\ &= \frac{1}{2} (u_2 - c)^2 - \alpha \frac{1}{2} (\hat{m} + 2) u_2 c \end{aligned} \quad (3.3.16)$$

and

$$u_2 \pi_2 - \frac{1}{2} u_2^2 = \frac{1}{2} u_2^2 + \frac{\rho_\ell}{2\rho_g} \hat{m} u_2 c - \alpha \frac{\rho_\ell}{2\rho_g} (\hat{m} + 2) u_2 c . \quad (3.3.17)$$

The momentum density and flux are determined according to

$$P = \rho_\ell (u_2 - c) + \alpha (\rho_g - \rho_\ell) u_2 \quad (3.3.18)$$

and

$$\Pi = \rho_\ell (u_2 - c)^2 + p_g + \frac{1}{4} \hat{m} \rho_\ell c^2 + \alpha (\rho_g - \rho_\ell) u_2^2 . \quad (3.3.19)$$

In a similar way the kinetic energy density is given by

$$K = \frac{1}{2} \rho_\ell (u_2 - c)^2 + \alpha \left\{ \frac{1}{2} (\rho_g - \rho_\ell) u_2^2 + \frac{1}{4} (\hat{m} + 2) \rho_\ell c^2 \right\} , \quad (3.3.20)$$

while the free energy density may be expressed as a linear function of  $\alpha$  by means of

$$F = \rho_\ell \mu_1 - p_g + \alpha (\rho_g \mu_2 - \rho_\ell \mu_1) . \quad (3.3.21)$$

The pressure is determined according to

$$p = p_g + \frac{1}{4} \hat{m} \rho_\ell c^2 - \alpha \frac{1}{2} (\hat{m} + 2) \rho_\ell c^2 . \quad (3.3.22)$$

The energy density and flux are finally given by

$$\begin{aligned}
 H = & \frac{1}{2} \rho_{\ell} (u_2 - c)^2 + \rho_{\ell} \mu_1 - p_g + \\
 & + \alpha \left\{ \frac{1}{2} (\rho_g - \rho_{\ell}) u_2^2 + \frac{1}{4} (\hat{m} + 2) \rho_{\ell} c^2 + \rho_g \mu_2 - \rho_{\ell} \mu_1 \right\}
 \end{aligned} \tag{3.3.23}$$

and

$$\begin{aligned}
 Q = & \rho_{\ell} (u_2 - c) \left\{ \mu_1 + \frac{1}{2} (u_2 - c)^2 + \frac{1}{4} \hat{m} c^2 \right\} + \\
 & + \alpha u_2 \left\{ \frac{1}{2} (\rho_g - \rho_{\ell}) u_2^2 + \frac{1}{4} (\hat{m} + 2) \rho_{\ell} c^2 + \rho_g \mu_2 - \rho_{\ell} \mu_1 \right\} .
 \end{aligned} \tag{3.3.24}$$

The results (3.3.12) to (3.3.24) are obtained in a non-trivial way by using (3.3.2) and (3.3.11). It follows from (3.3.20) and (3.3.21) that the Lagrangian density  $L = K - F$  is a linear function of  $\alpha$ . Using the Bernoulli equations (3.3.4) and (3.3.5) and the equation (3.3.7) we obtain

$$L = \frac{1}{2} \rho_{\ell} (u_2 - c)^2 - \rho_{\ell} \mu_1 + p_g + \alpha (\rho_g c_2 - \rho_{\ell} c_1) . \tag{3.3.25}$$

It is immediately inferred from (3.3.25) that

$$\frac{\partial}{\partial \alpha} \{ L - c_1 \rho_{\ell} (1 - \alpha) - c_2 \rho_g \alpha \} = 0 . \tag{3.3.26}$$

The result (3.3.26) suggests a particular form of Hamilton's principle of least action. It is discussed in the next section.

### 3.4 Variational principle

In the case of a void-fraction wave Hamilton's principle of least action takes the form

$$\delta \int_{t_1}^{t_2} dt \int_{x_1}^{x_2} dx L(\alpha) = 0, \quad (3.4.1)$$

where

$$\begin{aligned} L(\alpha) = & \frac{1}{2} \rho_\ell (u_2 - c)^2 - \frac{1}{2} \rho_\ell c^2 - \rho_\ell \mu_1 + p_g + \\ & + \alpha \left\{ \frac{1}{2} (\rho_g - \rho_\ell) u_2^2 + \rho_\ell \mu_1 - \rho_g \mu_2 \right\} + \\ & + \frac{1}{2} \rho_\ell c^2 \left[ \frac{m(\alpha)}{(1 - \alpha)^2} + \frac{1}{1 - \alpha} \right]. \end{aligned} \quad (3.4.2)$$

The Lagrangian density  $L(\alpha)$  is obtained from the expression (3.2.9) and (3.2.11) for the kinetic and free energy densities by expressing  $u_1$  in terms of  $\alpha$  according to (3.3.2). The behaviour of the void fraction as a function of position and time is given by (3.3.1). All the other quantities in (3.4.2) are constant. The form of the virtual-mass coefficient  $m(\alpha)$  as a function of  $\alpha$  is unknown. The variation of  $\alpha$  is subject to two constraints. They require that the total masses of the liquid and the gas are constant. The constraints may be put in the following form:

$$(t_2 - t_1) M_1 - \int_{t_1}^{t_2} dt \int_{x_1}^{x_2} dx \rho_\ell (1 - \alpha) = 0 \quad (3.4.3)$$

and

$$(t_2 - t_1) M_2 - \int_{t_1}^{t_2} dt \int_{x_1}^{x_2} dx \rho_g \alpha = 0. \quad (3.4.4)$$

Here  $M_1$  and  $M_2$  represent the total masses of the liquid and the gas.

Changing to new coordinates  $(\xi, \theta)$  according to

$$\xi = x - u_2 t, \quad \theta = t + \frac{x}{u_2} \quad (3.4.5)$$

and introducing Lagrange multipliers to take account of the constraints we obtain the following variational principle for  $\alpha$  as a function of  $\xi$ :

$$\delta \int_{\xi_1}^{\xi_2} d\xi \int_{\theta_1(\xi)}^{\theta_2(\xi)} d\theta \hat{L}(\alpha) = 0, \quad (3.4.6)$$

where

$$\hat{L}(\alpha) = L(\alpha) - \lambda_1 \rho_\ell (1 - \alpha) - \lambda_2 \rho_g \alpha \quad (3.4.7)$$

and

$$\xi_1 = x_1 - u_2 t_2, \quad \xi_2 = x_2 - u_2 t_1. \quad (3.4.8)$$

For the sake of convenience it is assumed that  $u_2 > 0$ . Note that (3.4.6) may be reduced to

$$\delta \int_{\xi_1}^{\xi_2} \hat{L}(\alpha) g(\xi) d\xi = 0, \quad (3.4.9)$$

where  $g(\xi) = \theta_2(\xi) - \theta_1(\xi)$ .

The Euler–Lagrange equation associated with (3.4.9) is given by

$$\frac{\partial \hat{L}}{\partial \alpha} = 0. \quad (3.4.10)$$

Using (3.4.2) and (3.4.7) we derive from (3.4.10) that

$$\begin{aligned} \frac{d}{d\alpha} \{ (1 - \alpha)^{-2} m(\alpha) \} + (1 - \alpha)^{-2} = \\ = - \left[ \frac{1}{2} \rho_\ell c^2 \right]^{-1} \left[ \frac{1}{2} (\rho_g - \rho_\ell) u_2^2 + \right. \\ \left. + \rho_\ell (\mu_1 + \lambda_1) - \rho_g (\mu_2 + \lambda_2) \right]. \end{aligned} \quad (3.4.11)$$

The right-hand side of (3.4.11) represents an arbitrary constant. By taking that constant equal to  $(1/2)(\hat{m} + 2)$  the equation (3.4.11) passes into (3.3.9). The differential equation (3.3.9) is solved by (3.3.11). The expression (3.3.11) for the virtual-mass coefficient is thereby derived directly from Hamilton's variational principle. The analysis shows again that void-fraction waves are dynamically allowed in a two-phase bubbly medium if and only if the virtual-mass coefficient satisfies (3.3.11).

### 3.5 Nonlinear void-fraction waves and bubble deformation

In Chapter II the equations of G (1985a) were extended to include the effect of bubble deformation and the energy associated with the surface tension of the gas bubbles. A linear stability analysis demonstrated that at marginal stability the virtual-mass coefficient  $m^*(\alpha, We)$  and the mass coefficient  $m(\alpha, We)$  take specific forms as functions of the void fraction and the Weber number (see expressions (2.4.31) and (2.4.32)). At marginal stability the drift velocity  $u_2$  of the gas bubbles becomes a triple root of the characteristic equation (dispersion equation). That root represents a linear bubble size wave (one root) and a linear void-fraction wave (two roots). We now wish to investigate whether the equations of motion presented in Chapter II allow nonlinear void-fraction waves as exact solutions and how bubble deformation and surface tension affect the relations given in sections 3.3 and 3.4. It is further analysed how the possible existence of nonlinear concentration waves is related to the functional form of the coefficient  $m(\alpha, We)$ .

A nonlinear void-fraction wave may be characterised by the properties (i) and (ii) given in section 3.3. Since the gas density is constant the gas pressure  $p_g$  can not vary and therefore the equivalent bubble volume  $\tau$  and the equivalent bubble radius  $a$  are constant as well. The mass conservation equations lead to (3.3.1) and (3.3.2) while equation (2.2.9), expressing the conservation of the number of bubbles, is satisfied when

$$n = \frac{1}{\tau} f(x - u_2 t), \quad (3.5.1)$$

which follows from  $\alpha = n\tau$ . Equation (2.2.9) and equation (3.2.3), expressing the conservation of mass for the gas phase, become dependent when  $\rho_g$  and  $\tau$  are constant. It follows from (3.3.2) and (2.2.7) that in the case of a nonlinear void-fraction wave the Weber number is given by

$$We = \frac{\eta_0}{(1 - \alpha)^2}, \quad (3.5.2)$$

where the constant  $\eta_0$  is equal to

$$\eta_0 = \frac{2a \rho_l c^2}{\gamma}. \quad (3.5.3)$$

In a similar way as in section 3.3 the Euler-Lagrange equations (2.2.13) to (2.2.17) are obviously satisfied, when

$$\varphi_i = \beta_i t - \nu_i x + \hat{\varphi}_i(x - u_2 t), \quad (i=1,2), \quad (3.5.4)$$

and

$$\lambda = \beta_3 t - \nu_3 x + \hat{\lambda}(x - u_2 t). \quad (3.5.5)$$

The constants  $\beta_i$  and  $\nu_i$ , ( $i=1,2,3$ ), are unknown. By introducing (3.5.4) into the Bernoulli equation (2.2.13) and using (2.2.16) it follows that

$$\begin{aligned} \mu_1 + \frac{1}{2} \left[ 1 + 2 \frac{m^*}{1 - \alpha} + m_\alpha + \frac{We}{3\alpha} m_{We} \right] (u_2 - u_1)^2 + \\ - \frac{1}{2} u_2^2 + c_1 = 0. \end{aligned} \quad (3.5.6)$$

By substituting (3.5.4) and (3.5.5), the Euler-Lagrange equations (2.2.14) and (2.2.15) reduce to, respectively,

$$\mu_2 - \frac{1}{2} u_2^2 + c_2 = 0 \quad (3.5.7)$$

and

$$\frac{\rho_\ell}{6n} \text{We} m_{\text{We}} (u_2 - u_1)^2 + c_3 = 0. \quad (3.5.8)$$

The constants  $c_i$  satisfy  $c_i = \beta_i - u_2 \nu_i$ , ( $i=1,2,3$ ). Equations (3.5.6) and (3.5.7) should be compared with, respectively, (3.3.4) and (3.3.5).

We further analyse equation (3.5.6). When the Weber number satisfies (3.5.2) the mass coefficient  $m(\alpha, \text{We})$  becomes a function of  $\alpha$  only, which we write as

$$\bar{m}(\alpha) = m(\alpha, \eta_0 / (1-\alpha)^2). \quad (3.5.9)$$

Since the derivative of that function obeys

$$\frac{d\bar{m}}{d\alpha} = m_\alpha + m_{\text{We}} \frac{2\eta_0}{(1-\alpha)^3} = m_\alpha + 2 \text{We} m_{\text{We}} \frac{1}{1-\alpha}, \quad (3.5.10)$$

equation (3.5.6) may take the form

$$\mu_1 + \frac{1}{2} \left[ 1 + 2 \frac{\bar{m}}{1-\alpha} + \frac{d\bar{m}}{d\alpha} \right] \frac{c^2}{(1-\alpha)^2} - \frac{c_3}{\rho_\ell \tau} - \frac{1}{2} u_2^2 + c_1 = 0, \quad (3.5.11)$$

where (2.2.8) and (3.5.8) have been used. By introducing  $\hat{m}_0$  according to

$$\mu_1 - \frac{1}{2} u_2^2 + \frac{1}{4} (\hat{m}_0 + 2) c^2 + c_1 - \frac{c_3}{\rho_\ell \tau} = 0, \quad (3.5.12)$$

relation (3.5.11) changes into

$$\frac{1}{2} \left[ 1 + 2 \frac{\bar{m}(\alpha)}{1-\alpha} + \frac{d\bar{m}(\alpha)}{d\alpha} \right] \frac{1}{(1-\alpha)^2} = \frac{1}{4} (\hat{m}_0 + 2), \quad (3.5.13)$$

a result similar to equation (3.3.7) for  $m(\alpha)$ . The solution of (3.5.13) satisfying  $\bar{m}(0) = 0$  is obviously given by



$$\bar{m}(\alpha) = \frac{1}{2} \alpha (1 - \alpha) (\hat{m}_0 - (\hat{m}_0 + 2) \alpha) . \quad (3.5.14)$$

It follows from (3.5.9) that  $\hat{m}_0$  may still be an arbitrary function of  $\eta_0 = We (1-\alpha)^2$ . By taking

$$C(We(1-\alpha)^2) = \frac{\hat{m}_0 + 2}{2} \quad (3.5.15)$$

it is seen that

$$m(\alpha, We) = \alpha (1 - \alpha) \{ (1-\alpha) C(We(1-\alpha)^2) - 1 \} . \quad (3.5.16)$$

Expression (3.5.16) is obtained from relation (2.4.31) for  $m(\alpha, We)$  by taking  $B = 0$  (since  $m(0, We) = 0$  must hold) and by including the term containing the constant  $A$  in the function  $C(\cdot)$ . We therefore conclude that the requirement of marginal stability and the existence of nonlinear void-fraction waves yield equivalent expressions for the mass coefficient  $m(\alpha, We)$ .

The same kinematic and dynamic quantities that were mentioned in section 3.3 become a linear function of the void fraction  $\alpha$  when the relations for a nonlinear void-fraction wave are used. The mass fluxes are not affected by the inclusion of bubble deformation effects and are given by (3.3.12) and (3.3.13). The generalised momenta  $\pi_1$  and  $\pi_2$  satisfy

$$\pi_1 = u_2 - c - \alpha \frac{1}{2} (\tilde{m}(\eta_0) + 2) c \quad (3.5.17)$$

and

$$\pi_2 = u_2 + \frac{\rho_\ell}{2\rho_g} \tilde{m}(\eta_0) c - \alpha \frac{\rho_\ell}{2\rho_g} (\tilde{m}(\eta_0) + 2) c . \quad (3.5.18)$$

When bubble deformation effects are accounted for the generalised momenta are defined by (3.2.14) and (3.2.15), where  $m(\alpha)$  must be replaced by the virtual-mass coefficient  $m^*(\alpha, We)$  (see the Euler-Lagrange equations (2.2.16) and (2.2.17)). As a result, (3.5.17) and (3.5.18) follow from (3.3.14) and (3.3.15) by substituting  $\tilde{m}(\eta_0) = \hat{m}_0(\eta_0) + \eta_0 \hat{m}'_0(\eta_0)$  for  $\hat{m}$ .

The function  $\tilde{m}(\eta)$  occurs in expression (2.4.35) for  $m^*(\alpha, We)$ . The momentum density  $P$  is given by (3.3.18) and the momentum flux  $\Pi$ , defined by (2.3.10), is determined according to

$$\begin{aligned} \Pi = \rho_{\ell} (u_2 - c)^2 + p_g + \frac{1}{4} \{ \hat{m}_0(\eta_0) + \frac{1}{3} \eta_0 \hat{m}'_0(\eta_0) \} \rho_{\ell} c^2 + \\ + \alpha (\rho_g - \rho_{\ell}) u_2^2, \end{aligned} \quad (3.5.19)$$

which generalises (3.3.19). The kinetic energy density  $K^*$  follows from (3.3.20) by replacing  $\hat{m}$  by  $\hat{m}(\eta_0)$  while the free energy density  $F^*$  is written as a linear function of  $\alpha$  by means of

$$F^* = \rho_{\ell} \mu_1 - p_g + \alpha (\rho_g \mu_2 - \rho_{\ell} \mu_1 + \frac{1}{4} \eta_0 \hat{m}'_0(\eta_0) \rho_{\ell} c^2). \quad (3.5.20)$$

$K^*$  and  $F^*$  are defined by (2.3.14) and (2.3.15) (see Chapter II). The pressure  $p$  (defined by (2.3.11)) satisfies

$$\begin{aligned} p = p_g + \frac{1}{4} \{ \hat{m}_0(\eta_0) + \frac{1}{3} \eta_0 \hat{m}'_0(\eta_0) \} \rho_{\ell} c^2 + \\ - \alpha \frac{1}{2} (\hat{m}(\eta_0) + 2) \rho_{\ell} c^2. \end{aligned} \quad (3.5.21)$$

It finally follows from (2.3.7) and (2.3.8) that the energy density and flux are given by

$$\begin{aligned} H = \frac{1}{2} \rho_{\ell} (u_2 - c)^2 + \rho_{\ell} \mu_1 - p_g + \\ + \alpha \{ \frac{1}{2} (\rho_g - \rho_{\ell}) u_2^2 + \frac{1}{4} (\hat{m}_0(\eta_0) + 2 \eta_0 \hat{m}'_0(\eta_0) + 2) \rho_{\ell} c^2 + \rho_g \mu_2 - \rho_{\ell} \mu_1 \} \end{aligned} \quad (3.5.22)$$

and

$$\begin{aligned} Q = \rho_{\ell} (u_2 - c) \{ \mu_1 + \frac{1}{2} (u_2 - c)^2 + \frac{1}{4} (\hat{m}_0(\eta_0) + \frac{1}{3} \eta_0 \hat{m}'_0(\eta_0)) c^2 \} + \\ + \alpha u_2 \{ \frac{1}{2} (\rho_g - \rho_{\ell}) u_2^2 + \frac{1}{4} (\hat{m}_0(\eta_0) + 2 \eta_0 \hat{m}'_0(\eta_0) + 2) \rho_{\ell} c^2 + \rho_g \mu_2 - \rho_{\ell} \mu_1 \}. \end{aligned} \quad (3.5.23)$$

It follows from (3.5.22) and (3.5.23) that equation (3.2.20), expressing the conservation of energy, reduces to

$$\frac{\partial \alpha}{\partial t} + u_2 \frac{\partial \alpha}{\partial x} = 0, \quad (3.5.24)$$

which is satisfied when  $\alpha = f(x - u_2 t)$ . As a result of (3.3.18) and (3.5.19) the equation for the conservation of momentum (3.2.16) reduces to (3.5.24) as well.

The Hamilton principle for a nonlinear concentration wave was treated in section 3.4. It will be clear that the extended variational principle, including bubble deformation effects as well as surface-tension energy, leads to expression (3.5.14) for  $\bar{m}(\alpha)$  in a similar way as expression (3.3.11) for  $m(\alpha)$  was derived in section 3.4.

### 3.6 Nonlinear void-fraction waves and gas motion inside bubbles

The two-phase flow equations developed by G (1985a) and the extended version presented in Chapter II account for the additional kinetic energy of the liquid phase resulting from a relative motion between the two phases. The additional kinetic energy of the gas, associated with the circulating motion of the gas inside the bubbles, has been neglected in both models. In the case of bubbly air/water mixtures the motion of the gas inside the bubbles does not make a substantial contribution to the total kinetic energy density due to the large difference between the values of the mass densities of both phases; it may therefore be omitted. However, when a bubbly mixture consisting of a heavy gas and a light liquid (compared to air and water) is considered it could become essential to include that effect. In the limit, where both phases have the same mass density, for example, Hill's spherical vortex may represent one of the possible flow structures inside the bubbles (see Batchelor 1967, p. 526, and Lamb 1945, p. 245). In the present section the macroscopic inclusion of the above mentioned effect is analysed. In addition, it is investigated how the flow induced motion of the gas inside the bubbles affects the equations of motion and the possible existence of nonlinear void-fraction waves.

The Lagrangian energy density  $L$  is defined by

$$L = K - F, \quad (3.6.1)$$

where the kinetic energy density  $K$  takes the form

$$K = \frac{1}{2} \rho_1 u_1^2 + \frac{1}{2} \rho_2 u_2^2 + \frac{1}{2} \{ \rho_l m(\alpha) + \rho_g k(\alpha) \} (u_2 - u_1)^2. \quad (3.6.2)$$

The mass coefficient  $k(\alpha)$  accounts for the motion of the gas inside the bubbles, in cases where the difference velocity does not vanish. The free energy density  $F$  satisfies the relations presented in section 3.2. The constraints (3.2.2) and (3.2.3), expressing the conservation of mass for the liquid and the gas phase, are included by means of the Lagrange multipliers  $\varphi_1$  and  $\varphi_2$ , and after partial integration the variational principle is transformed into

$$\delta \int_{t_1}^{t_2} dt \int_{x_1}^{x_2} dx L^* = 0, \tag{3.6.3}$$

where

$$L^* = L - \rho_1 \left[ \frac{\partial \varphi_1}{\partial t} + u_1 \frac{\partial \varphi_1}{\partial x} \right] - \rho_2 \left[ \frac{\partial \varphi_2}{\partial t} + u_2 \frac{\partial \varphi_2}{\partial x} \right] \tag{3.6.4}$$

(see section 1.6, Chapter I). The Euler–Lagrange equations following from (3.6.1) to (3.6.4) are written

$$\begin{aligned} \delta \rho_1: \frac{1}{2} u_1^2 - \frac{1}{2} \left\{ m'(\alpha) + \frac{\rho_g}{\rho_l} \left( k'(\alpha) - \frac{k(\alpha)}{\alpha} \right) \right\} (u_2 - u_1)^2 + \\ - \mu_1 - \frac{\partial \varphi_1}{\partial t} - u_1 \frac{\partial \varphi_1}{\partial x} = 0, \end{aligned} \tag{3.6.5}$$

$$\delta \rho_2: \frac{1}{2} u_2^2 + \frac{1}{2} \frac{k(\alpha)}{\alpha} (u_2 - u_1)^2 - \mu_2 - \frac{\partial \varphi_2}{\partial t} - u_2 \frac{\partial \varphi_2}{\partial x} = 0, \tag{3.6.6}$$

$$\delta u_1: \rho_1 u_1 - \left\{ \rho_l m(\alpha) + \rho_g k(\alpha) \right\} (u_2 - u_1) - \rho_1 \frac{\partial \varphi_1}{\partial x} = 0, \tag{3.6.7}$$

$$\delta u_2: \rho_2 u_2 + \left\{ \rho_l m(\alpha) + \rho_g k(\alpha) \right\} (u_2 - u_1) - \rho_2 \frac{\partial \varphi_2}{\partial x} = 0. \tag{3.6.8}$$

The equations of motion for the liquid and the gas phase are obtained by eliminating the potentials  $\varphi_1$  and  $\varphi_2$  from the Euler–Lagrange equations (3.6.5) to (3.6.8). They are written, respectively,

$$\begin{aligned}
 & \left[ \frac{\partial}{\partial t} + u_1 \frac{\partial}{\partial x} \right] \left\{ u_1 - \frac{\rho_\ell m(\alpha) + \rho_g k(\alpha)}{\rho_1} (u_2 - u_1) \right\} + \\
 & - \frac{\rho_\ell m(\alpha) + \rho_g k(\alpha)}{\rho_1} (u_2 - u_1) \frac{\partial u_1}{\partial x} + \\
 & + \frac{\partial}{\partial x} \left[ \frac{1}{2} \left\{ m'(\alpha) + \frac{\rho_g}{\rho_\ell} \left( k'(\alpha) - \frac{k(\alpha)}{\alpha} \right) \right\} (u_2 - u_1)^2 \right] = \\
 & = - \frac{1}{\rho_\ell} \frac{\partial p_g}{\partial x} \quad (3.6.9)
 \end{aligned}$$

and

$$\begin{aligned}
 & \left[ \frac{\partial}{\partial t} + u_2 \frac{\partial}{\partial x} \right] \left\{ u_2 + \frac{\rho_\ell m(\alpha) + \rho_g k(\alpha)}{\rho_2} (u_2 - u_1) \right\} + \\
 & + \frac{\rho_\ell m(\alpha) + \rho_g k(\alpha)}{\rho_2} (u_2 - u_1) \frac{\partial u_2}{\partial x} - \frac{\partial}{\partial x} \left[ \frac{1}{2} \frac{k(\alpha)}{\alpha} (u_2 - u_1)^2 \right] = \\
 & = - \frac{1}{\rho_g} \frac{\partial p_g}{\partial x} \quad (3.6.10)
 \end{aligned}$$

The generalised momenta per unit mass  $\pi_1$  and  $\pi_2$  are given by

$$\pi_1 = u_1 - \frac{\rho_\ell m(\alpha) + \rho_g k(\alpha)}{\rho_1} (u_2 - u_1) \quad (3.6.11)$$

and

$$\pi_2 = u_2 + \frac{\rho_\ell m(\alpha) + \rho_g k(\alpha)}{\rho_2} (u_2 - u_1) \quad (3.6.12)$$

Noether's theorem (see section 2.3, Chapter II) yields expression (3.2.17) for the momentum density P and

$$\Pi = \rho_1 u_1^2 + \rho_2 u_2^2 + \{ \rho_\ell m(\alpha) + \rho_g k(\alpha) \} (u_2 - u_1)^2 + p \quad (3.6.13)$$

for the momentum flux  $\Pi$ . The hydrodynamic pressure  $p$  is written

$$p = p_g + \frac{1}{2} \{ \rho_\ell [ m(\alpha) + (1-\alpha) m'(\alpha) ] + \rho_g [ (1-\alpha) k'(\alpha) - \frac{1-\alpha}{\alpha} k(\alpha) ] \} (u_2 - u_1)^2. \quad (3.6.14)$$

The energy density  $H$  satisfies (3.2.21),  $K$  is determined by (3.6.2), while the energy flux  $Q$  is now given according to

$$Q = \rho_1 u_1 \left\{ \frac{1}{2} u_1^2 - \frac{\rho_\ell m(\alpha) + \rho_g k(\alpha)}{\rho_1} u_1 (u_2 - u_1) + \mu_1 + \frac{1}{2} \left\{ m'(\alpha) + \frac{\rho_g}{\rho_\ell} \left( k'(\alpha) - \frac{k(\alpha)}{\alpha} \right) \right\} (u_2 - u_1)^2 \right\} + \rho_2 u_2 \left\{ \frac{1}{2} u_2^2 + \frac{\rho_\ell m(\alpha) + \rho_g k(\alpha)}{\rho_2} u_2 (u_2 - u_1) + \mu_2 - \frac{1}{2} \frac{k(\alpha)}{\alpha} (u_2 - u_1)^2 \right\}. \quad (3.6.15)$$

The equations (3.2.16) and (3.2.20), expressing the conservation of linear momentum and the conservation of energy, obviously remain valid for the present case.

The properties (i) and (ii) which were first mentioned in section 3.3 and characterise a nonlinear void-fraction wave again lead to expression (3.3.3) for the potentials  $\varphi_1$  and  $\varphi_2$ . With the use of that relation the Bernoulli equation (3.6.5) may be written

$$\mu_1 + \frac{1}{2} \left[ 1 + 2 \frac{m(\alpha)}{1-\alpha} + m'(\alpha) \right] (u_2 - u_1)^2 + \frac{\rho_g}{2\rho_\ell} \left[ \frac{3\alpha - 1}{\alpha(1-\alpha)} k(\alpha) + k'(\alpha) \right] (u_2 - u_1)^2 - \frac{1}{2} u_2^2 + c_1 = 0, \quad (3.6.16)$$

while the Euler-Lagrange equation (3.6.6) for the gas phase reduces to

$$\mu_2 - \frac{1}{2} \frac{k(\alpha)}{\alpha} (u_2 - u_1)^2 - \frac{1}{2} u_2^2 + c_2 = 0. \quad (3.6.17)$$

By substituting (3.3.2) into (3.6.17) it follows that the mass coefficient  $k(\alpha)$  must take the form

$$k(\alpha) = \hat{k} \alpha (1 - \alpha)^2 \quad (3.6.18)$$

to allow a nonlinear concentration wave as an exact solution of the equations of motion. In that case, the constant  $c_2$  follows from

$$\mu_2 - \frac{1}{2} \hat{k} c^2 - \frac{1}{2} u_2^2 + c_2 = 0. \quad (3.6.19)$$

The kinetic energy of the gas inside the bubbles as a result of the relative motion between the phases should determine the value of the constant  $\hat{k}$  (compare with  $\hat{m}$  which occurs in expression (3.3.11) for  $m(\alpha)$ ). Since (3.6.18) constitutes the general solution of the differential equation

$$\frac{3\alpha - 1}{\alpha (1 - \alpha)} k(\alpha) + k'(\alpha) = 0, \quad (3.6.20)$$

relation (3.6.16) changes into (3.3.4), which determines the virtual-mass coefficient  $m(\alpha)$  by means of (3.3.11). It may therefore be concluded that the additional inclusion of the kinetic energy associated with the gas circulating inside the bubbles as a result of the relative motion between the phases still allows the existence of nonlinear concentration waves. That conclusion also applies to the situation where the value of the mass density of the fluid contained by the bubbles is comparable to the value of the mass density of the surrounding fluid. In the limit that the mass densities are equal, the value of  $\hat{k}$  may be determined by assuming the occurrence of Hill's spherical vortex inside each bubble (droplet). The vortex energy  $(10/7) \pi a^3 \rho U^2$  (see Lamb 1945, p. 246) yields the value  $\hat{k} = 15/7$ ;  $\rho$  denotes the mass density and  $U$  the velocity of the bubble relative to the surrounding fluid. Chaabane (1989) found the same expressions for  $m(\alpha)$  and  $k(\alpha)$  by means of an extensive and elaborate linear stability analysis of a solution of the equations of motion representing uniform two-phase flow.

Finally, we restrict ourselves to mentioning that the expressions for  $m(\alpha)$  and  $k(\alpha)$  may also be derived from Hamilton's principle for a nonlinear void-fraction wave (see section 3.4) and conclude the present section by briefly listing the linear behaviour in  $\alpha$  of several physical quantities. In the case of a nonlinear concentration wave the generalised momenta per unit mass  $\pi_1$  and  $\pi_2$ , defined by (3.6.11) and (3.6.12), behave as

$$\pi_1 = u_2 - c - \alpha \left\{ \frac{1}{2} (\hat{m} + 2) + \frac{\rho_g}{\rho_\ell} \hat{k} \right\} c \quad (3.6.21)$$

and

$$\pi_2 = u_2 + \left\{ \frac{\rho_\ell}{2\rho_g} \hat{m} + \hat{k} \right\} c - \alpha \left\{ \frac{\rho_\ell}{2\rho_g} (\hat{m} + 2) + \hat{k} \right\} c. \quad (3.6.22)$$

The constant  $\hat{k}$  does not enter the momentum density and flux  $P$  and  $\Pi$ , which remain to be given by (3.3.18) and (3.3.19). The kinetic energy density  $K$  reads

$$K = \frac{1}{2} \rho_\ell (u_2 - c)^2 + \alpha \left[ \frac{1}{2} (\rho_g - \rho_\ell) u_2^2 + \left\{ \frac{1}{4} (\hat{m} + 2) + \frac{1}{2} \frac{\rho_g}{\rho_\ell} \hat{k} \right\} \rho_\ell c^2 \right], \quad (3.6.23)$$

while the free energy density  $F$  is still given by (3.3.21). The pressure  $p$  takes the form

$$p = p_g + \frac{1}{4} \hat{m} \rho_\ell c^2 - \alpha \left\{ \frac{1}{2} (\hat{m} + 2) + \frac{\rho_g}{\rho_\ell} \hat{k} \right\} \rho_\ell c^2. \quad (3.6.24)$$

The energy density and flux  $H$  and  $Q$  are written

$$H = \frac{1}{2} \rho_\ell (u_2 - c)^2 + \rho_\ell \mu_1 - p_g + \alpha \left[ \frac{1}{2} (\rho_g - \rho_\ell) u_2^2 + \left\{ \frac{1}{4} (\hat{m} + 2) + \frac{1}{2} \frac{\rho_g}{\rho_\ell} \hat{k} \right\} \rho_\ell c^2 + \rho_g \mu_2 - \rho_\ell \mu_1 \right] \quad (3.6.25)$$

and



$$\begin{aligned}
 Q = & \rho_\ell (u_2 - c) \left\{ \mu_1 + \frac{1}{2} (u_2 - c)^2 + \frac{1}{4} \hat{m} c^2 \right\} + \\
 & + \alpha u_2 \left[ \frac{1}{2} (\rho_g - \rho_\ell) u_2^2 + \left\{ \frac{1}{4} (\hat{m} + 2) + \frac{1}{2} \frac{\rho_g}{\rho_\ell} \hat{k} \right\} \rho_\ell c^2 + \right. \\
 & \left. + \rho_g \mu_2 - \rho_\ell \mu_1 \right]. \tag{3.6.26}
 \end{aligned}$$

### 3.7 Conclusions

Nonlinear void-fraction waves were characterised by properties (i) and (ii) in section 3.3. They require that the gas density  $\rho_g$  and the gas velocity  $u_2$  are constant. The other physical quantities, viz., the void fraction  $\alpha$ , the liquid velocity  $u_1$  and the bubble number density  $n$ , are determined as functions of position and time by the kinematic equations expressing the conservation of mass and the conservation of the number of bubbles. Void-fraction waves therefore constitute *kinematic* waves. The concept of a kinematic wave was introduced by Lighthill & Whitham (1955). Kinematic waves are also discussed in Whitham (1974). Since the physical variable  $\mathbf{z} = (\rho_1, \rho_2, n, u_1, u_2)^T$  may be written as a function of  $\alpha$  only, according to the properties (i) and (ii) mentioned above and the relations (3.3.1), (3.3.2) and (3.5.1), void-fraction waves belong to the class of generalised simple waves in the sense of Jeffrey (1976). By giving  $f(\cdot)$  in (3.3.1) and (3.5.1) the form of a step function, it is seen that concentration waves may also occur as contact discontinuities.

We have shown that a two-phase bubbly medium does not admit void-fraction waves under all circumstances. In fact, kinematic void-fraction waves are *dynamically* possible if and only if the local distribution of the gas bubbles satisfies a certain condition. That condition is expressed by the particular form (3.3.11) of the virtual-mass coefficient  $m(\alpha)$  as a function of the volume density  $\alpha$  of the gas bubbles. The 'microscopic' distribution of gas bubbles that underlies the expression (3.3.11) for the 'macroscopic' quantity  $m(\alpha)$  is not known. It may be asserted, however, that the distribution is not random (see G (1985a)). In the case that bubble deformation effects and surface tension are included the above mentioned condition yields expression (2.4.31) for the coefficient  $m(\alpha, We)$  (with  $B = 0$ ) as a function of  $\alpha$  and the Weber number  $We$ . In the case that the flow induced motion of the gas inside the bubbles is accounted for the condition leads to the functional relation (3.6.18) for the coefficient  $k(\alpha)$ .

The expression (3.3.11) for the virtual-mass coefficient changes sign at  $\alpha = \alpha_c$ , where  $\alpha_c = \hat{m}/(\hat{m}+2)$ . In the case of spherical bubbles ( $\hat{m} = 1$ ) the critical value  $\alpha_c$  is given by  $\alpha_c = 1/3$ . The change of sign of  $m(\alpha)$  may be related to the breakdown of bubbly flow, which is observed at values of the void-fraction near 0.3 (see e.g. Matuszkiewicz et al. 1987).

The analysis shows that nonlinear void-fraction waves are not affected by a change of sign of  $m(\alpha)$ . The acoustic waves, however, are influenced strongly. According to G (1985a) the phase velocity of the acoustic linear mode becomes infinitely large near  $\alpha = \alpha_c$ . It should be observed that acoustic waves, no less than void-fraction waves, give rise to perturbations of the void fraction  $\alpha$ .

The stability of nonlinear void-fraction waves is investigated numerically in Chapter IV according to some well-defined initial-value problem: the interaction with an acoustic disturbance. Computations with high Courant numbers are performed to investigate the behaviour of the disturbed void-fraction wave on a large time scale.

## CHAPTER IV

# NUMERICAL AND ANALYTICAL INVESTIGATION OF WAVES AND WAVE-INTERACTIONS IN BUBBLY TWO-PHASE FLOW †)

### 4.1 Introduction

A mathematical description of the dynamical behaviour of bubbly liquid/gas mixtures is indispensable for the correct understanding of a variety of industrial processes. Several mathematical techniques and physical models have been used for the derivation of macroscopic two-phase flow equations. As a result of the complicated nature of that type of flow many models now exist which are essentially different (see, for example, the models treated in Chapter I).

Several bubbly flow models suffer from complex characteristics. They accordingly lead to ill-posed initial-value problems and give rise to numerical instabilities. In Geurst (1985a)<sup>‡)</sup> it is shown that the appropriate inclusion of virtual-mass terms is sufficient in order to arrive at two-phase flow equations having real characteristics. The corresponding set of equations (called model 1) and an extended version (called model 2) which is treated in Chapter II, including flow induced bubble deformation, are studied in the present chapter. Our purpose here is to investigate whether the two models are suitable for producing stable and reliable numerical results. The models allow fast acoustic waves and slow void-fraction waves. A code has to be developed which can efficiently cope with steady and unsteady situations at the same time. The numerical method should therefore be implicit and time accurate. Possible steady states are then obtained by time iteration at high Courant numbers. In addition the two models turn out to be hyperbolic in a very specific sense. This fact has important consequences for the selection of the appropriate method. A method that has proved to be both robust and promising in gas dynamic computations is the one based on

---

†) *Parts of this chapter were presented at the XVII<sup>th</sup> International Congress of Theoretical and Applied Mechanics, August 1988, Grenoble, France. See Vreenegoor & Geurst (1988) and Vreenegoor, Wilders & Geurst (1988).*

‡) *Hereafter referred to as G (1985a).*

a scheme proposed by Lerat (1985). That scheme is applied for the numerical integration of the two-phase flow equations of model 1 and model 2.

In addition, we want to investigate whether the phenomena observed in the numerical computations are supported by linear theory. Agreement may contribute to the reliability of the numerical method. The equations of model 1 are linearised and the right eigenvectors are determined so that linear initial-value problems may be solved. The derivation of the eigenvectors and the general solution of the linearised equations bring about some typical aspects of model 1, which may be investigated numerically as well.

In Chapter III it was shown that both models possess a class of non-linear exact solutions. The solutions were analysed in some detail and interpreted as nonlinear void-fraction waves. The investigation of nonlinear void-fraction waves is continued here numerically.

In section 4.2 a brief account is given of the dimensionless equations governing bubbly two-phase flow. The equations presented in G (1985a) and in Chapter II are not ready for numerical computations. It is possible, however, to formulate equivalent sets of equations, which have the desired properties. The eigenvalues and right eigenvectors are presented in section 4.3. Section 4.4 deals with Lerat's scheme and the results of several numerical experiments. The performance of the scheme is tested, the interaction of acoustic waves and nonlinear concentration waves is computed and the stability of the void-fraction waves is investigated by performing computations with high Courant numbers. Section 4.5 contains the results which follow from linear theory. A comparison is made with the numerical results. The acoustics of a bubbly liquid/gas medium is derived from a variational principle.

The reader is warned that all formulas in the present chapter are expressed in dimensionless physical variables to avoid an additional notation and to facilitate the comparison with the numerical computations.

## 4.2 Flow equations

When the equations derived in G (1985a) (see also section 1.6 of Chapter I) are made dimensionless (model 1), they are given by

$$\frac{\partial \rho_1}{\partial t} + \frac{\partial}{\partial x} (\rho_1 u_1) = 0, \quad (4.2.1)$$

$$\frac{\partial \rho_2}{\partial t} + \frac{\partial}{\partial x} (\rho_2 u_2) = 0, \quad (4.2.2)$$

$$\begin{aligned} & \frac{\partial}{\partial t} \left[ u_1 - \frac{m(\alpha)}{\rho_1} (u_2 - u_1) \right] + \\ & + \frac{\partial}{\partial x} \left[ \frac{1}{2} u_1^2 - \frac{m(\alpha)}{\rho_1} (u_2 - u_1) u_1 + \rho_g + \frac{1}{2} m'(\alpha) (u_2 - u_1)^2 \right] = 0, \end{aligned} \quad (4.2.3)$$

$$\begin{aligned} & \frac{\partial}{\partial t} \left[ u_2 + \frac{m(\alpha)}{\rho_2} (u_2 - u_1) \right] + \\ & + \frac{\partial}{\partial x} \left[ \frac{1}{2} u_2^2 + \frac{m(\alpha)}{\rho_2} (u_2 - u_1) u_2 + \ln(\rho_g) \right] = 0. \end{aligned} \quad (4.2.4)$$

The mass densities are made dimensionless by means of the constant mass density  $\rho_\ell$  of the liquid, the velocities by means of the isothermal acoustic velocity  $U_0$  of the gas, which is determined by  $U_0 = (RT/M)^{\frac{1}{2}}$ . Note that  $R$  is the gas constant, while  $M$  denotes the molecular mass of the gas. The pipe length  $L_0$  is used to non-dimensionalise the space variable  $x$ . The time variable is accordingly made dimensionless by means of  $L_0/U_0$ . The reduced mass density of the liquid phase is denoted by  $\rho_1 = 1 - \alpha$ , the reduced mass density of the gas by  $\rho_2 = \alpha \rho_g$ , where  $\alpha$  represents the void fraction and  $\rho_g$  is the dimensionless mass density of the pure gas. A uniform two-phase flow is, according to G (1985a), marginally stable if and only if the virtual-mass coefficient  $m(\alpha)$  takes the form

$$m(\alpha) = \frac{1}{2} \hat{m} \alpha (1 - \alpha) \left( 1 - \frac{\hat{m} + 1}{\hat{m}} \alpha \right). \quad (4.2.5)$$

The derivative  $(d/d\alpha)m(\alpha)$  is denoted by  $m'(\alpha)$ . Note that  $\hat{m} = 1$ , when the bubbles have a spherical shape. Expression (4.2.5) for the virtual-mass coefficient allows the existence of nonlinear void-fraction waves (see Chapter III). Model 1 is evidently characterised by the

two mass-conservation equations (4.2.1) and (4.2.2) and the two equations of motion (4.2.3) and (4.2.4).

The system of equations (4.2.1) to (4.2.4) has the general conservation form

$$\frac{\partial \mathbf{q}}{\partial t} + \frac{\partial \mathbf{g}(\mathbf{q})}{\partial x} = 0, \quad (4.2.6)$$

where  $\mathbf{q} \in \mathbb{R}^m$ ,  $\mathbf{g}: \mathbb{R}^m \rightarrow \mathbb{R}^m$  and  $m=4$ . The conserved variable  $\mathbf{q}$  and its corresponding flux  $\mathbf{g}$  are given as vector functions of the physical variable  $\mathbf{z} \in \mathbb{R}^m$  where  $\mathbf{z} = (\rho_1, \rho_2, u_1, u_2)^T$ . If  $|\partial \mathbf{q} / \partial \mathbf{z}| \neq 0$ , the physical variable clearly satisfies the system of equations

$$\frac{\partial \mathbf{z}}{\partial x} + \mathbf{A} \frac{\partial \mathbf{z}}{\partial x} = 0, \quad (4.2.7)$$

where  $\mathbf{A} = (\partial \mathbf{q} / \partial \mathbf{z})^{-1} (\partial \mathbf{g} / \partial \mathbf{q}) (\partial \mathbf{q} / \partial \mathbf{z})$ . The conservation form (4.2.6) of the equations should be preferred, however, since it facilitates the formulation of conservative numerical schemes. It will be clear that a transformation from  $\mathbf{z}$  to  $\mathbf{q}$  is needed in that case. Details on the transformation may be found in subsection 4.4.1.

The variational analysis presented in G (1985a) is extended in Chapter II by including surface tension and flow induced bubble deformation. The corresponding equations constitute model 2. They contain as additional variables the equivalent bubble radius  $a$  and the bubble number density  $n = \alpha / \tau$ , where  $\tau$  represents the local average of the bubble volume  $4\pi a^3/3$ . When all physical quantities are made dimensionless in a similar way as for model 1, the five equations of model 2 are given by the two mass-conservation equations (4.2.1), (4.2.2), the equation for the conservation of bubble number density

$$\frac{\partial n}{\partial t} + \frac{\partial}{\partial x} (n u_2) = 0 \quad (4.2.8)$$

and the two equations of motion

$$\begin{aligned} \frac{\partial}{\partial t} \left[ u_1 - \frac{m^*}{\rho_1} (u_2 - u_1) \right] + \frac{\partial}{\partial x} \left[ \frac{1}{2} u_1^2 - \frac{m^*}{\rho_1} (u_2 - u_1) u_1 + \rho_g + \right. \\ \left. + \frac{1}{2} \left( m_\alpha + \frac{We}{3\alpha} m_{We} \right) (u_2 - u_1)^2 \right] = 0, \quad (4.2.9) \end{aligned}$$

$$\frac{\partial}{\partial t} [\rho_1 u_1 + \rho_2 u_2] + \frac{\partial}{\partial x} \left[ \rho_1 u_1^2 + \rho_2 u_2^2 + \rho_g + \right. \\ \left. + \frac{1}{2} (2m^* + m + (1-\alpha)m_\alpha + \frac{We}{3\alpha} m_{We}) (u_2 - u_1)^2 \right] = 0. \quad (4.2.10)$$

In dimensionless variables the Weber number  $We$  is defined by

$$We = \beta a (u_2 - u_1)^2, \quad (4.2.11)$$

where  $\beta = 2 \rho_l U_0^2 L_0 / \gamma$ , while  $\gamma$  denotes the surface tension coefficient. Note that  $m_\alpha$  and  $m_{We}$  represent the partial derivatives  $(\partial/\partial\alpha)m(\alpha, We)$  and  $(\partial/\partial We)m(\alpha, We)$ . At marginal stability the virtual-mass coefficient  $m^* = m^*(\alpha, We)$  and the mass coefficient  $m = m(\alpha, We)$  are determined by (2.5.13) and (2.5.14), where the coefficients  $b_k$ , ( $k=1, \dots, 4$ ), are given by (2.5.6).

Equation (4.2.8) which expresses the conservation of the number of bubbles implies that the coalescence and fragmentation of bubbles are neglected. Equation (4.2.9) represents the equation of motion for the liquid. In order to put the set of equations of model 2 in conservation form the equation of motion for the gas phase is replaced by equation (4.2.10), which expresses the conservation of total linear momentum. The use of the equation for the conservation of energy should be avoided, since it may lead to singularities in the transformation from the conserved variable  $q$  to the physical variable  $z$  (see subsection 4.4.1).

### 4.3 Some remarks on stability

#### 4.3.1 Eigenvalues and eigenvectors

The virtual-mass coefficient should take a non-negative value. A negative value would yield a negative additional contribution to the kinetic energy density which can not be allowed. It follows from (4.2.5) and (2.5.14) that the virtual-mass coefficient becomes negative when  $\alpha$  surpasses a critical value  $\alpha_c$ . In the case of model 1 that value is given by  $\alpha_c = 1/3$  (spherical bubbles) and in the case of model 2 it is determined by  $\alpha_c = 1/3 + (1/60)We + O(We^2)$  (see (2.6.6)). It is therefore concluded that bubbly flow is not possible at void fractions  $\alpha > \alpha_c$ . At  $\alpha = \alpha_c$  a transition to a different type of two-phase flow may be expected. As a

consequence, both models should only be applied to bubbly flows for which the void fraction is smaller than the critical void fraction.

It turns out that the matrix  $\mathbf{A}$  in (4.2.7) is well defined for  $\alpha < \alpha_c$  since the Jacobian determinants  $|\partial \mathbf{q} / \partial \mathbf{z}|$  for model 1 and model 2, given, respectively, by

$$|\partial \mathbf{q} / \partial \mathbf{z}| = 1 + \left( \frac{1}{\rho_1} + \frac{1}{\rho_2} \right) m(\alpha) \quad (4.3.1.1)$$

and

$$|\partial \mathbf{q} / \partial \mathbf{z}| = \rho_2 \left\{ 1 + \left( \frac{1}{\rho_1} + \frac{1}{\rho_2} \right) (m^* + 2We m^* We) \right\}, \quad (4.3.1.2)$$

are positive for positive values of the virtual-mass coefficients  $m(\alpha)$  and  $m^*(\alpha, We)$ . The eigenvalues of  $\mathbf{A}$  are real. They read

$$\lambda_1 = u_2 + a_1,$$

$$\lambda_2 = u_2 + a_2, \quad (4.3.1.3)$$

$$\lambda_3 = \lambda_4 = \lambda_5 = u_2.$$

The acoustic modes are represented by  $\lambda_1$  and  $\lambda_2$ . The eigenvalue equal to the gas velocity  $u_2$  is a multiple one, two-fold for model 1 and three-fold for model 2. In a first order of approximation with respect to the Weber number the dimensionless acoustic velocities  $a_1$  and  $a_2$  follow from (2.6.1) to (2.6.4). They are determined by the quadratic equation

$$c_2 a_k^2 + c_1 a_k + c_0 = 0, \quad (k=1,2), \quad (4.3.1.4)$$

where

$$c_2 = 1 - 3\alpha + 3b_1 \rho_1^3 We + \rho_g (2 + 3\alpha + 3b_1 \alpha \rho_1^2 We) + O(We^2), \quad (4.3.1.5)$$

$$c_1 = \left\{ 2\rho_g \left( 3 + \frac{4}{3} b_1 \rho_1^2 We \right) + \frac{10}{3} b_1 \rho_1^2 We \right\} \rho_1 w + O(We^2), \quad (4.3.1.6)$$



$$c_0 = -\frac{1}{\alpha} \left\{ \frac{1}{2} \rho_1^2 w^2 \left[ 1 + \frac{4}{3} b_1 \rho_1^2 \text{We} \right]^2 + \left[ \rho_g - \left( \frac{1}{18} b_1 \rho_1^4 \text{We} + \frac{4}{3\text{We}} \right) w^2 \right] \times \right. \\ \left. \times \left[ 1 + 2\rho_g + 3b_1 \rho_1^2 \text{We} \right] \right\} + O(\text{We}^2) \quad (4.3.1.7)$$

and the constant  $b_1$  takes the value 27/160 (see (2.A.1)). We recall that  $w$  denotes the steady-state value of the relative velocity  $u_2 - u_1$ . The dimensionless acoustic phase velocities of model 1 are obtained from (4.3.1.4) to (4.3.1.7) by deleting the terms, which depend on the Weber number  $\text{We}$ .

Model 1 will be analysed here in more detail by deriving the right eigenvectors and constructing the general solution of the linearised equations of model 1. The acoustic right eigenvectors, corresponding to the eigenvalues  $\lambda_k = u_2 + a_k$ , ( $k=1,2$ ), are given by

$$\mathbf{r}_k = \left( - \left[ \frac{1}{2} \rho_1 w - \left( \frac{1}{2} (1-3\alpha) + \rho_g \right) a_k \right] \rho_1, \frac{1}{2} \rho_1 \left( \frac{\rho_1 w}{\alpha} + 3a_k \right) \rho_2, \right. \\ \left. - \left[ \frac{1}{2} \rho_1 w - \left( \frac{1}{2} (1-3\alpha) + \rho_g \right) a_k \right] (w + a_k), \frac{1}{2} \rho_1 \left( \frac{\rho_1 w}{\alpha} + 3a_k \right) a_k \right)^T, \\ (k=1,2). \quad (4.3.1.8)$$

Only one independent eigenvector  $\mathbf{r}_3$  corresponds to the two-fold eigenvalue  $\lambda_3 = \lambda_4 = u_2$ . It is represented by

$$\mathbf{r}_3 = \left( 1, -\rho_g, \frac{w}{\rho_1}, 0 \right)^T. \quad (4.3.1.9)$$

The generalised eigenvector  $\mathbf{r}_4$ , which satisfies

$$\mathbf{A} \mathbf{r}_4 = \lambda_4 \mathbf{r}_4 + \mathbf{r}_3, \quad (4.3.1.10)$$

is given by

$$\mathbf{r}_4 = \left( 0, \frac{1}{2} \rho_1 w, \frac{1}{\rho_1}, -\frac{1}{\alpha} \right)^T. \quad (4.3.1.11)$$

Note that the eigenvalues and corresponding eigenvectors are presented in dimensionless form. The matrix  $\mathbf{A}$  is obviously defect. Model 1 is not hyperbolic since there is no complete set of eigenvectors. As a consequence, model 1 can not be written in characteristic form. We

also remark that the characteristic field related to  $\lambda_3$  and  $\lambda_4$  is linearly degenerate in the sense of Lax (1973), which allows contact discontinuities to occur as solutions. In the previous chapter it was already mentioned that concentration waves may appear in the form of contact discontinuities.

When we substitute  $\mathbf{z} = \mathbf{z}_0 + \hat{\mathbf{z}}$  into (4.2.1) to (4.2.4), the linearised equations of model 1 are written

$$\frac{\partial \hat{\rho}_1}{\partial t} + \frac{\partial}{\partial x} \{ \rho_1 \hat{u}_1 + u_1 \hat{\rho}_1 \} = 0, \quad (4.3.1.12)$$

$$\frac{\partial \hat{\rho}_2}{\partial t} + \frac{\partial}{\partial x} \{ \rho_2 \hat{u}_2 + u_2 \hat{\rho}_2 \} = 0, \quad (4.3.1.13)$$

$$\begin{aligned} \frac{\partial}{\partial t} \left\{ \left(1 + \frac{m}{\rho_1}\right) \hat{u}_1 - \frac{m}{\rho_1} \hat{u}_2 + \left(\frac{m}{\rho_1}\right)' w \hat{\rho}_1 \right\} + \\ \frac{\partial}{\partial x} \left\{ \left[\left(1 + \frac{m}{\rho_1}\right) u_1 - \rho_1 \left(\frac{m}{\rho_1}\right)' w\right] \hat{u}_1 + \left[m' w - \frac{m}{\rho_1} u_1\right] \hat{u}_2 + \hat{\rho}_g + \right. \\ \left. + \left[\left(\frac{m}{\rho_1}\right)' w u_1 - \frac{1}{2} m' w^2\right] \hat{\rho}_1 \right\} = 0, \end{aligned} \quad (4.3.1.14)$$

$$\begin{aligned} \frac{\partial}{\partial t} \left\{ -\frac{m}{\rho_2} \hat{u}_1 + \left(1 + \frac{m}{\rho_2}\right) \hat{u}_2 - \frac{m' w}{\rho_2} \hat{\rho}_1 - \frac{m w}{\rho_2^2} \hat{\rho}_2 \right\} + \\ \frac{\partial}{\partial x} \left\{ -\frac{m}{\rho_2} u_2 \hat{u}_1 + \left[\left(1 + \frac{m}{\rho_2}\right) u_2 + \frac{m w}{\rho_2}\right] \hat{u}_2 - \frac{m' w}{\rho_2} u_2 \hat{\rho}_1 + \right. \\ \left. - \frac{m w}{\rho_2^2} u_2 \hat{\rho}_2 + \frac{1}{\rho_g} \hat{\rho}_g \right\} = 0. \end{aligned} \quad (4.3.1.15)$$

The subscripts zero indicating steady-state values have been omitted while a prime denotes differentiation with respect to the void fraction  $\alpha$ . In short form those equations may be written as

$$\frac{\partial \hat{\mathbf{z}}}{\partial t} + \mathbf{A}_0 \frac{\partial \hat{\mathbf{z}}}{\partial x} = \mathbf{0}, \quad (4.3.1.16)$$

which is the linearised version of equation (4.2.7).  $\mathbf{A}_0 = \mathbf{A}(\mathbf{z}_0)$  has the eigenvalues  $\lambda_{k0} = \lambda_k(\mathbf{z}_0)$  and the eigenvectors  $\mathbf{r}_{k0} = \mathbf{r}_k(\mathbf{z}_0)$ , ( $k=1, \dots, 4$ ). The general solution of system (4.3.1.16) is constructed by combining the eigenvectors and eigenvalues to form the superposition of four independent solutions. It is determined by

$$\hat{\mathbf{z}}(x, t) = \sum_{k=1}^4 [ f_k(x - \lambda_k t) \mathbf{r}_k ] - t f_4(x - \lambda_4 t) \mathbf{r}_3, \quad (4.3.1.17)$$

where  $f_k(\cdot)$ , ( $k=1, \dots, 4$ ), are arbitrary functions and  $f_4'(\xi)$  denotes  $(d/d\xi)f_4(\xi)$ . In (4.3.1.17) the subscripts zero have been omitted as well. In the case of a strictly hyperbolic set of equations the general solution would obviously be given by just the first part of the right-hand side of (4.3.1.17), containing the summation. The second part, growing linearly in time along a  $\lambda = u_2$  characteristic, exists as a result of the deficiency of the matrix  $\mathbf{A}_0$ .

The linear growth property requires some comment. It may be clarified by considering the wave equation

$$\varphi_{tt} - \epsilon^2 \varphi_{xx} = 0 \quad (4.3.1.18)$$

for  $\varphi = \varphi(x, t)$ . The general solution of (4.3.1.18) is given by

$$\varphi(x, t) = h_1(x - \epsilon t) + h_2(x + \epsilon t), \quad (4.3.1.19)$$

where  $h_1(\cdot)$  and  $h_2(\cdot)$  are arbitrary functions. However, when the characteristic roots  $\lambda_{1,2} = \pm \epsilon$  coincide ( $\epsilon = 0$ ), the wave equation degenerates to

$$\varphi_{tt} = 0 \quad (4.3.1.20)$$

with the general solution

$$\varphi(x, t) = h_1(x) + t h_2(x), \quad (4.3.1.21)$$

demonstrating the linear behaviour in  $t$  along the multiple  $\lambda = 0$  characteristic. When dissipative effects are introduced in the model described by (4.3.1.20), they may be expected to appear as higher order spatial derivatives, thereby allowing solutions which decay exponentially in time. We therefore see that the occurrence of solutions growing linearly in time in an inviscid theory for bubbly two-phase flow does not present a fundamental

difficulty. It may be removed by means of the inclusion of dissipative terms. In addition, the linear growth in time is only present in the marginally stable case, obtained by choosing the virtual-mass coefficient  $m(\alpha)$  of the form given by (4.3.2.1) (see the next subsection) with  $p_1 = p_2 = 0$ . When the marginally stable equilibrium is disturbed by giving  $p_1$  and  $p_2$  values which slightly differ from zero, the coinciding roots may split into two distinct real roots, thus yielding a strictly hyperbolic system of equations with a complete set of eigenvectors. Finally dispersive terms like the one considered in Chapter V, may provide for strictly stable behaviour. It is therefore concluded that in practice there may be various effects which suppress the linear growth property.

### 4.3.2 Effect of the functional form of $m(\alpha)$ on the eigenvalues of model 1

By writing the virtual-mass coefficient  $m(\alpha)$  in the form

$$m(\alpha) = \frac{1}{2} \alpha + (p_1 - 2) \alpha^2 + (p_2 + 3/2) \alpha^3 \quad (4.3.2.1)$$

and assuming that  $p_1$  and  $p_2$  are small, we investigate now the behaviour of the eigenvalues, or characteristic roots, of model 1 close to marginal stability. Note that the linear stability of a uniform flow and the property of real characteristics are equivalent for model 1 : the dispersion equation is obtained by substituting  $\lambda = \omega/k$  and  $\mathbf{A} = \mathbf{A}_0$  in the characteristic polynomial  $|\mathbf{A} - \lambda\mathbf{I}| = 0$ . This may be seen by making the substitution  $\hat{\mathbf{z}} = \hat{\mathbf{z}}_1 \exp\{i(\omega t - kx)\}$  in (4.3.1.16), which yields  $|\mathbf{kA}_0 - \omega\mathbf{I}| = 0$  as a condition for the existence of constant vectors  $\hat{\mathbf{z}}_1$ .

We recall that the relative velocity  $w$  has been made dimensionless by means of the isothermal acoustic velocity of the gas and the mass density  $\rho_g$  of the gas by means of the constant mass density  $\rho_l$  of the liquid. By making the reasonable assumption that those quantities are small, it may be shown with the use of the results presented in G (1985a) that the discriminant  $D$  of the characteristic polynomial is approximately given by

$$\begin{aligned}
 D = & -16 \left[ 1 + \frac{m(\alpha)}{\alpha^2(1-\alpha)} \right]^3 \left[ \frac{1}{\rho_g} \frac{m(\alpha)}{\alpha} \right]^{-5} \left\{ \left[ 1 + \frac{m(\alpha)}{\alpha^2(1-\alpha)} \right] \times \right. \\
 & \times \left[ 1 + \frac{3m(\alpha)}{1-\alpha} + 2m'(\alpha) + \frac{1}{2}(1-\alpha)m''(\alpha) \right] + \\
 & \left. - \left[ 1 - \frac{3\alpha}{\alpha^2(1-\alpha)} m(\alpha) + \frac{m'(\alpha)}{\alpha} \right]^2 \right\} w^2 + O(w^4) + O(\rho_g^6). \quad (4.3.2.2)
 \end{aligned}$$

By substituting (4.3.2.1) into (4.3.2.2) it is derived that, for small  $w$  and  $\rho_g$ ,  $D \geq 0$  in the region  $S_\alpha$  of the  $(p_1, p_2)$ -plane, determined by

$$\begin{aligned}
 S_\alpha = \{ (p_1, p_2) \mid p_2 \leq p_1 + \frac{3(1-\alpha)^2}{4\alpha^2} \left[ 1 - \sqrt{\frac{8\alpha}{9(1-\alpha)}} p_1 + 1 \right] \wedge \\
 \wedge p_2 \geq -\frac{1}{\alpha} p_1 - \frac{(1-\alpha)(1-3\alpha)}{2\alpha^2} \}. \quad (4.3.2.3)
 \end{aligned}$$

The first inequality in (4.3.2.3) ensures that the characteristic roots associated with concentration waves are real, the second inequality follows from  $m(\alpha) \geq 0$  and ensures that the acoustic eigenvalues are real. Close to the origin of the  $(p_1, p_2)$ -plane, which represents marginal stability,  $S_\alpha$  may be approximated by  $S_\alpha^0$  given by

$$\begin{aligned}
 S_\alpha^0 = \{ (p_1, p_2) \mid p_2 \leq -\frac{1+2\alpha}{3\alpha} p_1 + O(p_1^2) \wedge \\
 \wedge p_2 \geq -\frac{1}{\alpha} p_1 - \frac{(1-\alpha)(1-3\alpha)}{2\alpha^2} \}. \quad (4.3.2.4)
 \end{aligned}$$

For several void fractions  $\alpha$  the regions  $S_\alpha^0$  are illustrated in figure 4.3.2.1. The arrows  $A \rightarrow$  denote the crossing of a line into a region where the acoustic roots are real, while the arrows  $C \rightarrow$  point in a similar way into a region where the roots associated with concentration waves are real. For  $\alpha = .3$  it is seen that the lines  $D = 0$  have a point of intersection. That point is shifted to the origin for  $\alpha = 1/3$ . For all void fractions exhibited values for  $p_1$  and  $p_2$  are available which will lead to linear stability of model 1. However, when we are bound to use the virtual-mass coefficient as a completely determined function of  $\alpha$  and demand the linear stability of model 1 for a maximal range of void fractions, then figure 4.3.2.1 shows

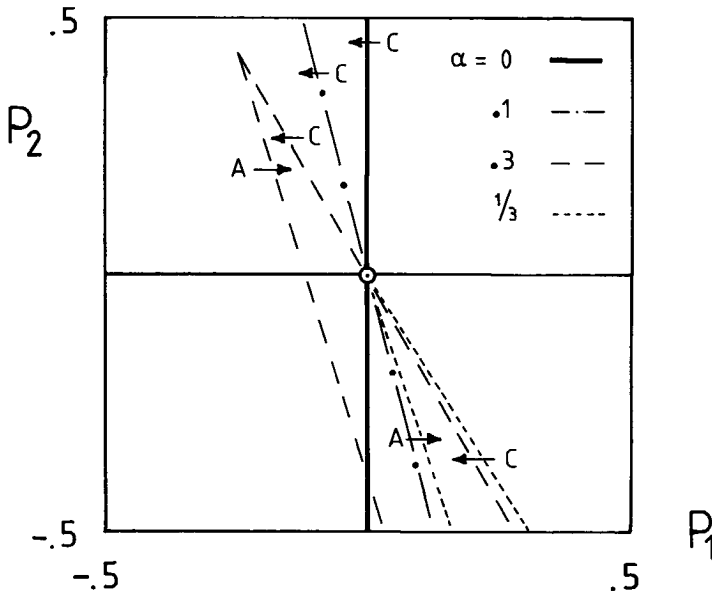


Figure 4.3.2.1. Regions of real characteristic roots in the neighbourhood of marginal stability, depending on the void fraction  $\alpha$  and the coefficients  $p_1$  and  $p_2$  which determine the virtual-mass coefficient according to (4.3.2.1);  $A \rightarrow$  : acoustic roots become real;  $C \rightarrow$  : roots associated with concentration waves become real.

that model 1 can only be (marginally) stable for  $\alpha$  varying from zero to  $1/3$ . This is a consequence of the fact that

$$\lim_{\alpha=0}^{1/3} S_\alpha = (0,0). \quad (4.3.2.5)$$

For higher void fractions the intersection is empty. In addition it can be concluded that hydrodynamical bubble interaction effects, represented by the higher order terms in  $\alpha$  in the virtual-mass coefficient, have to be included since  $p_1 = 2$  and  $p_2 = -3/2$  will lead to unstable behaviour of model 1 for small void fractions  $\alpha$ .

In the literature many forms of the virtual-mass coefficient may be found, often given different names, like added-mass coefficient or mass coefficient of the kinetic energy density due to relative motion (some coefficients are treated by Kok (1988)). Oshima (1979), for example, finds a virtual-mass coefficient equal to

$$m_0(\alpha) = \frac{1}{2} \alpha (1 - \alpha) + O(\alpha^3), \quad (4.3.2.6)$$

while Kok (1988) determines it to be

$$m_K(\alpha) = \frac{1}{2} \alpha (1 - .676 \alpha) + O(\alpha^3). \quad (4.3.2.7)$$

In Kok (1988) it is asserted that the added-mass coefficient of the bubbly mixture and the coefficient of the kinetic energy density due to relative motion become different quantities when bubble interaction effects are taken into account. The latter coefficient is identified with our virtual-mass coefficient. When we write expressions (4.3.2.6) and (4.3.2.7) in the form of (4.3.2.1), it is clear that  $p_1$  must be chosen equal to, respectively,  $p_1 = 3/2$  and  $p_1 = 1.662$  ( $p_2$  can not be determined). Figure 4.3.2.1 shows that both values of  $p_1$  lead to waves with a complex velocity of propagation when  $O(\alpha^3)$  terms are neglected by taking  $p_2 = 0$ . In subsection 4.4.5 expression (4.3.2.7) is substituted into model 1 to demonstrate numerically the appearance of a rapidly growing void fraction. Subsequently,  $p_1$  and  $p_2$  are chosen equal to  $p_1 = p_2 = -1/4$  to show the occurrence of two distinct and stable waves.

## 4.4 Numerical method and results

### 4.4.1 Numerical method

In view of the appearance of complex characteristics in the analysis of many two-phase flow models, robust numerical methods are strongly needed. We refer to Stewart & Wendroff (1984) for a review. The major part of the methods which have been developed makes use of an explicit or semi-implicit scheme. Since in that case the time step is restricted, steady or quasi-steady computations become time consuming. That is the reason, why Sha (1986) stresses the need for implicit numerical procedures.

Since the models 1 and 2 possess only real characteristics (see subsection 4.3.1), we are in a different situation. In fact it is one of our aims to investigate whether known and established schemes for hyperbolic conservation laws may be applied to the equations treated in the

present chapter. The conservation form ensures conservation on the difference level and enables a good resolution for shock waves. Familiar and robust schemes are upwind differencing schemes (see Harten et al. 1983) and TVD schemes (Chakravarthy & Osher 1985). Both types of schemes, however, have only been developed for hyperbolic systems with a complete set of eigenvectors. It is not clear whether a generalisation of such schemes is possible to the case of the equations considered here. A commonly used alternative is the application of space-centered schemes. We have chosen for the method of Lerat (1985), which is known from numerical gas dynamics.

Lerat's scheme is linearly implicit and second order accurate. For equation (4.2.6) the scheme reads in delta form

$$\begin{aligned} \Delta \mathbf{q} + \frac{1}{2} \tilde{\beta} \sigma^2 \delta [ \tilde{\mathbf{A}}^2(\bar{\mathbf{q}}) \delta(\Delta \mathbf{q}) ] + \frac{1}{2} \tilde{\gamma} \delta^2(\Delta \mathbf{q}) = \\ = -\sigma \bar{\delta} \mathbf{g}(\mathbf{q}) + \frac{1}{2} \sigma^2 \delta [ \tilde{\mathbf{A}}(\bar{\mathbf{q}}) \delta \mathbf{g}(\mathbf{q}) ], \end{aligned} \quad (4.4.1.1)$$

where the spatial and temporal difference operators are given, respectively, by

$$\begin{aligned} (\delta \mathbf{q})_i^n &= \mathbf{q}_{i+1/2}^n - \mathbf{q}_{i-1/2}^n, \\ (\bar{\delta} \mathbf{q})_i^n &= \frac{1}{2} ( \mathbf{q}_{i+1}^n - \mathbf{q}_{i-1}^n ), \end{aligned} \quad (4.4.1.2)$$

$$\Delta \mathbf{q} = \mathbf{q}_i^{n+1} - \mathbf{q}_i^n.$$

Furthermore  $\bar{\mathbf{q}} = (\mathbf{q}_i^n + \mathbf{q}_{i+1}^n)/2$ , while  $\tilde{\mathbf{A}}$  denotes the Jacobian matrix  $\partial \mathbf{g} / \partial \mathbf{q}$  and  $\sigma = \Delta t / \Delta x$  is the ratio of the time step  $\Delta t$  and the space increment  $\Delta x$ . Note that  $\mathbf{q}_i^n$  is the approximate solution at  $x = i \Delta x$ , ( $i=0, \dots, I$ ), and  $t = n \Delta t$ , ( $n=0, \dots, N$ ). The values of the two parameters  $\tilde{\beta}$  and  $\tilde{\gamma}$  may be chosen in an appropriate way. It has been proved that for a linear hyperbolic system the scheme (4.4.1.1) is linearly solvable and unconditionally stable for  $\tilde{\beta} \leq -1/2$  and  $\tilde{\gamma} < 1/2$  (see Lerat 1985). A third parameter  $\tilde{\alpha}$  which appears in Lerat's scheme has been taken equal to the commonly used value zero. The dispersive and dissipative properties of the scheme can be studied on the corresponding fourth order system, also known as the modified equation. For a second-order accurate scheme that system can be written as



$$\frac{\partial \mathbf{q}}{\partial t} + \tilde{\mathbf{A}} \frac{\partial \mathbf{q}}{\partial x} = \Delta x^2 \tilde{\mathbf{B}} \frac{\partial^3 \mathbf{q}}{\partial x^3} + \Delta x^3 \tilde{\mathbf{C}} \frac{\partial^4 \mathbf{q}}{\partial x^4}. \quad (4.4.1.3)$$

The first term on the right-hand side of (4.4.1.3) constitutes the dispersive error, the second term represents the dissipative error. In the case of Lerat's scheme the matrices  $\tilde{\mathbf{B}}$  and  $\tilde{\mathbf{C}}$  which appear in those error terms are determined by, respectively,

$$\tilde{\mathbf{B}} = -\frac{1}{6} \tilde{\mathbf{A}} [ (1-3\tilde{\gamma}) \mathbf{I} - (1+3\tilde{\beta}) (\sigma \tilde{\mathbf{A}})^2 ] \quad (4.4.1.4)$$

and

$$\tilde{\mathbf{C}} = -\frac{1}{8} \sigma \tilde{\mathbf{A}}^2 [ (1-2\tilde{\gamma}) \mathbf{I} - (1+2\tilde{\beta}) (\sigma \tilde{\mathbf{A}})^2 ]. \quad (4.4.1.5)$$

Expression (4.4.1.4) shows that for a linearly solvable and unconditionally stable scheme the numerical dispersion is minimized by choosing

$$\tilde{\beta} = -1/2, \quad \tilde{\gamma} = 1/3. \quad (4.4.1.6)$$

That value for  $\tilde{\beta}$  also makes the second term in  $\tilde{\mathbf{C}}$  vanish, as may be seen from (4.4.1.5), and partially reduces the numerical dissipation as well. We remark that, to our knowledge, Lerat's scheme has never been applied to hyperbolic systems with an incomplete set of eigenvectors. A theory is not available for that special case. Numerical experiments, however, indicate that the scheme works well. Some of those experiments are discussed in the remaining subsections of the present section.

The system (4.2.6) consists of complicated equations. The analytical determination of the Jacobian matrix  $\tilde{\mathbf{A}}$  therefore requires a considerable amount of calculations, which makes the code expensive. A novel and efficient feature in our code is the numerical determination of  $\tilde{\mathbf{A}}$  according to

$$\tilde{\mathbf{A}}_{ij} = \frac{g_i(\mathbf{q}_j + d\mathbf{q}) - g_i(\mathbf{q}_j)}{dq}, \quad (i, j = 1, \dots, m), \quad (4.4.1.7)$$

where  $dq$  is taken equal to  $|q_j| \times 10^{-6}$ . For model 1 the Jacobian was determined analytically as well as numerically. A comparison of the corresponding numerical values showed an agreement of the first five digits for the physical variable  $\mathbf{z}$ .

New values  $q_i^{n+1}$  become available after each time step. From these values the new values of the physical variable have to be determined by means of a transformation. In the case of model 1 the transformation can be performed analytically. In the case of model 2 the transformation reduces to a linear and a non-linear equation for  $u_1$  and  $u_2$ . Those equations were solved numerically by using the C05PBF NAG-routine. Relations (4.3.1.1) and (4.3.1.2) guarantee that the Jacobian of the transformation does not vanish. It should be emphasised that this is due to a careful selection of the equations that make part of model 1 and of model 2. We remark that the equation for the conservation of energy was not included in explicit form in any of the two models. The reason for this procedure is that when the equation for the conservation of energy is combined, respectively, with the equation for the conservation of total linear momentum, the equation of motion for the liquid, or the equation of motion for the gas phase in addition to the two equations for the conservation of mass, the Jacobian  $|\partial \mathbf{q} / \partial \mathbf{z}|$ , in the case of model 1, is given, respectively, by  $(u_2 - u_1) \{ \rho_1 \rho_2 + (\rho_1 + \rho_2) m(\alpha) \}$ ,  $(u_2 / \rho_1) \{ \rho_1 \rho_2 + (\rho_1 + \rho_2) m(\alpha) \}$ , or  $(u_1 / \rho_2) \{ \rho_1 \rho_2 + (\rho_1 + \rho_2) m(\alpha) \}$ . In each case the Jacobian therefore vanishes for certain values of the flow velocities  $u_1$  and  $u_2$  so that the numerical transformation breaks down. We finally mention that the CPU time required for the numerical experiments with model 2 could be reduced by a factor three when the corresponding results of model 1 were used as starting values for the numerical transformation.

#### 4.4.2 Testing the method

The numerical experiments presented in this subsection will serve as test cases for the numerical method. The experiments have the form of initial-value problems. They concern nonlinear void-fraction waves and acoustic waves. Void-fraction waves are used for comparing an exact solution with its numerical representation, while acoustic waves are used for a demonstration of the effect of the values of  $\tilde{\beta}$  and  $\tilde{\gamma}$  on the numerical dispersion. The initial values are determined by giving the physical variable  $\mathbf{z}$  as a vector function of  $\mathbf{x}$  at  $t=0$ . Concentration waves are included by using the properties (i) and (ii) and the relations (3.3.1), (3.3.2) and (3.5.1) (see sections 3.3 and 3.5 in Chapter III), where  $f(x)$  is the initial value of  $\alpha$ . Acoustic waves are generated by perturbing the value of  $\rho_g$  at  $t=0$ . Note that  $\rho_g$  is equal to the dimensionless gas pressure. The values of  $\mathbf{z}$  at the boundaries  $x=0$  and  $x=1$  are determined through overspecification and are kept equal to their initial values. Since one of our aims is to investigate waves and wave interactions at a certain distance from the boundaries of the region  $0 < x < 1$ , that overspecification is not a severe restriction.

As a first test of Lerat's scheme we compute a propagating nonlinear concentration wave in the case of model 1. The space increment and the time step are given, respectively, by  $\Delta x = .005$  and  $\Delta t = .04$  so that  $I = 200$  and the Courant number is close to one (for a void fraction  $\alpha = .1$  (see below) the maximal eigenvalue is approximately equal to .12). The number of time steps is determined by  $N = 200$ . The initial value of  $\alpha$  is given by (3.3.1), where

$$f(x) = f_0 + f_1 e^{-\xi_0(x-x_0)^2}, \quad (4.4.2.1)$$

with  $f_0 = .1$ ,  $f_1 = .025$ ,  $\xi_0 = 200$  and  $x_0 = .4$ . The other quantities occurring in the relations describing a concentration wave are determined by  $u_2 = .025$ ,  $\rho_g = 10^{-3}$  and  $\rho_1 w = -9 \times 10^{-4}$ . The initial values of the physical variable  $\mathbf{z} = (\rho_1, \rho_2, u_1, u_2)^T$  are thereby completely fixed. They represent at  $t=0$  a nonlinear void-fraction wave centered around  $x=.4$  and propagating with a velocity  $u_2 = .025$ . Note that the difference velocity  $w \neq 0$ . Figure 4.4.2.1 shows the values of  $\alpha$  at  $t=0$ ,  $t=4$  (hundred time steps) and  $t=8$  (two hundred time steps). The shape

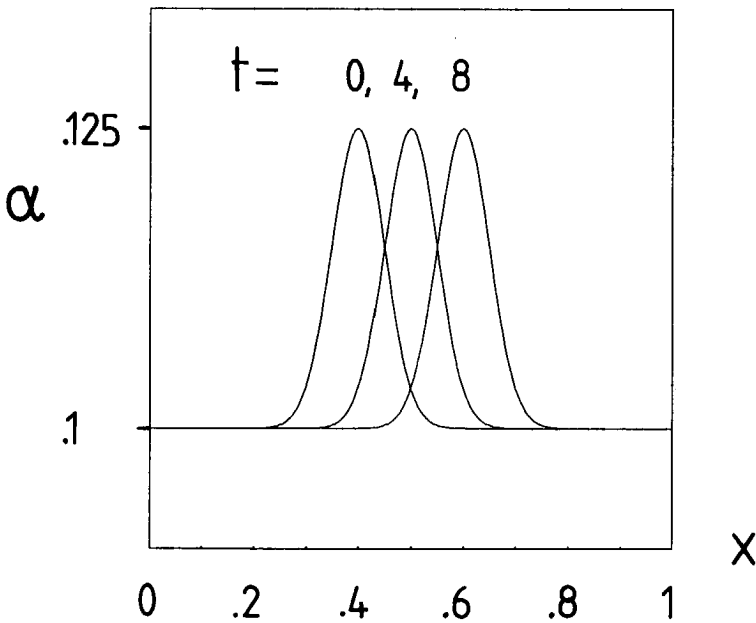


Figure 4.4.2.1. Propagating nonlinear concentration wave.  
Void fraction  $\alpha$  at  $t=0$ ,  $t=4$  and  $t=8$  (model 1).

of the curve representing the void fraction  $\alpha$  as a function of position is perfectly conserved in the course of time. At  $t=8$  the maximum value of  $\alpha$  has travelled from  $x=.4$  to  $x=.6$  and is equal to  $\alpha_{\max} = .12500$ . The numerical results are in excellent agreement with the exact solution.

Next we investigate the influence of  $\tilde{\beta}$  and  $\tilde{\gamma}$  on the numerical dispersion associated with scheme (4.4.1.1). A modified initial-value problem is solved for two different sets of values for  $\tilde{\beta}$  and  $\tilde{\gamma}$  by using model 1. The initial values given above are left unchanged, with the exception of the values of  $u_2$  and  $f_1$ . By taking them equal to  $u_2 = 0$  and  $f_1 = 0$ , the gas phase is initially at rest and uniformly distributed. The uniform value of  $\rho_g$  is slightly disturbed at  $t = 0$  by letting the dimensionless gas pressure take the form

$$\rho_g = \rho_{g0} + \rho_{g1} e^{-\xi_1(x-x_1)^2}, \quad (4.4.2.2)$$

where  $\rho_{g0} = 10^{-3}$ ,  $\rho_{g1} = 10^{-4}$ ,  $\xi_1 = 250$  and  $x_1 = .5$ . Acoustic waves will originate from the disturbance centered around  $x = .5$ . The initial-value problem is solved with  $\Delta x = .02$  and  $\Delta t = .16$ . The Courant number is therefore approximately one. Fifty time steps are taken ( $I = 50$ ,  $N = 50$ ). First, we take  $\tilde{\beta}$  and  $\tilde{\gamma}$  equal to the commonly used values  $\tilde{\beta} = -1$  and  $\tilde{\gamma} = 0$ . In figure 4.4.2.2 the result is presented in the form of a  $(x,t)$ -plot of the drift velocity  $u_2$  of the gas bubbles. The damped oscillations at the rear of the acoustic waves are a result of the numerical dispersion of the scheme (see the previous subsection). Subsequently, we take  $\tilde{\beta}$  and  $\tilde{\gamma}$  equal to the optimal values  $\tilde{\beta} = -1/2$  and  $\tilde{\gamma} = 1/3$ , and solve the same initial-value problem. The results are plotted in figure 4.4.2.3. They clearly demonstrate the importance of a correct tuning of the parameters which occur in the numerical scheme. The numerical dispersion is greatly reduced by choosing the optimal values of  $\tilde{\beta}$  and  $\tilde{\gamma}$ . However, a small oscillation at the rear of the wave is still visible. In the next subsection it may be seen (figure 4.4.3.1) that a refining of the grid ( $I = 200$ ) is sufficient to make that small oscillation disappear as well. We finally remark that only the gas velocity is plotted because it turned out to be the variable that is most sensitive to numerical errors.

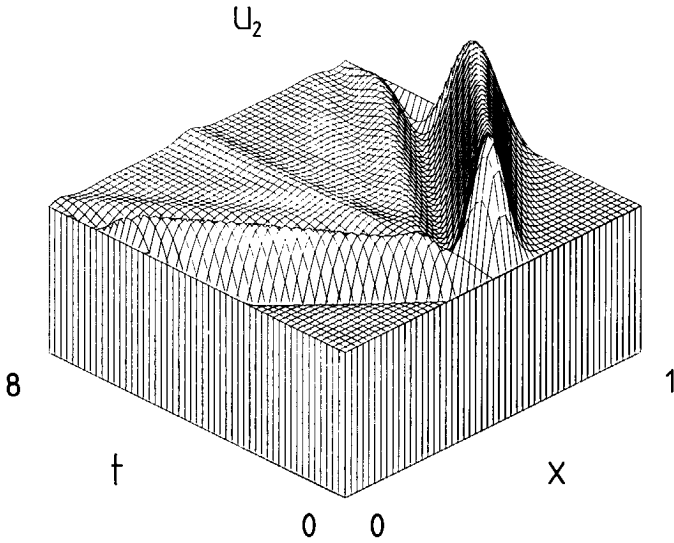


Figure 4.4.2.2. Numerical dispersion in acoustic waves for  $\tilde{\beta} = -1$  and  $\tilde{\gamma} = 0$ . Gas velocity  $u_2$  plotted as a function of  $x$  and  $t$  (model 1).

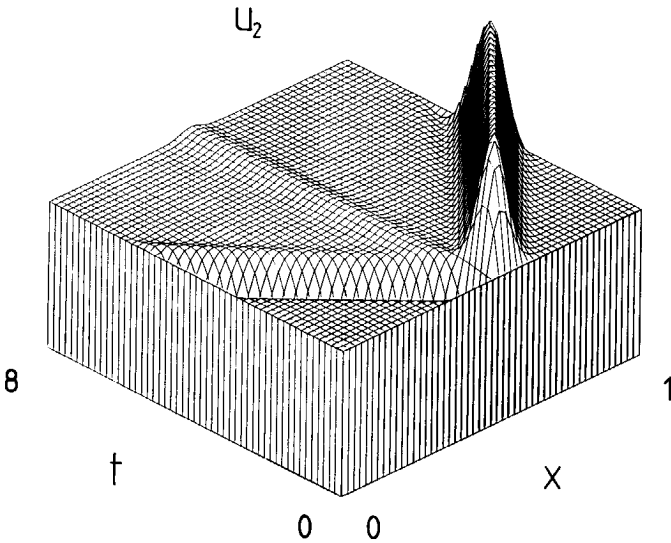


Figure 4.4.2.3. Numerical dispersion in acoustic waves for  $\tilde{\beta} = -1/2$  and  $\tilde{\gamma} = 1/3$ . Gas velocity  $u_2$  plotted as a function of  $x$  and  $t$  (model 1).

#### 4.4.3 Numerical investigation of wave–interaction

The numerical initial–value problems treated in this subsection concern the interaction of acoustic waves with nonlinear concentration waves. At the same time we further investigate the feasibility of Lerat's method. Next to model 1, model 2 is used to investigate the effect of bubble deformation. The experiments are performed with a space increment  $\Delta x = .005$ , giving  $I = 200$ . The time step is determined by  $\Delta t = .04$ , so that the computations of the present subsection will be performed with a Courant number that is approximately equal to one. The number of time steps is taken equal to  $N = 200$ . As a consequence the numerical experiments cover a period of 8 dimensionless units. For a pipe of one meter length filled with a bubbly mixture at room temperature, that period would correspond to approximately .03 seconds. The computations are therefore performed on a small time scale, characterised by the time of propagation of the fast acoustic waves. The possibly unstable behaviour of acoustically disturbed concentration waves may not appear on that time scale. In the next subsection they are investigated on a large time scale by numerically integrating at a high Courant number.

We investigate the stability of a nonlinear void–fraction wave of the form (4.4.2.1) by letting it interact with an acoustic wave originating from a disturbance of the form (4.4.2.2). The parameters take the values  $f_0 = .1$ ,  $f_1 = .025$ ,  $\xi_0 = 200$ ,  $x_0 = .7$  and  $x_1 = .3$ . The values of the remaining constants are left unchanged. They may be found in the previous subsection. In view of the relations describing a nonlinear concentration wave (see sections 3.3 and 3.5, Chapter III), the gas velocity is taken equal to  $u_2 = 0$  and the liquid velocity  $u_1$  is determined by taking  $\rho_{1w} = -9 \times 10^{-4}$ . Figure 4.4.3.1 presents the interaction in the form of  $(x,t)$ –plots of the void fraction  $\alpha$  and the bubble velocity  $u_2$ . That presentation is sufficient for a qualitative discussion of the results. Three waves originate from the disturbance of the gas pressure at  $x=.3$ , viz., two fast acoustic waves, both having a minimum in  $\alpha$ , and one slow wave, having a maximum in  $\alpha$ . The acoustic wave propagating to the right interacts with the nonlinear concentration wave at  $x=.7$ . On the small time scale the void–fraction wave reassumes its initial shape after interaction.

In order to investigate the influence of bubble deformations a similar initial–value problem is computed using model 2. The initial value of the bubble number density  $n$  follows from (3.5.1), where the constant value of the average bubble volume  $\tau$  is determined by choosing a constant equivalent bubble radius  $a_0$ . The initial–value problem was solved for  $a_0 = .216 \times 10^{-3}$ , associated with a Weber number of the undisturbed flow  $We_0 \approx .5$ , and for  $a_0 = 1.08 \times 10^{-3}$ , corresponding to  $We_0 \approx 2.5$ . The results are presented in figure 4.4.3.2 and

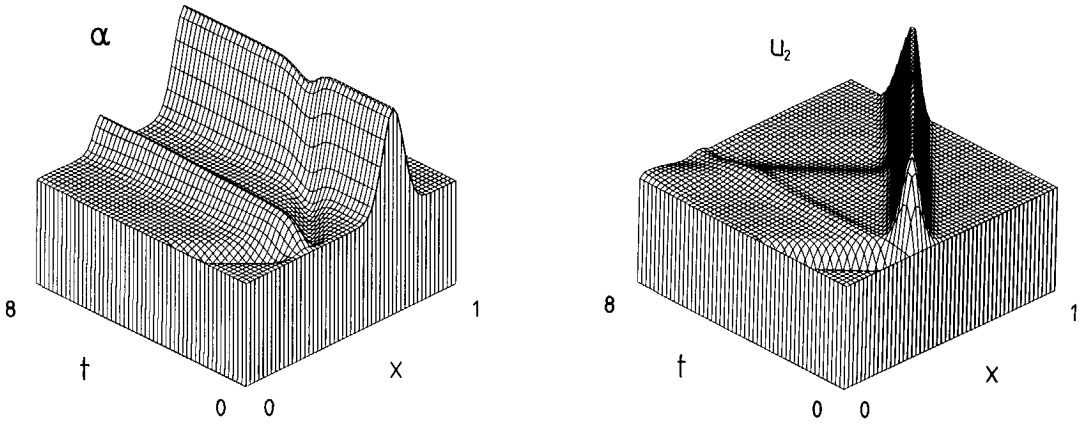


Figure 4.4.3.1. Interaction of an acoustic wave and a nonlinear concentration wave. Void fraction  $\alpha$  and gas velocity  $u_2$  plotted as functions of  $x$  and  $t$  (model 1).

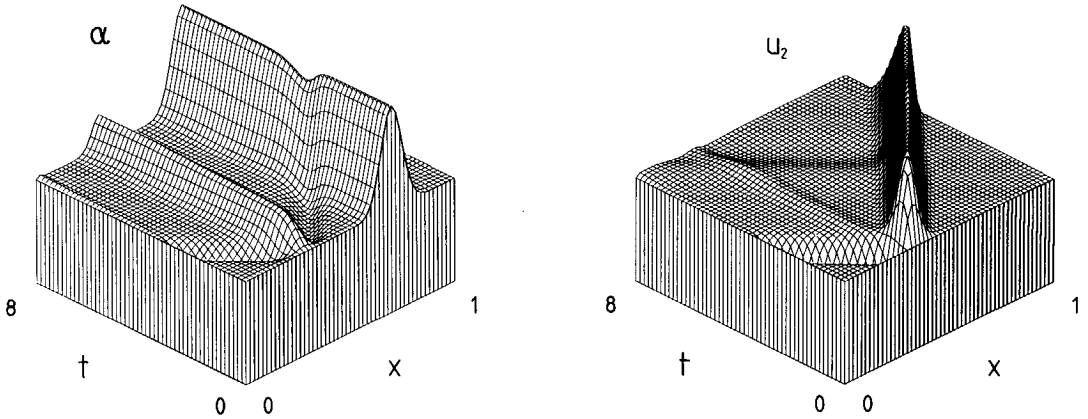


Figure 4.4.3.2. Bubble deformation effects in the interaction of an acoustic wave and a nonlinear concentration wave;  $We_0 \approx .5$ .

Void fraction  $\alpha$  and gas velocity  $u_2$  plotted as functions of  $x$  and  $t$  (model 2).

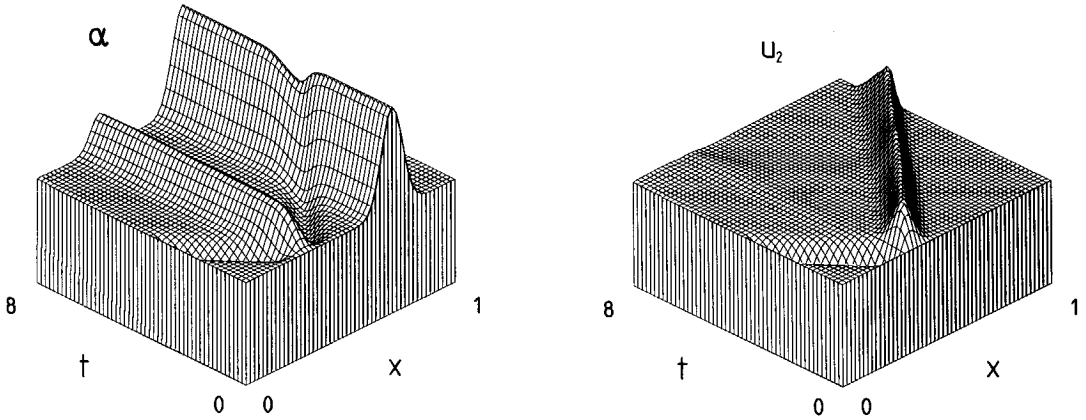


Figure 4.4.3.3. Bubble deformation effects in the interaction of an acoustic wave and a nonlinear concentration wave;  $We_0 \approx 2.5$ .  
 Void fraction  $\alpha$  and gas velocity  $u_2$  plotted as functions of  $x$  and  $t$  (model 2).

figure 4.4.3.3, respectively. The small Weber number  $We_0 \approx .5$  ensures that the bubbles have a nearly spherical shape. Indeed we see from figures 4.4.3.1 and 4.4.3.2 that, for small Weber numbers, model 2 yields nearly the same results as model 1, where the bubbles are assumed to be spherical. In the case where  $We_0 \approx 2.5$ , the bubbles take the approximate form of oblate ellipsoids. Figure 4.4.3.3 clearly demonstrates the effect of bubble deformations. The amplitude of  $u_2$  decreases, while the velocity of propagation of the acoustic disturbance diminishes (the wave in figure 4.4.3.2 arrives at the boundary  $x=1$  at an earlier time than the wave in figure 4.4.3.3). The void-fraction wave reassumes its original shape on the small time scale considered.

The plot of  $u_2$  in figure 4.4.3.1 displays a weak reflection. To investigate whether the reflection may become more pronounced, a void-fraction wave having a much higher gradient in the bubble concentration is introduced around  $x=.7$  by means of

$$f(x) = f_0 + f_1 \frac{1 + \tanh\{\xi_0(x-x_0)\}}{2}, \quad (4.4.3.1)$$

where  $f_0 = .1$ ,  $f_1 = .075$ ,  $\xi_0 = 100$  and  $x_0 = .7$ ; in the limit  $\xi_0 \rightarrow \infty$  the function  $f(\cdot)$  takes the



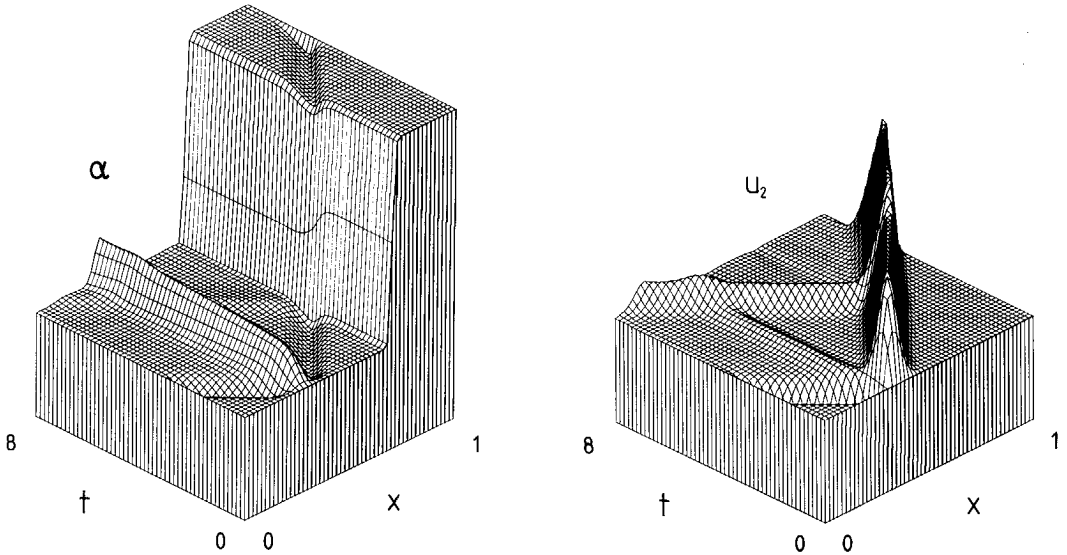


Figure 4.4.3.4. Reflection and transmission of an acoustic wave as a result of its interaction with a nonlinear concentration wave.

Void fraction  $\alpha$  and gas velocity  $u_2$  plotted as functions of  $x$  and  $t$  (model 1).

form of a step function. The pressure disturbance is increased by taking  $\rho_{g1} = 1.75 \times 10^{-4}$ . Other constants are left unchanged. Figure 4.4.3.4 shows the results obtained with model 1. The acoustic wave is partially reflected and partially transmitted. A close look at the plot of  $u_2$  shows that the acoustic disturbance travels slower with a larger amplitude in the region of high void fraction after transmission. A decrease of  $\alpha$  is observed at  $x = .7$  after interaction. It suggests that the pressure wave has pushed the concentration wave to the right. After interaction the void-fraction wave reassumes its initial shape, again on the small time scale considered. In the next section the initial-value problem discussed here is approximately solved by replacing (4.4.3.1) by a step function and using the linearised equations of model 1. An extensive comparison of the numerical results with the results following from linear theory is also presented there.

We finally point out two more aspects. First, it should be noted that the dispersive errors, still visible in figure 4.4.2.3, have disappeared completely as a result of the optimal values of  $\tilde{\beta}$  and  $\tilde{\gamma}$  in combination with the refined grid. Secondly, it should be observed that none of the results presented here demonstrate the linear growth property which is discussed in subsection 4.3.1. This may be understood by realising that the linear growth in time is carried by a slow wave and will therefore only manifest itself clearly on a large time scale. In the following subsection that effect is investigated by performing computations with a high Courant number.

#### 4.4.4 Stability of nonlinear concentration waves and linear stability of model 1

The stability of the acoustically disturbed nonlinear concentration wave presented in figure 4.4.3.1 is investigated here on a large time scale by continuing the numerical integration of the solution at  $t = 8$  with a high Courant number. The time step is fixed to  $\Delta t = .4$  and two hundred time steps are taken ( $N = 200$ ). The corresponding Courant number is approximately equal to ten. In figure 4.4.4.1 the void fraction  $\alpha$  is plotted at  $t = 8, 48, 88$ . The nonlinear void-fraction wave centered around  $x = .7$  preserves its initial shape on the large time scale considered and proves to be stable for an acoustic disturbance. A considerable change of the solution is observed around  $x = .3$ , where the acoustic waves were generated by means of a pulse in the gas pressure. At  $t = 88$  we may recognise the derivative of the initial value of the pressure  $\rho_g$ , given by (4.4.2.2). Note that the general solution (4.3.1.17) of the linearised equations contains a derivative which is multiplied by the time  $t$ . We therefore expect to find a similar behaviour in the numerical solution around  $x = .3$ . That the linear growth is indeed present is shown in figure 4.4.4.2, where the maximum void fraction around  $x = .3$ , denoted as  $\alpha_{\max}$ , is plotted as a function of time. An almost linear behaviour in time of the void fraction may be observed. We recall that this is a result of the fact that model 1 does not have a complete set of eigenvectors. In subsection 4.5.1 it is demonstrated that linear theory predicts the effects observed in the neighbourhood of the centre of a disturbance in the gas pressure. The linearly growing solutions are qualified in subsection 4.3.1 as an artefact of the model. They will disappear, when dissipative effects or higher order derivatives are taken into account.

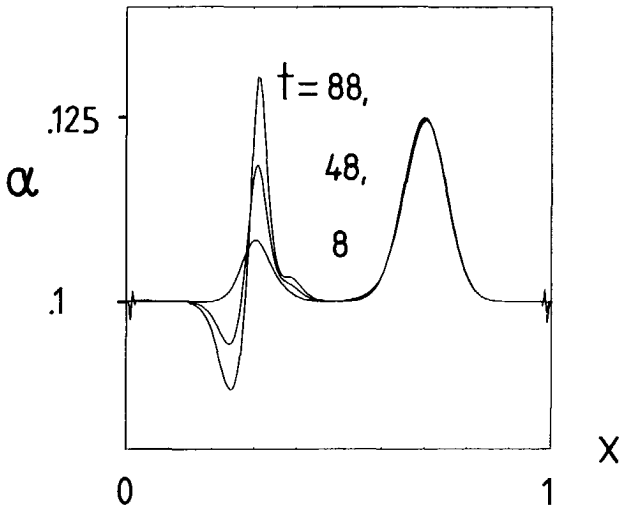


Figure 4.4.4.1. The void fraction  $\alpha$  at  $t = 8, 48, 88$  after the interaction of an acoustic wave and a nonlinear concentration wave(model 1).

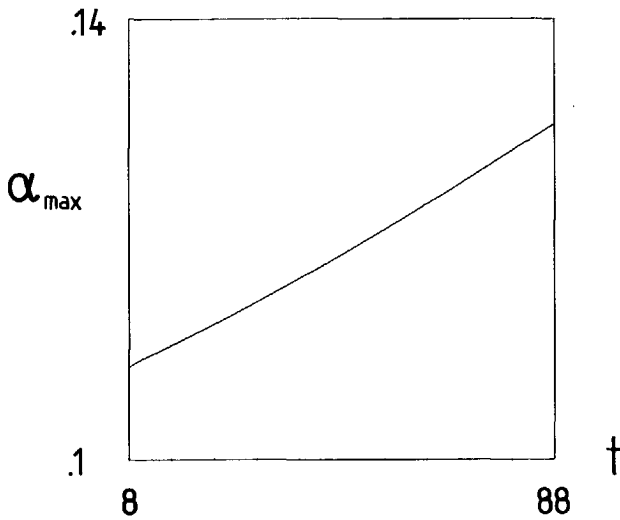


Figure 4.4.4.2. The maximum void fraction  $\alpha_{\max}$  as a function of time in the neighbourhood of the origin of a disturbance in the gas pressure (model 1).

It is analysed in subsection 4.3.2 in what way the form of the virtual–mass coefficient  $m(\alpha)$  may influence the linear stability of model 1 and, consequently, the behaviour of void–fraction waves. Here, the results of subsection 4.3.2 are illustrated numerically. First, we substitute the virtual–mass coefficient  $m_K(\alpha)$ , given by (4.3.2.7) and presented by Kok (1988), into model 1. It is shown in subsection 4.3.2 that for this case model 1 possesses two complex characteristics. The initial values are taken as in the first experiment of subsection 4.4.2 (a propagating nonlinear concentration wave), except for the values of the gas velocity and  $x_0$ , which are determined by  $u_2 = 0$  and  $x_0 = .5$ . At  $t = 0$  the void fraction has the shape of a Gaussian curve, the gas phase is at rest and the liquid has a positive velocity. The space increment and the time step are fixed to  $\Delta x = .02$  ( $I = 50$ ) and  $\Delta t = .6$ . Subsequently, two hundred time steps are taken ( $N = 200$ ) with a Courant number of approximately four. Figure 4.4.4.3 gives the maximum void fraction  $\alpha_{max}$  as a function of time. A rapid, more or less exponential growth of the void fraction is displayed in figure 4.4.4.3, which is a result of the complex characteristics of model 1. Model 1 is linearly unstable when the virtual–mass coefficient  $m_K(\alpha)$  is substituted and does not allow stable numerical computations.

Secondly, we take a virtual–mass coefficient of the form (4.3.2.1), where  $p_1$  and  $p_2$  are taken equal to  $p_1 = p_2 = -1/4$ . Figure 4.3.2.1 shows that for void fractions of about .1 model 1 is linearly stable and possesses two concentration waves with real and distinct velocities of propagation. The initial–value problem described above is solved numerically by making use of the modified virtual–mass coefficient. The space increment as well as the amount of time steps are left unchanged. Since  $p_1 = p_2 = -1/4$ , model 1 is close to marginal stability. As a result the two velocities of propagation of the concentration waves do not differ much from  $u_2 = 0$  and the two waves split very slowly. To make both waves clearly visible the time step is therefore increased to the value of  $\Delta t = 4$ . As a consequence, the computations are performed with a high Courant number of approximately twentyfour. The void fraction  $\alpha$  is plotted as a function of  $x$  and  $t$  in figure 4.4.4.4. It is seen that two stable void–fraction waves originate from the Gaussian curve at  $t = 0$ . Figure 4.4.4.4 demonstrates that two stable and distinct concentration waves may exist when expression (4.2.5) for the virtual–mass coefficient, corresponding to marginal stability, is slightly disturbed. In addition it is shown that the linear growth in time vanishes.

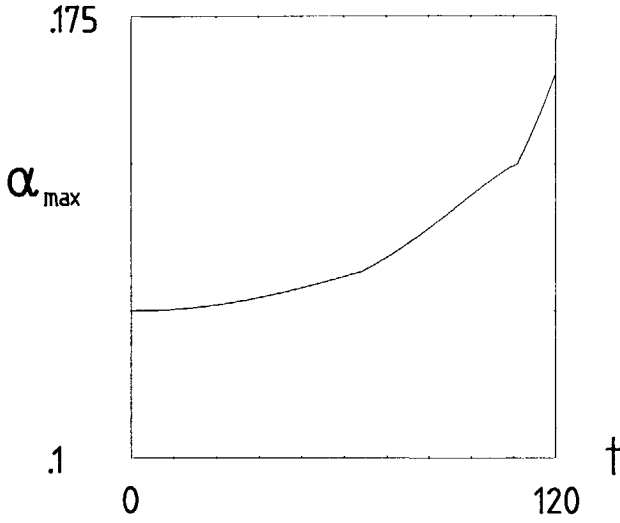


Figure 4.4.4.3. The maximum void fraction  $\alpha_{\max}$  in a concentration wave as a function of time;  $m_K(\alpha)$ , given by (4.3.2.7), substituted into model 1.

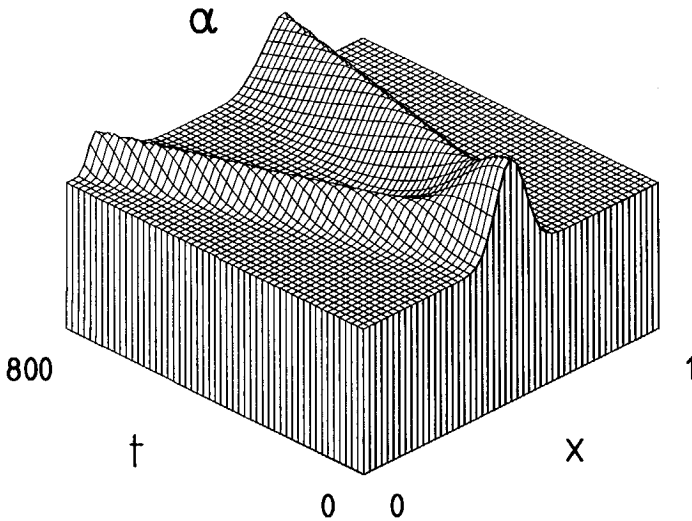


Figure 4.4.4.4. The void fraction  $\alpha$  plotted as a function of  $x$  and  $t$ ; virtual-mass coefficient  $m(\alpha)$  determined by (4.3.2.1) ( $p_1 = p_2 = -1/4$ ) and substituted into model 1.

## 4.5 Linear theory and acoustics

The effects which may be observed in the numerical results of the previous section require some analytical support. It is the aim of the present section to derive such a support from the analytical solution of the linearised equations of model 1. It will contribute to the reliability of the numerical calculations and will give more insight in the behaviour of waves and wave-interactions in bubbly two-phase flow. It constitutes a generalisation of the acoustics of one-phase fluids. The acoustic properties of a bubbly liquid/gas mixture are presented in dimensionless form to serve the readability of the present chapter.

### 4.5.1 Waves originating from a disturbance in the gas pressure (linear theory)

The initial-value problem characterised by a disturbance in the gas pressure, which was formulated in subsections 4.4.2 and 4.4.3, is solved here by means of linear theory. In concise form the linearised equations of model 1 are given by (4.3.1.16) which has the general solution (4.3.1.17). Note that  $\hat{\mathbf{z}}$  is equal to  $\hat{\mathbf{z}} = (\hat{\rho}_1, \hat{\rho}_2, \hat{u}_1, \hat{u}_2)^T$ . The disturbance in the dimensionless gas pressure  $\rho_g$  is given by (4.4.2.2), so that the initial value of  $\hat{\mathbf{z}}$  at  $t = 0$  is determined by

$$\hat{\mathbf{z}}(\mathbf{x}, 0) = (0, \hat{a} e^{-\xi_1(\mathbf{x}-\mathbf{x}_1)^2}, 0, 0)^T, \quad (4.5.1.1)$$

where  $\hat{a} = \alpha_0 \rho_{g1}$ . It follows from (4.3.1.17) that the general solution at  $t = 0$  is written

$$\hat{\mathbf{z}}(\mathbf{x}, 0) = \sum_{\mathbf{k}=1}^4 f_{\mathbf{k}}(\mathbf{x}) \mathbf{r}_{\mathbf{k}}. \quad (4.5.1.2)$$

The functions  $f_{\mathbf{k}}(\cdot)$ , ( $\mathbf{k} = 1, \dots, 4$ ), are unknown and have to be determined. When we write them as

$$f_{\mathbf{k}}(\mathbf{x}) = \hat{a} e^{-\xi_1(\mathbf{x}-\mathbf{x}_1)^2} d_{\mathbf{k}}, \quad (\mathbf{k} = 1, \dots, 4), \quad (4.5.1.3)$$

the coefficients  $d_{\mathbf{k}}$ , ( $\mathbf{k} = 1, \dots, 4$ ), are obtained by solving

$$\sum_{\mathbf{k}=1}^4 d_{\mathbf{k}} \mathbf{r}_{\mathbf{k}} = (0, 1, 0, 0)^T. \quad (4.5.1.4)$$

The eigenvectors  $\mathbf{r}_{\mathbf{k}}$ , ( $\mathbf{k}=1, \dots, 4$ ), are given by (4.3.1.8), (4.3.1.9) and (4.3.1.11). When they

are substituted the solution of (4.5.1.4) reads

$$d_1 = \frac{2}{\xi \rho_1 a_1 \left(1 - \frac{a_1}{a_2}\right)}, \quad d_2 = \frac{2}{\xi \rho_1 a_2 \left(1 - \frac{a_2}{a_1}\right)}, \quad (4.5.1.5)$$

$$d_3 = -\frac{1}{\xi} \left(1 - 3\alpha + 2\rho_g - \frac{a_1 + a_2}{a_1 a_2} \rho_1 w\right), \quad d_4 = \frac{\rho_1 w}{\xi},$$

where  $\xi = (1 + 2\rho_g)\rho_g + (1/2)\rho_1^2 w^2$ . By substituting (4.5.1.5) into (4.5.1.3) the solution of the present initial-value problem is determined by (4.3.1.17).

For a qualitative understanding of the solution we make some simplifying assumptions. In most practical situations  $\rho_g \ll 1$  and  $|w| \ll 1$ . When in addition the void fraction is not close to  $1/3$  the acoustic velocities  $a_1$  and  $a_2$  may be approximated by  $a_1 \cong \tilde{a}$  and  $a_2 \cong -\tilde{a}$ , where

$$\tilde{a} = \left[ \frac{\tilde{\xi}}{\alpha(1-3\alpha)} \right]^{1/2} \quad (4.5.1.6)$$

and  $\tilde{\xi} = \rho_g + (1/2)\rho_1^2 w^2$ . The coefficients  $d_k$ , ( $k = 1, \dots, 4$ ), then satisfy

$$d_1 \cong \frac{1}{\tilde{\xi} \rho_1 \tilde{a}}, \quad d_2 \cong -\frac{1}{\tilde{\xi} \rho_1 \tilde{a}}, \quad d_3 \cong -\frac{1-3\alpha}{\tilde{\xi}}, \quad d_4 \cong \frac{\rho_1 w}{\tilde{\xi}} \quad (4.5.1.7)$$

and the acoustic eigenvectors become approximately

$$\mathbf{r}_1 \cong \left( \frac{1}{2}(1-3\alpha) \rho_1 \tilde{a}, \frac{3}{2} \rho_1 \rho_2 \tilde{a}, \frac{1}{2}(1-3\alpha) \tilde{a}^2, \frac{3}{2} \rho_1 \tilde{a}^2 \right)^T \quad (4.5.1.8)$$

and

$$\mathbf{r}_2 \cong \left( -\frac{1}{2}(1-3\alpha) \rho_1 \tilde{a}, -\frac{3}{2} \rho_1 \rho_2 \tilde{a}, \frac{1}{2}(1-3\alpha) \tilde{a}^2, \frac{3}{2} \rho_1 \tilde{a}^2 \right)^T. \quad (4.5.1.9)$$

Since  $d_1$  and the first element of  $\mathbf{r}_1$  are positive, according to (4.5.1.6), (4.5.1.7) and (4.5.1.8), it is clear that the acoustic wave travelling to the right shows a maximum in  $\hat{\rho}_1$  and therefore a minimum in the void fraction ( $\hat{\rho}_1 = -\hat{\alpha}$ ). A similar result holds for the wave travelling to the left. When  $\rho_1 w$  has a negative value, both coefficients  $d_3$  and  $d_4$  are negative. The first

element of  $r_3$  is equal to one (see (4.3.1.9)) so that the void-fraction wave originating from the pressure disturbance has a maximum in  $\alpha$ . Due to (4.5.1.3) all modes take the form of a Gaussian curve. Considering expression (4.3.1.17) for the general solution, we see that the linear growth in time of the void fraction is multiplied by minus the derivative of a Gaussian curve. All effects mentioned above may be found in the numerical results of the previous section; see, for example, figure 4.4.3.4 and figure 4.4.4.1.

The initial-value problem displayed in figure 4.4.3.4 (reflection and transmission) and formulated in subsection 4.4.3, is used in the present subsection for a quantitative comparison between the numerical solution and the solution following from linear theory. In this subsection we focus on the region around the origin of the pressure disturbance. A comparison of the amplitudes is given in table 4.5.1.1. Taking into account that the

AMPL.	LEFT AC. WAVE		SLOW WAVE		RIGHT AC. WAVE	
	LIN.	NUM.	LIN.	NUM.	LIN.	NUM.
$\hat{\alpha}$	$-6.1 \times 10^{-3}$	$-5.6 \times 10^{-3}$	$1.2 \times 10^{-2}$	$1.2 \times 10^{-2}$	$-6.2 \times 10^{-3}$	$-5.7 \times 10^{-3}$
$\hat{\rho}_2$	$2.7 \times 10^{-6}$	$2.6 \times 10^{-6}$	$1.2 \times 10^{-5}$	$1.2 \times 10^{-5}$	$2.6 \times 10^{-6}$	$2.5 \times 10^{-6}$
$\hat{u}_1$	$-8.1 \times 10^{-4}$	$-7.8 \times 10^{-4}$	$-3.8 \times 10^{-6}$	$-3.4 \times 10^{-6}$	$8.2 \times 10^{-4}$	$7.8 \times 10^{-4}$
$\hat{u}_2$	$-3.2 \times 10^{-3}$	$-3.1 \times 10^{-3}$	$1.6 \times 10^{-4}$	$1.3 \times 10^{-4}$	$3.1 \times 10^{-3}$	$3.0 \times 10^{-3}$

*Table 4.5.1.1. Amplitudes of waves originating from a disturbance in the gas pressure. A comparison of numerical computations and linear analysis (model 1).*

disturbance in the gas pressure is 17.5 % ( $\rho_{g0} = 10^{-3}$ ,  $\rho_{g1} = 1.75 \times 10^{-4}$ ), we may conclude that linear theory supports the numerical results quite well. Furthermore, it is seen that the linear analysis gives a systematical overestimation of the numerical data. In the next subsection the reflected and transmitted waves are determined by means of the linearised equations in order to complete the comparison with the numerical calculations.



#### 4.5.2 Interaction of an acoustic wave and a discontinuous concentration wave (linear theory)

The interaction of an acoustic wave and a discontinuous void–fraction wave is analysed here according to linear theory. The concentration wave is characterised by means of some continuity relations across the interface which are derived from model 1. By linearising those relations the reflection and transmission of the acoustic disturbance may be determined. In this way, linear theory is used to analyse the phenomena which are present in figure 4.4.3.4 around  $x = .7$ . The corresponding initial–value problem is formulated in subsection 4.4.3. Mathematically spoken, a discontinuous concentration wave constitutes a contact discontinuity.

Model 1 is written in the conservation form (4.2.6). The corresponding continuity relations are given by

$$[\bar{g}(z)] - s [q(z)] = 0 , \quad (4.5.2.1)$$

where  $[q(z)] = q(z^+) - q(z^-)$ ,  $z^+$  being the state in front of the interface,  $z^-$  the state at the back, and  $\bar{g}(z) = g(q(z))$ . The velocity  $s$  of the interface is positive when the interface travels in the direction of the  $z^+$  region. With a view to linearisation we write

$$z^- = z_0^- + \hat{z}^- ,$$

$$z^+ = z_0^+ + \hat{z}^+ , \quad (4.5.2.2)$$

$$s = s_0 + \hat{s} .$$

It is assumed that the undisturbed flow, characterised by  $z_0^-$  and  $z_0^+$ , contains a discontinuous concentration wave. The relations for a nonlinear void–fraction wave, given in section (3.3) (see Chapter III), may be used to show that in that case

$$u_{z_0}^- = u_{z_0}^+ = u_{z_0} ,$$

$$\rho_{g_0}^+ = \rho_{g_0}^- = \rho_{g_0} ,$$

$$(4.5.2.3)$$

$$(\rho_{10}W_0)^+ = (\rho_{10}W_0)^- = \rho_{10}W_0 ,$$

$$s_0 = u_{20}$$

must hold. As a consequence, the undisturbed flow satisfies

$$[\bar{g}(z_0)] - u_{20} [q(z_0)] = 0 . \tag{4.5.2.4}$$

By substituting (4.5.2.2) into the continuity relations (4.5.2.1) and making use of (4.5.2.3) and (4.5.2.4), it is shown that the linearised continuity relations may be written as

$$C_{u_2}^+ \hat{z}^+ - C_{u_2}^- \hat{z}^- - [q(z)] \hat{s} = 0 , \tag{4.5.2.5}$$

where the 4x4 matrix  $C_{u_2}$  is given by  $C_{u_2} = \partial \bar{g} / \partial z - u_2 \partial q / \partial z$ . For convenience, the subscripts zero have been omitted.

The incident and the reflected acoustic waves make part of  $\hat{z}^-$  while  $\hat{z}^+$  should only contain the transmitted acoustic wave since the initial conditions and the conditions at  $+\infty$  do not allow a wave travelling to the left in that region. The amplitudes of the incident wave are known. They are determined by  $d_1^- \hat{a} r_1^-$ , where the coefficient  $d_1^-$  is given in (4.5.1.5),  $\hat{a} = \alpha_0 \rho_{g1}$  and the eigenvector  $r_1^-$  is determined by (4.3.1.8). When we assume, in an obvious way, that the amplitudes of the reflected wave are of the form  $e_2^- \hat{a} r_2^-$  and write the amplitudes of the transmitted wave as  $e_1^+ \hat{a} r_1^+$ , with unknown coefficients  $e_2^-$  and  $e_1^+$ ,  $\hat{z}^+$  and  $\hat{z}^-$  are determined by

$$\hat{z}^+ = e_1^+ \hat{a} r_1^+ , \tag{4.5.2.6}$$

$$\hat{z}^- = d_1^- \hat{a} r_1^- + e_2^- \hat{a} r_2^- .$$

Note that the modes associated with the eigenvectors  $r_3$  and  $r_4$  are not included in  $\hat{z}^+$  and  $\hat{z}^-$ . The reason for this is that those modes travel with the velocity of a concentration wave and therefore run parallel to the discontinuity in the (x,t)-plane. As a consequence, their coefficients have to be taken equal to zero since they would otherwise disturb the initial values. In addition, the  $r_3$  mode would vanish in the linearised continuity relations (4.5.2.5)

since  $C_{\mathbf{u}_2} \mathbf{r}_3 = 0$ . When (4.5.2.6) is substituted into (4.5.2.5), the continuity relations become

$$e_1^+ C_{\mathbf{u}_2}^+ \mathbf{r}_1^+ - e_2^- C_{\mathbf{u}_2}^- \mathbf{r}_2^- - \hat{s} \frac{[\mathbf{q}(\mathbf{z})]}{\hat{a}} = d_1^- C_{\mathbf{u}_2}^- \mathbf{r}_1^- . \quad (4.5.2.7)$$

We remark that expression (4.5.2.7) constitutes four equations for the three unknowns  $e_1^+$ ,  $e_2^-$  and  $\hat{s}$ . By making use of (4.5.2.3) it is shown that

$$[\mathbf{q}(\mathbf{z})] = - \left( 1, -\rho_g, \frac{3}{2} \rho_{1W}, \frac{3}{2} \frac{\rho_{1W}}{\rho_g} \right)^T [\alpha] . \quad (4.5.2.8)$$

When the eigenvectors are substituted into (4.5.2.7) and use is made of (4.5.2.8), it is derived that (4.5.2.7) is equivalent to

$$\mathbf{B} \mathbf{e} = \mathbf{c} , \quad (4.5.2.9)$$

where

$$\mathbf{B} = \begin{bmatrix} (\rho_1 a_2^2)^+ & -(\rho_1 a_2^2)^- & 0 \\ \left(\frac{1}{2} (\rho_{1W} + 3\alpha a_1) \rho_1 a_1\right)^+ & -\left(\frac{1}{2} (\rho_{1W} + 3\alpha a_2) \rho_1 a_2\right)^- & -1 \\ \left[\frac{\rho_1 a_1}{\alpha}\right]^+ & -\left[\frac{\rho_1 a_2}{\alpha}\right]^- & 0 \\ (\rho_1 a_1^2)^+ & -(\rho_1 a_2^2)^- & 0 \end{bmatrix} , \quad (4.5.2.10)$$

$$\mathbf{e} = ( e_1^+ , e_2^- , [\alpha] \hat{s} / \hat{a} )^T \quad (4.5.2.11)$$

and

$$\mathbf{c} = \left( (\rho_1 a_1^2)^- , \left(\frac{1}{2} (\rho_{1W} + 3\alpha a_1) \rho_1 a_1\right)^- , \right. \\ \left. (\rho_1 a_1 / \alpha)^- , (\rho_1 a_1^2)^- \right)^T . \quad (4.5.2.12)$$

We see that the four equations (4.5.2.9) are dependent and reduce to three independent equations with three unknowns. The solution is given by

$$e_1^+ = \frac{(\rho_1 a_1^2)^- \left[ 1 - \frac{a_2^-}{a_1^-} \right]}{(\rho_1 a_1^2)^+ \left[ 1 - \frac{\alpha^- a_2^-}{\alpha^+ a_1^+} \right]} d_1^-, \quad (4.5.2.13)$$

$$e_2^- = - \frac{(a_1^2)^- \left[ 1 - \frac{\alpha^+ a_1^+}{\alpha^- a_1^-} \right]}{(a_2^2)^- \left[ 1 - \frac{\alpha^+ a_1^+}{\alpha^- a_2^-} \right]} d_1^-, \quad (4.5.2.14)$$

$$\hat{s} = \frac{1}{2} (\rho_1 w + 3\alpha a_1)^+ \frac{a_1^- - a_2^-}{\alpha^+ a_1^+ - \alpha^- a_2^-} (\rho_1 a_1)^- \hat{a} d_1^-. \quad (4.5.2.15)$$

Relation (4.5.2.13) determines the transmission, (4.5.2.14) the reflection and (4.5.2.15) expresses the motion of the discontinuous void-fraction wave as a result of the incidence of the acoustic wave. When the limit  $\mathbf{z}^+ \rightarrow \mathbf{z}^-$  is taken it is inferred from (4.5.2.13) to (4.5.2.15) that  $e_1^+ \rightarrow d_1^-$ ,  $e_2^- \rightarrow 0$  and  $\hat{s} \rightarrow \hat{u}_2 = (1/2) \rho_1 (\rho_1 w / \alpha + 3a_1) a_1 d_1 \hat{a}$ . As a consequence, the acoustic wave is completely transmitted and not reflected. The reflection and transmission coefficients for the four components of the incident wave may now be defined, respectively, as

$$C_{R, z_k} = \frac{r_{2k}^- e_2^-}{r_{1k}^- d_1^-}, \quad (k = 1, \dots, 4), \quad (4.5.2.16)$$

and

$$C_{T, z_k} = \frac{r_{1k}^+ e_1^+}{r_{1k}^- d_1^-}, \quad (k = 1, \dots, 4), \quad (4.5.2.17)$$

where  $r_{ik}$  denotes the  $k^{\text{th}}$  element of the  $i^{\text{th}}$  eigenvector, ( $i = 1, 2$ ), ( $k = 1, \dots, 4$ ).

In practice, when  $\rho_g$  and  $|w|$  are small, the reflection and transmission coefficient of the void fraction  $\alpha$  may be approximated by

$$C_{R,\alpha} \approx - \frac{\alpha^+ - \alpha^-}{(\sqrt{\alpha^-(1-3\alpha^+)} + \sqrt{\alpha^+(1-3\alpha^-)})^2} \quad (4.5.2.18)$$

and

$$C_{T,\alpha} \approx 2 \frac{1-3\alpha^+}{1-3\alpha^-} \left[ \left[ \frac{\alpha^-(1-3\alpha^-)}{\alpha^+(1-3\alpha^+)} \right]^{1/2} + \frac{\alpha^-}{\alpha^+} \right]^{-1} \quad (4.5.2.19)$$

Relations (4.5.2.18) and (4.5.2.19) demonstrate that for  $\alpha^+ > \alpha^-$  a minimum in the void fraction is reflected as a maximum and transmitted as a minimum. Since the reflection coefficient of the gas velocity  $C_{R,u_2}$  may be approximated by the right hand side of (4.5.2.18) multiplied by minus one, a maximum in the gas velocity is reflected as a maximum. Those effects are also present in figure 4.4.3.4. A quantitative comparison of the numerically computed amplitudes and the amplitudes following from the linear analysis is made in table 4.5.2.1. The comparison concerns the initial-value problem which is displayed in figure 4.4.3.4 and formulated in subsection 4.4.3. The numerical integration is also performed for a void-fraction wave with a higher gradient by taking  $\xi_0 = 150$ . In that way the

AMPL.	REFLECTED ACOUSTIC WAVE			TRANSMITTED ACOUSTIC WAVE		
	LINEAR	NUMERICAL		LINEAR	NUMERICAL	
		$\xi_0=100$	$\xi_0=150$		$\xi_0=100$	$\xi_0=150$
$\hat{\alpha}$	$1.4 \times 10^{-3}$	$1.3 \times 10^{-3}$	$1.3 \times 10^{-3}$	$-5.7 \times 10^{-3}$	$-5.5 \times 10^{-3}$	$-5.5 \times 10^{-3}$
$\hat{p}_2$	$-6.2 \times 10^{-7}$	$-5.5 \times 10^{-7}$	$-5.8 \times 10^{-7}$	$6.1 \times 10^{-6}$	$6.1 \times 10^{-6}$	$6.1 \times 10^{-6}$
$\hat{u}_1$	$1.9 \times 10^{-4}$	$1.6 \times 10^{-4}$	$1.8 \times 10^{-4}$	$7.5 \times 10^{-4}$	$7.4 \times 10^{-4}$	$7.4 \times 10^{-4}$
$\hat{u}_2$	$7.4 \times 10^{-4}$	$6.6 \times 10^{-4}$	$6.9 \times 10^{-4}$	$3.8 \times 10^{-3}$	$3.8 \times 10^{-3}$	$3.8 \times 10^{-3}$

Table 4.5.2.1. Amplitudes of a reflected and transmitted acoustic wave. A comparison of numerical computations and linear analysis (model 1).

concentration wave shows a closer resemblance with a step function, or discontinuity, and it may be investigated whether the comparison improves or not. The comparison is focused on the amplitudes of the reflected and transmitted acoustic waves. Again the linear results prove to support the numerical computations very well. As in the previous subsection, linear theory systematically overestimates the numerical data. In addition it is seen that the comparison improves when we consider a concentration wave with a higher gradient ( $\xi_0 = 150$ ).

We finally want to investigate the displacement of the concentration wave due to the incident acoustic wave. It is easily seen from expression (4.5.2.15) that linear theory predicts that the void-fraction wave moves to the right when  $(\rho_1 w + 3\alpha a_1)^+ > 0$  and  $\hat{a} d_1^- > 0$ . Since both inequalities hold in the corresponding numerical experiment, the decrease of the void fraction at  $x = .7$  in figure 4.4.3.4 must indeed be interpreted as a translation to the right of the concentration wave as a result of the collision with a pressure disturbance. When we assume that the concentration wave, centered around  $x = x_0$  at  $t = 0$ , preserves its shape and the void fraction at  $x = x_0$  is known as a function of time, the displacement  $\hat{x}_c(t)$  of the void-fraction wave may be derived from (4.4.3.1) and is given by

$$\hat{x}_c(t) = x_0 + \frac{1}{2\xi_0} \ln \left[ \frac{\alpha^+ - \alpha(x_0, t)}{\alpha(x_0, t) - \alpha^-} \right]. \quad (4.5.2.20)$$

Expression (4.5.2.20) may be used to determine the displacement from the numerical data. In order to derive the displacement of the interface from linear theory we assume that a pressure pulse of the shape  $\hat{a} e^{-\xi_1(x-x_1-a_1t)^2}$  is travelling from  $x = x_1$  to the right, where at  $t = 0$  the discontinuous void-fraction wave is located at  $x = x_0$ . From (4.5.2.15) it is inferred that the pulse induced interface velocity  $\hat{s}(t)$  at the position of the interface  $x_{int}(t)$  is given by

$$\hat{s}(t) = \hat{s} e^{-\xi_1(x_{int}(t) - x_1 - a_1t)^2}, \quad (4.5.2.21)$$

where  $x_{int}(0) = x_0$ . When we write the position of the interface as  $x_{int}(t) = x_0 + \hat{x}_{int}(t)$ , the displacement  $\hat{x}_{int}(t)$  of the interface is obtained by integrating (4.5.2.21) with respect to time. It satisfies

$$\hat{x}_{int}(t) = \hat{s} \int_0^t e^{-\xi_1(x_0 - x_1 + \hat{x}_{int}(\theta) - a_1\theta)^2} d\theta. \quad (4.5.2.22)$$

For the same initial-value problem as is mentioned above the displacement of the concentration wave according to (4.5.2.20) and according to (4.5.2.22) are compared in table 4.5.2.2. For completeness the reflection coefficients, defined by (4.5.2.16), are also included. Both the displacement and the reflection coefficients compare quite well. Again, the agreement improves when a void-fraction wave with a higher gradient ( $\xi_0 = 150$ ) is used in the numerical computations. Considering the comparisons in this subsection and in the previous one, we may conclude that the major part of the phenomena observed in the numerical experiments is supported by linear theory.

	LINEAR	NUMERICAL	
		$\xi_0 = 100$	$\xi_0 = 150$
$\hat{x}_{\text{int}} (\text{lin.})$	$3.64 \times 10^{-3}$	$3.87 \times 10^{-3}$	$3.79 \times 10^{-3}$
$\hat{x}_c (\text{num.})$			
$C_{R,\alpha}$	-.23	-.22	-.23
$C_{R,\rho_2}$	-.24	-.22	-.23
$C_{R,u_1}$	.23	.22	.22
$C_{R,u_2}$	.24	.22	.23

Table 4.5.2.2. A comparison of the displacement of the concentration wave  $\hat{x}_{\text{int}}$ ,  $\hat{x}_c$  and the reflection coefficients as a result of the interaction of an acoustic wave and a concentration wave; numerical results versus linear theory (model 1).

### 4.5.3 Acoustics of bubbly two-phase flow

In this subsection relevant acoustic quantities are derived from the linearised equations of model 1. The acoustic energy and the acoustic intensity, for one-phase fluids given in Lighthill (1978), are here generalised for application to a bubbly liquid/gas mixture. We emphasize again that the expressions are given in dimensionless form. Note that bubble pulsation effects are not taken into account in model 1. Therefore, the linearised equations of model 1 only describe the behaviour of sound waves of frequencies which are smaller than the isothermal resonance frequency of the individual bubbles  $\omega_b = [3p_w/(\rho_\ell a_0^2)]^{1/2}$  (see van Wijngaarden 1972), where  $a_0$  denotes the bubble radius and  $p_w$  the undisturbed pressure. For acoustic shock waves or, in general, waves of a high frequency the Rayleigh–Plesset equation should be included, as is done by Noordzij & van Wijngaarden (1974), for example.

In Lighthill (1978) the acoustic energy and intensity for a one-component fluid are derived by means of a physical argument. Bubbly two-phase flow is too complicated for such an approach. As a result, the linearised equations of motion have to be used to derive the equation describing the conservation of acoustic energy. The linearised equations of model 1 are given by (4.3.1.12) to (4.3.1.15) and may be applied to derive expressions for the acoustic energy  $W$  and the acoustic intensity  $I$  in their dimensionless form. They should be quadratic in the disturbances  $\hat{\rho}_1, \hat{\rho}_2, \hat{u}_1, \hat{u}_2$  and must satisfy

$$\frac{\partial W}{\partial t} + \frac{\partial I}{\partial x} = 0. \tag{4.5.3.1}$$

A way to obtain equation (4.5.3.1) is to multiply (4.3.1.14) by  $\rho_1 \hat{u}_1 + u_1 \hat{\rho}_1$ , multiply (4.3.1.15) by  $\rho_2 \hat{u}_2 + u_2 \hat{\rho}_2$ , add the obtained equations and make use of (4.3.1.12) and (4.3.1.13) to bring the result into conservation form. This procedure, however, requires a lot of tedious calculations and gives little insight. An alternative and more systematic approach is to formulate a variational principle which generates (4.3.1.12) to (4.3.1.15) and derive the conservation of acoustic energy (4.5.3.1) from Noether's invariance theorem.

Consider the case that the nonlinear equations of motion for a variable  $\mathbf{u}(x,t)$  are derived from a Lagrangian energy density  $\tilde{L}(\mathbf{u})$ . By writing  $\mathbf{u} = \mathbf{u}_0 + \hat{\mathbf{u}}$ ,  $\hat{\mathbf{u}}$  being a relatively small disturbance of a solution  $\mathbf{u}_0$ , it is shown in a straightforward way that the corresponding linearised equations of motion may be obtained by means of an associated Lagrangian  $\bar{L}(\hat{\mathbf{u}})$  which follows from  $\tilde{L}$  by expanding  $\tilde{L}(\mathbf{u}_0 + \hat{\mathbf{u}})$  in powers of  $\hat{\mathbf{u}}$  and retaining only the terms that are quadratic in the disturbance. In the present case of bubbly two-phase flow, that



procedure is most readily applied to the dimensionless form of the Lagrangian  $L^*$  defined by (1.6.11) (see section 1.6, Chapter I). It reduces to a quadratic expression in the disturbances  $\hat{\rho}_1, \hat{\rho}_2, \hat{u}_1, \hat{u}_2, \hat{\varphi}_1$  and  $\hat{\varphi}_2$  which is given by

$$\begin{aligned}
 L^* = & \frac{1}{2} \rho_1 \hat{u}_1^2 + \hat{\rho}_1 u_1 \hat{u}_1 + \frac{1}{2} \rho_2 \hat{u}_2^2 + \hat{\rho}_2 u_2 \hat{u}_2 + \\
 & + \frac{1}{4} m'' w^2 \hat{\rho}_1^2 - m' w \hat{\rho}_1 (\hat{u}_2 - \hat{u}_1) + \frac{1}{2} m (\hat{u}_2 - \hat{u}_1)^2 - \frac{1}{2} \frac{\alpha}{\rho_g} \hat{\rho}_g^2 + \\
 & - \hat{\rho}_1 \left[ \frac{\partial}{\partial t} + u_1 \frac{\partial}{\partial x} \right] \hat{\varphi}_1 - \hat{\rho}_1 \hat{u}_1 \frac{\partial \varphi_1}{\partial x} - \rho_1 \hat{u}_1 \frac{\partial \hat{\varphi}_1}{\partial x} + \\
 & - \hat{\rho}_2 \left[ \frac{\partial}{\partial t} + u_2 \frac{\partial}{\partial x} \right] \hat{\varphi}_2 - \hat{\rho}_2 \hat{u}_2 \frac{\partial \varphi_2}{\partial x} - \rho_2 \hat{u}_2 \frac{\partial \hat{\varphi}_2}{\partial x}. \tag{4.5.3.2}
 \end{aligned}$$

Since it follows from the Euler-Lagrange equations (1.6.14) and (1.6.15) that

$$\begin{aligned}
 \hat{\rho}_1 \hat{u}_1 \frac{\partial \varphi_1}{\partial x} + \hat{\rho}_2 \hat{u}_2 \frac{\partial \varphi_2}{\partial x} = & \hat{\rho}_1 \hat{u}_1 u_1 + \hat{\rho}_2 \hat{u}_2 u_2 + \\
 & + m w \left( \frac{\hat{\rho}_2 \hat{u}_2}{\rho_2} - \frac{\hat{\rho}_1 \hat{u}_1}{\rho_1} \right), \tag{4.5.3.3}
 \end{aligned}$$

equation (4.5.3.2) may be written in the form

$$\begin{aligned}
 L^* = L - & \left[ \hat{\rho}_1 \frac{\partial}{\partial t} + (\rho_1 \hat{u}_1 + u_1 \hat{\rho}_1) \frac{\partial}{\partial x} \right] \hat{\varphi}_1 + \\
 & - \left[ \hat{\rho}_2 \frac{\partial}{\partial t} + (\rho_2 \hat{u}_2 + u_2 \hat{\rho}_2) \frac{\partial}{\partial x} \right] \hat{\varphi}_2, \tag{4.5.3.4}
 \end{aligned}$$

where

$$\begin{aligned}
 L = & \frac{1}{2} \rho_1 \hat{u}_1^2 + \frac{1}{2} \rho_2 \hat{u}_2^2 + \frac{1}{2} m (\hat{u}_2 - \hat{u}_1)^2 - m' w \hat{\rho}_1 (\hat{u}_2 - \hat{u}_1) + \frac{1}{4} m'' w^2 \hat{\rho}_1^2 + \\
 & - m w \left( \frac{\hat{\rho}_2 \hat{u}_2}{\rho_2} - \frac{\hat{\rho}_1 \hat{u}_1}{\rho_1} \right) - \frac{1}{2} \frac{\alpha}{\rho_g} \hat{\rho}_g^2. \tag{4.5.3.5}
 \end{aligned}$$

Partial integration shows that the last two terms on the right-hand side of (4.5.3.4) yield the linearised mass conservation equations (4.3.1.12) and (4.3.1.13), multiplied, respectively, by  $\hat{\varphi}_1$  and  $\hat{\varphi}_2$ . Performing the independent variations of the four quantities  $\hat{\rho}_1$ ,  $\hat{\rho}_2$ ,  $\hat{u}_1$  and  $\hat{u}_2$ , we derive the following Euler-Lagrange equations from (4.5.3.4):

$$\delta\hat{\rho}_1: L_{\hat{\rho}_1} - \frac{\partial\hat{\varphi}_1}{\partial t} - u_1 \frac{\partial\hat{\varphi}_1}{\partial x} = 0, \quad (4.5.3.6)$$

$$\delta\hat{\rho}_2: L_{\hat{\rho}_2} - \frac{\partial\hat{\varphi}_2}{\partial t} - u_2 \frac{\partial\hat{\varphi}_2}{\partial x} = 0, \quad (4.5.3.7)$$

$$\delta\hat{u}_1: L_{\hat{u}_1} - \rho_1 \frac{\partial\hat{\varphi}_1}{\partial x} = 0, \quad (4.5.3.8)$$

$$\delta\hat{u}_2: L_{\hat{u}_2} - \rho_2 \frac{\partial\hat{\varphi}_2}{\partial x} = 0, \quad (4.5.3.9)$$

where  $L_{\hat{f}}$  denotes  $\partial L / \partial \hat{f}$ . It is easily inferred from (4.5.3.6) to (4.5.3.9) that the Lagrange multipliers satisfy

$$\frac{\partial\hat{\varphi}_1}{\partial x} = \frac{1}{\rho_1} L_{\hat{u}_1}, \quad (4.5.3.10)$$

$$\frac{\partial\hat{\varphi}_1}{\partial t} = L_{\hat{\rho}_1} - \frac{u_1}{\rho_1} L_{\hat{u}_1}, \quad (4.5.3.11)$$

$$\frac{\partial\hat{\varphi}_2}{\partial x} = \frac{1}{\rho_2} L_{\hat{u}_2}, \quad (4.5.3.12)$$

$$\frac{\partial\hat{\varphi}_2}{\partial t} = L_{\hat{\rho}_2} - \frac{u_2}{\rho_2} L_{\hat{u}_2}. \quad (4.5.3.13)$$

Combining relations (4.5.3.10) and (4.5.3.11) it is seen that

$$\frac{\partial}{\partial t} \left\{ \frac{1}{\rho_1} L_{\hat{u}_1} \right\} + \frac{\partial}{\partial x} \left\{ \frac{u_1}{\rho_1} L_{\hat{u}_1} - L_{\hat{\rho}_1} \right\} = 0. \quad (4.5.3.14)$$

In the same way relations (4.5.3.12) and (4.5.3.13) give

$$\frac{\partial}{\partial t} \left\{ \frac{1}{\rho_2} L_{\hat{u}_2} \right\} + \frac{\partial}{\partial x} \left\{ \frac{u_2}{\rho_2} L_{\hat{u}_2} - L_{\hat{\rho}_2} \right\} = 0 . \quad (4.5.3.15)$$

When (4.5.3.5) is substituted for L, relations (4.5.3.14) and (4.5.3.15) take the form of, respectively, (4.3.1.14) and (4.3.1.15), which constitute the linearised equations of motion for the liquid and the gas. Since the Lagrangian density L is quadratic in the disturbances, it is true that

$$\hat{\rho}_1 L_{\hat{\rho}_1} + \hat{\rho}_2 L_{\hat{\rho}_2} + \hat{u}_1 L_{\hat{u}_1} + \hat{u}_2 L_{\hat{u}_2} = 2 L . \quad (4.5.3.16)$$

Multiplying the Euler-Lagrange equations (4.5.3.6) to (4.5.3.9) by, respectively,  $\hat{\rho}_1$ ,  $\hat{\rho}_2$ ,  $\hat{u}_1$  and  $\hat{u}_2$ , and adding the results, we derive with the use of (4.5.3.16) that

$$2 L - \left[ \hat{\rho}_1 \frac{\partial}{\partial t} + (\rho_1 \hat{u}_1 + u_1 \hat{\rho}_1) \frac{\partial}{\partial x} \right] \hat{\varphi}_1 + \\ - \left[ \hat{\rho}_2 \frac{\partial}{\partial t} + (\rho_2 \hat{u}_2 + u_2 \hat{\rho}_2) \frac{\partial}{\partial x} \right] \hat{\varphi}_2 = 0 . \quad (4.5.3.17)$$

By substituting expression (4.5.3.4) for  $L^*$  it is seen that L and  $L^*$  are simply related by means of

$$L^* = -L . \quad (4.5.3.18)$$

We now return to equation (4.5.3.1), which expresses the conservation of acoustic energy. In the case of a bubbly liquid/gas medium it may be derived in dimensionless form by applying Noether's first invariance theorem to  $L^*$ , given by (4.5.3.4). We recall that the invariance theorem was treated in section 2.3, Chapter II. The acoustic energy and intensity are shown to satisfy, respectively,

$$W = -\hat{\rho}_1 \frac{\partial \hat{\varphi}_1}{\partial t} - \hat{\rho}_2 \frac{\partial \hat{\varphi}_2}{\partial t} - L^* \quad (4.5.3.19)$$

and

$$I = -(\rho_1 \hat{u}_1 + u_1 \hat{\rho}_1) \frac{\partial \hat{\varphi}_1}{\partial t} - (\rho_2 \hat{u}_2 + u_2 \hat{\rho}_2) \frac{\partial \hat{\varphi}_2}{\partial t} . \quad (4.5.3.20)$$

By substituting (4.5.3.4), (4.5.3.5) and (4.5.3.10) to (4.5.3.13) it follows that

$$\begin{aligned} W &= \frac{1}{2} \rho_1 \hat{u}_1^2 + \frac{1}{2} \rho_2 \hat{u}_2^2 + \frac{1}{2} m (\hat{u}_2 - \hat{u}_1)^2 + \frac{1}{2} \frac{\alpha}{\rho_g} \hat{\rho}_g^2 + \\ &+ u_1 \hat{\rho}_1 \hat{u}_1 + u_2 \hat{\rho}_2 \hat{u}_2 + m \left( \frac{u_2 \hat{\rho}_2}{\rho_2} - \frac{u_1 \hat{\rho}_1}{\rho_1} \right) (\hat{u}_2 - \hat{u}_1) - m w \left[ \frac{u_2 \hat{\rho}_2^2}{\rho_2^2} - \frac{u_1 \hat{\rho}_1^2}{\rho_1^2} \right] + \\ &- m' w \hat{\rho}_1 \left( \frac{u_2 \hat{\rho}_2}{\rho_2} - \frac{u_1 \hat{\rho}_1}{\rho_1} \right) - \frac{1}{4} m'' w^2 \hat{\rho}_1^2 , \end{aligned} \quad (4.5.3.21)$$

$$\begin{aligned} I &= (\rho_1 \hat{u}_1 + u_1 \hat{\rho}_1) \left\{ u_1 \hat{u}_1 - \frac{m}{\rho_1} u_1 (\hat{u}_2 - \hat{u}_1) - \frac{m}{\rho_1} w \hat{\rho}_1 + \left( \frac{m}{\rho_1} \right)' w u_1 \hat{\rho}_1 + \right. \\ &\quad \left. + m' w (\hat{u}_2 - \hat{u}_1) + \hat{\rho}_g - \frac{1}{2} m'' w^2 \hat{\rho}_1 \right\} + \\ &+ (\rho_2 \hat{u}_2 + u_2 \hat{\rho}_2) \left\{ u_2 \hat{u}_2 + \frac{m}{\rho_2} u_2 (\hat{u}_2 - \hat{u}_1) + \frac{m}{\rho_2} w \hat{u}_2 - \frac{m' w}{\rho_2} u_2 \hat{\rho}_1 + \right. \\ &\quad \left. - \frac{m w}{\rho_2^2} u_2 \hat{\rho}_2 + \frac{1}{\rho_g} \hat{\rho}_g \right\} . \end{aligned} \quad (4.5.3.22)$$

Clearly, these expressions are too complicated to construct them by means of a physical argument, like Lighthill (1978) does for an ordinary fluid. The corresponding dimensional relations for W and I are obtained by multiplying (4.5.3.21) and (4.5.3.22) by, respectively,  $\rho_\ell U_0^2$  and  $\rho_\ell U_0^3$ , where  $U_0^2 = RT/M$ , and rewriting the right-hand sides in dimensional variables.

The conservation of acoustic momentum is also derived from Noether's theorem. It is written

$$\frac{\partial P}{\partial t} + \frac{\partial \Pi}{\partial x} = 0 , \quad (4.5.3.23)$$

where the acoustic momentum density P is given by

$$\begin{aligned}
 P &= \hat{\rho}_1 \frac{\partial \hat{\varphi}_1}{\partial x} + \hat{\rho}_2 \frac{\partial \hat{\varphi}_2}{\partial x} \\
 &= \hat{\rho}_1 \hat{u}_1 + \hat{\rho}_2 \hat{u}_2 + m \left( \frac{\hat{\rho}_2}{\rho_2} - \frac{\hat{\rho}_1}{\rho_1} \right) (\hat{u}_2 - \hat{u}_1) - m w \left[ \frac{\hat{\rho}_2^2}{\rho_2^2} - \frac{\hat{\rho}_1^2}{\rho_1^2} \right] + \\
 &\qquad\qquad\qquad - m' w \hat{\rho}_1 \left( \frac{\hat{\rho}_2}{\rho_2} - \frac{\hat{\rho}_1}{\rho_1} \right) \tag{4.5.3.24}
 \end{aligned}$$

and the acoustic momentum flux  $\Pi$  by

$$\begin{aligned}
 \Pi &= (\rho_1 \hat{u}_1 + u_1 \hat{\rho}_1) \frac{\partial \hat{\varphi}_1}{\partial x} + (\rho_2 \hat{u}_2 + u_2 \hat{\rho}_2) \frac{\partial \hat{\varphi}_2}{\partial x} + L^* \\
 &= -\hat{\rho}_1 \frac{\partial \hat{\varphi}_1}{\partial t} - \hat{\rho}_2 \frac{\partial \hat{\varphi}_2}{\partial t} + L \\
 &= \frac{1}{2} \rho_1 \hat{u}_1^2 + \frac{1}{2} \rho_2 \hat{u}_2^2 + \frac{1}{2} m (\hat{u}_2 - \hat{u}_1)^2 + \frac{1}{2} \frac{\alpha}{\rho_g} \hat{\rho}_g^2 + \\
 &\qquad\qquad\qquad + u_1 \hat{\rho}_1 \hat{u}_1 + u_2 \hat{\rho}_2 \hat{u}_2 + m \left( \frac{u_2 \hat{\rho}_2}{\rho_2} - \frac{u_1 \hat{\rho}_1}{\rho_1} \right) (\hat{u}_2 - \hat{u}_1) - m w \left[ \frac{u_2 \hat{\rho}_2^2}{\rho_2^2} - \frac{u_1 \hat{\rho}_1^2}{\rho_1^2} \right] + \\
 &\qquad\qquad\qquad - m' w \hat{\rho}_1 \left( \frac{u_2 \hat{\rho}_2}{\rho_2} - \frac{u_1 \hat{\rho}_1}{\rho_1} \right) - \frac{1}{4} m'' w^2 \hat{\rho}_1^2. \tag{4.5.3.25}
 \end{aligned}$$

The corresponding dimensional relations for  $P$  and  $\Pi$  are obtained by multiplying (4.5.3.24) and (4.5.3.25) by, respectively,  $\rho_\ell U_0$  and  $\rho_\ell U_0^2$  and rewriting the right-hand sides in dimensional variables. Since  $L = -L^*$  according to (4.5.3.18), it follows from the second line of (4.5.3.25) that in the one-dimensional case  $\Pi = W$  (see expression (4.5.3.19) for  $W$ ). Note that in general  $\Pi$  is a tensor and  $W$  a scalar. When we apply a Galilean transformation  $u_i \rightarrow u_i + \nu$ , ( $i = 1, 2$ ), it may be shown with the use of (4.5.3.24) that the acoustic energy is transformed according to

$$W \rightarrow W + \nu P. \tag{4.5.3.26}$$

Transformation (4.5.3.26) demonstrates the Galilean character of the acoustic energy.

Relation (4.5.3.22) for the acoustic intensity  $I$  is used in the following subsection to investigate whether the reflected and transmitted acoustic waves analysed in the previous subsection satisfy the conservation of acoustic energy.

#### 4.5.4 Comparison with ordinary acoustics

In this subsection we compare the acoustics of a bubbly liquid/gas mixture with the acoustics of an ordinary fluid, as it is described by Lighthill (1978) (see also Whitham 1974). Since Lighthill assumes the fluid to be at rest, we take the unperturbed velocities of the liquid phase and the gas phase equal to zero, i.e.  $u_1 = u_2 = 0$ . In that case it is derived from relations (4.3.1.4) to (4.3.1.7) that the acoustic velocities  $a_1$  and  $a_2$  satisfy  $a_1 = -a_2 = \bar{a}$ , where  $\bar{a} = (-c_0/c_1)^{1/2}$ . When we define the "excess pressure"  $\hat{p}_g$  as  $\hat{p}_g = \hat{\rho}_g$  and substitute  $u_1 = u_2 = 0$  into (4.5.3.21) and (4.5.3.22), the dimensionless acoustic energy and intensity reduce to

$$W = \frac{1}{2} \rho_1 \hat{u}_1^2 + \frac{1}{2} \rho_2 \hat{u}_2^2 + \frac{1}{2} m (\hat{u}_2 - \hat{u}_1)^2 + \frac{1}{2} \frac{\alpha}{\rho_g} \hat{p}_g^2 \quad (4.5.4.1)$$

and

$$I = ((1-\alpha) \hat{u}_1 + \alpha \hat{u}_2) \hat{p}_g. \quad (4.5.4.2)$$

The corresponding relations for an ordinary fluid (see Lighthill 1978) are given by

$$\tilde{W} = \frac{1}{2} \rho \hat{u}^2 + \frac{1}{2} \frac{1}{\rho c^2} \hat{p}^2 \quad (4.5.4.3)$$

and

$$\tilde{I} = \hat{u} \hat{p}. \quad (4.5.4.4)$$

To enable a convenient comparison the undisturbed mass density  $\rho$  of the fluid has been made dimensionless by means of  $\rho_\ell$ , the disturbance  $\hat{u}$  in the velocity and the speed of sound  $c$  by means of  $U_0$  and the excess pressure  $\hat{p}$  by means of  $\rho_\ell U_0^2$ . When the bubbly medium is assumed to consist of gas only ( $\alpha = 1$ ), it is seen from (4.5.4.2) and (4.5.4.4) that the acoustic intensities become identical. Since  $\rho_1 = 0$  for  $\alpha = 1$ ,  $m(1) = 0$  and  $c = 1$  for an isothermal fluid, the acoustic energies (4.5.4.1) and (4.5.4.3) become identical as well.

By assuming the excess pressure of the form  $\hat{p}_g = \hat{f}(x - \bar{a} t)$ , the equations of motion for the liquid and the gas, given by (4.3.1.14) and (4.3.1.15), yield

$$\hat{u}_1 = Y_1 \hat{p}_g \quad (4.5.4.5)$$

and

$$\hat{u}_2 = Y_2 \hat{p}_g, \quad (4.5.4.6)$$

where the dimensionless acoustic admittance of the liquid  $Y_1$  is determined by

$$Y_1 = \frac{\rho_g + \left(\frac{1}{\rho_1} + \frac{1}{\alpha}\right) m}{\left(1 + \left(\frac{1}{\rho_1} + \frac{1}{\rho_2}\right) m\right) \rho_g \bar{a}} \quad (4.5.4.7)$$

and the dimensionless acoustic admittance of the gas  $Y_2$  by

$$Y_2 = \frac{1 + \left(\frac{1}{\rho_1} + \frac{1}{\alpha}\right) m}{\left(1 + \left(\frac{1}{\rho_1} + \frac{1}{\rho_2}\right) m\right) \rho_g \bar{a}}. \quad (4.5.4.8)$$

When the total acoustic admittance  $Y$  is defined as

$$Y = (1-\alpha) Y_1 + \alpha Y_2, \quad (4.5.4.9)$$

it is shown with the use of (4.5.4.4), (4.5.4.5) and (4.5.4.6) that the acoustic intensity satisfies

$$I = Y \hat{p}_g^2. \quad (4.5.4.10)$$

Substitution of (4.5.4.7) and (4.5.4.8) into (4.5.4.9) demonstrates that the total dimensionless admittance is equal to

$$Y = \frac{\alpha \bar{a}}{\rho_g}. \quad (4.5.4.11)$$

The associated dimensional relations for  $Y_1$ ,  $Y_2$  and  $Y$  are obtained by multiplying (4.5.4.7), (4.5.4.8) and (4.5.4.11) by  $1/(\rho_\ell U_0^2)$  and rewrite the right-hand sides in dimensional

variables. In the case of an ordinary fluid the velocity  $\hat{u}$  and the excess pressure  $\hat{p}$  are related by

$$\hat{u} = \tilde{Y} \hat{p}, \quad (4.5.4.12)$$

where the admittance  $\tilde{Y}$  is given by

$$\tilde{Y} = \frac{1}{\rho c}. \quad (4.5.4.13)$$

Since  $\bar{a} = 1$  when the liquid is absent and  $c = 1$  for an isothermal fluid, it follows from (4.5.4.11) and (4.5.4.13) that the admittances  $Y$  and  $\tilde{Y}$  become identical. Note that  $Y_2$ , given by (4.5.4.8), and  $\tilde{Y}$  also become identical when virtual-mass effects are neglected.

It is shown by Lighthill (1978) that the reflection and transmission of a pressure wave propagating through a medium containing a discontinuity, is completely determined by the ratio  $\tilde{n} = \tilde{Y}^+/\tilde{Y}^-$  of the admittances of the fluid in front and at the back of the discontinuity. Clearly, the quantity  $\tilde{n}$  satisfies

$$\tilde{n} = \frac{\rho^- c^-}{\rho^+ c^+}. \quad (4.5.4.14)$$

When the incident pressure wave has an amplitude  $A$ , the amplitudes of the reflected and transmitted wave are respectively given by (see Lighthill 1978, p. 105)

$$R_A = -\frac{\tilde{n} - 1}{\tilde{n} + 1} A \quad (4.5.4.15)$$

and

$$T_A = \frac{2}{\tilde{n} + 1} A. \quad (4.5.4.16)$$

In optics (see Born & Wolf 1959, p. 40) the relations (4.5.4.15) and (4.5.4.16) constitute the so-called Fresnel formulas. The quantity  $\tilde{n}$  is there identified as the refractive index  $\bar{n} = v^-/v^+$ , where  $v^-$  and  $v^+$  denote the velocities of electromagnetic waves. We now demonstrate that the interaction of an acoustic wave and a discontinuous concentration wave, analysed in subsection 4.5.2, may also be written in terms of the reflection and



transmission relations (4.5.4.15) and (4.5.4.16). Following the notation of subsection 4.3.1, we write the acoustic wave travelling to the right as  $\hat{z} = f_1(x-\bar{a}t) \mathbf{r}_1$ , where  $\mathbf{r}_1$  is given by (4.3.1.8). The excess pressure therefore follows as

$$\hat{p}_g = \frac{\rho_g}{\alpha} \hat{\rho}_1 + \frac{1}{\alpha} \hat{\rho}_2 = \rho_g \left( \frac{1}{2} + \rho_g \right) \frac{\rho_1 \bar{a}}{\alpha} f_1(x-\bar{a}t), \quad (4.5.4.17)$$

which determines the amplitude of the incident pressure wave. The reflection and transmission of an acoustic wave are determined by relations (4.5.2.13) and (4.5.2.14). When those relations are used in combination with (4.5.4.17), it is seen that the reflection and transmission of a pressure wave propagating through a stationary bubbly liquid/gas mixture containing a discontinuous concentration wave is described by

$$R_A = - \frac{\left[ -\frac{\rho_1 \bar{a}}{\alpha} \right]^- 1 - \frac{\alpha^+ \bar{a}^+}{\alpha^- \bar{a}^-}}{\left[ \frac{\rho_1 \bar{a}}{\alpha} \right]^- 1 + \frac{\alpha^+ \bar{a}^+}{\alpha^- \bar{a}^-}} A \quad (4.5.4.18)$$

and

$$T_A = \frac{\left[ \frac{\rho_1 \bar{a}}{\alpha} \right]^+ (\rho_1 \bar{a}^2)^- 2}{\left[ \frac{\rho_1 \bar{a}}{\alpha} \right]^- (\rho_1 \bar{a}^2)^+ 1 + \frac{\alpha^- \bar{a}^-}{\alpha^+ \bar{a}^+}} A. \quad (4.5.4.19)$$

Note that the concentration wave implies that  $\rho_g^+ = \rho_g^-$ . Similar as in Lighthill (1978) we define the "refractive index"  $n_b$  for a bubbly liquid/gas mixture as the ratio of the acoustic admittances:

$$n_b = \frac{Y^+}{Y^-}. \quad (4.5.4.20)$$

By substituting (4.5.4.11) it becomes equal to

$$n_b = \frac{\alpha^+ \bar{a}^+}{\alpha^- \bar{a}^-}. \quad (4.5.4.21)$$

With the use of (4.5.4.21) the reflection and transmission relations (4.5.4.18) and (4.5.4.19) may be written in the form

$$R_A = -\frac{n_b - 1}{n_b + 1} A \quad (4.5.4.22)$$

and

$$T_A = \frac{2}{n_b + 1} A, \quad (4.5.4.23)$$

which agree completely with the reflection and transmission relations as they appear in optics and in ordinary acoustics.

Finally, we verify the conservation of acoustic energy by checking whether the acoustic intensity of the incident wave is equal to the sum of the acoustic intensities of the reflected wave and the transmitted one. By means of (4.5.4.10) this is formulated as

$$Y^- A^2 = Y^- R_A^2 + Y^+ T_A^2. \quad (4.5.4.24)$$

Multiplying equation (4.5.4.24) by  $1/(Y^- A^2)$  and substituting (4.5.4.20), (4.5.4.22) and (4.5.4.23) we arrive at

$$1 = \left[ \frac{n_b - 1}{n_b + 1} \right]^2 + \frac{4n_b}{(n_b + 1)^2}, \quad (4.5.4.25)$$

which is obviously valid. The acoustic energy is therefore conserved. The motion of the concentration wave due to the incident acoustic wave does not have to be accounted for since it has a higher order effect on the acoustic intensity.

## 4.6 Conclusions

We have shown that model 1 and model 2 give rise to stable and reliable numerical results. The fact that both models do not have a complete set of eigenvectors does not introduce unexpected numerical errors. Lerat's method works well and proves to be a feasible method for the numerical computation of transient inviscid bubbly two-phase flows. Although there is a large spreading in the order of magnitude of the dimensionless physical variables ( $\rho_1=O(1)$ ,  $\rho_2=O(10^{-4})$ ,  $n=O(10^{13})$ ), the computations proceed without any problems, also at high Courant numbers.

Numerical experiments have demonstrated that acoustic waves may be reflected by nonlinear void-fraction waves exhibiting a high gradient in the gas fraction. Linear theory fully supports the observed phenomena. Even for a considerable disturbance in the gas pressure a good agreement between the numerical data and the results following from a linear analysis is obtained. The linear growth in time, predicted by the linear theory is shown to be present in the numerical computations as well. The experiments making use of model 2 illustrate that bubble deformation reduces the amplitudes and the velocity of propagation of acoustic waves.

The stability of nonlinear concentration waves for an acoustic disturbance has been investigated numerically on a large time scale by performing computations with high Courant numbers. Nonlinear void-fraction waves reassume their initial shape after interaction and prove to be stable. Numerical experiments as well as linear theory show that a concentration wave may be set into motion by an acoustic wave. Furthermore, it is demonstrated that the expression for the virtual-mass coefficient  $m(\alpha)$  has great influence on the linear stability of model 1 and, consequently, on the behaviour of concentration waves.

The linearised equations of model 1 have been used to formulate the acoustics of a bubbly liquid/gas mixture in the form of a variational principle. Conservation laws are derived from Noether's invariance theorem and a comparison is made with the acoustics of an ordinary fluid. The expressions for the acoustic energy and the acoustic intensity of waves propagating through a bubbly liquid/gas mixture may be interpreted as a generalisation of the corresponding quantities for a single-phase fluid. The interaction of an acoustic wave and a discontinuous concentration wave may be formulated in terms of reflection and transmission relations like in ordinary acoustics.



## CHAPTER V

# TWO-PHASE BUBBLY FLOW THROUGH VERTICAL TUBE : VOID-FRACTION DISTRIBUTION AND VELOCITY PROFILES

### 5.1 Introduction

It is already known for a long time that the bubbles in the vertical upward flow of a bubbly liquid/gas mixture tend to concentrate near the wall of the tube (see Kobayashi, Iida & Kanegae 1970, Serizawa, Kataoka & Michiyoshi 1975, Beyerlein, Cossmann & Richter 1985, Wang, Lee, Jones & Lahey 1987 and references contained in these papers; similar phenomena were observed in a system of converging and diverging tube sections by de Jong, 1987). Several attempts have been made to explain the observed void-fraction distribution by means of lateral forces acting on the bubbles. Some examples of those forces are the shear 'lift' force considered by Zun, Richter & Wallis (1975), the turbulent pressure in the liquid taken into account by Drew & Lahey (1982) and the non-dissipative 'lift' force used recently by Wang et al. (1987) in addition to the Reynolds stress. Up till now, however, despite repeated attempts no satisfactory prediction of the distribution of the bubbles over a cross-section of the tube could be given by starting from first hydrodynamic principles (see the short review of bubbly flow in Batchelor 1989). It is one of the purposes of this chapter to present such a derivation of the void-fraction distribution by using a properly extended form of the general theory for two-phase bubbly flow developed by Geurst (1985a)<sup>†</sup>).

In Geurst (1986)<sup>‡</sup>) the two-phase flow equations derived in G (1985a) are examined in more detail. It is shown there, by going to the limit of vanishingly small values of the void fraction, that the theory implies the following equation for the non-dissipative motion of a single gas bubble through liquid:

$$m_1 \frac{d\mathbf{u}_2}{dt} = (1 + m_1) \left[ \frac{\partial}{\partial t} + \mathbf{u}_1 \cdot \nabla \right] \mathbf{u}_1 - m_1 (\mathbf{u}_2 - \mathbf{u}_1) \times (\nabla \times \mathbf{u}_1) . \quad (5.1.1)$$

---

†) Hereafter referred to as G (1985a).

‡) Hereafter referred to as G (1986).

In this equation  $\mathbf{u}_1$  represents the velocity of the liquid in the absence of the bubble,  $\mathbf{u}_2$  equals the velocity of the bubble when moving through the liquid and  $m_1$  denotes the virtual-mass coefficient of the bubble ( $m_1 = 1/2$  for a sphere). The volume of the bubble is taken constant and the mass density of the gas is disregarded compared to the mass density of the liquid. External forces like the buoyancy force have been omitted. The last term at the right-hand side of (5.1.1) shows that a non-dissipative 'lift' force is obviously contained in the theory of G (1985a). That may be understood in the following way. According to the analysis in G (1986) the virtual-mass terms appearing in (5.1.1) should have an objective, i.e., material frame indifferent character. The 'lift' force apparently equals the Coriolis force experienced by a bubble when its motion is considered with respect to a frame attached to the locally rotating liquid. The 'lift' force therefore contributes to making the acceleration of the bubbles in (5.1.1) material frame indifferent (Drew & Lahey 1987). The equation of motion (5.1.1) may accordingly be written in the form

$$m_1 \mathbf{a}_{\text{rel}} = \left[ \frac{\partial}{\partial t} + \mathbf{u}_1 \cdot \nabla \right] \mathbf{u}_1, \quad (5.1.2)$$

where  $\mathbf{a}_{\text{rel}}$  represents the acceleration of the bubble *relative* to the rotating liquid. See section 5.2, where the theory of G (1985a) is reviewed in a form suitable for the purposes of this paper. The 'lift' force is discussed extensively in recent papers by Auton (1987), Drew & Lahey (1987) and Auton, Hunt & Prud'homme (1988).

In addition to the non-dissipative 'lift' force and well known forces like the viscous stress of the bubbly liquid/gas mixture, the buoyancy force, the Levich-Moore drag force and the dissipative Faxén force (see section 5.4), some other force appears to be required in order to explain the fact that the maximum of the void-fraction profile in cocurrent upward flow occurs at a certain distance from the wall of the tube. At the location of a solid boundary the probability to encounter a gas bubble vanishes. The void fraction accordingly assumes a zero-value at a solid wall. It is known from experiments that very large gradients of the void fraction occur in the immediate vicinity of the wall. The corresponding characteristic lengths appear to be of the order of magnitude of the diameter of the bubbles. The condition required for the application of a macroscopic theory, viz. local equilibrium of the distribution of the gas bubbles in a volume element, seems therefore violated in a relatively thin layer adjacent to the wall. It is possible to cope with that situation by admitting additional terms in the energy density of the two-phase mixture that depend on the gradient of the void fraction. We accordingly extend the theory developed in G (1985a) by introducing the following additional contributions  $\Delta F$  and  $\Delta K$  to, respectively, the free energy density  $F$  and the kinetic energy density  $K$ :

$$\Delta F = \frac{1}{2} g_{11} \rho_l^2 (\nabla \alpha)^2, \quad (5.1.3)$$

$$\Delta K = \frac{1}{2} \rho_l^3 [ (m_{||} - m_{\perp}) \mathbf{w} \mathbf{w} + m_{\perp} w^2 \mathbf{I} ] : \nabla \alpha \nabla \alpha. \quad (5.1.4)$$

Here  $\alpha$  denotes the fraction of the volume occupied by the bubbles (void fraction),  $\mathbf{w} = \mathbf{u}_2 - \mathbf{u}_1$  represents the drift velocity of the bubbles with respect to the liquid, while  $g_{11} \rho_l^2$ ,  $\rho_l^3 m_{\perp}$  and  $\rho_l^3 m_{||}$  are relatively small material coefficients which characterise the bubbly mixture and which are roughly proportional to the square of a bubble radius. The material coefficients may depend weakly on the local value of the void fraction.

Since the expressions for  $\Delta F$  and  $\Delta K$  model in a macroscopic way deviations of the distribution of the gas bubbles from local equilibrium, the right-hand side of (5.1.3) may be attributed partly to the entropy portion  $-TS$  of the free energy density  $F$ . A distribution of the bubbles, which deviates appreciably from equilibrium as a result of a large gradient of the void fraction, has a relatively small probability, in particular at large values of the void fraction due to the excluded volume effect. The corresponding contribution to the entropy density is therefore negative. The major part of  $\Delta F$ , however, comprising the energy associated with the small irregular motions executed by the bubbles during steady flow, has to be attributed to the internal energy portion  $U$  of the free energy density. The small random motions, which come into prominence in the neighbourhood of the wall because of the locally modified bubble distribution, may have a dispersive effect on the macroscopic distribution of the bubbles (see section 5.5). It will be plausible from the preceding remarks that  $g_{11} \geq 0$ .

As a result of the large gradient of the bubble concentration in the vicinity of a solid boundary the local bubble distribution is no more symmetric with respect to an imaginary plane that is locally parallel to the wall. A bubble in the neighbourhood of the wall is consequently subject to a net non-vanishing Bernoulli force which acts in a direction away from the boundary. In a similar way the atoms and molecules at a free surface of a liquid or a solid body experience a net non-vanishing van der Waals force directed towards the interior of the body. It will be clear that the net Bernoulli force should follow from an additional contribution to that part of the kinetic energy density of a bubble dispersion that is associated with the local 'backflow' of the liquid around the bubbles. When terms at most quadratic in the gradient of the void fraction are taken into account, that additional contribution is represented by the right-hand side of (5.1.4). The expression for  $\Delta K$  implies that the virtual-mass coefficient of a bubble dispersion depends on the gradient of the

volume density of the bubbles. In view of (5.1.4) it takes the form of an anisotropic tensor given by

$$[ m(\alpha) + \rho_l^2 m_{\perp} (\nabla\alpha)^2 ] \mathbf{I} + \rho_l^2 ( m_{\parallel} - m_{\perp} ) \nabla\alpha \nabla\alpha . \quad (5.1.5)$$

The virtual-mass coefficient for uniform two-phase flow has been denoted by  $m(\alpha)$ .

Experiments indicate that the dispersive action of the small irregular motions of the bubbles in the neighbourhood of the wall is probably the most prominent effect in the vertical two-phase flow of a bubbly liquid/gas mixture (see e.g. Wang et al. 1987). It will therefore be sufficient for the purposes of this chapter to consider only the modifications brought about in the two-phase flow equations by the addition of expression (5.1.3) to the free energy density (see section 5.3).

The possible importance of an expression like (5.1.3) for describing the macroscopic behaviour of a two-fluid system in the immediate vicinity of a solid boundary was recognised more than three decades ago by Ginzburg & Pitaevskii (1958) in the case of superfluid  $^4\text{He}$  (He II). In He II the superfluid mass density, which vanishes at a solid boundary, attains its bulk value within a few atomic distances from the wall. This so called 'healing' effect was also studied by Hills & Roberts (1977) and Geurst (1980). Expression (5.1.3) may play a role in smoothing out the sharp transition in a discontinuous void-fraction wave (concentration wave) (Wallis, private communication, 1986). The effect of dispersive forces on the propagation of void-fraction waves is now under investigation. It is important to realise that already at the turn of the century Korteweg (1901) introduced terms including gradients of the mass density in the expression of the pressure tensor in order to arrive at a general theory of capillarity in which the changes of the mass density proceed continuously (Truesdell & Noll 1965, p. 514). Similar terms appear in the expression of the pressure tensor derived in section 5.3.

Reynolds stresses will not be considered in this chapter. The tendency of bubbles to concentrate near the boundary in upward cocurrent flow has been observed under laminar as well as turbulent conditions as mentioned by Beyerlein et al. (1985). Even in the case where gas bubbles are allowed to rise in a stagnant liquid, a maximum of the void fraction is found close to the wall of the tube (Zun 1980 and Kapteyn, private communication, 1989). It will be shown, however, in sections 5.5 and 5.6 that although Reynolds stresses are not taken into account, velocity profiles for the liquid phase are obtained which look very similar to the velocity profiles known from one-phase turbulent flow.



## 5.2 Equations governing non-dissipative bubbly flow

The non-dissipative equations of motion for a bubbly liquid/gas mixture were derived in G (1985a) from a generalised form of Hamilton's principle of least action (see Chapter I, section 1.6). Special attention was given to the virtual mass of a bubble dispersion. Hamilton's principle was formulated in terms of Euler coordinates. A similar variational principle formulated in terms of Lagrange coordinates was discussed in G (1986). Surface tension was not considered in these two papers. It was later taken into account by Geurst & Vreenegoor (1987) in their analysis of flow induced bubble deformation (see Chapter II for a more complete account). We review in this section the macroscopic theory just mentioned in a form suitable for the purposes of this chapter.

The reduced densities  $\rho_1$  and  $\rho_2$  of the liquid and the gas phase of a bubbly liquid/gas mixture are defined by

$$\rho_1 = \rho_l (1 - \alpha) , \quad \rho_2 = \rho_g \alpha . \quad (5.2.1)$$

It is assumed that the liquid is incompressible (constant mass density  $\rho_l$ ) and the gas satisfies the ideal gas law ( $p_g = (RT/M)\rho_g$ ). The volume density of the bubbles (void fraction) is denoted by  $\alpha$  in accordance with the notation in section 5.1. The conservation of mass for the two phases and the conservation of the number of bubbles (bubble number density  $n$ ) are expressed, respectively, by

$$\frac{\partial \rho_i}{\partial t} + \nabla \cdot (\rho_i \mathbf{u}_i) = 0 \quad (i=1,2) , \quad (5.2.2)$$

$$\frac{\partial n}{\partial t} + \nabla \cdot (n \mathbf{u}_2) = 0 . \quad (5.2.3)$$

It is usual to assume that the flow proceeds isothermally.

The free energy density  $F^*(\rho_i, n)$  of the bubbly liquid/gas mixture may be decomposed into the sum  $F(\rho_i)$  of the free energy densities of the two phases and the interfacial energy density of the bubbles in the following way :

$$F^*(\rho_i, n) = F(\rho_i) + n \gamma 4\pi a^2 . \quad (5.2.4)$$

The surface tension coefficient is denoted by  $\gamma$ , while the equivalent bubble radius  $a$  is determined by

$$a = \left( \frac{3}{4\pi} \frac{\alpha}{n} \right)^{\frac{1}{3}}. \quad (5.2.5)$$

It is shown in G (1985a) that the free energy density  $F(\rho_i)$  and the thermodynamic potentials  $\mu_i$  ( $i=1,2$ ) satisfy

$$dF = \sum_{i=1}^2 \mu_i d\rho_i, \quad (5.2.6)$$

$$d\mu_1 = \frac{1}{\rho_l} dp_g, \quad d\mu_2 = \frac{1}{\rho_g} dp_g, \quad (5.2.7)$$

$$\sum_{i=1}^2 \rho_i \mu_i = F + p_g. \quad (5.2.8)$$

It follows from (5.2.4) that

$$dF^* = \mu_1^* d\rho_1 + \mu_2 d\rho_2 + \mu_n dn, \quad (5.2.9)$$

where

$$\mu_1^* = \mu_1 - \frac{2\gamma}{\rho_l a}, \quad \mu_n = \frac{\gamma \alpha}{a n}. \quad (5.2.10)$$

Furthermore

$$\rho_1 \mu_1^* + \rho_2 \mu_2 + n \mu_n = F^* + p^* \quad (5.2.11)$$

with

$$p^* = p_g - \frac{2\gamma}{a}. \quad (5.2.12)$$

The kinetic energy density  $K(\rho_i, u_i)$  of the two-phase mixture is composed of the kinetic energy densities of the separate phases and the kinetic energy density associated with the

local backflow of the liquid around the bubbles in the case of relative flow. We accordingly have

$$K(\rho_i, \mathbf{u}_i) = \sum_{i=1}^2 \frac{1}{2} \rho_i u_i^2 + \frac{1}{2} \rho_\ell m(\alpha) w^2, \quad (5.2.13)$$

where  $\mathbf{w} = \mathbf{u}_2 - \mathbf{u}_1$  denotes the relative velocity. The virtual-mass coefficient is represented by  $m(\alpha)$ . The validity of expression (5.2.13), in particular the additivity of the contributions at the right-hand side, is discussed at some length in G (1986). In Geurst & Vreenegoor (1987) the virtual-mass coefficient is allowed to be a function of the Weber number defined by

$$We = \frac{\rho_\ell w^2}{\gamma/2a}. \quad (5.2.14)$$

We assume here that  $We \ll 1$ , so that in a first order of approximation the virtual-mass coefficient depends only on the volume density of the bubbles.

The dynamic equations governing the non-dissipative flow of a bubbly liquid/gas mixture are obtained from Hamilton's principle of least action in the form

$$\delta \int_{t_0}^{t_1} dt \int_{\Omega} dV L(\rho_i, n, \mathbf{u}_i) = 0, \quad (5.2.15)$$

where the Lagrangian density  $L(\rho_i, n, \mathbf{u}_i)$  is given by

$$L(\rho_i, n, \mathbf{u}_i) = K(\rho_i, \mathbf{u}_i) - F^*(\rho_i, n). \quad (5.2.16)$$

The variations in (5.2.15) are subject to the side conditions (5.2.2), (5.2.3) and the two Lin constraints expressed by (see Geurst 1988)

$$\frac{\partial \Psi_i}{\partial t} + \nabla \cdot (\Psi_i \mathbf{u}_i) = 0 \quad (i=1,2). \quad (5.2.17)$$

Introducing the quantities  $\psi_i$  ( $i=1,2$ ) according to  $\Psi_i = \rho_i \psi_i$  we obtain from (5.2.17)

$$\left( \frac{\partial}{\partial t} + \mathbf{u}_i \cdot \nabla \right) \psi_i = 0 \quad (i=1,2). \quad (5.2.18)$$

Variational principle (5.2.15) yields the following equations of motion for the liquid and the gas:

$$\begin{aligned} \frac{\partial \boldsymbol{\pi}_1}{\partial t} + \nabla \left[ \mathbf{u}_1 \cdot \boldsymbol{\pi}_1 + \mu_1^* + \frac{1}{2} m'(\alpha) w^2 - \frac{1}{2} u_1^2 \right] \\ - \mathbf{u}_1 \times (\nabla \times \boldsymbol{\pi}_1) = 0, \end{aligned} \quad (5.2.19)$$

$$\begin{aligned} \frac{\partial \boldsymbol{\pi}_2}{\partial t} + \nabla \left[ \mathbf{u}_2 \cdot \boldsymbol{\pi}_2 + \mu_2 - \frac{1}{2} u_2^2 \right] + \frac{\mathbf{n}}{\rho_2} \nabla \mu_n \\ - \mathbf{u}_2 \times (\nabla \times \boldsymbol{\pi}_2) = 0. \end{aligned} \quad (5.2.20)$$

The generalised momenta  $\boldsymbol{\pi}_i$  ( $i=1,2$ ) taken per unit mass are given by

$$\begin{aligned} \boldsymbol{\pi}_1 &= \mathbf{u}_1 - \frac{\rho_\ell m(\alpha)}{\rho_1} \mathbf{w}, \\ \boldsymbol{\pi}_2 &= \mathbf{u}_2 + \frac{\rho_\ell m(\alpha)}{\rho_2} \mathbf{w}. \end{aligned} \quad (5.2.21)$$

We remark that

$$\begin{aligned} d\mu_1^* &= \frac{1}{\rho_\ell} dp^*, \\ d\mu_2 + \frac{\mathbf{n}}{\rho_2} d\mu_n &= \frac{1}{\rho_g} dp^*. \end{aligned} \quad (5.2.22)$$

The variational procedure yields the following Clebsch representations:

$$\begin{aligned} \boldsymbol{\pi}_1 &= \nabla \varphi_1 + \psi_1 \nabla \chi_1, \\ \boldsymbol{\pi}_2 &= \nabla \varphi_2 + \psi_2 \nabla \chi_2 + \frac{\mathbf{n}}{\rho_2} \nabla \varphi_n. \end{aligned} \quad (5.2.23)$$

The quantities  $\varphi_i$  ( $i=1,2$ ),  $\varphi_n$  and  $\chi_i$  ( $i=1,2$ ) represent Lagrange multipliers associated, respectively, with the constraints (5.2.2), (5.2.3) and (5.2.17) (see Geurst 1988). The Clebsch representations are valid locally (Salmon 1988).

The equations expressing the conservation of total momentum and energy read, respectively,

$$\frac{\partial \mathbf{P}}{\partial t} + \nabla \cdot \mathbf{\Pi} = 0, \quad (5.2.24)$$

$$\frac{\partial \mathbf{H}}{\partial t} + \nabla \cdot \mathbf{Q} = 0, \quad (5.2.25)$$

where

$$\mathbf{P} = \sum_{i=1}^2 \rho_i \boldsymbol{\pi}_i = \sum_{i=1}^2 \rho_i \mathbf{u}_i, \quad (5.2.26)$$

$$\mathbf{\Pi} = \sum_{i=1}^2 \rho_i \mathbf{u}_i \boldsymbol{\pi}_i + p \mathbf{I}, \quad (5.2.27)$$

$$\mathbf{H} = \mathbf{K} + \mathbf{F}^*, \quad (5.2.28)$$

$$\begin{aligned} \mathbf{Q} = & \rho_1 \mathbf{u}_1 \left( \mathbf{u}_1 \cdot \boldsymbol{\pi}_1 + \mu_1^* + \frac{1}{2} m'(\alpha) w^2 - \frac{1}{2} u_1^2 \right) \\ & + \rho_2 \mathbf{u}_2 \left( \mathbf{u}_2 \cdot \boldsymbol{\pi}_2 + \mu_2 + \frac{n}{\rho_2} \mu_n - \frac{1}{2} u_2^2 \right). \end{aligned} \quad (5.2.29)$$

The average pressure  $p$  of the two-phase mixture is given by

$$p = p^* + \frac{1}{2} \rho_\ell (1 - \alpha)^2 \frac{d}{d\alpha} \left( \frac{m(\alpha)}{1 - \alpha} \right) w^2. \quad (5.2.30)$$

Expression (5.2.30) evidently includes the Bernoulli effects that are associated with the local backflow of the liquid around the bubbles in the case of a relative motion of the two phases.

A detailed stability analysis of the system of two-phase flow equations determined by (5.2.2), (5.2.3), (5.2.19) and (5.2.20) shows that a uniform two-phase bubbly flow is marginally stable if and only if the virtual-mass coefficient satisfies

$$m(\alpha) = \frac{1}{2} \alpha (1 - \alpha) (1 - 3\alpha) . \quad (5.2.31)$$

For details see G (1985a) and Geurst & Vreenegoor (1987). Expression (5.2.31) is valid when  $We \ll 1$  (see Chapter II, expression (2.5.14)). The virtual-mass coefficient may be regarded as an order parameter that represents the local microscopic distribution of the gas bubbles on a macroscopic level. The bubble distribution underlying (5.2.31) is apparently anisotropic (G (1985a)).

When the mass ratio  $\rho_g/\rho_l$  is disregarded and the bubble radius  $a$  is taken constant (ping-pong ball approximation) we obtain<sup>†</sup>) from (5.2.2), (5.2.3), (5.2.19) and (5.2.20) in the limit of vanishingly small values of the void fraction equation (5.1.1) for the motion of a single gas bubble in liquid. Indeed, in the limit of an infinitely dilute dispersion of bubbles the expression  $(\partial/\partial t + \mathbf{u}_2 \cdot \nabla) \mathbf{u}_2$  may be identified with the acceleration  $d\mathbf{u}_2/dt$  of a single bubble. Equation (5.1.1) may be put in the form (5.1.2), where the left-hand side represents  $m_1$  times the relative acceleration of a bubble with respect to a frame that is rigidly attached to the locally rotating liquid. The left-hand side is accordingly objective (G (1986) and Drew and Lahey 1987).

### 5.3 Additional terms required near solid boundary

It was discussed at some length in the introductory section of this chapter that the free energy density  $F^*(\rho_{i,n})$  of a two-phase bubbly mixture has to be extended to the free energy density  $\hat{F}(\rho_{i,n}, \nabla \rho_1)$  determined by (see (5.1.3))

$$\hat{F}(\rho_{i,n}, \nabla \rho_1) = F^*(\rho_{i,n}) + \frac{1}{2} g_{11} (\nabla \rho_1)^2 \quad (5.3.1)$$

in order to take into account the small irregular motions of the bubbles observed in two-phase bubbly flow near a solid boundary. If  $g_{11}$  is constant, it follows from (5.3.1) that

$$d\hat{F} = \hat{\mu}_1 d\rho_1 + \mu_2 d\rho_2 + \mu_n dn + \nabla \cdot (g_{11} \nabla \rho_1 d\rho_1) , \quad (5.3.2)$$

---

†) We take the opportunity to make the following correction in expression (6.3) of G (1986): the factor preceding  $\nabla \cdot \mathbf{v}_2$  should read  $m(\alpha)/\alpha - m'(\alpha)$ . The correction does not have consequences for the subsequent results of the paper.

where

$$\hat{\mu}_1 = \frac{\delta \hat{F}}{\delta \rho_1} = \mu_1^* - \nabla \cdot (g_{11} \nabla \rho_1). \quad (5.3.3)$$

When expression (5.3.1) is used in the Lagrangian density (5.2.16), it is recognised by comparing (5.2.9) and (5.3.2) that the equations of motion resulting from Hamilton's principle of least action (5.2.15) may be obtained from (5.2.19) and (5.2.20) by substituting the thermodynamic potential  $\hat{\mu}_1$  for  $\mu_1^*$ . In that case the pressure  $p^*$  appearing in (5.2.30) has to be replaced by  $\hat{p}$  determined by (cf. (5.2.11))

$$\hat{p} = \rho_1 \hat{\mu}_1 + \rho_2 \mu_2 + n \mu_n - \hat{F}. \quad (5.3.4)$$

By virtue of (5.2.11), (5.3.1), (5.3.3) and (5.3.4) we have

$$\hat{p} = p^* - g_{11} \left[ \rho_1 \Delta \rho_1 + \frac{1}{2} (\nabla \rho_1)^2 \right], \quad (5.3.5)$$

where  $\Delta$  denotes the Laplacian operator. It is derived in a straightforward way that the momentum flux  $\Pi$  (see (5.2.27)), the energy density  $H$  (see (5.2.28)) and the energy flux  $Q$  (see (5.2.29)) are extended, respectively, to

$$\Pi = \sum_{i=1}^2 \rho_i \mathbf{u}_i \boldsymbol{\pi}_i + p \mathbf{I} + g_{11} \nabla \rho_1 \nabla \rho_1, \quad (5.3.6)$$

$$H = K + \hat{F}, \quad (5.3.7)$$

$$\begin{aligned} Q = & \rho_1 \mathbf{u}_1 \left( \mathbf{u}_1 \cdot \boldsymbol{\pi}_1 + \hat{\mu}_1 + \frac{1}{2} m'(\alpha) w^2 - \frac{1}{2} u_1^2 \right) \\ & + \rho_2 \mathbf{u}_2 \left( \mathbf{u}_2 \cdot \boldsymbol{\pi}_2 + \mu_2 + \frac{n}{\rho_2} \mu_n - \frac{1}{2} u_2^2 \right) \\ & - g_{11} \nabla \rho_1 \frac{\partial \rho_1}{\partial t}. \end{aligned} \quad (5.3.8)$$

In view of expression (5.2.30) and the remark preceding (5.3.4) the pressure  $p$  of the bubbly liquid/gas mixture is given by

$$p = \hat{p} + \frac{1}{2} \rho_\ell (1 - \alpha)^2 \frac{d}{d\alpha} \left( \frac{m(\alpha)}{1 - \alpha} \right) w^2. \quad (5.3.9)$$

The two terms that appear at the right-hand side of (5.3.6) and (5.3.8) with the coefficient  $g_{11}$  originate from the divergence term in (5.3.2). Similar expressions have been derived in the macroscopic analysis of 'healing' phenomena in He II near a solid boundary (see e.g. Geurst 1980).

#### 5.4 Dissipative effects and external forces

The terms which represent dissipative effects have to be introduced in the equations of motion in such a way that the conservation of mass and the conservation of total linear momentum are not violated. In spite of these restrictions, however, there may be some arbitrariness in the selection of the dissipative forces. That is the reason, why the presentation in this section looks somewhat different from the discussion given in the appendix of G (1985a). The different approaches, however, prove to be equivalent.

The two-phase flow equations for the liquid and the gas are extended, respectively, to

$$\begin{aligned} \frac{\partial \boldsymbol{\pi}_1}{\partial t} + \nabla [ \mathbf{u}_1 \cdot \boldsymbol{\pi}_1 + \hat{\mu}_1 + \frac{1}{2} m'(\alpha) w^2 - \frac{1}{2} u_1^2 ] - \mathbf{u}_1 \times (\nabla \times \boldsymbol{\pi}_1) = \\ = \frac{1}{\rho_1} \mathbf{F} + \frac{1}{\rho_1} \nabla \cdot \boldsymbol{\sigma} - \frac{1}{\rho} \nabla \cdot \boldsymbol{\tau} + \frac{1}{\rho_1} \mathbf{F}_1 \end{aligned} \quad (5.4.1)$$

and

$$\begin{aligned} \frac{\partial \boldsymbol{\pi}_2}{\partial t} + \nabla [ \mathbf{u}_2 \cdot \boldsymbol{\pi}_2 + \mu_2 - \frac{1}{2} u_2^2 ] + \frac{n}{\rho_2} \nabla \mu_n - \mathbf{u}_2 \times (\nabla \times \boldsymbol{\pi}_2) = \\ = - \frac{1}{\rho_2} \mathbf{F} - \frac{1}{\rho_2} \nabla \cdot \boldsymbol{\sigma} - \frac{1}{\rho} \nabla \cdot \boldsymbol{\tau} + \frac{1}{\rho_2} \mathbf{F}_2 . \end{aligned} \quad (5.4.2)$$

The external force densities are represented by  $\mathbf{F}_1$  and  $\mathbf{F}_2$ . The viscous stress tensor of the bubbly liquid/gas mixture is denoted by  $\boldsymbol{\tau}$ , while  $\mathbf{F}$  and  $\nabla \cdot \boldsymbol{\sigma}$  are the densities of mutual friction forces which act on the two phases during relative flow. It is easily recognised that the balance of total momentum corresponding to (5.4.1) and (5.4.2) is expressed by

$$\frac{\partial \mathbf{P}}{\partial t} + \nabla \cdot \boldsymbol{\Pi} = \mathbf{F}_1 + \mathbf{F}_2 , \quad (5.4.3)$$

where the momentum density  $\mathbf{P}$  is given by (5.2.26) and the momentum flux  $\boldsymbol{\Pi}$  is determined by



$$\Pi = \sum_{i=1}^2 \rho_i \mathbf{u}_i \boldsymbol{\pi}_i + g_{11} \nabla \rho_1 \nabla \rho_1 + p \mathbf{I} + \boldsymbol{\tau}. \quad (5.4.4)$$

When dissipative effects are taken into account the energy conservation equation (5.2.25) has to be generalised to an equation expressing a balance of energy of the following form:

$$\frac{\partial H}{\partial t} + \nabla \cdot \mathbf{Q} = -R_d, \quad (5.4.5)$$

where  $R_d$  denotes the rate of dissipation. The energy density  $H$  is given according to (5.3.7) by

$$\begin{aligned} H = & \sum_{i=1}^2 \frac{1}{2} \rho_i u_i^2 + \frac{1}{2} \rho_\ell m(\alpha) w^2 \\ & + F(\rho_i) + 3 \frac{\gamma}{a} \alpha + \frac{1}{2} g_{11} (\nabla \rho_1)^2. \end{aligned} \quad (5.4.6)$$

It is easily verified that the energy flux  $\mathbf{Q}$  and the rate of dissipation  $R_d$  should take the form

$$\begin{aligned} \mathbf{Q} = & \rho_1 \mathbf{u}_1 \left( \mathbf{u}_1 \cdot \boldsymbol{\pi}_1 + \hat{\mu}_1 + \frac{1}{2} m'(\alpha) w^2 - \frac{1}{2} u_1^2 \right) \\ & + \rho_2 \mathbf{u}_2 \left( \mathbf{u}_2 \cdot \boldsymbol{\pi}_2 + \mu_2 + \frac{n}{\rho_2} \mu_n - \frac{1}{2} u_2^2 \right) \\ & - g_{11} \nabla \rho_1 \frac{\partial \rho_1}{\partial t} + \boldsymbol{\sigma} \cdot \mathbf{w} + \boldsymbol{\tau} \cdot \mathbf{u} \end{aligned} \quad (5.4.7)$$

and

$$R_d = \mathbf{F} \cdot \mathbf{w} - \boldsymbol{\sigma} : \nabla \mathbf{w} - \boldsymbol{\tau} : \nabla \mathbf{u}. \quad (5.4.8)$$

The average mass velocity of the two-phase mixture is denoted by  $\mathbf{u}$ , i.e.,

$$\rho \mathbf{u} = \sum_{i=1}^2 \rho_i \mathbf{u}_i, \quad (5.4.9)$$

where  $\rho = \rho_1 + \rho_2$ . Note that the fragmentation and coalescence of bubbles, which may be treated as an independent dissipative process, have been disregarded. A similar remark applies to the diffusive flux of the bubbles with respect to the average mass velocity  $\mathbf{u}_2$ .

A second order tensor like  $\tau$  can be decomposed in the following way:

$$\tau = \text{dev } \tau + \frac{1}{3} \text{tr}(\tau) \mathbf{I} + \frac{1}{2} (\tau - \tau^T), \quad (5.4.10)$$

where the deviatoric part is given by

$$\text{dev } \tau = \frac{1}{2} (\tau + \tau^T) - \frac{1}{3} \text{tr}(\tau) \mathbf{I}. \quad (5.4.11)$$

We apply the decomposition (5.4.10) to the second-order tensors that appear in the bilinear form (5.4.8) for the rate of dissipation  $R_d$  and use the thermodynamics of irreversible processes (see de Groot & Mazur 1962). On account of Curie's theorem for an isotropic medium (note that the anisotropy associated with the direction of  $\nabla \rho_1$  is disregarded as in the case of the virtual-mass coefficient) we introduce the following constitutive relations:

$$\begin{bmatrix} -\text{dev } \tau \\ -\text{dev } \sigma \end{bmatrix} = \begin{bmatrix} A_{11} & A_{12} \\ A_{21} & A_{22} \end{bmatrix} \begin{bmatrix} \text{dev } \nabla \mathbf{u} \\ \text{dev } \nabla \mathbf{w} \end{bmatrix}, \quad (5.4.12)$$

$$-\frac{1}{2} (\sigma - \sigma^T) = A \frac{1}{2} [ \nabla \mathbf{w} - (\nabla \mathbf{w})^T ], \quad (5.4.13)$$

$$\mathbf{F} = B \mathbf{w}, \quad (5.4.14)$$

$$\begin{bmatrix} -\frac{1}{3} \text{tr}(\tau) \\ -\frac{1}{3} \text{tr}(\sigma) \end{bmatrix} = \begin{bmatrix} C_{11} & C_{12} \\ C_{21} & C_{22} \end{bmatrix} \begin{bmatrix} \nabla \cdot \mathbf{u} \\ \nabla \cdot \mathbf{w} \end{bmatrix}. \quad (5.4.15)$$

The material coefficients, which are allowed to depend on  $\rho_1$  and  $\rho_2$ , should satisfy the Onsager relations

$$A_{12} = A_{21}, \quad C_{12} = C_{21}. \quad (5.4.16)$$

According to the second law of thermodynamics the matrices  $A_{ij}$  and  $C_{ij}$  ( $i, j=1, 2$ ) are positive semi-definite, while the material coefficients  $A$  and  $B$  can take only non-negative values. Since the constitutive relations have to fulfil the requirement of objectivity (material frame indifference; see e.g. Truesdell & Noll 1965) the viscous stress tensor  $\tau$  is symmetric. The equation that expresses the vanishing of the antisymmetric part of  $\tau$  has been deleted from the constitutive relations (5.4.12) to (5.4.15).

With a view to the analysis of the vertical flow of a bubbly liquid/gas mixture to be given in the next section and in order to indicate clearly the physical meaning of the various material coefficients we introduce the following notations and simplifications:

$$A_{11} = 2 \eta_u , \quad A_{12} = A_{21} = 0 , \quad A_{22} = 2 \eta_w , \quad (5.4.17)$$

$$A = 2 \eta_F , \quad (5.4.18)$$

$$B = \eta_{LM} \frac{1}{a^2} , \quad (5.4.19)$$

$$C_{11} = \zeta_u , \quad C_{12} = C_{21} = 0 , \quad C_{22} = \zeta_w . \quad (5.4.20)$$

The constitutive relations (5.4.12) to (5.4.15) now take the form

$$-\tau = \eta_u [ \nabla \mathbf{u} + (\nabla \mathbf{u})^T ] + (\zeta_u - \frac{1}{3} \eta_u) \nabla \cdot \mathbf{u} \mathbf{I} , \quad (5.4.21)$$

$$-\sigma = \eta_w [ \nabla \mathbf{w} + (\nabla \mathbf{w})^T ] + (\zeta_w - \frac{1}{3} \eta_w) \nabla \cdot \mathbf{w} \mathbf{I} \\ + \eta_F [ \nabla \mathbf{w} - (\nabla \mathbf{w})^T ] , \quad (5.4.22)$$

$$\mathbf{F} = \eta_{LM} \frac{1}{a^2} \mathbf{w} . \quad (5.4.23)$$

Note that the cross-effects determined by the (small) off-diagonal elements of the matrices  $A_{ij}$  and  $C_{ij}$  ( $i, j=1, 2$ ) have been disregarded. It will be clear from (5.4.21) that  $\eta_u$  and  $\zeta_u$  represent, respectively, the dynamic and second viscosity of the bubbly mixture. The last term at the right-hand side of (5.4.22) determines a couple of the Faxén type. When the interactions of the bubbles are neglected we may write

$$\eta_F = \eta_e \alpha , \quad (5.4.24)$$

where  $\eta_e$  denotes an effective viscosity of the bubble dispersion. In a local Stokes flow, where a no-slip boundary condition prevails at the surface of the bubbles, it is true that

$$\eta_e = \frac{3}{4} \eta , \quad (5.4.25)$$

where  $\eta$  represents the viscosity of the liquid (see e.g. Happel & Brenner 1973). Expression (5.4.23) for  $F$  corresponds to the Levich–Moore mutual friction force. In the case where the interactions of the bubbles are disregarded, we have (Levich 1962)

$$\eta_{LM} = 9 \eta \alpha . \tag{5.4.26}$$

In view of the simplifications which have been introduced it will be clear that the viscosity coefficients in the constitutive relations (5.4.21) to (5.4.23) are not completely independent of the physical conditions under which the two–phase flow of a bubbly liquid/gas mixture proceeds. Their values may in fact be adjusted somewhat in order to meet the requirements of a particular type of flow. A mild form of that procedure is adopted in section 5.6, where the theoretical results of section 5.5 concerning vertical two–phase flow are compared with some known experimental data. Matching of the theoretical and experimental results proves to be successful in producing reasonable values for the material coefficients.

### 5.5 Bubbly flow through vertical tube : asymptotic solution

We consider a two–phase bubbly flow through a vertical cylindrical tube of circular cross–section (radius  $R_0$ ). It is assumed that the flow is steady, vertically uniform and rotationally symmetric (no swirl). A system of cylindrical coordinates  $(r, \theta, z)$  is used with symmetry axis along the centre line of the tube. The external forces experienced by the liquid and the gas of the bubbly mixture result from gravity, i.e.,

$$F_i = - \rho_i g i_z \tag{5.5.1} \quad (i=1,2) .$$

It will be assumed in the analysis of this section that the masses of the gas bubbles are approximately equal. In addition, the mass density  $\rho_g$  of the gas is taken constant. The spherical bubbles are accordingly characterised by a constant radius  $a$  (ping–pong ball approximation). That approximation seems to be justified *locally*, when the Mach number itself and the Mach number divided by the local Froude number are small, i.e.,

$$w^2 / \left[ \frac{\rho_g}{\rho_l} \right] \left[ \frac{RT}{M} \right] \ll 1 \quad \text{and} \quad gh / \left[ \frac{\rho_g}{\rho_l} \right] \left[ \frac{RT}{M} \right] \ll 1, \tag{5.2.2}$$

where  $h$  denotes the height of the tube section. The ping–pong ball approximation is

evidently not valid *globally* because the bubble radius will vary (weakly) with vertical position. Since we are only interested in local properties of vertical two-phase flow, that variation is disregarded here. It is also in accordance with the assumption of uniformity of the flow in vertical direction.

In view of the assumptions of steadiness, vertical uniformity and rotational symmetry of the flow all quantities with the exception of the pressure depend only on the radial coordinate  $r$ . In the case of axial flow the pressure  $p^*$  should in addition be a function of the coordinate  $z$ . The mass conservation equations (5.2.2) and equation (5.2.3) expressing the conservation of bubble number are satisfied when  $\mathbf{u}_i = (0, 0, u_i)^T$ , where  $u_i = u_i(r)$ . Accordingly  $\boldsymbol{\pi}_i = (0, 0, \pi_i)^T$  with  $\pi_i = \pi_i(r)$ . The equations of motion (5.4.1) and (5.4.2) now take the following form in cylindrical coordinates:

$$\begin{aligned} \frac{d}{dr} \left[ u_1 \pi_1 - \frac{1}{2} u_1^2 + \frac{1}{2} m'(\alpha) w^2 + \rho_\ell \frac{1}{r} \frac{d}{dr} \left( g_{11} r \frac{d\alpha}{dr} \right) \right] \\ - u_1 \frac{d\pi_1}{dr} = - \frac{1}{\rho_\ell} \frac{\partial p^*}{\partial r}, \end{aligned} \quad (5.5.3)$$

$$\begin{aligned} - \frac{1}{\rho_\ell} \frac{\partial p^*}{\partial z} + \frac{1}{\rho_1 a^2} \eta_{LM} w - \frac{1}{\rho_1} \frac{1}{r} \frac{d}{dr} \left( (\eta_w + \eta_F) r \frac{dw}{dr} \right) \\ + \frac{1}{\rho_1 + \rho_2} \frac{1}{r} \frac{d}{dr} \left( \eta_u r \frac{du}{dr} \right) - g = 0, \end{aligned} \quad (5.5.4)$$

$$\frac{d}{dr} \left( u_2 \pi_2 - \frac{1}{2} u_2^2 \right) - u_2 \frac{d\pi_2}{dr} = - \frac{1}{\rho_g} \frac{\partial p^*}{\partial r}, \quad (5.5.5)$$

$$\begin{aligned} - \frac{1}{\rho_g} \frac{\partial p^*}{\partial z} - \frac{1}{\rho_2 a^2} \eta_{LM} w + \frac{1}{\rho_2} \frac{1}{r} \frac{d}{dr} \left( (\eta_w + \eta_F) r \frac{dw}{dr} \right) \\ + \frac{1}{\rho_1 + \rho_2} \frac{1}{r} \frac{d}{dr} \left( \eta_u r \frac{du}{dr} \right) - g = 0. \end{aligned} \quad (5.5.6)$$

In deriving these equations the constitutive relations (5.4.21) to (5.4.23) have been used.

It follows from (5.5.3) to (5.5.6) that

$$p^* = -Cz + h(r), \quad (5.5.7)$$

where C is a constant. By combining (5.5.4), (5.5.6) and (5.5.7) we obtain the equations

$$C + \frac{1}{r} \frac{d}{dr} (\eta_u r \frac{du}{dr}) - (\rho_1 + \rho_2) g = 0 \quad (5.5.8)$$

and

$$\begin{aligned} - (1 - \frac{\rho_g}{\rho_\ell}) C + (1 + \frac{\rho_g}{\rho_\ell} \frac{\alpha}{1-\alpha}) [ \frac{1}{\alpha a^2} \eta_{LM} w \\ - \frac{1}{\alpha} \frac{1}{r} \frac{d}{dr} ( (\eta_w + \eta_F) r \frac{dw}{dr} ) ] = 0. \end{aligned} \quad (5.5.9)$$

Equation (5.5.8) expresses the balance of total linear momentum in the axial direction. Elimination of the pressure gradient between (5.5.3) and (5.5.5) yields

$$\begin{aligned} - \frac{m(\alpha)}{\alpha(1-\alpha)} w \frac{du_1}{dr} + [ m'(\alpha) - \frac{m(\alpha)}{\alpha} ] w \frac{dw}{dr} + \frac{1}{2} m'(\alpha) w^2 \frac{d\alpha}{dr} \\ + \rho_\ell \frac{d}{dr} [ \frac{1}{r} \frac{d}{dr} (g_{11} r \frac{d\alpha}{dr}) ] = 0. \end{aligned} \quad (5.5.10)$$

Since  $\rho_g/\rho_\ell$  is very small, equations (5.5.8) and (5.5.9) may be reduced to

$$C + \frac{1}{r} \frac{d}{dr} (\eta_u r \frac{du_1}{dr}) - \rho_\ell (1 - \alpha) g = 0 \quad (5.5.11)$$

and

$$- C + \frac{1}{\alpha a^2} \eta_{LM} w - \frac{1}{\alpha} \frac{1}{r} \frac{d}{dr} ( (\eta_w + \eta_F) r \frac{dw}{dr} ) = 0. \quad (5.5.12)$$

Equations (5.5.10), (5.5.11) and (5.5.12) constitute a seventh order system of ordinary differential equations for the determination of  $\alpha$ ,  $u_1$  and  $w$  as a function of  $r$ . Note the role of the axial pressure gradient C as one of the external parameters characterising the physical conditions of the flow. In view of axial symmetry the solutions have to fulfil at the tube axis the requirements

$$(\frac{d\alpha}{dr})_{r=0} = (\frac{du_1}{dr})_{r=0} = (\frac{dw}{dr})_{r=0} = 0. \quad (5.5.13)$$

Furthermore

$$(u_1)_{r=0} = (u_1)_0, \quad (5.5.14)$$

where  $(u_1)_0$  is the given value of the liquid velocity at the tube axis. It seems natural to impose at the wall of the tube the boundary conditions

$$\begin{aligned} (\alpha)_{r=R_0} &= 0 && \text{(excluded volume),} \\ (u_1)_{r=R_0} &= 0 && \text{(no slip),} \\ \left(\frac{dw}{dr}\right)_{r=R_0} &= 0 && \text{(vanishing Faxén couple).} \end{aligned} \quad (5.5.15)$$

When the viscosity coefficient  $\eta_{LM}$  is expressed according to (5.4.26), we derive from (5.5.12) on account of the boundary conditions (5.5.13) and (5.5.15)

$$w = w_0, \quad (5.5.16)$$

where  $w_0$  denotes the value of the relative velocity at the tube axis. Equation (5.5.12) accordingly reduces to

$$C = \frac{9\eta}{a^2} w_0. \quad (5.5.17)$$

It will be assumed that the value of the dynamic viscosity  $\eta_u$  of the bubbly mixture is constant and that the virtual-mass coefficient  $m(\alpha)$  is determined by its expression (5.2.31) corresponding to marginal stability of a uniform two-phase flow. When the velocities and the radial coordinate are made dimensionless by means of, respectively, the constant relative velocity  $w_0$  and the tube radius  $R_0$ , equations (5.5.10) and (5.5.11) take the form

$$\alpha - \alpha_e + \epsilon_1 \frac{1}{r} \frac{d}{dr} \left( r \frac{du_1}{dr} \right) = 0, \quad (5.5.18)$$

$$(1 - 3\alpha) \frac{du_1}{dr} + (4 - 9\alpha) \frac{d\alpha}{dr} - \gamma_{11} \frac{d}{dr} \left[ \frac{1}{r} \frac{d}{dr} \left( r \frac{d\alpha}{dr} \right) \right] = 0, \quad (5.5.19)$$

where

$$\alpha_e = 1 - \frac{9\eta w_0}{\rho_l g a^2}, \quad \epsilon_1 = \frac{a^2 Fr}{R_0^2 Re},$$

$$Re = \frac{\rho_l a w_0}{\eta_u}, \quad Fr = \frac{w_0^2}{g a}, \quad (5.5.20)$$

$$\gamma_{11} = 2 \frac{a^2 g_{11} \rho_l}{R_0^2 w_0^2 a^2}.$$

Equation (5.5.18) expresses the balance of forces acting on the bubbly mixture in vertical direction. The term  $\alpha_e$  appearing in (5.5.18) clearly vanishes when the bubbles of a dilute dispersion attain their terminal velocity, while the last term takes account of the viscous shear force. The three terms in (5.5.19) represent, respectively, the lift force experienced by bubbles in a shear flow, the gradient of the Bernoulli pressure associated with the local backflow of the liquid around a bubble (see the third term in the expression between square brackets appearing in (5.4.1)) and the dispersive force resulting from the small irregular motions of the bubbles. By eliminating  $u_1$  between (5.5.18) and (5.5.19) we finally obtain

$$\alpha - \alpha_e - \epsilon_1 \frac{1}{r} \frac{d}{dr} \left[ \frac{4-9\alpha}{1-3\alpha} r \frac{d\alpha}{dr} \right]$$

$$+ \epsilon_2 \frac{1}{r} \frac{d}{dr} \left\{ \frac{1}{1-3\alpha} r \frac{d}{dr} \left[ \frac{1}{r} \frac{d}{dr} \left( r \frac{d\alpha}{dr} \right) \right] \right\} = 0, \quad (5.5.21)$$

where  $\epsilon_2 = \gamma_{11} \epsilon_1$ .

When  $\alpha$  is small, the equations may be linearised in order to arrive at an approximate solution. The linearised versions of (5.5.19) and (5.5.21) read

$$\frac{du_1}{dr} + 4 \frac{d\alpha}{dr} - \gamma_{11} \frac{d}{dr} \left[ \frac{1}{r} \frac{d}{dr} \left( r \frac{d\alpha}{dr} \right) \right] = 0, \quad (5.5.22)$$

$$\alpha - \alpha_e - 4 \epsilon_1 \frac{1}{r} \frac{d}{dr} \left( r \frac{d\alpha}{dr} \right)$$

$$+ \epsilon_2 \frac{1}{r} \frac{d}{dr} \left\{ r \frac{d}{dr} \left[ \frac{1}{r} \frac{d}{dr} \left( r \frac{d\alpha}{dr} \right) \right] \right\} = 0. \quad (5.5.23)$$



The boundary conditions to be associated with these equations should follow from (5.5.13), (5.5.14) and (5.5.15). We first infer from (5.5.22) that

$$\left\{ \frac{d}{dr} \left[ \frac{1}{r} \frac{d}{dr} \left( r \frac{d\alpha}{dr} \right) \right] \right\}_{r=0} = 0. \quad (5.5.24)$$

By integrating (5.5.23) and (5.5.22) we then obtain

$$\int_0^r (\alpha - \alpha_e) r \, dr = 4 \epsilon_1 r \frac{d\alpha}{dr} - \epsilon_2 r \frac{d}{dr} \left[ \frac{1}{r} \frac{d}{dr} \left( r \frac{d\alpha}{dr} \right) \right], \quad (5.5.25)$$

$$u_1 = -4 \alpha + \gamma_{11} \left\{ \frac{1}{r} \frac{d}{dr} \left( r \frac{d\alpha}{dr} \right) - \left[ \frac{1}{r} \frac{d}{dr} \left( r \frac{d\alpha}{dr} \right) \right]_{r=1} \right\}, \quad (5.5.26)$$

$$\begin{aligned} \int_0^r u_1 r \, dr = & - \left\{ 2 \alpha_e + \frac{\gamma_{11}}{2} \left[ \frac{1}{r} \frac{d}{dr} \left( r \frac{d\alpha}{dr} \right) \right]_{r=1} \right\} r^2 \\ & + (\gamma_{11} - 16 \epsilon_1) r \frac{d\alpha}{dr} + 4 \epsilon_2 r \frac{d}{dr} \left[ \frac{1}{r} \frac{d}{dr} \left( r \frac{d\alpha}{dr} \right) \right]. \end{aligned} \quad (5.5.27)$$

The average  $\langle u_1 \rangle$  of the liquid velocity is accordingly given by

$$\begin{aligned} \langle u_1 \rangle = 2 \int_0^1 u_1 r \, dr = & -4 \alpha_e + (\gamma_{11} - 32 \epsilon_1 - 8 \epsilon_2) \left( \frac{d\alpha}{dr} \right)_{r=1} \\ & - (\gamma_{11} - 8 \epsilon_2) \left( \frac{d^2\alpha}{dr^2} \right)_{r=1} + 8 \epsilon_2 \left( \frac{d^3\alpha}{dr^3} \right)_{r=1}, \end{aligned} \quad (5.5.28)$$

while the void fraction averaged over a cross-section of the tube is determined by

$$\begin{aligned} \langle \alpha \rangle = 2 \int_0^1 \alpha r \, dr = & \alpha_e + 2 (4 \epsilon_1 + \epsilon_2) \left( \frac{d\alpha}{dr} \right)_{r=1} \\ & - 2 \epsilon_2 \left[ \left( \frac{d^2\alpha}{dr^2} \right)_{r=1} + \left( \frac{d^3\alpha}{dr^3} \right)_{r=1} \right]. \end{aligned} \quad (5.5.29)$$

It will be clear that the solutions of the fourth order linear differential equation (5.5.23) have to satisfy the boundary conditions (5.5.24) and (5.5.28). Note that expression (5.5.28) may

be used as an alternative for boundary condition (5.5.14). In view of (5.5.13) and (5.5.15) the set of boundary conditions is completed by requiring that

$$\left(\frac{d\alpha}{dr}\right)_{r=0} = (\alpha)_{r=1} = 0. \quad (5.5.30)$$

The quantity  $\alpha_e$  and the average  $\langle u_1 \rangle$  of the liquid velocity play the role of external physical parameters.

Equation (5.5.23) is not readily solved in closed form. We therefore attempt an asymptotic analysis. Experimental results (see e.g. Wang et al. 1987) indicate that a reasonable value for  $\gamma_{11}$  is given by

$$\gamma_{11} \approx 10^{-2}. \quad (5.5.31)$$

The following orders of magnitude are commonly encountered in vertical bubbly flow (see the next section):

$$\frac{a}{R_0} \approx 10^{-2}, \quad \frac{Re}{Fr} \approx 10. \quad (5.5.32)$$

It follows from (5.5.20) and (5.5.32) that

$$\epsilon_1 \approx 10^{-5}. \quad (5.5.33)$$

In view of (5.5.31) and (5.5.33) the *outer* solution satisfying (5.5.22) and (5.5.23) is, in a first order of approximation, given by

$$\alpha = \alpha_e, \quad u_1 = (u_1)_0. \quad (5.5.34)$$

We now apply the coordinate transformation

$$y = -\ln r. \quad (5.5.35)$$

Equation (5.5.23) takes in that case the form

$$\epsilon_2 e^{2y} \frac{d^2}{dy^2} ( e^{2y} \frac{d^2 \alpha}{dy^2} ) - 4 \epsilon_1 e^{2y} \frac{d^2 \alpha}{dy^2} + \alpha - \alpha_e = 0 , \quad (5.5.36)$$

while equation (5.5.22) is transformed into

$$\frac{d u_1}{dy} + 4 \frac{d \alpha}{dy} - \gamma_{11} \frac{d}{dy} ( e^{2y} \frac{d^2 \alpha}{dy^2} ) = 0 . \quad (5.5.37)$$

By introducing the strained coordinate  $\bar{y}$  by means of

$$y = \epsilon_2^{\frac{1}{4}} \bar{y} \quad (5.5.38)$$

we derive from (5.5.36) and (5.5.37) that the *inner* solution is, in a first order of approximation, determined by

$$\frac{d^4 \alpha}{d\bar{y}^4} + \alpha - \alpha_e = 0 , \quad (5.5.39)$$

$$\frac{d \bar{u}_1}{d\bar{y}} - \frac{d^3 \alpha}{d\bar{y}^3} = 0 , \quad (5.5.40)$$

where  $u_1 = (\gamma_{11}/\epsilon_1)^{\frac{1}{2}} \bar{u}_1$ . According to (5.5.31) and (5.5.33) we have  $(\epsilon_1/\gamma_{11})^{\frac{1}{2}} \approx 3 \times 10^{-2}$ . The boundary conditions to be associated with equation (5.5.39) are expressed by (see (5.5.28))

$$(\alpha)_{\bar{y}=0} = 0 , \quad \left[ \frac{d^2 \alpha}{d\bar{y}^2} \right]_{\bar{y}=0} = - \langle \bar{u}_1 \rangle , \quad (5.5.41)$$

and

$$\alpha - \alpha_e \rightarrow 0 , \quad \frac{d \alpha}{d\bar{y}} \rightarrow 0 , \quad \text{when } \bar{y} \rightarrow \infty .$$

The conditions at infinity provide for the matching of the inner and outer solutions. Note that the average  $\langle \bar{u}_1 \rangle$  of the strained liquid velocity has been introduced according to  $\langle u_1 \rangle = (\gamma_{11}/\epsilon_1)^{\frac{1}{2}} \langle \bar{u}_1 \rangle$ . The solution of (5.5.40) requires the additional boundary condition

$$(\bar{u}_1)_{\bar{y}=0} = 0 . \quad (5.5.42)$$

The inner solution determined by the differential equations (5.5.39), (5.5.40) with the boundary conditions (5.5.41), (5.5.42) is now given by

$$\frac{\alpha - \alpha_e}{\alpha_e} = - \left[ \cos y^* - \frac{(\bar{u}_1)_0}{\alpha_e} \sin y^* \right] e^{-y^*}, \quad (5.5.43)$$

$$\frac{\bar{u}_1 - (\bar{u}_1)_0}{(\bar{u}_1)_0} = - \left[ \cos y^* + \frac{\alpha_e}{(\bar{u}_1)_0} \sin y^* \right] e^{-y^*},$$

where  $y^* = 2^{-\frac{1}{2}} \bar{y} = -2^{-\frac{1}{2}} \epsilon_2^{-\frac{1}{4}} \ln r$ . It is easily verified by means of (5.5.41) and (5.5.43) that

$$\langle \bar{u}_1 \rangle = (\bar{u}_1)_0. \quad (5.5.44)$$

The equality expressed by (5.5.44) is valid in a first order of approximation. It results from the fact that in that order of approximation the velocity profile of the liquid may be considered as flat (turbulent-like profile; see the next section). In the same order of approximation we have according to (5.5.29)

$$\langle \alpha \rangle = \alpha_e. \quad (5.5.45)$$

It is easily verified by means of (5.5.28), (5.5.29) and (5.5.44) that in a first order of approximation

$$(\bar{u}_1)_0 = - \left[ \frac{d^2 \alpha}{d\bar{y}^2} \right]_{\bar{y}=0}. \quad (5.5.46)$$

Equation (5.5.46) implies that for upward (downward) flow of the liquid the void-fraction profile at the wall of the tube is concave (convex) when considered as a function of  $y = -\ln r$ . That property of vertical two-phase flow is also found experimentally. We refer the reader for more details to the next section, where the solutions of equations (5.5.18) and (5.5.19) satisfying some appropriate dimensionless forms of the boundary conditions (5.5.13), (5.5.14) and (5.5.15) are studied numerically together with their linear and asymptotic approximations. The numerical results are matched there with some known experimental data.

### 5.6 Numerical results

In section 5.5 equations (5.5.18) and (5.5.19) were linearised and solved by deriving the first order asymptotic approximation (5.5.43). We now wish to deal with the solutions of (5.5.18) and (5.5.19) in more detail. After integrating the equations numerically we are able to compare the asymptotic solution, the numerical solution of the linearised equations and the numerical solution of the nonlinear equations. The correlation of theoretical and experimental results is analysed next. In order to substantiate the theory a rather complete picture of vertical two-phase flow is given by making a comparison with experiments on upward flow (Serizawa et al. 1975 and Wang et al. 1987), downward flow (Wang et al. 1987) and the collective rise of bubbles in a stagnant liquid (Kapteyn, private communication, 1989).

The numerical integration of (5.5.18) and (5.5.19) is not straightforward due to the singular behaviour at  $r=0$ . In addition, the conditions (5.5.13), (5.5.14) and (5.5.15) constitute a boundary-value problem which requires an iterative numerical procedure. The first difficulty may be removed by means of the transformation  $y^* = 2^{-\frac{1}{2}} \bar{y} = -2^{-\frac{1}{2}} \epsilon_2^{-\frac{1}{4}} \ln r$ , which was also used in section 5.5. As a consequence, the wall of the tube is positioned at  $y^* = 0$  and the axis of the tube at  $y^* = \infty$ . Since the case  $y^* = \infty$  can not be treated numerically, some boundary values have to be given at a finite value  $y_0^*$  of  $y^*$ . The flat behaviour of the asymptotic solution suggests to take

$$(\alpha)_{y^*=y_0^*} = \alpha_e(1+\delta), \quad (u_1)_{y^*=y_0^*} = (u_1)_0, \quad (5.6.1)$$

$$\left[ \frac{du_1}{dy^*} \right]_{y^*=y_0^*} = 0,$$

where  $\delta$  is a small parameter. At the wall of the tube we require that

$$(\alpha)_{y^*=0} = (u_1)_{y^*=0} = 0, \quad (5.6.2)$$

in accordance with (5.5.15). The transformed equations (5.5.18) and (5.5.19) are subsequently written as a set of five first-order differential equations.

Robust methods, based on shooting techniques, may be applied to obtain numerical solutions of the set of equations that satisfy the boundary conditions (5.6.1) and (5.6.2). We have

chosen for the D02HBF routine from the NAG library, which is described in detail by Gladwell (1979). The routine requires, at each of the two boundaries, initial estimates of the quantities that are left unspecified there. In the case of the transformed version of the equations (5.5.18) and (5.5.19) the initial estimates at  $y^* = y_0^*$  follow from the outer solution given by (5.5.34). They read

$$\left[ \frac{d\alpha}{dy^*} \right]_{y^*=y_0^*} = \left[ \frac{d^2\alpha}{dy^{*2}} \right]_{y^*=y_0^*} = 0 . \quad (5.6.3)$$

At the wall of the tube  $y^* = 0$  the asymptotic solution (5.5.43) is used to obtain the estimates

$$\begin{aligned} \left[ \frac{d\alpha}{dy^*} \right]_{y^*=0} &= \alpha_e \left( 1 + \frac{(\bar{u}_1)_0}{\alpha_e} \right) , \\ \left[ \frac{d^2\alpha}{dy^{*2}} \right]_{y^*=0} &= -2 (\bar{u}_1)_0 , \\ \left[ \frac{du_1}{dy^*} \right]_{y^*=0} &= (u_1)_0 \left[ 1 - \frac{\alpha_e}{(\bar{u}_1)_0} \right] . \end{aligned} \quad (5.6.4)$$

A numerical exploration showed that it is favourable to impose the boundary conditions (5.6.1) at  $y^* = y_0^* = 12$  with  $\delta = 10^{-3}$ . It also demonstrated that the direction of integration (shooting direction) should be taken from  $y^* = y_0^*$  to the wall of the tube at  $y^* = 0$ .

The physical parameters which may take various values are given by  $\epsilon_1$  and  $\gamma_{11}$ , defined in (5.5.20). It follows from (5.5.20) that  $\epsilon_1$  is determined by

$$\epsilon_1 = \frac{\eta_u}{\rho_l g R_0^2} w_0 \approx 1.25 \times 10^{-4} w_0 , \quad (5.6.5)$$

when the value of the tube radius reported by Serizawa et al. (1975) ( $2R_0 = 57.15$  mm) is substituted and  $\eta_u$  is taken, in a preliminary way, equal to the dynamic viscosity  $\eta$  of water at 20°C ( $\eta = 10^{-3}$  kg/ms). A moderate value (in m/s) for the difference velocity corresponds to the estimate (5.5.33) for  $\epsilon_1$ . That value also applies to the experiments by Wang et al. (1987), since their tube diameter is equal to 60 mm. The equivalent spherical diameters  $2a$

reported by Serizawa et al. (1975) vary from 3.5 mm to 4 mm. They lead to the estimates given by (5.5.32). Wang et al. (1987) do not discuss the bubble size.

In view of the preceding analysis we take  $\alpha_e = .05$ ,  $(u_1)_0 = 5$ ,  $\epsilon_1 = 4 \times 10^{-5}$  and  $\gamma_{11} = 10^{-2}$ , which represent typical values that may be encountered in practice for the case of upflow. It follows from (5.6.5) that a reasonable value of the difference velocity  $w_0$ , viz. .3 m/s, is associated with the value of  $\epsilon_1$ . Since the liquid velocity is made dimensionless by means of  $w_0$ ,  $(u_1)_0 = 5$  implies that the liquid flows with a velocity of approximately 1.5 m/s at the centre of the tube. That is certainly an acceptable value. Figure 5.6.1 gives the void-fraction distribution  $\alpha$  and the velocity profile  $u_1$  for three different cases: (1) the numerical solution of (5.5.18) and (5.5.19), (2) the numerical solution of the equations (5.5.18) and (5.5.19) when linearised and (3) the asymptotic solution (5.5.43). The numerical solutions are obtained by means of the transformed equations with the boundary conditions (5.6.1) and (5.6.2) as discussed before. Clearly a distinct maximum in the void fraction occurs near the tube wall. The value of the maximum may exceed twice the value of the void fraction at the centre of the tube. The velocity profiles are flat and look similar to turbulent profiles, although turbulence has not been taken into account. The asymptotic solution and the

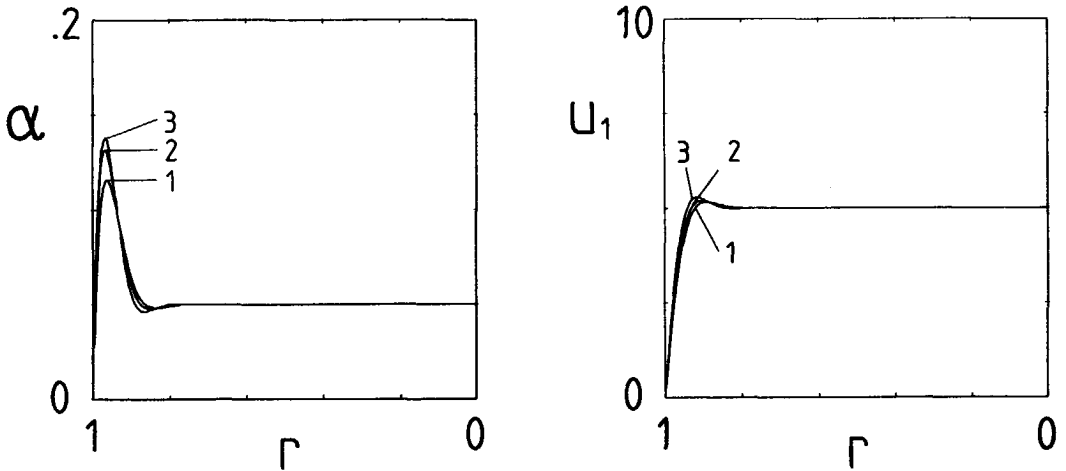


Figure 5.6.1 Void fraction  $\alpha$  and dimensionless liquid velocity  $u_1$  as functions of  $r$  in vertical upward flow for  $\alpha_e = .05$ ,  $(u_1)_0 = 5$ ,  $\epsilon_1 = 4 \times 10^{-5}$ ,  $\gamma_{11} = 10^{-2}$ ; (1) : numerical solution of (5.5.18) and (5.5.19), (2) : numerical solution of the equations (5.5.18) and (5.5.19) when linearised, (3) : asymptotic solution (5.5.43).

numerical solution of the linearised equations overestimate the behaviour of the numerical solution of the nonlinear equations. That effect increases with increasing  $\alpha_e$ . Use of the linearised instead of the original non-linear equations leads to a maximum in  $\alpha$  slightly closer to the wall. Varying  $\gamma_{11}$  and  $\epsilon_1$  shows that these parameters have a distinct effect on the value and the position of the maximum in the gas fraction  $\alpha$ : increasing  $\gamma_{11}$  decreases the maximum and moves it away from the wall of the tube, increasing  $\epsilon_1$  increases the maximum and also moves it away from the wall. Both effects will be used to obtain agreement with experiments reported in the literature. Note that in the present theory the void fraction can not exceed 1/3, since at that value the virtual-mass coefficient  $m(\alpha)$  given by (5.2.31) changes sign. All theoretical curves to be presented below are obtained by numerically integrating the transformed version of the nonlinear equations (5.5.18) and (5.5.19) subject to the modified boundary conditions (5.6.1) and (5.6.2).

Serizawa et al. (1975) report on an experimental investigation of vertical upward flow. They measured the bubble velocity in addition to the liquid velocity. In the case of low void fractions their measurements indicate that a constant difference velocity  $w_0$  is a good approximation. From their figure 14(A) we obtain  $\alpha_e = .035$ ,  $w_0 = .14$  m/s and  $u_1 = .94$  m/s at the axis of the tube, which yields  $(u_1)_0 \approx 7$ . We now vary  $\epsilon_1$  and  $\gamma_{11}$  in such a way that the position and magnitude of the maximum of  $\alpha$  are close to their measured values. That is achieved by taking  $\epsilon_1 = 6.7 \times 10^{-5}$  and  $\gamma_{11} = 2 \times 10^{-2}$ . Figure 5.6.2 shows that for those values of the physical parameters the theoretical and experimental curves for the void fraction nearly coincide. The calculated velocity profile for the liquid, however, is flatter than the measured one. The matching is clearly not as good as in the case of the void fraction. The value of the dynamic viscosity  $\eta_u$  of the bubbly mixture that corresponds to the value of  $\epsilon_1$  is given by  $\eta_u = 3.8 \times 10^{-3}$  kg/ms. Obviously, the presence of the bubbles increases the viscosity ( $\eta = 10^{-3}$  kg/ms for pure water at 20°C). This may be expected since the small irregular motions of the bubbles result in an additional contribution to the dynamic viscosity comparable with the eddy viscosity known from the theory of turbulence.

Wang et al. (1987) investigated both upflow and downflow. They report on measurements of the void fraction, the liquid velocity and turbulent fluctuations in the liquid. The gas velocity, however, is not measured. It is therefore not possible to obtain an estimate of the difference velocity  $w_0$  directly from their figures. They do present, however, the values of the superficial liquid velocity  $j_1$  and the superficial gas velocity  $j_2$  which are determined by

$$j_1 = \langle (1-\alpha) u_1 \rangle, \quad j_2 = \langle \alpha u_2 \rangle, \quad (5.6.6)$$



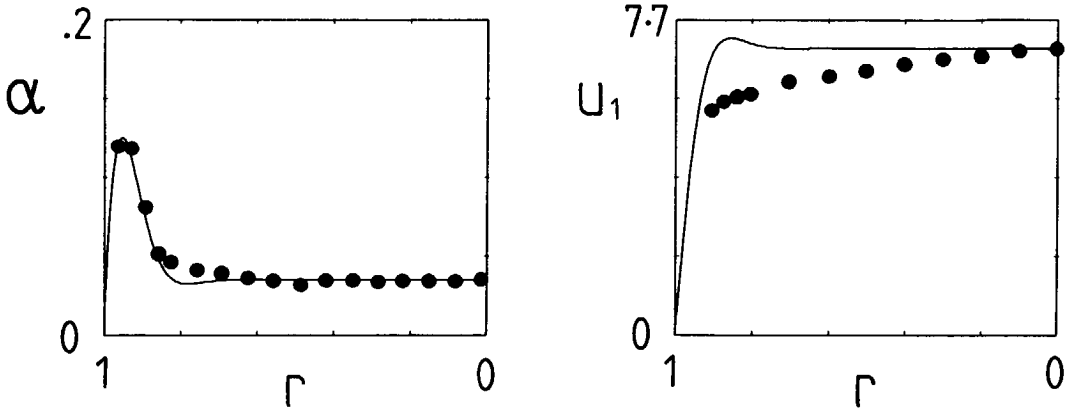


Figure 5.6.2 Void fraction  $\alpha$  and dimensionless liquid velocity  $u_1$  as functions of  $r$  in vertical upward flow for  $\alpha_e = .035$ ,  $(u_1)_0 = 7$ ,  $\epsilon_1 = 6.7 \times 10^{-5}$ ,  $\gamma_{11} = 2 \times 10^{-2}$ ; — : numerical solution of (5.5.18) and (5.5.19), • : experiments (Serizawa et al. 1975, figure 14(A)).

where

$$\langle \cdot \rangle = 2 \int_0^1 \cdot r \, dr . \tag{5.6.7}$$

Adding  $j_1$  and  $j_2$  and assuming a constant difference velocity we derive

$$j_1 + j_2 = \langle u_1 \rangle + w_0 \langle \alpha \rangle . \tag{5.6.8}$$

Relation (5.6.8) is used to obtain an approximate value for the difference velocity  $w_0$ .

We selected figures 6 (void fraction) and 11 (liquid velocity) from Wang et al. (1987) for a comparison with our theoretical results on upward flow. Wang et al. (1987) report  $j_1 = .71$  m/s and  $j_2 = .10$  m/s. By integrating the measured values for  $\alpha$  and  $u_1$  we estimated the difference velocity by means of (5.6.8) to be approximately given by  $w_0 = .10$  m/s. We also determined  $j_1$  from the measured values and arrived at  $j_1 = .72$  m/s, in accordance with the reported value. Figure 6 (Wang et al. 1987) shows that  $\alpha_e = .1$  while the value .84 m/s of the liquid velocity  $u_1$  at the tube axis, which is inferred from figure 11 (Wang et al. 1987), yields  $(u_1)_0 = 8.4$  by using the estimated value of the difference velocity. Figure 5.6.3

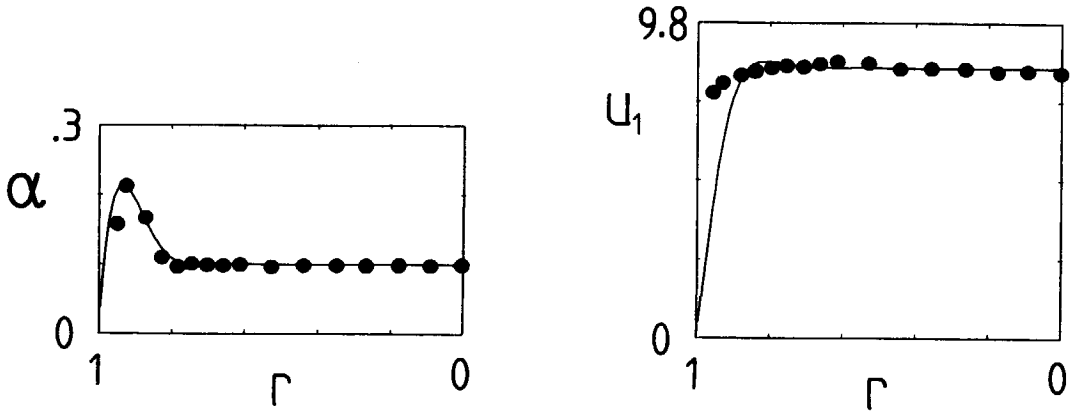


Figure 5.6.3 Void fraction  $\alpha$  and dimensionless liquid velocity  $u_1$  as functions of  $r$  in vertical upward flow for  $\alpha_e = .1$ ,  $(u_1)_0 = 8.4$ ,  $\epsilon_1 = 1.2 \times 10^{-4}$ ,  $\gamma_{11} = 1.6 \times 10^{-2}$ ; — : numerical solution of (5.5.18) and (5.5.19), • : experiments (Wang et al. 1987, figures 6 and 11).

displays the good agreement that is obtained with regard to the void fraction and the liquid velocity when  $\epsilon_1 = 1.2 \times 10^{-4}$  and  $\gamma_{11} = 1.6 \times 10^{-2}$ . By choosing a slightly different value for the difference velocity according to  $w_0 = .102$  m/s but keeping  $(u_1)_0 = 8.4$  the computed values of the liquid velocity are increased only slightly, while the superficial velocities take the values  $j_1 = .683$  m/s and  $j_2 = .104$  m/s. These values deviate not more than four percent from the values reported by Wang et al. (1987). The dynamic viscosity  $\eta_u$  of the bubbly mixture that corresponds to the value of  $\epsilon_1$  is equal to  $10^{-2}$  kg/ms. The value of  $\eta_u$  therefore increases as a result of the presence of the bubbles (see the remarks made above).

A comparison of figures 5.6.2 and 5.6.3 shows that the velocity profile measured by Wang et al. (1987) is much flatter than the profile obtained by Serizawa et al. (1975). It is therefore not surprising that Wang et al. (1987) observe turbulent fluctuations in the liquid. The magnitude of the fluctuations does not exceed 10 percent of the value of the liquid velocity at the tube axis. Since the fluctuations measured by Wang et al. (1987) increase with the value of the void fraction, they may be related to the presence of the bubbles. The fluctuations are also larger near the wall of the tube. Wang et al. (1987) therefore conclude that the turbulence level in the liquid consists of wall induced and bubble induced turbulence. It would be interesting to know more about the origin of the turbulent fluctuations. As long as a detailed knowledge is lacking it seems natural to assume that the

irregular motions of the gas bubbles which are particularly prominent in the neighbourhood of the wall, make a substantial contribution to the turbulent fluctuations of the liquid velocity. We recall that the energy associated with the irregular bubble motions is incorporated in the present theory by means of an additional term in the free energy density that is given by (5.1.3). Apparently, turbulence does not necessarily have to be included in order to arrive at the trends which are observed in the experiments.

The void-fraction profiles presented in figures 5.6.1, 5.6.2 and 5.6.3 satisfy in the neighbourhood of the wall the inequality  $\Delta\alpha < 0$ , where  $\Delta$  denotes the Laplacian operator. The profiles when considered as a function of  $y = -\ln r$  are therefore concave near the wall in the case of upflow. That behaviour was already concluded from the asymptotic analysis in section 5.5 (see expression (5.5.46)). Since as a consequence  $\Delta\rho_1 > 0$  in the vicinity of the boundary it follows from expression (5.3.5) for  $\hat{p}$  that wall effects decrease the pressure  $p$  determined by (5.3.9).

Wang et al. (1987) also investigated downflow. Their figures 9 (void fraction) and 13 (liquid velocity) were selected for a comparison with the present theory. We discuss the case where the superficial velocities have both a negative sign and are given by  $j_1 = -0.71$  m/s and  $j_2 = -0.10$  m/s. Wang et al. (1987) use positive values for  $j_1$  and  $j_2$  in view of the fact that their test section was turned upside down to measure downflow. By using their measurements and expression (5.6.8) in the way like was done earlier in the case of upflow, the difference velocity  $w_0$  is estimated to be .38 m/s, a somewhat large value to our opinion. In addition, it follows from the integration of the measured values that  $j_1 = -0.64$  m/s, a value which deviates considerably from the value reported by Wang et al. (1987). We do not have an explanation for this discrepancy. We will assume here that  $j_1$  has the value which follows from the measured gas-fraction distribution and velocity profile, i.e.,  $j_1 = -0.64$  m/s. From the graphs in Wang et al. (1987) it is inferred that  $\alpha_e = 0.17$  and  $u_1 = -0.78$  m/s at the tube axis. By varying  $\epsilon_1$  and  $\gamma_{11}$  and performing computations with several difference velocities we arrived at a satisfactory agreement with the experimental results when  $(u_1)_0 = -3$ ,  $\epsilon_1 = 1.25 \times 10^{-4}$  and  $\gamma_{11} = 1.9 \times 10^{-2}$ , as demonstrated in figure 5.6.4. The corresponding difference velocity and dynamic viscosity are given by  $w_0 = 0.26$  m/s and  $\eta_u = 4.2 \times 10^{-3}$  kg/ms. The superficial velocities computed from the numerical results are given by  $j_1 = -0.65$  m/s and  $j_2 = -0.08$  m/s, which again demonstrates that  $j_1$  can not be equal to the reported value of  $-0.71$  m/s. The measured void-fraction distribution shows a weakly oscillating behaviour before going to zero at the wall. The computed distribution behaves similarly although it is hardly visible in the plot of figure 5.6.4. The computed and the measured velocity profile both display a minimum near the tube wall. The fact that the

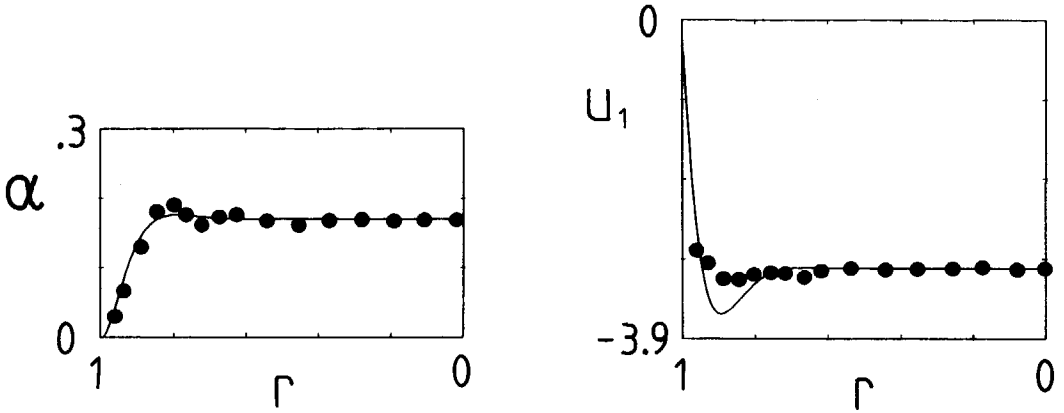


Figure 5.6.4 Void fraction  $\alpha$  and dimensionless liquid velocity  $u_1$  as functions of  $r$  in vertical downward flow for  $\alpha_e = .17$ ,  $(u_1)_0 = -3$ ,  $\epsilon_1 = 1.25 \times 10^{-4}$ ,  $\gamma_{11} = 1.9 \times 10^{-2}$ ; — : numerical solution of (5.5.18) and (5.5.19), • : experiments (Wang et al. 1987, figures 9 and 13).

minimum of the computed curve is lower explains why the calculated value  $j_1 = -.65$  m/s is somewhat smaller than the value  $j_1 = -.64$  m/s determined from the measurements.

Vertical two-phase flow in a stagnant liquid was investigated by C. Kapteyn (Twente University, Enschede, The Netherlands). That type of flow is characterised by  $j_1 = 0$  m/s and forms the transition between upflow and downflow. Kapteyn (private communication, 1989) measured a void-fraction distribution for a superficial gas velocity  $j_2 = .015$  m/s. The pipe radius  $R_0$  was equal to 40 mm. From his measurements we obtained  $\alpha_e = .067$ . Starting with  $(u_1)_0 = .5$  we varied  $\epsilon_1$  and  $\gamma_{11}$  until a satisfactory agreement was achieved. Subsequently we lowered  $(u_1)_0$  to the value .225 which hardly affected the void-fraction distribution but made the dimensionless quantity  $j_1/w_0$  approximately equal to zero ( $O(10^{-4})$ ). The corresponding values of  $\epsilon_1$  and  $\gamma_{11}$  are given by  $\epsilon_1 = 2.5 \times 10^{-5}$  and  $\gamma_{11} = 7 \times 10^{-2}$ . Figure 5.6.5 shows the void-fraction distribution and the velocity profile for those values. The dimensionless superficial gas velocity computed from the numerical results is given by  $j_2/w_0 = 6.6 \times 10^{-2}$ . Taking into account that  $j_2 = .015$  m/s we therefore arrive at a difference velocity  $w_0 = .23$  m/s, which is an acceptable value. The dynamic viscosity of the bubbly mixture is determined by  $\eta_u = 1.7 \times 10^{-3}$  kg/ms. From figure 5.6.5 we see that the liquid velocity shows an interesting behaviour. At the tube axis the velocity is positive but near the wall there is a local backflow where  $u_1$  becomes negative. There is even a region

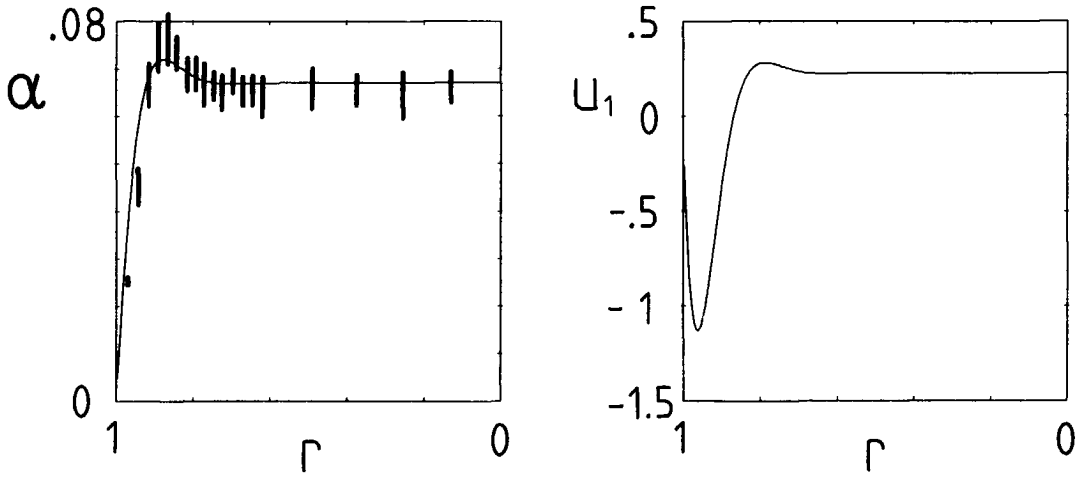


Figure 5.6.5 Void fraction  $\alpha$  and dimensionless liquid velocity  $u_1$  as functions of  $r$  in a stagnant liquid for  $\alpha_e = .067$ ,  $(u_1)_0 = .225$ ,  $\epsilon_1 = 2.5 \times 10^{-5}$ ,  $\gamma_{11} = 7 \times 10^{-2}$ ; — : numerical solution of (5.5.18) and (5.5.19), | : experiments (Kapteyn, private communication, 1989).

near the wall where  $u_1 < -1$ , which means that the bubbles attain a negative velocity in this region and move downwards. Kapteyn (private communication, 1989) has observed that effect experimentally for average gas fractions  $\langle \alpha \rangle$  varying from .2 to .3. Thanks are due to him for the kind permission to use some of his experimental results before publication (these results may now be found in Kapteyn 1989).

### 5.7 Higher order asymptotic solution

The asymptotic analysis in section 5.5 was kept as simple as possible. Only the first term of the asymptotic expansion for the inner solution was determined. In the present section we consider the asymptotic analysis in more detail and derive a higher order asymptotic solution of the equations (5.5.36) and (5.5.37).

The small parameters  $\epsilon_1$  and  $\gamma_{11}$  are assumed to satisfy  $\epsilon_1 \ll \gamma_{11}$ , which is a reasonable assumption under normal experimental conditions (see section 5.5). When the coordinate transformation  $y = -\ln r$  is applied and the strained coordinate  $\bar{y}$  is introduced by means of (5.5.38), the equations (5.5.36) and (5.5.37) are respectively written

$$e^{2\epsilon_3\bar{y}} \frac{d^2}{d\bar{y}^2} \left[ e^{2\epsilon_3\bar{y}} \frac{d^2\alpha}{d\bar{y}^2} \right] - 4 \frac{\epsilon_3^2}{\gamma_{11}} e^{2\epsilon_3\bar{y}} \frac{d^2\alpha}{d\bar{y}^2} + \alpha - \alpha_e = 0, \quad (5.7.1)$$

$$\frac{d\bar{u}_1}{d\bar{y}} - \frac{d}{d\bar{y}} \left[ e^{2\epsilon_3\bar{y}} \frac{d^2\alpha}{d\bar{y}^2} \right] + 4 \frac{\epsilon_3^2}{\gamma_{11}} \frac{d\alpha}{d\bar{y}} = 0, \quad (5.7.2)$$

where  $u_1 = (\gamma_{11}/\epsilon_1)^{\frac{1}{2}} \bar{u}_1$  and  $\epsilon_3 = \epsilon_2^{\frac{1}{2}} = (\gamma_{11}\epsilon_1)^{\frac{1}{4}}$ . Equations (5.7.1) and (5.7.2) govern the inner solution, which is written as an asymptotic expansion of the form

$$\alpha = \alpha^0 + \mu_1(\epsilon_3, \gamma_{11}) \alpha^1 + \dots, \quad (5.7.3)$$

$$\bar{u}_1 = \bar{u}_1^0 + \mu_1(\epsilon_3, \gamma_{11}) \bar{u}_1^1 + \dots,$$

where  $\mu_1(\epsilon_3, \gamma_{11})$  is a small parameter depending on  $\epsilon_3$  and  $\gamma_{11}$ . Substitution of (5.7.3) into (5.7.1) and (5.7.2) demonstrates that the first order terms in the asymptotic expansion (5.7.3) satisfy

$$\frac{d^4\alpha^0}{d\bar{y}^4} + \alpha^0 - \alpha_e = 0, \quad (5.7.4)$$

$$\frac{d\bar{u}_1^0}{d\bar{y}} - \frac{d^3\alpha^0}{d\bar{y}^3} = 0.$$

These equations coincide with (5.5.39) and (5.5.40). The solution of (5.7.4) satisfying the boundary conditions (5.5.41) and (5.5.42) and matching the outer solution (5.5.34) was obtained in section 5.5 in the form (5.5.43).

The next order case is more complicated. It follows from (5.7.1) that a convenient choice for  $\mu_1(\epsilon_3, \gamma_{11})$  is given by

$$\mu_1(\epsilon_3, \gamma_{11}) = 2 \epsilon_3. \quad (5.7.5)$$

In that case the differential equations for  $\alpha^1$  and  $\bar{u}_1^1$  contain terms of the order of  $\epsilon_3/\gamma_{11} = (\epsilon_1/\gamma_{11}^3)^{\frac{1}{4}}$ . Three cases may be distinguished: 1)  $\epsilon_1 = O(\gamma_{11}^3)$ , 2)  $\epsilon_1 \ll \gamma_{11}^3$  and

3)  $\gamma_{11}^3 \ll \epsilon_1 \ll \gamma_{11}$ . In the analysis of case 1  $\lambda$  is introduced according to

$$\epsilon_3 = \lambda \gamma_{11}. \tag{5.7.6}$$

Case 2 may be obtained from case 1 by letting  $\lambda \rightarrow 0$ . In the third case  $\epsilon_3/\gamma_{11}$  takes a large value and (5.7.5) is no more a suitable choice for  $\mu_1$ . The differential equations for  $\alpha^1$  and  $\bar{u}_1^1$  show that it should be replaced by

$$\mu_1(\epsilon_3, \gamma_{11}) = 4 \frac{\epsilon_3^2}{\gamma_{11}}. \tag{5.7.7}$$

We now analyse the three cases in more detail.

Case 1):  $\epsilon_1 = O(\gamma_{11}^3), \quad \mu_1 = 2 \epsilon_3 = 2 (\gamma_{11}\epsilon_1)^{\frac{1}{2}}.$

Substitution of (5.7.3) into (5.7.1) and (5.7.2) with  $\mu_1$  given by (5.7.5) yields the differential equations

$$\frac{d^4 \alpha^1}{d\bar{y}^4} + \alpha^1 = 2 \lambda \frac{d^2 \alpha^0}{d\bar{y}^2} - \frac{d^2}{d\bar{y}^2} \left[ \bar{y} \frac{d^2 \alpha^0}{d\bar{y}^2} \right] - \bar{y} \frac{d^4 \alpha^0}{d\bar{y}^4} \tag{5.7.8}$$

and

$$\frac{d\bar{u}_1^1}{d\bar{y}} = -2 \lambda \frac{d\alpha^0}{d\bar{y}} + \frac{d}{d\bar{y}} \left[ \bar{y} \frac{d^2 \alpha^0}{d\bar{y}^2} + \frac{d^2 \alpha^1}{d\bar{y}^2} \right], \tag{5.7.9}$$

where  $\alpha^0$  is a known function given by (5.5.43). The boundary conditions and the conditions which provide for the matching with the outer solution are given by

$$(\alpha^1)_{\bar{y}=0} = 0, \tag{5.7.10}$$

$$\alpha^1 \rightarrow 0, \quad \frac{d\alpha^1}{d\bar{y}} \rightarrow 0, \quad \text{when } \bar{y} \rightarrow \infty$$

and

$$(\bar{u}_1^1)_{\bar{y}=0} = 0, \tag{5.7.11}$$

$$\bar{u}_1^1 \rightarrow 0, \quad \text{when } \bar{y} \rightarrow \infty.$$

Note that it follows from (5.5.36) and (5.5.37) that the higher order terms of the outer solution are equal to zero as a result of the fact that the first order approximations for  $\alpha$  and  $\bar{u}_1$  are constant (see (5.5.34)). The outer solution is therefore completely given by (5.5.34). As a consequence, the asymptotic expansion for the inner solution is uniformly valid as well. The solution of (5.7.8) and (5.7.9) satisfying the boundary conditions (5.7.10) and (5.7.11) reads

$$\begin{aligned} \frac{\alpha^1}{\alpha_e} = & \left\{ 2 \lambda \sin y^* + \right. \\ & - \frac{1}{4} y^* \left[ \left[ 2^{\frac{1}{2}} - 2\lambda \left[ 1 - \frac{(\bar{u}_1)_0}{\alpha_e} \right] \right] \cos y^* - \left[ 2^{\frac{1}{2}} \frac{(\bar{u}_1)_0}{\alpha_e} - 2\lambda \left[ 1 + \frac{(\bar{u}_1)_0}{\alpha_e} \right] \right] \sin y^* \right] + \\ & \left. - \frac{1}{4} 2^{\frac{1}{2}} y^{*2} \left[ \left[ 1 + \frac{(\bar{u}_1)_0}{\alpha_e} \right] \cos y^* + \left[ 1 - \frac{(\bar{u}_1)_0}{\alpha_e} \right] \sin y^* \right] \right\} e^{-y^*}, \end{aligned} \tag{5.7.12}$$

$$\begin{aligned} \frac{\bar{u}_1^1}{(\bar{u}_1)_0} = & \left\{ - \lambda \sin y^* + \right. \\ & - \frac{1}{4} y^* \left[ \left[ 2^{\frac{1}{2}} - 2\lambda \left[ 1 + \frac{\alpha_e}{(\bar{u}_1)_0} \right] \right] \cos y^* + \left[ 2^{\frac{1}{2}} \frac{\alpha_e}{(\bar{u}_1)_0} + 2\lambda \left[ 1 - \frac{\alpha_e}{(\bar{u}_1)_0} \right] \right] \sin y^* \right] + \\ & \left. - \frac{1}{4} 2^{\frac{1}{2}} y^{*2} \left[ \left[ 1 - \frac{\alpha_e}{(\bar{u}_1)_0} \right] \cos y^* + \left[ 1 + \frac{\alpha_e}{(\bar{u}_1)_0} \right] \sin y^* \right] \right\} e^{-y^*}, \end{aligned} \tag{5.7.13}$$



where  $y^* = 2^{-\frac{1}{2}} \bar{y} = -2^{-\frac{1}{2}} \epsilon_2^{\frac{1}{2}} \ln r$ . It will be clear that the higher order contribution to the liquid velocity  $\bar{u}_1^1$  is obtained in a straightforward way by integrating (5.7.9).

Case 2):  $\epsilon_1 \ll \gamma_{11}^3$ ,  $\mu_1 = 2 \epsilon_3 = 2 (\gamma_{11} \epsilon_1)^{\frac{1}{2}}$ .

When  $\epsilon_1 \ll \gamma_{11}^3$ ,  $\lambda = \epsilon_3/\gamma_{11}$  has a small value. The solution for case 2 is therefore obtained from case 1 by letting  $\lambda \rightarrow 0$  in (5.7.12) and (5.7.13).

Case 3):  $\gamma_{11}^3 \ll \epsilon_1 \ll \gamma_{11}$ ,  $\mu_1 = 4 \frac{\epsilon_3^2}{\gamma_{11}} = 4 \left[ \frac{\epsilon_1}{\gamma_{11}} \right]^{\frac{1}{2}}$ .

By assuming an expansion according to (5.7.3), the differential equations for  $\alpha^1$  and  $\bar{u}_1^1$  now take the form

$$\frac{d^4 \alpha^1}{d\bar{y}^4} + \alpha^1 = \frac{d^2 \alpha^0}{d\bar{y}^2} \tag{5.7.14}$$

and

$$\frac{d\bar{u}_1^1}{d\bar{y}} = -\frac{d\alpha^0}{d\bar{y}} + \frac{d^3 \alpha^1}{d\bar{y}^3}. \tag{5.7.15}$$

The solutions of (5.7.14) and (5.7.15), satisfying the boundary conditions (5.7.10) and (5.7.11), are given by

$$\frac{\alpha^1}{\alpha_e} = \left\{ \sin y^* + \frac{1}{4} y^* \left[ \left[ 1 - \frac{(\bar{u}_1)_0}{\alpha_e} \right] \cos y^* - \left[ 1 + \frac{(\bar{u}_1)_0}{\alpha_e} \right] \sin y^* \right] \right\} e^{-y^*}, \tag{5.7.16}$$

and

$$\frac{\bar{u}_1^1}{(\bar{u}_1)_0} = \left\{ -\frac{1}{2} \sin y^* + \frac{1}{4} y^* \left[ \left[ 1 + \frac{\alpha_e}{(\bar{u}_1)_0} \right] \cos y^* - \left[ 1 - \frac{\alpha_e}{(\bar{u}_1)_0} \right] \sin y^* \right] \right\} e^{-y^*}. \tag{5.7.17}$$

A numerical calculation shows that when the second order approximations (5.7.16) and (5.7.17) are included, the asymptotic solution in figure 5.6.1 can hardly be distinguished from the numerical solution of equations (5.5.18) and (5.5.19) when linearised.

By comparing (5.7.16) and (5.7.17) with (5.7.12) and (5.7.13) we conclude that the relative order of magnitude of  $\epsilon_1$  with respect to  $\gamma_{11}$  in the case where  $\epsilon_1 \ll \gamma_{11}$  has a distinct influence on the form of the higher order terms in the asymptotic expansions for  $\alpha$  and  $u_1$ : for instance, terms quadratic in  $y^*$  which are encountered in (5.7.12) and (5.7.13) are absent in (5.7.16) and (5.7.17). The numerical effect of increasing and decreasing the values of  $\epsilon_1$  and  $\gamma_{11}$  was already discussed in section 5.6.

## **5.8 Conclusions**

The macroscopic theory of two-phase bubbly flow developed in G (1985a) was extended with a dispersive force according to (5.1.3). That term models the energy of the small irregular motions of the bubbles which, in the case of vertical two-phase flow, come into prominence in the neighbourhood of a solid boundary. It was demonstrated by means of analytical and numerical calculations that the dispersive force and the 'lift' force already contained in the original theory (see (5.1.1)) combine to produce void-fraction distributions and velocity profiles for vertical flow in a cylindrical tube which are in good agreement with experimental results obtained by various investigators. In particular the 'turbulent' character of the velocity profile for the liquid phase is reflected by the computations. The calculated void-fraction distributions display, in conformity with the experiments, a distinct maximum in the vicinity of the tube wall both for the cocurrent upward flow of a bubbly liquid/gas mixture and the collective rise of bubbles in a stagnant liquid.

## REFERENCES

- van den Akker, H. E. A. 1986 Momentum equations in dispersed two-phase flows. In *Encyclopedia of Fluid Mechanics Vol. III*, Gulf, Houston.
- Assimacopoulos, D. 1986 Wave propagation in dispersed and gravity stratified gas-liquid flows. *PDR/CFDU/27*.
- Auton, T. R. 1987 The lift force on a spherical body in a rotational flow. *J. Fluid Mech.* **183**, 199–218.
- Auton, T. R., Hunt, J. C. R. & Prud'homme, M. 1988 The force exerted on a body in inviscid unsteady non-uniform rotational flow. *J. Fluid Mech.* **197**, 241–257.
- Batchelor, G. K. 1967 *An Introduction to Fluid Dynamics*. Cambridge University Press, Cambridge.
- Batchelor, G. K. 1988 A new theory of the instability of a uniform fluidized bed. *J. Fluid Mech.* **193**, 75–110.
- Batchelor, G. K. 1989 A brief guide to two-phase flow. In *Theoretical and Applied Mechanics* (Edited by Germain, P., Piau, M. & Caillerie, D.), Proceedings of the XVII<sup>th</sup> International Congress of Theoretical and Applied Mechanics, pp. 27–40. North-Holland, Amsterdam.
- Bateman, H. 1959 *Partial Differential Equations of Mathematical Physics*. Cambridge University Press, Cambridge.
- Bedford, A. & Drumheller, D. S. 1978 A variational theory of immiscible mixtures. *Arch. Ration. Mech. Anal.* **68**, 37–51.
- van Bekkum, A. J. 1985 *Theoretical and experimental investigation of the liquid flow around a gas bubble*. Ph.D. Thesis, Delft University of Technology, Delft, The Netherlands.
- Benjamin, T. B. 1987 Hamiltonian theory for motions of bubbles in an infinite liquid. *J. Fluid Mech.* **181**, 349–379.
- Beyerlein, S. W., Cossman, R. K. & Richter, H. J. 1985 Prediction of bubble concentration profiles in vertical turbulent two-phase flow. *Int. J. Multiphase Flow* **11**, 629–641.
- Biesheuvel, A. & Wijngaarden, L. van 1984 Two-phase flow equations for a dilute dispersion of gas bubbles in liquid. *J. Fluid Mech.* **148**, 301–318.
- Born, M. A. & Wolf, E. 1959 *Principles of Optics*. Pergamon Press, London.

- Bouré, J. A. 1987 Two-phase flow models: the closure issue. In *Multiphase Science and Technology Vol. III* (Edited by Hewitt, G. F., Delhayé, J. M. & Zuber, N.). Hemisphere, Washington.
- Bouré, J. A. & Delhayé, J. M. 1982 General equations and two-phase flow modeling. In *Handbook of Multiphase Systems* (Edited by Hetsroni, G.). Hemisphere, Washington.
- Bouré, J. A. 1988 Properties of kinematic waves in two phase pipe flows; Consequences on the modeling strategy. *SETh/LEF/88-16*, Centre d'Etudes Nucleaires de Grenoble, Grenoble.
- Chaabane, M. 1989 Stability, virtual mass and compressibility of the liquid phase in bubbly liquid/gas mixtures. *Report 814.399*, TPD, TNO Delft.
- Chakravarthy, S. R. & Osher, S. 1985 A new class of high accuracy TVD schemes for hyperbolic conservation laws. *AIAA paper 85-0363*.
- Cook, T. L. & Harlow, F. H. 1984 Virtual mass in multiphase flow. *Int. J. Multiphase Flow* **10**, 691-696.
- Delhayé, J. M. 1981. In *Thermohydraulics of Two-Phase Systems for Industrial Design and Nuclear Engineering* (Edited by Delhayé, J. M., Giot, M. & Riethmuller, M. L.), Chapters 7-10. Hemisphere, Washington.
- Drew, D. A. 1983 Mathematical modeling of two-phase flow. In *Ann. Rev. Fluid Mech. Vol. XV* (Edited by Van Dyke, M., Wehausen, J. V. & Lumley, J. L.). Annual Reviews Inc., Palo Alto.
- Drew, D. A. & Lahey, R. T. 1982 Phase-distribution mechanisms in turbulent low-quality two-phase flow in a circular pipe. *J. Fluid Mech.* **117**, 91-106.
- Drew, D. A. & Lahey Jr., R. T. 1987 The virtual mass and lift force on a sphere in rotating and straining inviscid flow. *Int. J. Multiphase Flow* **13**, 113-121.
- Drew, D. A. & Wood, R. T. 1985 Overview and taxonomy of models and methods. Presented at *International Workshop on Two-Phase Flow Fundamentals*, National Bureau of Standards, Maryland, September.
- Drumheller, D. S. & Bedford, A. 1980 A thermomechanical theory for reacting immiscible mixtures. *Arch. Ration. Mech. Anal.* **73**, 257-284.
- Geurst, J. A. 1980 General theory unifying and extending the Landau-Khalatnikov, Ginzburg-Pitaevskii, and Hills-Roberts theories of superfluid  $^4\text{He}$ . *Phys. Rev. B* **22**, 3207-3220.
- Geurst, J. A. 1985a Virtual mass in two-phase bubbly flow. *Physica A* **129**, 233-261.
- Geurst, J. A. 1985b Two-fluid hydrodynamics of bubbly liquid/vapour mixture including phase change. *Philips J. Res.* **40**, 352-374.
- Geurst, J. A. 1986 Variational principles and two-fluid hydrodynamics of bubbly liquid/gas mixtures. *Physica A* **135**, 455-486.

- Geurst, J. A. 1988 Drift mass, multifluid modelling of two-phase bubbly flow and superfluid hydrodynamics. *Physica A* **152**, 1–28.
- Geurst, J. A. & Vreenegoor, A. J. N. 1987 Variational approach to bubble deformation in two-phase flow. In *Proceedings of the First International Conference on Industrial and Applied Mathematics (ICIAM 87), Contributions from the Netherlands* (Edited by van der Burgh, A. H. P. & Mattheij, R. M. M.), pp. 335–350. Dutch Mathematics Centre, Amsterdam.
- Geurst, J. A. & Vreenegoor, A. J. N. 1988 Nonlinear void-fraction waves in two-phase bubbly flow. *ZAMP* **39**, 376–386.
- Ginzburg, V. L. & Pitaevskii, L. P. 1958 On the theory of superfluidity. *Zh. Eksp. Teor. Fiz.* **34**, 1240–1245 [*Sov. Phys. JETP* **7**, 858–861].
- Gladwell, I. 1979 The development of the boundary value codes in the ordinary differential equations chapter of the NAG library. In *Codes for Boundary Value Problems in Ordinary Differential Equations* (Edited by Childs, B., Scott, M., Daniel, J. W., Denman, E. & Nelson, P.), Springer-Verlag Lecture Notes in Computer Science, Vol. 76.
- de Groot, S. R. & Mazur, P. 1962 *Non-Equilibrium Thermodynamics*. North-Holland, Amsterdam.
- Happel, J. & Brenner, H. 1973 *Low Reynolds Number Hydrodynamics*. Second revised edition, Noordhoff, Leyden.
- Harten, A., Lax, P. D. & van Leer, B. 1983 On upstream differencing and Godunov-type schemes for hyperbolic conservation laws. *SIAM Review* **25**, 35–61.
- Hewitt, G. F. & Roberts, D. N. 1969 Studies of two-phase flow patterns by simultaneous X-ray and flash photography. *Rept. AERA-M2159*, UKAEA, Harwell.
- Hills, R. N. & Roberts, P. H. 1977 Healing and relaxation in flows of Helium II –I Generalization of Landau's equations. *Int. J. Eng. Sci.* **15**, 305–316.
- Ishii, M. 1987 Interfacial area modelling. In *Multiphase Science and Technology Vol. III* (Edited by Hewitt, G. F., Delhay, J. M. & Zuber, N.). Hemisphere, Washington.
- Jeffrey, A. 1976 *Quasilinear Hyperbolic Systems and Waves*. Research Notes in Mathematics 5, Pitman, London.
- de Jong, J. J. Th., 1987 Modelling of a two-phase flow, Master's thesis, Laboratory of Aero- and Hydrodynamics, Delft University of Technology, Delft, The Netherlands.
- Kapteyn, C. 1989 *Measurements on concentration waves in bubbly liquids*. Ph.D. Thesis, Twente University, Enschede, The Netherlands.
- Kobayashi, K., Iida, Y. & Kanegae, N. 1970 Distribution of local void fraction of air-water two phase flow in a vertical channel. *Bull. JSME* **13**, 1005–1012.
- Kok, J. B. W. 1988 Kinetic energy and added mass of hydrodynamically interacting gas bubbles in liquid. *Physica A* **148**, 240–252.

- Kok, J. B. W. 1989 *Dynamics of gas bubbles moving through liquid*. Ph.D. Thesis, Twente University, Enschede, The Netherlands.
- Korteweg, D. J. 1901 Sur la forme que prennent les équations du mouvement des fluides si l'on tient compte des forces capillaires causées par des variations de densité considérables mais continues et sur la théorie de la capillarité dans l'hypothèse d'une variation continue de la densité. *Arch. Neerl. Sci. Ex. Nat. (2)* 6, 1–24.
- Kowe, R., Hunt, J. C. R., Couet, B. & Bradbury, L. J. S. 1988 The effects of bubbles on the volume fluxes and the pressure gradients in unsteady and non-uniform flow of liquids. *Int. J. Multiphase Flow* 14, 587–606.
- Lahey, R. T., Cheng, L. Y., Drew, D. A. & Flaherty, J. E. 1980 The effect of virtual mass on the numerical stability of accelerating two-phase flows. *Int. J. Multiphase Flow* 6, 281–294.
- Lamb, H. 1945 *Hydrodynamics*. Dover, New York.
- Lax, P. D. 1973 *Hyperbolic Systems of Conservation Laws and the Mathematical Theory of Shock Waves*. SIAM Regional Conference Series in Applied Mathematics 11, SIAM, Philadelphia.
- Lerat, A. 1985 Implicit methods of second-order accuracy for the Euler equations. *AIAA Journal* 23, 33–40.
- Levich, V. G. 1962 *Physicochemical Hydrodynamics*. Prentice-Hall, Englewood Cliffs, NJ.
- Lhuillier, D. 1985 Phenomenology of inertia effects in a dispersed solid-fluid mixture. *Int. J. Multiphase Flow* 11, 427–444.
- Lighthill, J. 1978 *Waves in Fluids*. Cambridge University Press, Cambridge.
- Lighthill, M. J. & Whitham, G. B. 1955 On kinematic waves. *Proc. R. Soc. A* 229, 281–316.
- Logan, J. D. 1977 *Invariant Variational Principles*. Academic Press, New York.
- MacSyma Reference Manual 1985. *Symbolics Inc.*, Version 11.
- Matuszkiewicz, A., Flamand, J. C. & Bouré, J. A. 1987 The bubble-slug flow pattern transition and instabilities of void-fraction waves. *Int. J. Multiphase Flow* 13, 199–217.
- Milne-Thomson, L. M. 1968 *Theoretical Hydrodynamics*. MacMillan, London.
- Moore, D. W. 1965 The velocity of rise of distorted gas bubbles in a liquid of small viscosity. *J. Fluid Mech.* 23, 749–766.
- Nigmatulin, R. I. 1979 Spatial averaging in the mechanics of heterogeneous and dispersed systems. *Int. J. Multiphase Flow* 5, 353–385.
- Noordzij, L. & van Wijngaarden, L. 1974 Relaxation effects, caused by relative motion, on shock waves in gas-bubble/liquid mixtures. *J. Fluid Mech.* 66, 115–143.
- Oshima, N. 1979 The method of calculating the mechanical coefficients of fluid mixtures. *Bull. J.S.M.E.* 22, 550–555.

- Pauchon, C. & Banerjee, S. 1986 Interphase momentum interaction effects in the averaged multifluid model, Part I: Void propagation in bubbly flows. *Int. J. Multiphase Flow* **12**, 559–573.
- Pauchon, C. & Banerjee, S. 1988 Interphase momentum interaction effects in the averaged multifluid model, Part II: Kinematic waves and interfacial drag in bubbly flows. *Int. J. Multiphase Flow* **14**, 253–264.
- Ramshaw, J. D. & Trapp, J. A. 1978 Characteristics, stability and short-wavelength phenomena in two-phase flow equation systems. *Nucl. Sci. Eng.* **66**, 93–102.
- Ransom, V. H. & Hicks, D. L. 1984 Hyperbolic two-pressure models for two-phase flow. *Journal of Computational Physics* **53**, 124–151.
- Salmon, R. 1988 Hamiltonian fluid mechanics. In *Annual Review of Fluid Mechanics Vol. 20* (Edited by Lumley, J. L., Van Dyke, M. & Reed, H. L.), pp. 225–256. Annual Reviews Inc., Palo Alto.
- Serizawa, A., Kataoka, I. & Michiyoshi, I. 1975 Turbulence structure of air–water bubbly flow – II. Local properties. *Int. J. Multiphase Flow* **2**, 235–246.
- Sha, W. T. 1986 Computational fluid dynamics for multiphase flow systems. In *Advances in Multiphase Flow and Related Problems* (Edited by Papanicolaou, G.). SIAM, Philadelphia.
- Stewart, H. B. & Wendroff, B. 1984 Two-phase flow: models and methods. *Journal of Computational Physics* **56**, 363–409.
- Truesdell, C. & Noll, W. 1965 The non-linear field theories of mechanics. In *Encyclopedia of Physics Vol. III/3* (Edited by Flügge, S.). Springer, Berlin.
- Turnbull, H. W. 1944 *Theory of Equations*. Oliver and Boyd, Edinburgh.
- Vreenegoor, A. J. N. & Geurst, J. A. A numerical study of nonlinear wave-interactions in bubbly two-phase flow. In *Theoretical and Applied Mechanics* (Edited by Germain, P., Piau, M. & Caillerie, D.), Proceedings of the XVII<sup>th</sup> International Congress of Theoretical and Applied Mechanics, p. 450. North-Holland, Amsterdam.
- Vreenegoor, A. J. N., Wilders, P. & Geurst, J. A. 1988 Numerical study of non-linear wave interactions in bubbly two-phase flow. *Report 88–50*, Faculty of Technical Mathematics and Informatics, Delft University of Technology, Delft, The Netherlands.
- Wallis, G. B. 1978 *Internal Memoranda*, Thayer School of Engineering, Dartmouth College, Hanover, NH, January–February.
- Wallis, G. B. 1987 Inertial coupling in two-phase flow: macroscopic properties of suspensions in an inviscid fluid. *Lecture Notes*, Thayer School of Engineering, Dartmouth College, Hanover, NH.

- Wallis, G. B. 1988a On Geurst's equations for inertial coupling in two-phase flow. Thayer School of Engineering, Dartmouth College, Hanover, NH. Prepared for the Institute for Mathematics and its Applications workshop *Two Phase waves in Fluidized Beds, Flowing Composites and Granular Media*, University of Minnesota, January, 1989.
- Wallis, G. B. 1988b Some tests of two-fluid models for two-phase flow. Presented at *U.S.-Japan Seminar on Two-Phase Flow Dynamics*, Ohtsu, Japan, July.
- Wang, S. K., Lee, S. J., Jones Jr., O. C. & Lahey Jr., R. T. 1987 3-D turbulence structure and phase distribution measurements in bubbly two-phase flows. *Int. J. Multiphase Flow* **13**, 327-343.
- Whitham, G. B. 1974 *Linear and Non-linear Waves*. Wiley, New York.
- van Wijngaarden, L. 1972 One-dimensional flow of liquids containing small gas bubbles. In *Ann. Rev. Fluid Mech. Vol. IV* (Edited by Van Dyke, M., Wehausen, J. V. & Lumley, J. L.). Annual Reviews Inc., Palo Alto.
- Zun, I. 1980 The transverse migration of bubbles influenced by walls in vertical bubbly flow. *Int. J. Multiphase Flow* **6**, 583-588.
- Zun, I., Richter, H. J. & Wallis, G. B. 1975 The transverse migration of bubbles in vertical two-phase flow. Dartmouth College, Thayer School of Engineering, Hanover, NH.



## ACKNOWLEDGMENT

The author of this thesis wishes to thank Prof. dr. J.A. Geurst for the stimulating and fruitful cooperation. The author is also indebted to Dr. P. Wilders (Delft University of Technology, Delft, The Netherlands) for his valuable suggestions concerning the numerical computations presented in Chapter IV.



## SUMMARY

In this thesis the dynamics of bubbly liquid/gas mixtures is studied. The basis is formed by an article of Geurst (1985), who demonstrated that bubbly two-phase flow may be described in a systematic way by making use of variational techniques. In the present work that theory is extended in various ways and it is used to analyse and clarify some not yet completely understood phenomena which are encountered in the two-phase flow of bubbly mixtures.

Chapter I summarizes some of the mathematical models which may be found in the literature, all claiming to be applicable to bubbly liquid/gas flow yet all being fundamentally different. It gives an overview of the present state of the art in the field of bubbly flow. The main difficulty that is encountered concerns the virtual-mass effects associated with the local backflow around the gas bubbles, which is present when the gas has a motion relative to the liquid. It is discussed how Geurst (1985) included those effects by means of a variational formulation. It is also indicated how that approach leads to a consistent modelling of the dynamics of bubbly two-phase flow.

In Chapter II the Hamilton principle of Geurst is extended to include the effect of flow induced bubble deformation. The energy associated with the surface tension of the gas bubbles is also taken into account. The equivalent bubble radius and the bubble number density appear as additional variables. The equations of motion are subjected to a linear stability analysis which proves the possible existence of so-called void-fraction waves travelling with the velocity of the gas bubbles in the case of marginal stability. The virtual-mass coefficient of the bubble dispersion takes in that case a special form. It is made compatible with the virtual-mass coefficient of a separate gas bubble by analysing the limit of small void fractions.

In Chapter III it is shown that Geurst's equations and the equations presented in Chapter II allow a certain class of exact solutions. The solutions are interpreted as nonlinear void-fraction waves and appear to be related to the specific form of the virtual-mass coefficient which follows from the linear stability analysis. Some properties of the waves are

discussed. A variational formulation demonstrates that the additional inclusion of the motion of the gas inside the gas bubbles does not affect the characteristic properties of a nonlinear void–fraction wave.

Chapter IV presents a numerical and analytical investigation of the interaction of acoustic waves and void–fraction waves. Nonlinear void–fraction waves appear to be stable for an acoustic disturbance. The numerical results show that an acoustic wave may be reflected by a void–fraction wave characterised by a high gradient in the bubble concentration. The linearised equations of motion are used to derive reflection and transmission coefficients which give an analytical support for the numerical results. The acoustics of a bubbly liquid/gas medium is derived from a variational principle. It constitutes a generalisation of the acoustics of single–phase fluids.

In Chapter V the inviscid theory for two–phase bubbly flow is made of practical use by including dissipative terms and terms accounting for high gradients in the void fraction, which may be present near a solid boundary. Subsequently it is investigated whether the theory might be successful in predicting the characteristic void–fraction distributions and velocity profiles which are observed in the vertical pipe flow of a bubbly liquid/gas mixture. The results are compared with measurements. A good agreement is obtained for the three cases of upflow, downflow and the collective rise of gas bubbles in a stagnant liquid.

## SAMENVATTING

In dit proefschrift wordt het dynamisch gedrag van vloeistof/bellenmengsels bestudeerd. De basis wordt gevormd door een artikel van Geurst (1985), die aantoont dat de tweefasenstroming van een vloeistof/bellenmengsel op een systematische wijze beschreven kan worden door gebruik te maken van variationele technieken. Deze theorie wordt hier op verschillende manieren uitgebreid en gebruikt ter analyse en verduidelijking van sommige nog niet volledig begrepen verschijnselen die optreden in de tweefasenstroming van een bellemengsel.

Hoofdstuk I geeft een opsomming van een aantal wiskundige modellen die in de literatuur te vinden zijn. Alle modellen beweren van toepassing te zijn op de tweefasenstroming van een vloeistof/bellenmengsel ondanks het feit dat zij op fundamentele wijze van elkaar verschillen. Het geeft een overzicht van de huidige stand van zaken op het gebied van belstromingen. De grootste moeilijkheid geven de virtuele-massa effecten, gerelateerd aan de lokale terugstroming rond de gasbellen welke optreedt wanneer het gas een relatieve snelheid heeft ten opzichte van de vloeistof. Besproken wordt hoe deze effecten door Geurst (1985) zijn opgenomen via een variationele formulering. Bovendien wordt aangetoond dat deze benaderingswijze leidt tot een consistente modellering van de dynamica van vloeistof/bellenmengsels.

Het Hamiltonprincipe van Geurst wordt in Hoofdstuk II uitgebreid door het effect van stromings-geïnduceerde belvormingen op te nemen. Tevens wordt de energie ten gevolge van de oppervlaktespanning van de gasbellen in rekening gebracht. De equivalente belstraal en het aantal bellen per volume-eenheid verschijnen als additionele variabelen. De bewegingsvergelijkingen worden onderworpen aan een lineaire stabiliteitsanalyse welke het mogelijk optreden van zogenaamde gasfractiegolven aantoont, die zich voortplanten met de snelheid van de gasbellen in het geval van marginale stabiliteit. De virtuele-massa coëfficiënt van een bellendispersie heeft in dat geval een speciale vorm. Deze wordt in overeenstemming gebracht met de virtuele-massa coëfficiënt van een afzonderlijke gasbel door de limiet van kleine gasfracties te analyseren.

In Hoofdstuk III wordt aangetoond dat de vergelijkingen van Geurst en de vergelijkingen gepresenteerd in Hoofdstuk II een bepaalde klasse van exakte oplossingen toelaten. De oplossingen worden geïnterpreteerd als niet—lineaire gasfractiegolven en blijken gerelateerd te zijn aan de specifieke vorm van de virtuele—massa coëfficiënt, die volgt uit de lineaire stabiliteitsanalyse. Enkele eigenschappen van de golven worden besproken. Een variationele formulering toont aan dat het additioneel opnemen van de beweging van het gas binnen de bellen de karakteristieke eigenschappen van een niet—lineaire gasfractiegolf niet verandert.

In Hoofdstuk IV wordt numeriek en analytisch de interactie tussen akoestische golven en gasfractiegolven onderzocht. Niet—lineaire gasfractiegolven blijken stabiel te zijn voor een akoestische verstoring. De numerieke resultaten geven aan dat een akoestische golf gereflecteerd kan worden door een gasfractiegolf, gekarakteriseerd door een hoge gradiënt in de bellenconcentratie. De gelineariseerde bewegingsvergelijkingen worden aangewend om reflectie— en transmissiecoëfficiënten af te leiden, welke de numerieke resultaten van een analytische ondersteuning voorzien. De akoestische eigenschappen van een vloeistof/bellenmedium worden afgeleid uit een variatieprincipe. Zij vormen een generalisatie van de akoestische eigenschappen van fluïda, die uit één component bestaan.

In Hoofdstuk V wordt de niet—viskeuze theorie voor de tweefasenstroming van een vloeistof/bellenmengsel bruikbaar gemaakt voor praktische toepassingen door dissipatieve termen op te nemen en termen die hoge gradiënten in de gasfractie in rekening brengen. Deze laatste kunnen optreden in de buurt van een vaste wand. Vervolgens wordt onderzocht of de theorie op succesvolle wijze de karakteristieke gasfractieverdelingen en snelheidsprofielen kan voorspellen, die worden waargenomen in de verticale pijpstroming van een water/bellenmengsel. De resultaten worden vergeleken met metingen. Een goede overeenstemming wordt bereikt voor de drie gevallen van opwaartse stroming, neerwaartse stroming en het gezamenlijk opstijgen van gasbellen in een stilstaande vloeistof.

## CURRICULUM VITAE

De auteur van dit proefschrift werd op 7 november 1960 geboren te Hillegom. Als basisschool doorliep hij van 1967 tot 1973 de Jozefschool aldaar. Vervolgens bezocht hij College Hageveld te Heemstede, waar hij in 1979 het Atheneum–B diploma behaalde. In augustus dat jaar begon de auteur met de studie Toegepaste Wiskunde aan de Technische Hogeschool Delft. Het propedeutisch examen werd afgelegd in juni 1982, het kandidaats–examen in maart 1984. Op 28 februari 1986 werd cum laude het doctoraal examen afgelegd. De doctoraalscriptie betrof de supersone omstroming van delta–vleugels en werd geschreven onder de begeleiding van Prof. dr. ir. P.G. Bakker en Prof. dr. ir. J.W. Reyn. De auteur trad op 1 maart 1986 in dienst van de Technische Hogeschool Delft (Technische Universiteit Delft vanaf september dat jaar) om als wetenschappelijk assistent onderzoek te verrichten, werkend op de Faculteit der Technische Wiskunde en Informatica. De tweefasenstroming van vloeistof/bellenmengsels vormde het onderwerp van het onderzoek, dat werd uitgevoerd onder de begeleiding van Prof. dr. J.A. Geurst. Op congressen in Zeist (Conferentie Numeriek Wiskundigen 1987), Parijs (ICIAM 1987) en Grenoble (ICTAM 1988) werden presentaties van het werk gegeven. In oktober 1989 hebben Prof. Geurst en de auteur op verzoek van het Samenwerkingsverband Stromingsleer Delft een colloquium *Tweefasenstromingen* georganiseerd.